

EFFECT OF VEHICLES' BLOCKAGE ON HEAT RELEASE RATE
IN CASE OF TUNNEL FIRE

A THESIS SUBMITTED TO
THE GRADUATE SCHOOL OF NATURAL AND APPLIED SCIENCES
OF
MIDDLE EAST TECHNICAL UNIVERSITY

BY

SERKAN KAYILI

IN PARTIAL FULFILLMENT OF THE REQUIREMENTS
FOR
THE DEGREE OF DOCTOR OF PHILOSOPHY
IN
MECHANICAL ENGINEERING

DECEMBER 2009

Approval of the thesis:

**EFFECT OF VEHICLES' BLOCKAGE ON HEAT RELEASE RATE
IN CASE OF TUNNEL FIRE**

submitted by **SERKAN KAYILI** in partial fulfillment of the requirements for the degree of **Doctor of Philosophy in Mechanical Engineering Department, Middle East Technical University** by,

Prof. Dr. Canan Özgen
Dean, Graduate School of **Natural and Applied Sciences**

Prof. Dr. Süha Oral
Head of Department, **Mechanical Engineering**

Prof. Dr. O. Cahit Eralp
Supervisor, **Mechanical Engineering Dept., METU**

Examining Committee Members:

Prof. Dr. A. Demir Bayka
Mechanical Engineering Dept., METU

Prof. Dr. O. Cahit Eralp
Mechanical Engineering Dept., METU

Prof. Dr. Ali Durmaz
Mechanical Engineering Dept., Gazi University

Prof. Dr. Kahraman Albayrak
Mechanical Engineering Dept., METU

Asst. Prof. Ahmet Yozgatlıgil
Mechanical Engineering Dept., METU

Date: 08.12.2009

I hereby declare that all information in this document has been obtained and presented in accordance with academic rules and ethical conduct. I also declare that, as required by these rules and conduct, I have fully cited and referenced all material and results that are not original to this work.

Serkan KAYILI

ABSTRACT

EFFECT OF VEHICLES' BLOCKAGE ON HEAT RELEASE RATE IN CASE OF TUNNEL FIRE

Kayılı, Serkan

Ph.D. , Department of Mechanical Engineering

Supervisor: Prof. Dr. O. Cahit Eralp

December 2009, 200 pages

Road and railways tunnels are constructed for decreasing the transportation time inside city or intercity. The fire safety systems are mounted for the safe use of tunnels. Therefore, it is important to accurately predict the fire-induced air velocity, temperature and smoke concentrations in tunnel fires in order to design efficient fire protection systems. To this end, scaled tunnel models are used and experiments are carried to understand the phenomena on these tunnel models. In addition, the studies for investigating the tunnel fire phenomena and their methods of modeling techniques for fire experiments are mentioned. In the literature, there is no sufficient information about vehicles' blockage effect on heat release rate and temperature distribution inside tunnel with different ventilation velocities. As a result, in order to research this subject, the scaled model tunnel is constructed in Fluid Mechanics Laboratory. Based on the Froude number scaling, wood sticks with different

configuration inside the model tunnel are burned in a controlled environment. The heat release rate measurement, sampling of gases after combustion, mass loss rate of burning models and temperature distribution along the tunnels with different longitudinal ventilation velocities are measured to investigate the effect of different cross-sectional areas of the burning substances. Furthermore, the model vehicles having a square base area are built according to wood crib theory. The results are investigated with statistical techniques called “Analysis of Variance” and general results have been tried to be reached. It is determined that the variation of air velocity inside tunnel is not so effective, but the model vehicle’s cross sectional area is directly proportional to heat release rate.

Keywords: Fire safety, Tunnel fire, Froude number scaling, Fire Load, Emergency Ventilation, Blockage Ratio

ÖZ

TÜNEL YANGINI SIRASINDA TAŞIT BLOKAJININ YANGIN YÜKÜNE ETKİSİ

Kayılı, Serkan

Doktora, Makina Mühendisliği Bölümü
Tez Yöneticisi: Prof. Dr. O. Cahit Eralp

Aralık 2009, 200 sayfa

Kara ve demiryolu tünelleri şehir içi ve şehirlerarası ulaşım zamanını kısaltmak amacıyla yapılmaktadır. Tüneller, güvenli bir şekilde kullanılabilmesi için, yangın güvenlik sistemleri ile donatılır. Bu nedenle, yangın güvenlik sistemlerinin yeterli bir şekilde tasarlanması için yangın sonucu oluşan hava hızlarının, sıcaklıklarının ve duman konsantrasyonunun doğru bir şekilde tahmin edilmesi önemlidir. Bu amaçla, küçük ölçekli tünel modelleri kullanılarak bu olgunun çözümlenmesi için deneyler yapılmaktadır. Literatürdeki çalışmalarda, tünel yangınları ve bunların modelleme metodları üzerine yapılan çalışmalardan bahsedilmiştir. Taşıtların blokaj etkisinin farklı havalandırma hızlarında yangın ısı gücüne ve sıcaklık dağılımına etkisi ile ilgili yeterli bilgi bulunmamaktadır. Küçük ölçekli bir tünel modeli Akışkanlar Mekaniği Laboratuvarında yapılmıştır. Froude sayısı temel alınarak yapılan ölçeklendirme ile değişik şekillerde dizilmiş tahta malzemeler model tünel içinde

kontrollü bir ortamda yakılmıştır. Değişik havalandırma hızlarında yangının ısı gücü, gaz konsantrasyonu, kütle azalma hızı ve tünel boyunca oluşan sıcaklık değerleri ölçülerek değişik kesit alanlarına sahip yanan parçaların etkisi araştırılmıştır. Yapılan deneylerde model araçlar tabanları kare olacak şekilde tahta kafes teorisine göre oluşturulmuştur. Sonuçlar istatistiksel bir yöntem olan varyans analizi methodu ile incelenmiş ve genel sonuçlar elde edilmeye çalışılmıştır. Tünel içindeki hava hızının değişimi yangın yüküne çok fazla etkili olmadığı fakat model taşıtın kesit alanı ile yangın yükü doğru orantılı olduğu tespit edilmiştir.

Anahtar Kelimeler: Yangın Güvenliği, Tünel Yangını, Froude numarası modellemesi, Yangın Yüğü, Acil durum havalandırması, Tıkama (Blokaj) Oranı

To My Family and My Destiny

ACKNOWLEDGMENTS

I would like to thank my advisor Professor Dr. O. Cahit Eralp for their direction, assistance, and his excellent guidance during the course of Ph. D. study. In particular, Professor Dr. Kahraman Albayrak and Assistant Professor Dr. Ahmet Yozgatlıgil 's recommendations and suggestions have been invaluable for this study.

Special thanks go to my friends Tolga Köktürk, Eren Musluođlu, Ekin Özgirgin Bingöl, Gençer Koç, Özgür Cem Ceylan, Alper Çelik, Ersin Yorgun, Şeniz Bilgi, Cihan Kayhan, Ozan Korkmaz. I would like to show my gratitude to specially Mehmet Özçiftçi for his dishonoured help and Rahmi Ercan.

I also wish to thank Dr. Songül Bayraktar, Neslim Hancılar and Elçin Kartal Koç, who help me to perform statistical analysis. It is a pleasure to thank the Scientific and Technological Research Council of Turkey (TÜBİTAK) who supports this work (Project No: 109M007).

Finally, this thesis would not be possible without the endless support of my family.

TABLE OF CONTENTS

ABSTRACT.....	iv
ÖZ	vi
ACKNOWLEDGMENTS	ix
TABLE OF CONTENTS	x
LIST OF TABLES	xii
LIST OF FIGURES	xiii
LIST OF SYMBOLS	xviii
CHAPTERS	
1.INTRODUCTION	1
1.1 Tunnel Fire	2
1.1.1 Emergency Ventilation in Tunnels for Fire Safety	6
1.1.2 Literature Survey on Tunnel Fire Studies	13
1.2 Aim of Thesis	32
2. SCALE MODELING IN TUNNEL FIRE.....	33
2.1 Introduction	33
2.1 Fundamental Equations in Fire	34
2.2 Dimensionless Groups of Fundamental Equation.....	35
2.2.1 Dimensionless Groups of Momentum Equation	35
2.2.2 Dimensionless Groups for Energy Equation.....	36
2.2.3 Dimensionless Groups from Species Conservation Equation.....	39
2.3 Summary of Length Scale Result.....	40
2.4 Scale Modelling Tests in Literature	41
2.5 Wood Cribs as a Burning Item.....	54
2.5.1 Description of Wood Crib Configuration	55

3. EXPERIMENTAL SETUP & INSTRUMENTATION.....	58
3.1 Experimental Setup	58
3.2 Instrumentation	63
3.2.1 Combustion Gas Concentration Measurement.....	63
3.2.2 Temperature Measurement and Data Acquisition System.....	65
3.2.3 Mass Loss Rate of Burning Specimen	68
3.2.4 Velocity Measurement	69
3.2.5. Measurement Chain	70
4. EXPERIMENTAL PROCEDURE	72
4.1 Experimental Design Parameters	72
4.2 Fractional Factorial Design	76
4.3 Steps of the Experimental Procedure	79
5. EXPERIMENTAL RESULTS.....	81
5.1 Introduction	81
5.2 Results of Fire Tests.....	81
6. STATISTICAL ANALYSIS-ANALYSIS OF VARIANCE.....	123
6.1 Introduction	123
6.2 Statistical Analysis of Experimental Results	126
7. DISCUSSION AND CONCLUSION.....	142
7.1 Comments on the Experimental Results	142
7.2 Recommendations for Future Work.....	145
REFERENCES.....	147
APPENDICES	153
VITA	198

LIST OF TABLES

TABLES

Table 1.1 Fires in Road and Rail Tunnels.....	5
Table 1.2 Tunnel Length Limitation in the Use of Longitudinal Ventilation.....	10
Table 1.3 Heat Release Rate Data from Fires in Different Types of Vehicles.....	17
Table 1.4 Heat Release Rate Data from Fires in Rail Vehicles	18
Table 1.5 Test Conditions and Results in H. Ingason Study	21
Table 1.6 Predicted Development of Heat Release Rate in R.O. Carvel et al. 's study	27
Table 2.1 Dimensionless Variables and Scalling in fire	40
Table 2.1 Summary of Compartment Dimensions	42
Table 2.2 Summary of π Group Scaling Results	44
Table 3.1 List of Measured Quantities and Data Acquisition System.....	70
Table 4.1 Experimental Design Parameters	74
Table 4.2 Full Factorial Design Table.....	75
Table 4.3 Experiment Design Matrix (L=W).....	76
Table 4.3 Experiment Design Matrix (L \neq W).....	79
Table 6.1 Typical Data for Single Factor Experiments.....	124
Table 6.2 The Analysis of Variance Table for the Single Factor, Fixed Effect Model	126
Table 6.3 Evaluation of Correlation Between Continuous Variables	127

LIST OF FIGURES

FIGURES

Figure 1.1 Stages of Fire	3
Figure 1.2 Longitudinal Ventilation	8
Figure 1.3 Working Principle of Underground Transportation System' Emergency Ventilation in Tunnel Fire.....	11
Figure 1.4 Fully Transverse Ventilation System	12
Figure 1.5 Semi-Transverse Ventilation System	13
Figure 1.6 Results of Smoke Control with Longitudinal Ventilation	19
Figure 1.7 Variation of the Critical Velocity with of the Tunnel Width for Several Fire HRR	23
Figure 1.8 Experimental Results of S.R. Lee and H. S. Ryou's Study	24
Figure 1.9 Smoke Propagation Distance in Real Tunnel	25
Figure 1.10 The Dimensionless Critical Velocity vs. the Dimensionless Heat Release Rate	28
Figure 1.11 Critical Velocity at Different Inclination Angle.....	29
Figure 1.12 Comparison of Tunnel Slope Correction Factor on Critical Velocity Calculation.....	31
Figure 2.4 Wood Crib Example Used as a Fire Load	42
Figure 2.5 The Scaled Burning Rate for Wood Cribs	45
Figure 2.6 Gas Temperature for Wood Cribs 1/8 Scale at Different Locations	46
Figure 2.7 Gas Temperature for Wood Cribs 1/4 Scale at Different Locations	47

Figure 2.8 Gas Temperature for Wood Cribs For Scaled Fire	
At Different Locations	48
Figure 2.9 The Wall Temperature for Wood Cribs for Scaled Fire	
At Different Locations	49
Figure 2.10 Scaled Radiation Heat Flux for Wood Cribs For Scaled Fire	
At Different Locations	50
Figure 2.11 Scaled Convection Heat Flux for Wood Cribs for Scaled Fire	
At Different Locations	51
Figure 2.12 The Results of the Scaled Conduction for Each of the Small Fires	52
Figure 2.13 Dimensionless Convective Heat Transfer Coefficient Correlation	
with Temperature Rise	53
Figure 2.15 Free-Burn Model for Croce’s Wood Crib Designs.....	56
Figure 3.1 Prototype Tunnel	58
Figure 3.2 Model Tunnel.....	59
Figure 3.3 Tunnel Model Dimensions	59
Figure 3.4 Flow Driven System and Auxiliary Connections	60
Figure 3.6 Experimental Setup.....	62
Figure 3.7 TESTO 350S Gas Analyzer.....	63
Figure 3.8 K Type Thermocouple.....	65
Figure 3.9 Omega OMB-DAQ–3005 with QMB–PDQ 30 Expansion Module	66
Figure 3.10 Temperature Measurement Points	67
Figure 3.12 Pitot Tube Rakes Orientation.....	69
Figure 3.13 Measurement Chain of the Setup.....	71
Figure 4.1 Dimensions of Model Vehicles and Their Layout inside tunnel	73
Figure 4.2 Description of Experiment Notation (L=W)	77
Figure 4.3 Description of Experiment Notation (L is not equal to W)	78
Figure 5.1 Mass Loss Rate versus Time Variation of Experiment No:	
(-1)000 - 0000 - 1000 - 20000.....	89
Figure 5.2 Heat Release Rate versus Time Variation of Experiment No:	
(-1)000 - 0000 - 1000 - 20000.....	90

Figure 5.3 Mass Loss Rate versus Time Variation of Experiment No: 00002 - 1002	91
Figure 5.4 Heat Release Rate versus Time Variation of Experiment No: 00002 - 1002	92
Figure 5.5 Mass Loss Rate versus Time Variation of Experiment No: (-1)101 - 0101 - 2101	93
Figure 5.6 Heat Release Rate versus Time Variation of Experiment No: (-1)101 - 0101 - 2101	94
Figure 5.7 Mass Loss Rate versus Time Variation of Experiment No: 02000 - 1200 - 2200	95
Figure 5.8 Heat Release Rate versus Time Variation of Experiment No: 02000 - 1200 - 2200	96
Figure 5.9 Mass Loss Rate versus Time Variation of Experiment No: (-1)011 - 1011 - (-1)012 - 0012.....	97
Figure 5.10 Heat Release Rate versus Time Variation of Experiment No: (-1)011 - 1011 - (-1)012 - 0012.....	98
Figure 5.11 Mass Loss Rate versus Time Variation of Experiment No: (-1)120 - 0110 - (-1)211 - 0211.....	99
Figure 5.12 Heat Release Rate versus Time Variation of Experiment No: (-1)120 - 0110 - (-1)211 - 0211.....	100
Figure 5.13 Mass Loss Rate versus Time Variation of Experiment No: (-1)021 - 0021 - 1020 - 20220.....	101
Figure 5.14 Heat Release Rate versus Time Variation of Experiment No: (-1)021 - 0021 - 1020 - 20220.....	102
Figure 5.15 Mass Loss Rate versus Time Variation of Experiment No: (-1)2200 - 22200 - (-1)2202 - 02202.....	103
Figure 5.16 Heat Release Rate versus Time Variation of Experiment No: (-1)2200 - 22200 - (-1)2202 - 02202.....	104
Figure 5.17 Mass Loss Rate versus Time Variation of Experiment No: 20022 - 00020 - 20202 - 00200.....	105

Figure 5.18 Heat Release Rate versus Time Variation of Experiment No: 20022 - 00020 - 20202 - 00200.....	106
Figure 5.19 Mass Loss Rate versus Time Variation of Experiment No: 0202 - 22002 - 1201	107
Figure 5.20 Heat Release Rate versus Time Variation of Experiment No: 0202 - 22002 - 1201	108
Figure 5.21 Mass Loss Rate versus Time Variation of Experiment No: (-1)221 - 2221 - 0220 - 2120.....	109
Figure 5.22 Heat Release Rate versus Time Variation of Experiment No: (-1)221 - 2221 - 0220 - 2120.....	110
Figure 5.23 Mass Loss Rate versus Time Variation of Experiment No: (-1)122 - 1121	111
Figure 5.24 Heat Release Rate versus Time Variation of Experiment No: (-1)122 - 1121 - 0122 - (-1)1121.....	112
Figure 5.25 Mass Loss Rate versus Time Variation of Experiment No: 2102 - 1112 - 1100 - 2001.....	113
Figure 5.26 Heat Release Rate versus Time Variation of Experiment No: 2102 - 1112 - 1100 - 2001.....	114
Figure 5. 27 Mass Loss Rate versus Time Variation of Experiment No: 1222 - 22222	115
Figure 5.28 Heat Release Rate versus Time Variation of Experiment No: (-1)222 - 1222 - 22222	116
Figure 5.29 Mass Loss Rate versus Time Variation of Experiment No: 1210 - 2010 - 2212	117
Figure 5.30 Heat Release Rate versus Time Variation of Experiment No: 1210 - 2010 - 2212	118
Figure 5.31 Mass Loss Rate versus Time Variation of Experiment No: (-1)111 - 2111 - 2022 - 00222.....	119
Figure 5.32 Heat Release Rate versus Time Variation of Experiment No: (-1)111 - 2111 - 2022 - 00222.....	120

Figure 5.33 Mass Loss Rate versus Time Variation of Experiment No: (-1)2020 - 22020 - 02022	121
Figure 5.34 Heat Release Rate versus Time Variation of Experiment No: (-1)2020 - 22020 - 02022	122
Figure 6.1 Main Effect Plots for Experiments in HRR ($L \neq W$).....	128
Figure 6.2 Main Effect Plots for Experiments in Mass Loss Rate ($L \neq W$).....	128
Figure 6.3 Minitab Output for ANOVA of Mass Loss Rate ($L \neq W$).....	129
Figure 6.4 Pie Chart for a Cause of Variation in Mass Loss Rate ($L \neq W$)	130
Figure 6.5 Minitab Output for ANOVA of HRR Data ($L \neq W$)	131
Figure 6.6 Pie Chart for a Cause of Variation in HRR ($L \neq W$)	132
Figure 6.7 Main Effect Plots of Mass Loss Rate and HRR ($L = W$)	134
Figure 6.8 Interaction Plots of Mass Loss Rate and HRR ($L = W$)	137
Figure 6.9 Velocity, Thickness and Blockage Ratio Variation Plots of Mass Loss Rate and HRR ($L = W$)	138
Figure 6.10 Minitab Output for ANOVA of HRR Data ($L = W$)	139
Figure 6.11 Pie Chart for a Cause of Variation in HRR ($L = W$)	140
Figure 6.12 Minitab Output for ANOVA of Mass Loss Rate Data ($L = W$)	140
Figure 6.13 Pie Chart for a Cause of Variation in Mass Loss Rate ($L = W$).....	141

LIST OF SYMBOLS

\dot{Q}	: Fire heat release rate	(W)
\dot{q}	: Heat loss rates	(W)
Q	: Energy Content	(GJ)
A	: Annular area , Cross sectional Area	(m ²)
A _s	: Exposed surface area of crib	(cm ²)
A _v	: Total cross-sectional area of vertical crib shafts	(cm ²)
b	: Stick thickness	(cm)
c _p	: Specific Heat at Constant Pressure	(J/kg.K)
C	: Specific Heat of Solid	(J/kg.K)
D _h	: Hydraulic tunnel height (diameter)	(m)
g	: Gravitational Acceleration	(m/s ²)
h	: Convective Heat Transfer Coefficient	(W/m ² K)
H	: Tunnel height	(m)
K ₁	: Dimensionless constant	
K _g	: Grade correction factor	
k	: Thermal conductivity	(W/m.K)
L	: Length	(cm)
L _e	: Mean beam length of the gas	
l	: characteristic length(height)- length of sticks	(cm)
\dot{m}	: Mass flow rate	(kg/s)
m	: specimen mass	(g)
n	: Number of Sticks per Layer	
V	: Volume	(m ³)
V _c	: Critical velocity	(m/s)
p	: Pressure	(Pa)
P	: Crib porosity	
s	: Spacing between sticks	(cm)
S	: Control volume surface area	(m ²)
U,v	: Velocity	(m/s)
\dot{V}	: Volumetric gas flow	(m ³ /s)
W	: Width	(cm)
t	: Time	(s)
T	: Temperature, Thickness.	(°K- cm)

Y	: Mass Fraction of Species	
Δh_c	: Heat of Combustion	(kJ/kg)
y_i	: Mass of Species i per Mass of Reacted Fuel	
X_{xx}^A	: Mole Fraction of Species in the Exhaust Flow Measured by analyzer	(% - ppm)
X_{xx}^o	: Actual mole fraction of gas in the incoming air	(% - ppm)
E'	: net heat release of combustion per unit volume of oxygen consumed referred to 25 °C assuming carbon goes to carbon dioxide.	($E' = 17.2 \text{ MJ/m}^3$)
E''	: net heat release of combustion per unit volume of oxygen consumed referred to 25 °C in the burning of carbon monoxide.	($E'' = 23.1 \text{ MJ/m}^3$)

Greek Letters

θ	: Inclination angle	
ϕ	: Oxygen depletion factor	
ρ	: Density	(kg/m^3)
π	: Dimensionless Group	
δ	: Wall thickness	(m)
κ	: Absorption coefficient,	
σ	: Stefan- Boltzman Constant	($5.67 \times 10^{-11} \text{ kW/m}^2 \text{K}^4$)
Γ	: Shear Stress	(Pa)
μ	: Absolute Viscosity	(Pa.s)
ε	: Gas emissivity of the smoke layer	

Abbreviations

CFD	: Computational Fluid Dynamics
HGV	: Heavy Goods Vehicle
HRR	: Heat Release Rate
FDS	: Fire Dynamics Simulator
NFPA	: National Fire Protection Association
PIARC	: World Road Association
Re	: Reynolds number
Gr	: Grashof number
Grade	: Absolute value of the slope grade expressed as percent

Subscripts

w	: Wall
---	--------

c : Convection
e : Exhaust
f : Flame
o : Vent/ Ambient condition
r : Radiation
i : Data Scan number/ species
 ∞ : Ambient condition
CO : Carbon Monoxide
O₂ : Oxygen
H₂O : Water vapor
sat : Saturation Pressure of water

CHAPTER 1

INTRODUCTION

New construction techniques are utilized in order to build longer tunnels. Today, engineers can build tunnels longer than 50 km. Tunnels are preferred not only in the mountainous regions between the cities but also under water or inside the cities. Due to the topographical or urban planning constraints, the shortest way to go between two points is to build tunnels. Therefore, the tunnels for road and railways transportation help the people travel in a short time.

The number of tunnels has increased all around the world since 1960. Nowadays, the huge number of modern tunnels is decided to be constructed for road and railway transportation including underground transportation inside cities in Turkey because they are inevitable means of transportation today. For model tunnels, the safety issue for transportation becomes important through tunnels. The safety regulations are implemented to use the tunnels safely [1]. The traffic and the atmospheric conditions are always monitored inside tunnels. Although a lot of safety measures are used, fire incidents occur during the tunnel operations. The fire could initiate due to the crash of vehicles, electrical fault, arson and the transportation system may get damaged heavily. Due to tunnel fire, people may lose their lives and properties. The number of fatalities in accidents in railway tunnels is possibly larger than accidents in road tunnels due to the large amount of people being transported in the rail tunnels.

In this section of the study, the tunnel fire characteristics, fire safety in tunnels, the fire studies done previously are mentioned. Moreover, the aim of the study is also given.

1.1 Tunnel Fire

Tunnel fire is a type of compartment fire, which is a fire confined with walls like in a room or similar enclosure. When an item burns inside an enclosure, two factors mainly influence the energy released and the burning rate [3]:

1. The temperature at the ceiling and the walls will increase due to the collection of the hot gases at the ceiling level. This causes a increase in burning rate, since the enclosure surfaces and the hot gas layer will radiate heat toward the fuel surface.
2. The availability of oxygen needed for combustion is limited by the enclosure openings. As a result, the amount of fuel burnt and energy release rate decreases.

Due to heat transfer from the compartment walls to the fuel surface, a fire in a compartment has a higher energy release rate than the fire in an open space. The heat release rate of fire within the tunnel is 4 times greater than the same material burning in the open environment [2]. The rate at which energy is released in a compartment fire depends mainly on the following factors [3]:

- the size and location of the ignition source,
- the type, amount, position, spacing , orientation and surface area of the fuel packages,
- the geometry of enclosure,
- the size and location of the compartment openings,
- the material properties of the enclosure boundaries.

Compartment fires are divided into different stages according to the temperature development in the compartment. They are ignition, growth, flashover, fully-developed fire and decay (Figure 1.1) .

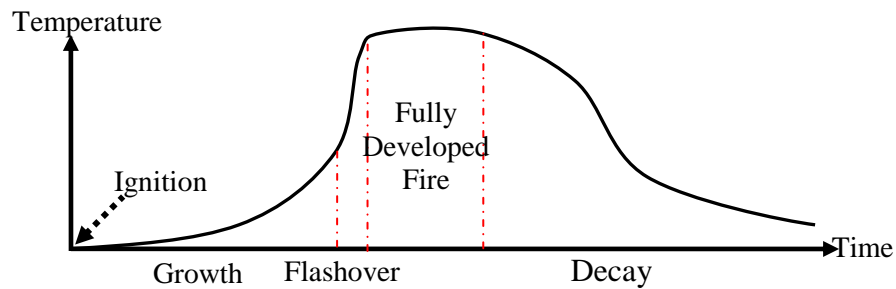


Figure 1.1 Stages of Fire [3]

Firstly, *ignition* is the process which triggers exothermic reaction releasing energy to the atmosphere [4]. Secondly, fire grows after the ignition in *growth* stage. The rate of fire growth differs from the type of fuel, compartment configuration and the type of combustion [3]. The combustible items start to burn when their temperatures reach to the ignition temperature. During this stage, hot gases with the buoyancy (stack) effect rise and form a layer at the upper part of the enclosure. A fuel-controlled (with sufficient amount of oxygen) fire occurs after ignition and during initial fire growth stage. Thirdly, the total surface of the combustible material is involved in *flashover* stage where a rapid transition from the growth period to a fully developed fire occurs [2]. In addition to these, *fully developed fire* occurs after a flashover. In this stage, the rate of heat release reaches to a maximum. The availability of oxygen (ventilation-controlled) limits the development of the fire [2]. Lastly, the energy release rate diminishes as the fuel becomes consumed during the *decay period* [3]. The fire may go from ventilation-controlled mode to fuel-controlled mode in this period.

There are differences between tunnel fires and building compartment fires. They are expressed by Carvel [2]:

1. The maximum heat release rate varies proportionally when the ventilation factor, defined as product of opening area and square root of opening height of the compartment, changes in the compartment. However, tunnel fires' development depends on the fire size, the tunnel slope, the cross-sectional area, length, type of the tunnel and meteorological conditions at the entrance. Due to mechanical ventilation systems installed in tunnels, the excess air always exists in case of tunnel fire. The heat release rate inside tunnels is affected by the ventilation differently.
2. Tunnel fire can grow more difficultly to flashover than compartment fire due to large heat losses from the fire to surrounding walls. Flashover can occur if the fire is inside the carriage of train in the tunnel.
3. The smoke in the tunnel fire rises to the ceiling and elongates on both direction along the tunnel length without longitudinal ventilation, the cold gases are located below this layer as in the compartment fire. On the other hand, due to heat loss, hot gases are getting cold and mixing with the cold layer away from the fire source. When the longitudinal ventilation starts, the smoke layer is swept. At the upstream side of fire, smoke travels opposite to the direction of ventilation, which is defined as backlayering.

There are different reasons of initiation of fire inside tunnels. They are listed as collision, overheating of braking systems and electrical fault of vehicle, sabotage etc. The risk of casualty in the rail tunnels is higher in road tunnel fire due to higher number of people transported by railway. In Table 1.1 some of the fires in the road and railways tunnels are listed. A detailed list can be found in the reference [2], [5] and [6].

Table 1.1 Fires in Road and Rail Tunnels ([2],[5] and [6])

Date	Tunnel /Length Location	Vehicles on Fire	Reason	Duration	Consequences		
					people	vehicles	structure
2005, 4 June	Frejus Road Tunnel (12900 m) France-Italy	1 Heavy Good Vehicles carrying tyres	Engine Fire	-	2 dead, 21 injured	4 Heavy Good Vehicles	10 km of equipment to be repaired
2003, 18 Feb	Jungangno Underground Daego, South Korea	Petrol and cigarette in Train	Arson	3.75 h	198 dead, 146 injured		
2003, 10 Nov	Flöfjell Road Tunnel (3100 m) Norway	Fire in car spread to tunnel lining	Collision between car and wall		1 dead	1 car	
2001, 24 Oct.	St. Gottharda Road Tunnel (16322) Switzerland	Collision between two HGVs	Collision	2 days	11 dead	13 HGVs 10 cars	Severe damage 230 m, additionally damage 700 m, closed for two months
2000, 11 Nov	Kitzsteinhorn funicular tunnel, Austria	Train	The rear driver's cab	3 h	155 dead	Train completely burnout	
1999, 23 May	Salerno, L=9000 m Italy	Train	Smoke bomb		4 dead, 9 injured		
1999, 29 May	Tauern, L= 6400 m Austria-Road	Multiple collision due to maintenance work	Leakage of paints and varnishes	15 h	12 dead	16 HGVs, 10 cars	Closed for three months

1.1.1 Emergency Ventilation in Tunnels for Fire Safety

Tunnel fires cause catastrophic damage to tunnel structure as well as the loss of lives. “Spalling” in tunnels constructed from high-strength, low-porosity concrete is the dominant failure process [2]. Under high-temperature, the pressure increases within the concrete due to formation of water vapor, the concrete layer separate or explode from the surface [7]. If the vapor pressure exceeds the capabilities of concrete pores to release the pressure, then the concrete will spall [7]. The direct exposure to fire is not the most immediate threat to human life in case of fire. Most of the casualties in fire are the results of smoke-inhalation. Precautions are taken not only to avoid or to decrease the possibility of a fire but also to increase the possibility of escape from fire. As a result, tunnel structures are protected and the number of death and injury is decreased.

The fire safety systems are mounted for the safe use of tunnels. Tunnel fire safety systems consist of ventilation system, detection system and suppression system, yet only ventilation systems are considered in this study.

Ventilation is used inside tunnel for dilution of air pollutants, smoke control and in order to decrease the temperature. In the past, ventilation system was only used to provide fresh air to the tunnel to decrease the temperature inside the tunnel. Ventilation in a tunnel can be classified as natural ventilation, mechanical ventilation, and emergency ventilation.

Air temperature, meteorological conditions and traffic are the causes of the natural ventilation. In railways tunnels, natural ventilation in the tunnel is primarily the result of vehicle operation in the tunnel (piston effect). However, in a road tunnel the piston effect has a small effect on ventilation due to the small blockage of vehicles. Wind and pressure difference between tunnel portals may provide sufficient

ventilation for the tunnel. For a short tunnel, the natural ventilation is widely used for smoke control. Some countries restrain the length of tunnel with natural ventilation. This length varies between 350 and 700 m in Germany [2], but the upper limit is 400 m [2] in United Kingdom, and 230 m in Hong Kong [8]. The smoke layer over the ceiling can start to descend due to cold wall around the layer. This can affect the evacuation period. Necessary time for evacuation in case of fire inside tunnel with natural ventilation depends on tunnel length, tunnel dimensions and slope, fire size and growth rate and meteorological conditions [2]. The safety of the system in case of emergency is inversely proportional to the tunnel length.

The mechanical ventilation is used for providing a reliable operation in case of normal and emergency operations. If the natural ventilation is not adequate during normal operation, it is supplemented by mechanical ventilation (i.e. fans). Another duty of mechanical ventilation is to provide outside air for people in tunnels in an emergency case. Lastly, extracting smoke from the system for the life safety of the passengers is another function of mechanical ventilation in case of fire.

Emergency ventilation is the major control strategy in a tunnel fire. During emergencies involving fire, the products of combustion will produce toxic gases. Particles in smoke also tend to limit visibility. The emergency ventilation equipment may be used to [14]: (1) move combustion products, and heat; (2) decrease the concentration of combustion products; and (3) reduce the heat and air temperatures in the tunnel.

The types of ventilation systems are used for emergency ventilation. These are:

- a) Longitudinal ventilation
- b) Fully transverse ventilation
- c) Semi-transverse ventilation
- d) Partial transverse system

Longitudinal ventilation is the type of ventilation, which creates a uniform longitudinal flow of air along the tunnel. This is an easy and cheap choice for a road tunnel. This ventilation system uses the traffic space as a duct for ventilation and it is not necessary to use extra ventilation ducts [2]. Two types of ventilation configurations exist for longitudinal ventilation. One of them uses jet fans and the other uses fans mounted at the vertical fan shafts. The operation of two types of longitudinal ventilation system in case of normal and emergency operation in case of fire is shown in Figure 1.2.

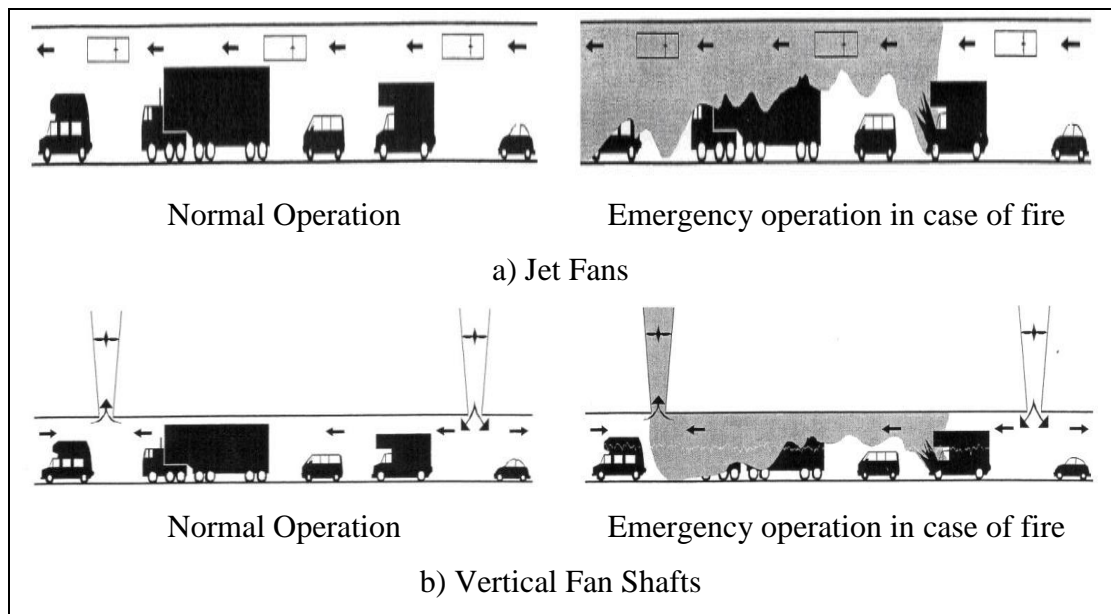


Figure 1.2 Longitudinal Ventilation [2]

The purpose of this system is to sweep smoke to preferred direction by ventilation. As a result, it creates a smoke free evacuation path and facilitates the emergency rescue services to attend the fire. Due to buoyancy effect, smoke and hot gases will flow upstream when the ventilation velocity in tunnel is relatively small. This phenomenon is called “backlayering”. Ventilation system has to prevent

backlayering. Therefore, the ventilation velocity in the tunnel for longitudinal ventilation system must be greater than a certain velocity limit. The term “Critical Velocity” is used to define the minimum air velocity past a fire to prevent backlayering. The critical velocity is calculated as:

$$V_c = K_1 K_g \left(\frac{gHQ}{\rho c_p AT_f} \right)^{1/3} \quad (1.1)$$

$$K_g = 1 + 0.0374(\text{grade})^{0.8} \quad (1.2)$$

$$T_f = \frac{Q}{\rho c_p AV_c} + T \quad (1.3)$$

where V_c is critical velocity (m/s), H is tunnel height (m), Q is fire heat release rate (W), A is annular area (tunnel - vehicle cross-sectional area) (m^2), g is gravitational acceleration (m/s^2), $K_1 = 0.61$ (dimensionless constant), K_g is Grade correction factor (For level and uphill grades, K_g is set to be 1.0.), T_f is Hot air temperature ($^{\circ}\text{K}$), Grade= absolute value of the slope grade expressed as percent, c_p is specific heat of air at constant pressure (J/kg.K), ρ (kg/m^3) and T ($^{\circ}\text{K}$) is ambient air density and temperature. The critical velocity is calculated by the simultaneous solution of equations (1.1) and (1.2) iteratively [12].

Jet fans may be installed along the tunnels. They pull the air from one side of the tunnel and push to the other side of tunnel in desired direction. Longitudinal ventilation systems with jet fans are the most common systems in Turkey for road tunnel. In road tunnel, some countries limit the tunnel length for the use of longitudinal ventilation (Table 1.2).

Table 1.2 Tunnel Length Limitation in the Use of Longitudinal Ventilation [5]

Country	Urban Area		Non urban	
	One way traffic	Two way traffic	One way traffic	Two way traffic
Germany	4 km with jetfans	2 km with jetfans	4 km with jetfans	2 km with jetfans
France	800 m	-----	4000 m	800 m
USA	900 m	900 m	900 m	900 m

In most underground transportation systems, emergency ventilation is performed by longitudinal ventilation with emergency ventilation fans at each side of the station. When the train in the system is on fire, emergency ventilation fans with nearly full reverse flow capacity start to operate. The fans at one side of the fire operate in supply mode; whereas the fans at the other side of the fire operate in exhaust mode (push-pull type). Figure 1.3 represents the working principles of emergency ventilation fans in case of tunnel fire in underground transportation system. The smoke sweeps towards the ventilation direction and passengers or occupants escape from the fire by walking towards the opposite direction of ventilation. In some cases, midtunnel, station over track ventilation fans and jet fans for directing the air flow may be used for the emergency ventilation system. The number of emergency fans working in case of fire varies depending on the fire location, design fire load and tunnel network configuration.

Emergency ventilation systems should be designed based on a design fire load that is related to the types of vehicles that use in the tunnel [14]. The fan capacities are selected in order to supply enough flow rate to the system to create air velocities above the critical velocity near the fire. For a train on fire in a tunnel, the air flow generated by the tunnel ventilation fans should be large enough to enable the passengers to sense the direction of airflow (minimum of 2.5 m/s) and not result in

such a high air speed that passengers would be prevented when walking against it (Maximum of 11 m/s) [14],[1].

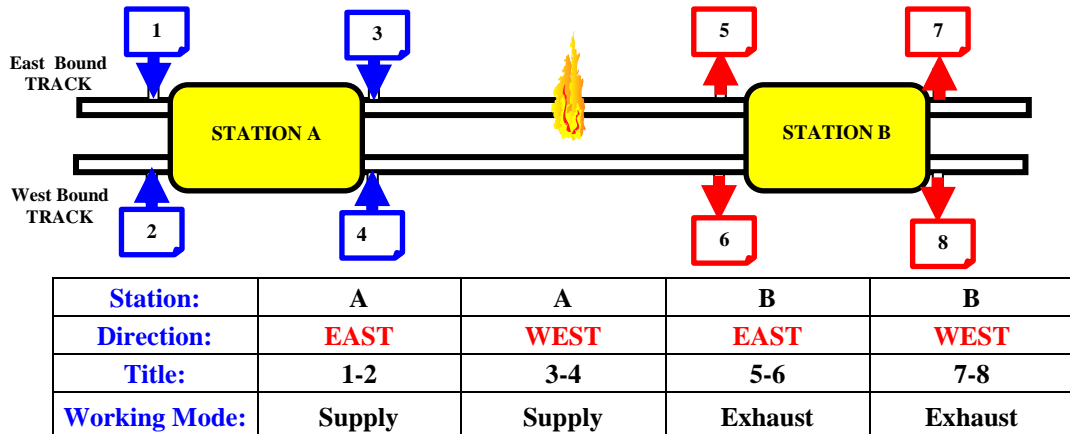


Figure 1.3 Working Principle of Underground Transportation System' Emergency Ventilation in Tunnel Fire [13]

For underground transportation system, the design objectives can be found in NFPA 130 Standard [1] as far as the evacuation (egress) routes are concerned. They are listed as follows [1]:

- “A stream of noncontaminated air is provided to evacuees on a path of evacuation away from fire.
- During emergency, evacuees should not be subjected to air temperatures that exceed 50 °C.
- Longitudinal airflow rates are produced to prevent backlayering of smoke on a path of evacuation away from fire. High ventilation rates can cause difficulties in walking. Evacuees under emergency conditions can tolerate velocities as high as 11 m/s.
- It is recommended that smoke obscuration levels should be continuously below the point at which a sign internally illuminated 80 lx is discernible at 30 m and doors and walls are discernible at 10 m.

- The fans should be designed to withstand elevated temperatures in the event of fire (remain operational for a minimum of 1 hour in an air stream temperature of 250 °C).”

Also, detail information can be found in Subway Environment Design Handbook [14] for ventilation issue in underground transportation system.

In fully-transverse system, ventilation is performed by two separate ducts with several registers on the ceiling of the tunnel. In normal operation, the fresh air is supplied from one of ducts along the tunnel in transverse to the longitudinal axis of the tunnel and the polluted air is extracted from the tunnel also in transverse direction by the other duct [2]. In case of fire, the fresh air supply channels are closed and only hot gases are extracted from the air exhaust ducts (Figure 1.4).

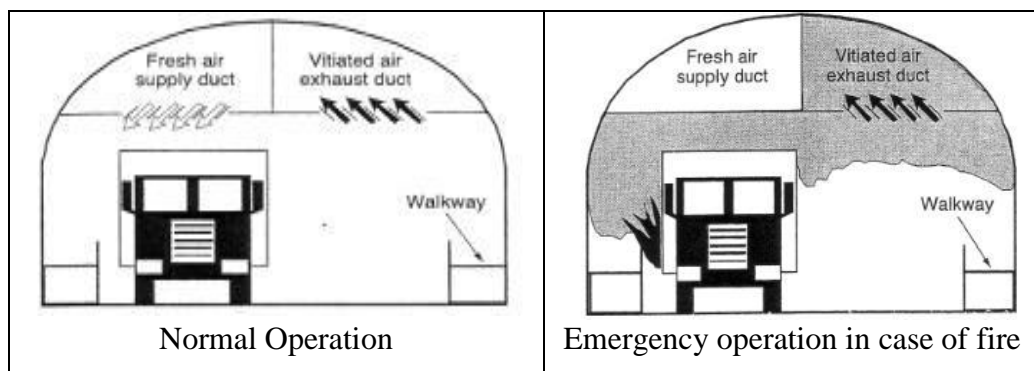


Figure 1.4 Fully Transverse Ventilation System [2]

In semi-transverse system, there is no separate duct for exhaust air from the tunnel [2]. In normal operation, fresh air is supplied to the tunnel and the polluted air leaves the tunnel from the tunnel portals. In case of fire, same ducts are used to extract the smoke from the tunnel (Figure 1.5).

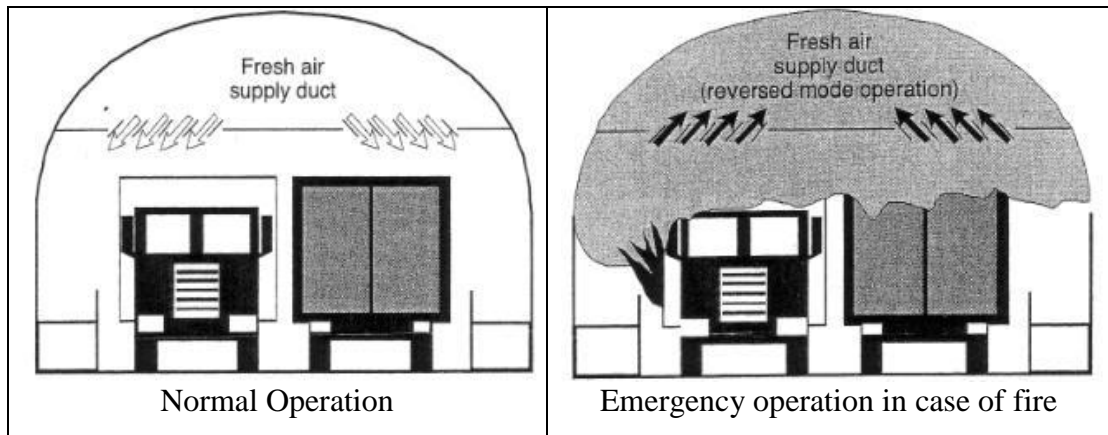


Figure 1.5 Semi- Transverse Ventilation System [2]

Depending on the percentage of supplied to extracted flow, partial transverse ventilation systems have intermediate characteristics between full transverse and semi-transverse ventilation system [2]. In all types of transverse ventilation systems, while extracting the smoke from the tunnel, the stratified smoke layer should not be destroyed [2],[8]. In the World Road Association (PIARC) [5] publication, the longitudinal velocity inside tunnel must be below 2 m/s and no fresh air must be supplied from the ceiling. Also, in a transverse type ventilation, the fresh air jets entering the tunnel at floor level cause the smoke layer down to the floor. Therefore, the fresh air rate should be throttled to 1/2 to 1/3 of full capacity [5]. The comparison of different ventilation systems can be found in reference [8],[2]and [5].

Emergency ventilation systems' requirements for road tunnels can be found in NFPA 502[15], PIARC publication [5]. Detailed list can be found for national guidelines and standard in "The Handbook of Tunnel Fire Safety" [2].

1.1.2 Literature Survey on Tunnel Fire Studies

The reasons for fire tests in tunnel are due to better understanding of fire dynamics and test the fire safety system inside tunnel. Different types of tunnel fire studies

have been performed in the literature. These studies are about backlayering related to obtain the minimum critical air velocity, the effect of the ventilation on the heat release rate, flame length and condition in tunnels. It is important to accurately predict the fire-induced air velocity, temperature and smoke concentrations in tunnel fires for designing efficient fire protection systems. The experiments investigating the enclosure fire are based on the Froude number scaling.

The full scale tunnel fire experiments have been performed. The Ofenegg tunnel fire experiments were performed in Switzerland in 1965. The tests were performed by using petrol with 3 different sizes (6.6 m², 47.5 m² and 95 m²) to investigate the natural, longitudinal and semi-transverse ventilation system [2]. Visibility inside tunnel, air velocity, temperature, carbon monoxide and oxygen concentrations were recorded [6], [2], [7]. It was observed that the burning rate of fuel in case of natural and semi-transverse ventilation due to limitation in oxygen availability was slower than equivalent fire in the open space [2]. The highest burning rate was estimated in case of longitudinal ventilation compared to other ventilation types [2]. Sprinkler system was also tested in the experiments. It was effective in extinguishing the fire [2].

Some fire tests were conducted in a disused railway tunnel with a 480 m long, 8 m wide and 6 m height in 1970, West Meon, United Kingdom. According to reference [2], the experiments were conducted with number of cars while the wind velocity was about 2 m/s at natural ventilation. It was observed that the height of the smoke layer was favorable to evacuate people safely.

Five experiments were done with kerosene fuel (1.44, 2.88 and 5.76 m²) in The railway tunnel with a length of 620 m , width 7.2 m wide , height of 5.2 m in Glasgow, United Kingdom 1970[6]. The temperature was recorded to obtain the smoke movements inside the tunnel. The smoke layer thickened as the fire size was larger and also the smoke descended to the surface of tunnel after the fire started.

30 fire tests (25 of 6.8 m petrol pool, three of 13.6 m petrol pool, one of in 6.8 m diesel pool and one test with a mixed load of wood, car tyres and sawdust) were performed in Austria, 1976 to visualize the effect of different ventilation systems. Temperature, velocity, gas concentrations (CO, CO₂, O₂, NO_x, hydrocarbon content) were recorded during the experiments [6]. It was found that the temperature at the ceiling was very high; the stratified smoke layer was dissolved in longitudinal ventilation with higher velocity [2]. The fans in fire location should be adjusted to maximum exhaust capacity and the fresh air supply fans were operated at 70-80 % of their normal working modes to maintain the stratification in case of transverse ventilation[2].

In Japan, 24 full-scale fire tests were conducted in 1980 [7]. 16 of them were in a 700-m long fire gallery with 57.3 m² cross-sectional area and eight of them in a 3.28 km long road tunnel with 58 m² cross-sectional area. 12 petrol pools, passenger cars and buses were used as burning items, the air velocity, mass loss rate of fuel, concentration measurements of carbon monoxide and in some tests also oxygen, optical density and radiation were recorded in case of natural and longitudinal ventilation. According to reference [2], “The stratification of smoke layer was partially or totally separated depending on velocity at longitudinal ventilation. When the ventilation velocity at longitudinal ventilation is increased, the heat release rate was also increased. The sprinkler was not able to extinguish the buses, cars and pool fires, but it reduced the development rate of heat release rate.

In 1985 in Finland, two large scale tests were done to model the subway car and collision of passenger cars using wood cribs as fuel in 183 m long tunnel with cross sectional area varying from 24 to 31 m² [2],[6].

Fire researchers from Austria, Finland, France, Germany, Italy, Norway, Sweden, Switzerland and the United Kingdom carried out the EUREKA EU-499 ‘Firetun’ test series, between 1990 and 1992. Cars, train carriages, wooden cribs, heptane pools, a ‘simulated truck load’ and heavy good vehicle loaded with a cargo of furniture were

burnt in the experiments in Norway near Hammerfest. Other fire tests were carried in Germany and Finland by using wood cribs as a fuel. Heat release rate, temperature, velocity, gas concentrations, visibility, mass loss rate etc. were recorded during tests [6]. The following conclusions were reached [2]: It was concluded that during most of the vehicle fires the temperatures reached to maximum values of 800-900 °C but heavy good vehicles to 1300 °C. The railway carriages burned between 15 and 20 MW; the heavy good vehicles burned at over 100 MW. Ventilation conditions affected the fire growth and burning pattern. Longitudinal ventilation destroyed stratified smoke layer in the downstream direction of ventilation in case of the HGV fire. Modern rail cars were ignited harder than older ones.

The Memorial Tunnel Fire Ventilation test program was carried out between 1993 and 1995 in USA [2], [7]. 98 pool fire tests were carried out in full scale. The 853 m long tunnel was modified to be capable of testing of natural, semi-transverse, fully transverse and longitudinal ventilation system. The objectives of the test series were to develop a database from full-scale fire tests and evaluate the capabilities of transverse and longitudinal ventilation systems to control the smoke movement and heat. The secondary objective were to test the ventilation system with different ventilation rates, system configurations and operation modes in case of different fire heat release rate and to decide their effects for smoke and heat control. Diesel fuel was used to perform the experiment. According to the test results, important conclusions were reached. In case of longitudinal ventilation, the fire with 10 MW reduced the longitudinal air flow by 10 %, a 100 MW reduced it by 50-60 %. It was concluded that the longitudinal air velocity which is dependent on the number of active fans and thrust, not on the configuration of the fans. If the ventilation velocity was between 2.5 and 3 m/s, it could prevent back-layering in a 100 MW pool fire. In case of transverse ventilation, it was necessary to extract air from the tunnel instead of only supplying air in case of fire. The longitudinal air velocity in transverse ventilation was the most effective factor to control smoke.

In Japan, 2001 ten fire tests were performed in a tunnel with 1119 m long, 8.5 m height and 115 m² cross-sectional area to understand fire behavior and smoke control and get data for verification of computational fluid dynamics (CFD) simulations [2],[7].

Four fire tests were done in Runehamar tunnel in Norway, 2003 [2]. A fire development in heavy good vehicle cargo loads, the influence of longitudinal ventilation fire heat release rate and fire growth, production of toxic gases, fire spread between vehicles, fire fighting possibilities and temperature development at the tunnel ceiling were the objectives of the test series. The combination of wooden pallets, mattresses and plastic materials were used in the experiments. The peak heat release rates were 203, 158, 125 and 70 MW.

Full scale fire tests were also performed in order to investigate fire safety system in building tunnel for commissioning. A detailed list of experiments can be found in reference [2], [7]. A heat release rate (HRR) data from vehicle fire obtained in full scale fire tests are listed in Table 1.3.

Table 1.3 Heat Release Rate Data from Fires in Different Types of Vehicles [6]

Vehicle	No. Of Tests	Energy [GJ]	Peak HRR [MW]	Time to Peak [min]
Passenger car	15	2-8	1.5-8.5	10-38
2 cars	7	5-10	5.6-10	13-55
3 cars	1	----	8.9	33
Bus	2	41 ^{a)}	29-30	7-8
Heavy Goods Vehicle Trailer	10	10-244	13-202	8-18

^{a)} Energy content only for one of the buses; the value 41 GJ gives a peak HRR of 29 MW.

From data obtained for vehicle fire tests, a correlation is found between the energy content and the maximum heat release rate. For passenger cars, the regression line forced to pass from the origin can be expressed as [6]:

$$\dot{Q}_{car} = 0.868 \left[\frac{\text{MW}}{\text{GJ}} \right] Q[\text{GJ}] \quad (R = 0.840) \quad (1.4)$$

For heavy goods vehicle trailers, the regression line passing from the origin can be expressed as [6]:

$$\dot{Q}_{HGV} = 0.866 \left[\frac{\text{MW}}{\text{GJ}} \right] Q[\text{GJ}] \quad (R = 0.910) \quad (1.5)$$

A heat release rate (HRR) data from rail vehicle fire obtained in full scale fire tests are listed in Table 1.4. The ratios of maximum heat release rate to energy content of the vehicles vary from 0.17 to 0.85 depending on the vehicle openings' dimensions such as doors and windows, vehicle material types and ignition source.

Table 1.4 Heat Release Rate Data from Fires in Rail Vehicles [6]

Type of Vehicle	Energy [GJ]	Peak HRR [MW]	HRR / Energy [MW/GJ]
A joined Railway car; two half cars, one of aluminum and one of steel, EUREKA 499	55	43	0.78
German Intercity-Express railway car (ICE), EUREKA 499	63	19	0.30
German Intercity passenger railway car (IC), EUREKA 499	77	13	0.17
British Rail 415, passenger railway car	-	16	-
British Rail Sprinter, passenger railway car, fire retardant upholstered seating	-	7	-
German subway car, EUREKA 499	41	35	0.85

Full-scale fire tests are very expensive to perform. Therefore, scientists have constructed small scale experimental tunnel to better understand the fire dynamics inside tunnel with fire safety system.

O. Vauquelin (2008) [17] investigated smoke control by longitudinal and transverse ventilation system experimentally at a 1:20 scale tunnel model with rectangular cross-section. The fire smoke was represented by air helium mixture (isothermal model). The calculation of necessary helium flow rate in the mixture, which was necessary for representing fire with certain convective heat release rate, was shown.

Froude number was preserved to transfer the results to full scale. The model which was equipped with both longitudinal and transverse ventilation had a modified height and width and it was possible to vary slope from -20 % to +20 %.

In longitudinal ventilation system model, experimentally calculated critical velocity was compared with other critical ventilation velocity model [17]. It was found that a good agreement was seen between all approaches (Figure 1.6a). In addition to this, the influence of tunnel slope was studied and it showed that the slope correction factor was necessary for calculation of the critical velocity (Figure 1.6b). According to the researchers, it was emphasized that “The tunnel height was roughly independent of the tunnel height except for small values of height.”(Figure 1.6c) The tunnel width was inversely proportional to critical velocity when the heat release rate of fire was high enough (Figure 1.6d) [17].

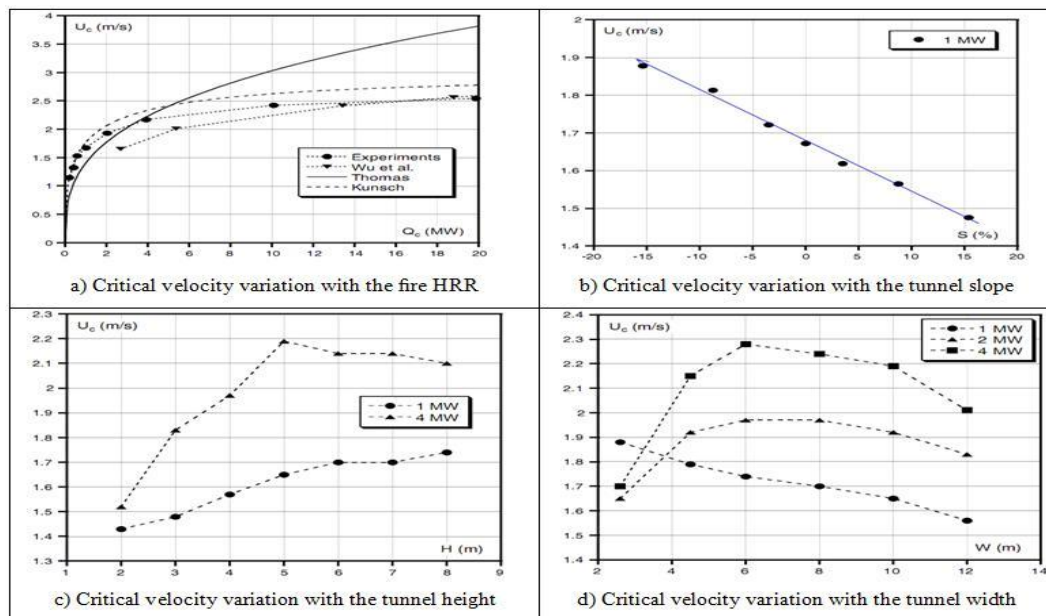


Figure 1.6 Results of Smoke Control with Longitudinal Ventilation [17]

Transverse ventilation system was investigated for several heat release rates and different values of the extraction flow rate. At certain value for the ratio of smoke

extraction flow rate to flow rate of smoke, the extraction flow rate increased with fire load, but decreased when compared with the ratio of extraction flow rate to smoke flow rate [17]. The researcher gave the corresponding full scale back flow length distance for several heat release rates and extraction flow rates. It was concluded that the back flow control was difficult due to its high sensitivity to longitudinal air flow variations.

J. S. Roh et al. (2006) [18] investigated the effect of longitudinal ventilation velocity on burning rate in tunnel fires. They performed experiments at 1/20 reduced-scale model using Froude scaling with heptane pool fires ranging from 3.71 to 15.6 kW and longitudinal ventilation velocity ranging from 0 to 1.68 m/s. The mass loss rate of the burning fuel was measured by the load cell platform. It was concluded that the burning rate of fuel increased because of larger oxygen supply effect compared to cooling effect as the ventilation velocity increased. The heat release rate in the experiment was about 4.45-11.3 times greater than the empirical calculated heat release rate.

J. S. Roh et al. (2006) [19] investigated the difference of backlayering between naturally ventilated heat release rate and varied heat release rate by longitudinal ventilation. They performed 1/20 reduced-scale experiments using Froude scaling with heptane pool fires to investigate the effects of ventilation velocity on burning rate. The sizes of each pool were 4.5, 5.5, 6.5, 8.5 cm, respectively and all fuel trays were 2 cm high. Fuel trays were mounted on the load cell platform to measure the mass loss rate of the burning fuel. The experimental results were compared with the numerical results performed by using Fire Dynamics Simulator; version 406. As the ventilation velocity increased, the burning rate of fuel increased because of larger oxygen supply effect compared to cooling effect. Although there was a small deviation in downstream temperature of fire, there was a good agreement with experimental and numerical results. It was concluded that the calculation of critical velocity should be done with the varied heat release rate by ventilation.

H. Ingason (2007) [20] performed tests in a 1/10 scale model of a Swedish intercity passenger train compartment. He tried to find the simple mathematical expressions for calculation of heat release rate in case of train compartment fire. Heat release rate, time, energy and mass were scaled based on a Froude number scaling technique with neglecting the material thermal inertia and radiation effects on fire. The model was constructed by using non-combustible boards, a plywood and corrugated cardboard which had different characteristics were used to cover the surfaces of the walls, ceiling and floor. The ventilation, the fuel load and the type of interior surface material were the varied parameters in the study. In all tests, one door was open and the number of windows varied from all windows closed, to all windows opened. The ignition took place in the corner of the model compartment opposite the door opening. The heat release rate from the fire was measured by oxygen consumption calorimetry technique. The tests conditions and results in this study were listed in Table 1.5.

Table 1.5 Test Conditions and Results in H. Ingason Study [20]

Start /end test conditions	TEST 1	TEST 2	TEST 3	TEST 4	TEST 5
Inside surface material	3.5 mm plywood	3.5 mm plywood	2 layers of 6.5 mm corrugated cardboard	2 layers of 6.5 mm corrugated cardboard	2 layers of 6.5 mm corrugated cardboard
Total weight of wall material (kg)	-	5.3	-	3.44	3.08
Total weight of wood cribs (kg)	1.12	-	-	0.97	0.91
Ambient temperature (°C)	18	19	17	19	20
Windows at Ignition	All opened	All closed	All opened	All opened	All closed
Sequence of opening of windows (min:s)		5:17 →4x2 windows opened 9:12 →5x2 windows opened			2:06 →4x2 windows opened 4:35 →5x2 windows opened

Table 1.5 Continued

Start /end test conditions	TEST 1	TEST 2	TEST 3	TEST 4	TEST 5
Test Results					
Peak HRR (kW)	148	136.5	142.8	147.6	113.2
Time to reach peak HRR (min)	6.5	11.1	3.8	3.9	6.5
Total energy released (kJ)	97828	96735	62359	62081	57451
Total mass consumed (kg)	9.58	-	4.8	4.2	4.5
Peak ceiling temperature (°C)	914	921	871	942	962
Peak radiation (kW/m ²)	74.2	71.2	63.4	68.1	63.7

From the experimental results, it was shown that the peak heat release rate was almost same when all the windows were open at the time of ignition, independent of interior surface materials used [20]. It was concluded that the body of the car and the quality and mounting of the windows were the most important parameters for fire development. The number of open windows was important for the fire development although the fire development is affected by the fuel load and the type of interior surface. Different types of surface interior material influenced initial fire growth rates and duration of the fire.

O. Vauquelin, Y. Wu (2006) [21] investigated the influence of tunnel width on critical velocity by experiments on scale models. Two different experimental reduced scale models were used: the first one was a thermal model using a propane gas flame to simulate the 1.4 to 28 kW fire and in the second experiment was performed by injecting a continuous release of an isothermal buoyant mixture (helium and air) in place of the fire induced smoke. Froude number was conserved in the 1/20 scaled road tunnel. The experimental studies were done in the tunnels with same height (250 mm); but different widths (136 mm, 250 mm, 500 mm, 1000 mm).

The experimental results were represented graphically (Figure 1.7). It was emphasized that there was no close correspondence between two models. In both cases, the critical velocity decreased when the tunnel width increased for aspect ratios width to height greater than unity. On the other hand, for low values of the aspect ratio and for high enough fire heat release rates, the critical velocity significantly increased with tunnel width.

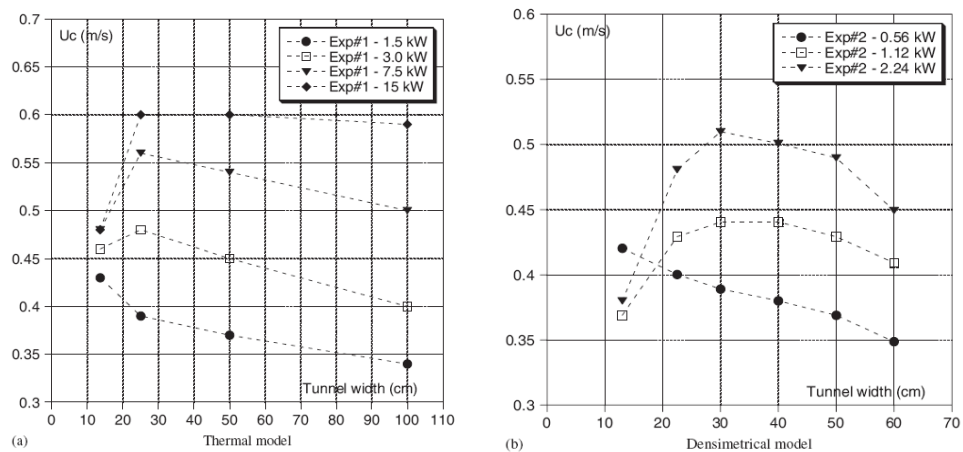


Figure 1.7 Variation of the Critical Velocity with of the Tunnel Width for Several Fire HRR [21]

S.R. Lee and H. S. Ryou (2005) [22] presented their study about the effect of aspect ratio of the tunnel cross section on the critical velocity. Based on Froude number scaling, the experiments were done in 1/20 scaled tunnels using ethanol as the fuel (12). The model tunnels with a rectangular cross section had the same aspect ratio but different aspect ratios (0.5, 0.667, 1.0 , 1.5 and 2.0). The variation of critical velocity with the aspect ratio is shown in Figure 1.8. It was confirmed that the critical velocity was dependent of the aspect ratio. It was found that as the aspect ratio increased for the tunnel with same hydraulic diameter, the critical velocity increased. They developed an expression to calculate critical velocity for medium size fire defined as dimensionless critical velocity (V^*) = 0.73 x cubic root of dimensionless heat release

rate (Q') where A_s is aspect ratio and D_h is hydraulic diameter (Figure 1.8). The researchers concluded that the growth and development of fire was affected by the aspect ratio of the tunnel. They emphasized that the smoke front velocity increased with the tunnel height and increasing the aspect ratio affected the fire growth.

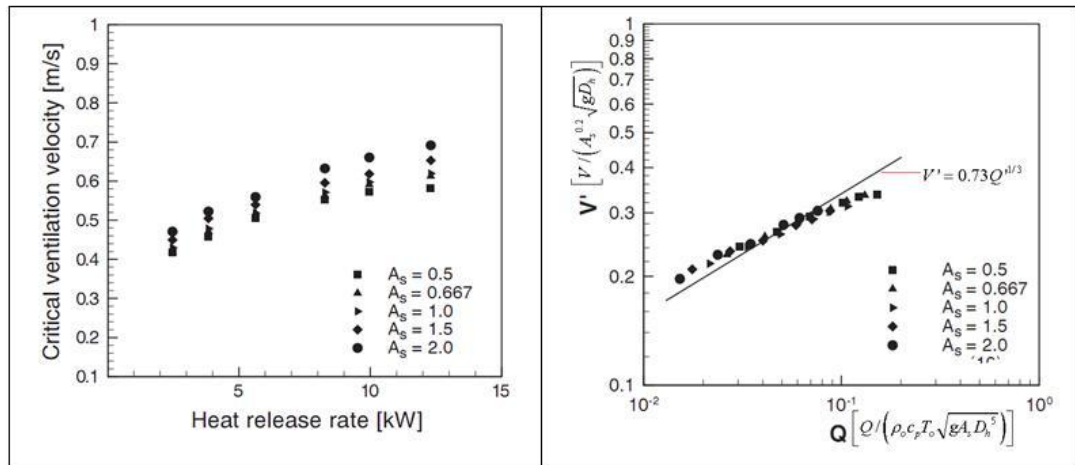


Figure 1.8 Experimental Results of S.R. Lee and H. S. Ryou's Study[22]

J.S. Choi, M.B. Kim and D.H. Choi (2005) [23] presented the results from experimental study for evaluating the smoke propagation characteristics in transverse ventilation systems as a function of fire size, fire location and supply and exhaust flow rates. The experiments were carried out 1/20 scale model of Memorial tunnel. The effects of fire location on the smoke propagation were also studied; for this purpose, fire at the center of the tunnel (symmetric case) and fire at the right hands side of the tunnels (asymmetric case) were two situations examined. Heptane was used as a fuel in the study and Froude number scaling was performed. In both cases, the smoke propagation distance variations with the exhaust flow rate per tunnel length with supplying flow rate on the tunnel floor for various fire sizes and without supplying flow rate at the given fire sizes were obtained in the model tunnel and the experimental data was converted to the case in real fire tunnel by using Froude number similarity (Figure 1.9). It was found that the smoke propagation distance

increased with the fire size and decreased with the exhaust ventilation rate. Also, the smoke propagation distance could not be decreased continuously whereas it had a constant value for off-centered fire. The smoke propagation distance in case of asymmetric case was smaller than the symmetric fire scenario. One of the important results was that the supply rate didn't affect the smoke propagation distance when it was smaller than the exhaust rate, but it had a negative affect as it was greater than the exhaust flow rate.

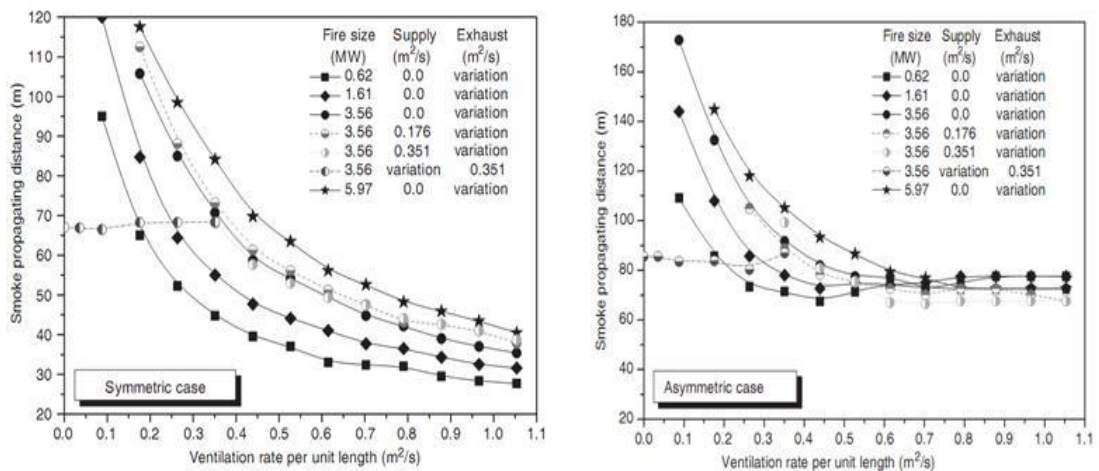


Figure 1.9 Smoke Propagation Distance in Real Tunnel [23]

B. H. Chiam (2005) [24] investigated the simulation of fire growth and flame spread within a metro train in an underground transportation system using Fire Dynamics Simulator (FDS) Computational Fluid Dynamics (CFD) model in his research thesis. The prediction of the peak value of heat release rate for emergency tunnel ventilation system design was the objective of his study. He mentioned the different models for estimating heat release rate of metro train fire and gave their drawbacks. He investigated the factors which were the burning material properties, the train and tunnel geometries and ventilation. A fire on top of the seat (arson), fire in the corner (arson and electrical fault) and undercarriage fire (electrical fault) were identified. For a corner fire case, fire grew up for low ventilation airflow but fire grew slowly in

case of high airflow. In undercarriage fire case, ventilation caused the fire spread to next railway car. It was concluded that a peak heat release was estimated as 5 MW at the station fire and 10 MW at the tunnel fire.

R.O. Carvel, A.N. Beard, P.W. Jowitt and D.D. Drysdale (2004) [25] investigated the influence of tunnel geometry and ventilation on the heat release rate of a fire. The heat release data from literature survey compared with the similar fire in open space. The values of enhancement coefficient in case of car, wooden crib and pool fire cases were listed. The ratio of heat release rate inside tunnel to heat release in open space was defined as enhancement coefficient. It was found that the enhancement coefficient increased up to a point and then it decreased due to existence of ventilation controlled fire in that region depending on the fire dimensions. The increasing behavior of enhancement coefficient was explained with the dominant behavior of re-radiation of heat in the fuel controlled regime. In case of tunnel fire the influence of geometrical factors, which were the hydraulic diameter, width and height of the tunnel and blockage ratio, was determined by using Bayesian methodology. It was shown that the heat release rate of fire in a tunnel was primarily influenced by the width of the tunnel. They found a relation (equation 1.6).

$$\text{HRR Enhancement Coefficient} = 24 \left[\frac{\text{width of the fuel}}{\text{width of the tunnel}} \right]^3 + 1 \quad \text{Eq. 1.6}$$

It is applicable for cars, wooden cribs, kerosene and heptane pools in naturally ventilated tunnels with rectangular cross sections for enhancement coefficient. The heat release rate of tunnel fire also increased with forced ventilation velocity. The authors gave values of ratio of ventilated tunnel fire heat release rate to naturally ventilated tunnel fire in case of medium and large pool fires and heavy good vehicle fires. It was demonstrated that the ventilation conditions in a tunnel may have a far more dramatic influence on the heat release rate than the geometry of the tunnel.

J. P. Kunsch (2002) [26] developed an analytical formula for estimating the critical velocity. The validation of the model was tested by comparison the derived model with the experimental data obtained from fire test. It was emphasized that the

formula of the critical ventilation velocity was applicable for ventilation rates and heat release rates occurring in real tunnel fires.

R. O. Carvel, A. N. Beard, P. W. Jowitt and D. D. Drysdale (2001) [27] investigated the effect of forced longitudinal ventilation on heat release rate for fires in tunnel. Data taken from car, wood cribs and heavy good vehicle fires were used to estimate this effect on heat release rate by using a Bayesian methodology. The main results obtained from R.O. Carvel et al. 's study is represented in tabular form in Table 1.6. In conclusion, it was shown that forced ventilation has a a great enhancing effect on the heat release rate of heavy goods vehicle fires like increasing the fire size up to 10 times in certain conditions, but has little effect on the heat release rate of car fires.

Table 1.6 Predicted Development of Heat Release Rate in R.O. Carvel et al. 's Study [27]

Type of Fire	Stage of fire	Ventilation Velocity	Increase of fire size
Heavy Good Vehicle	Growth Phase	3 m/s	5 times
	Growth Phase	10 m/s	10 times
	Fully Developed Phase	3 m/s	4 times
	Fully Developed Phase	10 m/s	10 times
Car Fire	----	1.5 m/s	No significant affect

Y. Wu and M. Z. A. Bakar (2000) [28] investigated the influence of the heat release rate of fire and the effect of the tunnel geometry on the critical velocity. A series of experimental tests in five model tunnels having the same height and 15 m long but different cross-sectional geometry were done. The propane was used as a fuel generating fires of 1.4 - 2.8 kW (approximately 2.5 - 50 MW in a tunnel of approximately 5 m diameter in full scale). Variations of critical velocity with heat released rate for 5 different model tunnels were represented in graphical form.

According to experimental results, it was emphasized that the magnitude of the critical velocity varied with tunnel geometry and heat release rate. When the hydraulic tunnel height ($D_h=4 \times \text{Cross-sectional area} / \text{tunnel wetted perimeter}$) was used, the critical velocity and heat release rate were non-dimensionalized as $V'' = V / \sqrt{gD_h}$ and $Q'' = Q / \rho_o c_p T_o \sqrt{gD_h^5}$ respectively (Figure 1.10).

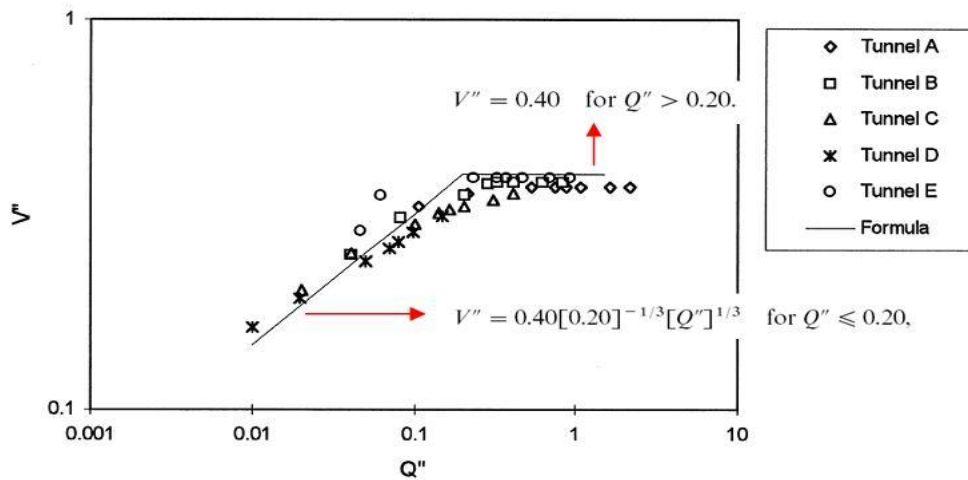


Figure 1.10 The Dimensionless Critical Velocity vs. the Dimensionless Heat Release Rate [28]

It was concluded that the critical velocity was proportional to the one-third power of the heat release rate at low rates of heat release; however, the critical velocity becomes independent of fire heat release rate at higher rates [28]. The correlation obtained in this study compared with the full scale fire tests and it was found that it is applicable to use in full scale tests. Furthermore, CFD simulations were performed to examine the flow behavior inside the tunnels and the results showed that CFD simulations predicted velocity profiles well, and gave a poor prediction of temperature in the near fire region.

H. Xue, T. C. Chew, K. L. Kay and Y. M. Cheng (2000) [29] investigated a longitudinally ventilated tunnel fire in a 1:20 scale tunnel in the laboratory. Liquefied petroleum gas (LPG) was used as a fuel. Froude number was preserved in this study. The main test section was 6 m long with 0.3 height and 0.9 m wide rectangular cross section. Heat release rates were controlled by the burner in the tunnel fire experiments. In the experimental study, two heat release rates, 3.15 and 4.75 kW were studied under four different ventilation flow velocities (0.13 , 0.31, 0.52 and 0.61 m/s) and for various tunnel slope from -5° to $+5^\circ$ at intervals 1° or 2° . It was shown that the heat and smoke movement was very sensitive to ventilation velocity in case of a tunnel fire. The flow was two dimensional when the ventilation velocity was smaller than the critical velocity. On the other hand, unstable smoke movement existed at downstream of fire when the flow velocity was greater than the critical velocity. According to the experimental results, a strong relation between the inclination angle of the tunnel with heat and smoke movement was shown. The results obtained from the experimental studies for the variation of tunnel inclination angle with the critical velocity were presented in Figure 1.11. In this figure, the negative values of the tunnel inclination angle shows descending flow.

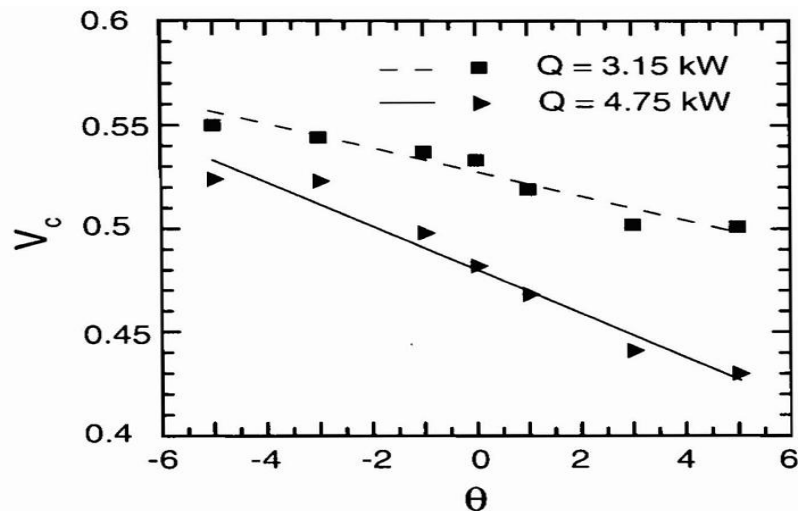


Figure 1.11 Critical Velocity at Different Inclination Angle[29]

O. Mégret and O. Vauquelin (2000) [30] developed a semi-empirical model for the determination of heat release rate, smoke flow rate and smoke temperature depending on the diameter of heptane pool fire . Correlations were applicable to be used for a wide range of fire size based on the analysis of the combustion process in heptane pool fires.

W. D. Kennedy, J. A. Gonzalez, J. G. Sanchez (1997) [31] presented the derivation of equation for calculating the critical velocity in Subway Environment simulation computer program. They emphasized that the annular area would be used in calculation for fire of subway car and the full tunnel area was used in calculation of fire in a tunnel with fuel spillage.

G. T. Atkinson and Y. Wu (1996) [32] performed a test in model tunnels with slopes between 0 and 10 degrees to study the effect of slope on the critical velocity. The researchers found an expression showing a relation with the critical velocity and slope of the tunnel. The critical velocity with the downhill slopes in the range of 0 to 10 ° is expressed as critical velocity for corresponding horizontal tunnel 0° times (1+0.014 x the slope of the tunnel in degrees). The slope factor is much lower than the one presented in W. D. Kennedy et al. study [12] or in other words given relation in Subway Simulation Program (Figure 1.12).

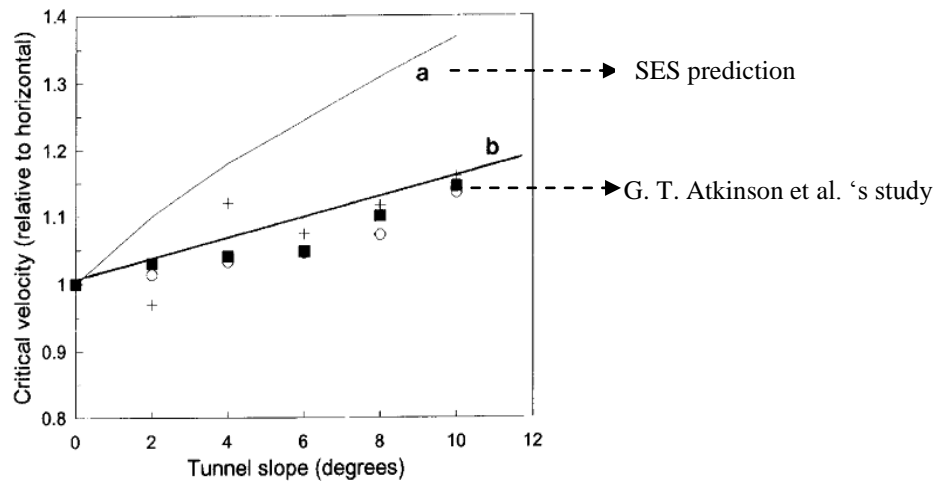


Figure 1.12 Comparison of Tunnel Slope Correction Factor on Critical Velocity Calculation [32]

Y. Oka and G.T. Atkinson (1995) [33] studied backlayering phenomena prevention in case of the longitudinal ventilation and found a formulae for critical velocity. The Froude number scaling technique was used. It was found that the critical velocity varied as the cube root of heat release rate for low rates of heat release rate, there was no dependence of the critical velocity on heat release rate at higher rate. They also studied the effect of solid blockage on heat release rate. Based on this study, the critical velocities were reduced when the fire occupied large portion of the width of the tunnel and was increased by raising the fire towards the ceiling. It was observed that solid blockages near the fire caused decrease in the critical velocity.

In summary, the experimental studies have been mentioned in this study. However, numerical investigations of ventilation systems have been done. In 2009, E. Musluoğlu [34] investigated the fire development and flame spread in the railway carriages by performing a set of simulations using Fire Dynamics Simulator. This study predicts the values of the peak heat release rates for simulated incident cases.

Prior to this investigation, theoretical research was carried out in Middle East Technical University for numerically simulating fire in station and tunnels of underground transportation systems station [35],[36].

1.2 Aim of Thesis

Since fire tests in full size tunnels are very expensive, limited numbers of full-size tunnel fire studies have been performed in the literature. However, they do not give detailed information about the behavior of fire and smoke. In order to understand the phenomena with a lower cost, scaled tunnel models have been used and small scale experiments have been carried. The studies for investigating the tunnel fire phenomena and their methods of modeling techniques are mentioned in tunnel fire studies section. In the literature, there is no information about tunnel vehicle (train, cars, truck etc.) blockage effect and its configuration on heat release rate and temperature distribution inside tunnel with different ventilation velocities. As a result, in order to research this subject, the scaled model tunnel configuration is constructed in Fluid Mechanics Laboratory of Mechanical Engineering Department, METU. Based on the Froude number scaling, materials with different geometrical configurations are burned in a controlled environment inside the model tunnel. The heat release rate measurement, sampling of gases after combustion, temperature distribution along the tunnels and the ceiling with different longitudinal ventilation velocities are measured in order to investigate the effect of different cross-sectional areas of the burning substances.

CHAPTER 2

SCALE MODELING IN TUNNEL FIRE

2.1 Introduction

The full scale model tests are expensive. Scientists learn how to scale down the physical phenomena with conservation of dimensionless parameters. By this way, the deeper understanding of the problem is possible and investigations can be made at the lower costs. Three methods exist for derivation of dimensionless π terms to scale the physical phenomena. The first one is Buckingham Pi theorem which shows the number of independent dimensionless parameters needed to correlate the variables in a given process. In the second method, the complete partial differential governing equations for a system are deriving and the equations are then made dimensionless. The third technique is deriving a simplest form of equations for representing the physics of the problem. Lastly, the simplified governing partial differential equations are made dimensionless. From the dimensionless partial differential equations, necessary π group terms are selected for scaling the compartment fires.

In this part of the dissertation, the scale modeling in the fire study is mentioned. The derivation of the dimensionless parameters in the fire study is presented based on summarizing studies in reference [11] and [37].

2.1 Fundamental Equations in Fire

The conservation of mass equation[11] is

$$\dot{m} = \rho u A \quad 2.1$$

An approximate form of the vertical momentum equation with a buoyancy term and the pressure is written for a control volume .The equation of momentum is [11]

$$\rho V \frac{du}{dt} + \dot{m}u \approx \rho_{\infty} - \rho gV + pA + \Gamma S \quad 2.2$$

where S = control volume surface area, ρ =density , ρ_{∞} = ambient density, V = volume, p = pressure, u =velocity, Γ =shear stress, g = gravitational acceleration. The equation-2.2 gives the relationship between the unsteady momentum and momentum advection to the buoyancy, pressure and shear forces respectively.

The simple form of the energy equation [11] is

$$\rho C_p V \frac{dT}{dt} + \dot{m}C_p T - T_{\infty} \approx \dot{Q} - \dot{q} \quad 2.3$$

The mass flows (\dot{m}) defines the sum of fuel flow (F), air flow (\dot{m}_{O_2} & \dot{m}_{Fan}). The chemical energy or heat release rate of fire is represented by \dot{Q} and all of the heat loss rates by \dot{q} .

A conservation equation of species in case of chemical reaction [11] can be represented by :

$$\rho V \frac{dY_i}{dt} + \dot{m}Y_i = \frac{y_i}{\Delta h_c} \dot{Q} \quad 2.4$$

where, Y_i is mass fraction of species, V is the volume, Δh_c is heat of combustion, y_i is mass of species i per mass of reacted fuel.

2.2 Dimensionless Groups of Fundamental Equation

2.2.1 Dimensionless Groups of Momentum Equation

In natural convection, the proportionality between momentum flux and buoyancy terms is represented in Equation 2.5 [11]. When this relation is written in terms of primary dimension term, Equation 2.6 [11] is obtained. After rearrangement of terms in Equation 2.6; Equation 2.7 [11] is derived.

$$\dot{m}u \sim \rho_{\infty} - \rho \ gV \quad 2.5$$

$$\rho u^2 l^2 \sim \rho_{\infty} - \rho \ gl^3 \quad 2.6$$

$$\frac{u}{gl^{1/2}} \sim \left(\frac{\rho_{\infty} - \rho}{\rho} \right)^{1/2} \quad 2.7$$

It is applicable to use the air as an ideal gas under constant pressure. As a result, the variation of density in the flow field can be represented as

$$\left(\frac{\rho_{\infty} - \rho}{\rho} \right) = \frac{T - T_{\infty}}{T_{\infty}} \quad 2.8$$

The equation 2.7 [11] becomes normalized factor for velocity

$$\tilde{u} = \left(\frac{T - T_{\infty}}{T_{\infty}} gl \right)^{1/2} \Rightarrow \tilde{u} \cong gl^{1/2} \quad 2.9$$

According to reference [11], “This value is very proper for natural convection and represents an ideal maximum velocity due to buoyancy”. The proportionality of unsteady momentum term and the buoyancy term gives time scale factor.

$$\rho V \frac{du}{dt} \sim \rho_{\infty} - \rho \ gV \quad 2.10$$

The above equation [11] is made dimensionless using the characteristic velocity (\tilde{u}) defined in equation 2.9

$$\rho \frac{gl^{1/2}}{\tilde{t}} \frac{d\hat{u}}{d\hat{t}} \sim \rho_{\infty} - \rho \ g \quad 2.11$$

After reordering the dimensionless equation, approximate form of the characteristic time [11] is

$$\tilde{t} \sim \frac{\tilde{u}}{g} = \left(\frac{l}{g} \right)^{1/2} \quad 2.12$$

The pressure and stress can be normalized as

$$\tilde{\Gamma} \sim \tilde{p} \sim \rho_{\infty} g l \quad 2.13$$

Using Newton's viscosity law,

$$\tilde{\Gamma} \sim \mu \frac{\partial u}{\partial x} \sim \mu \frac{\tilde{u}}{l} \quad 2.14$$

And equating momentum flux and stress terms gives

$$\rho_{\infty} \tilde{u}^2 l^2 \sim \mu \frac{\tilde{u}}{l} l^2 \quad 2.15$$

The equation can be defined as

$$\text{Re} = \pi_1 = \frac{\rho_{\infty} \tilde{u} l}{\mu} \sim \frac{\text{momentum}}{\text{shear force}} \quad 2.16$$

Alternatively, the above equation can be written in terms of the dimensionless velocity,

$$\hat{u} = \frac{u}{\tilde{u}} \sim \left[\frac{\mu}{\rho_{\infty} [T - T_{\infty} / T_{\infty}]^{1/2} \sqrt{g l}} \right]^{1/2} = \left(\frac{1}{Gr} \right)^{1/4} \quad 2.17$$

where Gr represents the Grashof number.

2.2.2 Dimensionless Groups for Energy Equation

The dimensionless energy equation [11] can be derived when temperature is normalized using ambient temperature, $\hat{T} = T / T_{\infty}$

$$\frac{d\hat{T}}{d\hat{t}} + \hat{T} - 1 \approx \frac{\dot{Q}}{\rho_{\infty} C_p T_{\infty} g^{1/2} l^{5/2}} - \frac{\dot{q}}{\rho_{\infty} C_p T_{\infty} g^{1/2} l^{5/2}} \quad 2.18$$

The second π group is derived from the dimensionless energy equation:

$$\pi_2 = Q^* = \frac{\dot{Q}}{\rho_{\infty} C_p T_{\infty} g^{1/2} l^{5/2}} \sim \frac{\text{Fire Power}}{\text{Enthalpy Flow}} \quad 2.19$$

Heat is transferred from compartment walls and to the ambient via the vent opening in the enclosure. Heat loss from compartment walls and from the vent of the compartment is defined as \dot{q}_w and \dot{q}_o , respectively. Total heat loss is summation of both terms.

$$\dot{q} = \dot{q}_o + \dot{q}_w \quad 2.20$$

Heat losses through the vent are combination of radiation from smoke layer and compartment walls.

$$\dot{q}_o = A_o \sigma \varepsilon T^4 - T_\infty^4 + 1 - \varepsilon T_w^4 - T_\infty^4 \quad 2.21$$

where ε is the gas emissivity of the smoke layer and A_o the area of the vent and the walls have been assumed as a blackbody. Convection losses from the vent are negligible. The gas emissivity may be expressed as

$$\varepsilon \sim 1 - e^{-\kappa L_e} \quad 2.22$$

with κ being the absorption coefficient, L_e is the mean beam length of the gas. Heat transfer both by convection and radiation to the compartment walls can be expressed as

$$\dot{q}_w = \dot{q}_k = \dot{q}_r + \dot{q}_c \quad 2.23$$

The radiation exchange for the blackbody walls can be expressed as

$$\dot{q}_r = \sigma \varepsilon T^4 - T_w^4 \quad 2.24$$

and convection as

$$\dot{q}_c = h_c S T - T_w \quad 2.24$$

where S is the wall surface area. The conduction loss is

$$\dot{q}_k = \frac{k_w S T - T_w}{\delta} \quad 2.25$$

where δ represents the physical wall thickness. For a thermally thick wall $\delta \sim \sqrt{k_w / \rho_w c_w t}$ and $\delta = \delta_w$ for a thermally thin one.

The dimensionless loss term of the energy equation gives

$$\hat{q} = \frac{\dot{q}_o + \dot{q}_w}{\rho_\infty C_p T_\infty g^{1/2} l^{5/2}} = \hat{q}_o + \hat{q}_w \quad 2.27$$

The dimensionless wall loss term is equivalent to the conduction losses through the wall. Normalizing the wall temperature with the ambient temperature and wall thickness with thermal penetration depth gives

$$\hat{q}_{w_k} = \left(\frac{Ak_w T_\infty \hat{T}_w - 1}{\delta_t \delta_w / \delta_t} \right) \frac{1}{\rho_\infty C_p T_\infty g^{1/2} l^{5/2}} = \frac{\pi_3 (\hat{T}_w - 1)}{\pi_4} \quad 2.28$$

First term gives a ratio of wall conduction to enthalpy flow. That is

$$\pi_3 = \left(\frac{l^2 k_w T_\infty \hat{T}_w - 1}{\delta_t} \right) \frac{1}{\rho_\infty C_p T_\infty g^{1/2} l^{5/2}} = \frac{k \rho C_w^{1/2}}{\rho_\infty C_p g^{1/4} l^{3/4}} \quad 2.29$$

The second term is

$$\pi_4 = \left(\frac{\delta_w}{\delta_t} \right) = \left(\frac{\rho C}{k} \right)_w^{1/2} \left(\frac{g}{l} \right)^{1/4} \delta_w \quad 2.30$$

The dimensionless wall conduction term can be expressed as the sum of the dimensionless convection and radiation heat transfer to the walls. The dimensionless convection heat transfer term is

$$\hat{q}_{w_c} = \frac{h_c \hat{T} - \hat{T}_w}{\rho_\infty C_p T_\infty g^{1/2} l^{1/2}} \quad 2.31$$

π term for convection is represented by the formula

$$\pi_5 = \frac{h_c}{\rho_\infty C_p g l^{1/2}} \quad 2.32$$

The dimensionless radiation flux and the π term for radiations are

$$\hat{q}_o = \frac{\sigma \varepsilon T_\infty^3 \hat{T}^4 - \hat{T}_w^4}{\rho_\infty C_p g^{1/2} l^{1/2}} \quad 2.33$$

$$\pi_6 = \frac{\sigma \varepsilon T_\infty^3}{\rho_\infty C_p g^{1/2} l^{1/2}} \quad 2.34$$

The emissivity of the smoke layer provides the π_7 term which scale emmissivity by preserving the absorbtivity and beam length.

$$\pi_7 = \kappa L_e \sim \frac{\text{radiation emitted}}{\text{blackbody radiation}} \quad 2.35$$

2.2.3 Dimensionless Groups from Species Conservation Equation

The dimensionless species transport equation can be derived by same procedure applied to momentum and energy equation.

$$\frac{\rho_{\infty} l^3}{l/g^{1/2}} \frac{dY_i}{d\hat{t}} + \rho_{\infty} g l^{1/2} l^2 Y_i = \frac{y_i \tilde{Q}}{\Delta h_c} \rho_{\infty} C_p T_{\infty} g^{1/2} l^{5/2} \quad 2.36$$

$$\frac{\Delta h_c}{y_i C_p T_{\infty}} \frac{dY_i}{d\tau} + \frac{\Delta h_c Y_i}{y_i C_p T_{\infty}} = \tilde{Q} \quad 2.37$$

The π term for species transport is

$$\pi_8 = \frac{\Delta h_c}{y_i C_p T_{\infty}} \quad 2.38$$

2.3 Summary of Length Scale Result

Dimensionless variables and scaling parameters are listed at Table 2.1

Table 2.1 Dimensionless variables and scaling in fire [5]

Variable/Pi group	Dimensionless	Scaling/comment
Velocity, u	$\hat{u} = \frac{u}{\sqrt{gl}}$	$u \sim l^{1/2}$
Temperature, T	$\hat{T} = \frac{T}{T_\infty}$	$T \sim l^0$
Pressure, p	$\hat{p} = \frac{p}{\rho_\infty gl}$	$p \sim l$
Concentration, Y_i	$\frac{Y_i}{Y_{i,\infty}}$	$Y_i \sim l^0$
Coordinates x,y,z	x_i/l	$x_i \sim l$
Time, t	$\hat{t} = \frac{t}{\sqrt{l/g}}$	$t \sim l^{1/2}$
Pi Groups		
$\pi_1 \left(\frac{\text{momentum}}{\text{shear force}} \right), \text{Re}$	$\text{Re} = \frac{\rho_\infty \sqrt{gl}^{3/2}}{\mu}$	Usually ignored
$\pi_2 \left(\frac{\text{fire power}}{\text{enthalpy rate}} \right), \tilde{Q}$	$\frac{\dot{Q}}{\rho_\infty C_p T_\infty g^{1/2} l^{5/2}}$	Significant for combustion $\dot{Q} \sim l^{5/2}$
$\pi_3 \left(\frac{\text{conduction}}{\text{enthalpy}} \right)$	$\frac{k \rho C_w^{1/2}}{\rho_\infty C_p g^{1/4} l^{3/4}}$	Conduction important $k \rho C_w \sim l^{3/4}$
$\pi_4 \left(\frac{\text{thickness}}{\text{thermal length}} \right)$	$\left(\frac{\rho C}{k} \right)_w^{1/2} \left(\frac{g}{l} \right)^{1/4} \delta_w$	Thickness of the boundary $\delta_w / \alpha_w^{1/2} \sim l^{1/4}$

Table 2.1 Continued [5]

Variable/Pi group	Dimensionless	Scaling/comment
$\pi_5 = \left(\frac{\text{convection}}{\text{enthalpy}} \right)$	$\frac{h_c}{\rho_\infty C_p g l^{1/2}}$	Convection is important $h_c \sim l^{1/2}$
$\pi_6 \left(\frac{\text{radiation}}{\text{enthalpy}} \right)$	$\frac{\sigma T_\infty^3}{\rho_\infty C_p g^{1/2} l^{1/2}}$	Inconsistent with other $T_\infty \sim l^{1/6}$
$\pi_7 = \kappa L_e \sim \frac{\text{radiation emitted}}{\text{blackbody radiation}}$		Thermally thick case $\varepsilon \sim l^{1/2}$
$\pi_8 \left(\frac{\text{ith enthalpy}}{\text{chemical energy}} \right)$	$\frac{\Delta h_c}{y_i C_p T_\infty}$	$y_i \sim l^0$

The scaling relation for convective heat transfer coefficient can be different depending on the correlation used in the turbulent flow. The scaling of temperature, velocity and species concentration is performed when the dimensionless terms are conserved in the model. In other words, the variables in enclosure fire are function of these dimensionless parameter [37].

$$\left\{ \frac{T}{T_\infty}, \frac{T_w}{T_\infty}, \frac{u}{g l^{1/2}}, y_i \right\} \approx \text{function} \left\{ \frac{x_i}{l}, \frac{t}{\left(\frac{l}{g} \right)^{1/2}}, \pi_{1-8} \right\} \quad 2.39$$

2.4 Scale Modelling Tests in Literature

P. S. Veloo (2006) [37] studied the scale modeling of the transient behavior of heat flux in enclosure fire. A new scaling technique is developed on the hypothesis about buoyancy driven flows in a compartment fire by Quintiere[11]. Scaling parameters for convective and radiative heat transfer within compartment fires are mentioned based on this hypothesis; Experiments performed to test the scaling hypotheses are conducted at different scales. A fuel load is modeled by wood cribs. (Figure 2.4) All

wood cribs are designed in this study to all fall under the category of porosity independent or openly packed burning regimes.

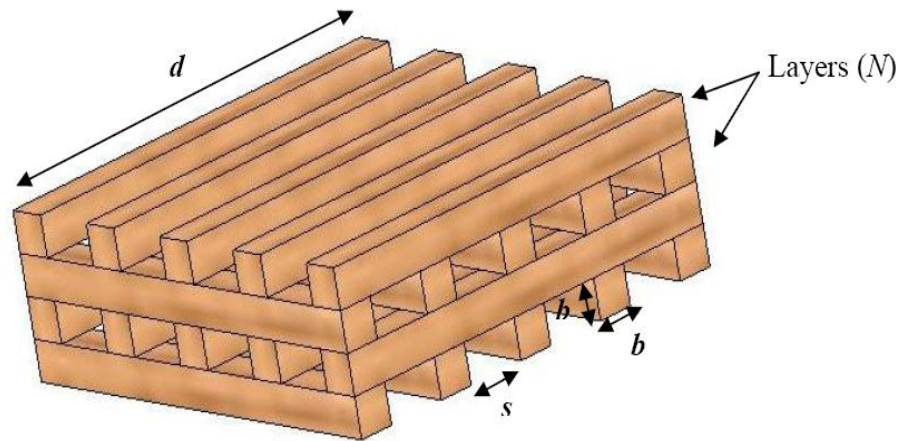


Figure 2.4 Wood Crib Example used as a fire load [37]

The full scale compartment of dimensions 3.76 x 3.76 x 2.54 m corresponding to its width, length and height respectively, has to be scaled geometrically to design three compartments at 1/8, 1/4 and 3/8 scales. These compartments have dimensions which are listed below in Table 2.1.

Table 2.1 Summary of Compartment Dimensions [37]

Compartment scale	Dimension (m) (WxLxH)
1/8	0.47 x 0.47 x 0.32
1/4	0.94 x 0.94 x 0.635
3/8	1.41 x 1.41 x 0.95
1/1	3.76 x 3.76 x 2.54

The repeatability of wood crib fires is demonstrated. This study is performed by comparing the data taken from J. A. Perricone's study [37]. His study is based on the scaling of transient behavior of wood cribs fire in the enclosure. Experimental results indicate that radiation heat flux scales according to the thermally thick emissivity criteria. Convective heat flux is demonstrated to scale with advected enthalpy. The convective heat transfer coefficient is correlated against temperature rise within the compartment for both the before and after extinction cases.

It is not possible to preserve all the π groups derived previously. In order to preserve convection, the convective heat transfer coefficient needs to be scaled. The scaling theory then presents two contradictory methods to scale the convective heat transfer coefficient. To preserve radiation requires knowledge of the gas layer emissivity. Herein lays the 'art' of scaling, examining the dominant physics of a problem and preserving the pertinent π groups.

The conductive resistance is the most dominant thermal resistor. Designing the compartment walls using insulation board and blanket further increases this dominance. For this reason the π_3 and π_4 groups are preserved and the π_5 , π_6 , and π_7 groups discarded, i.e. conduction is preserved in favor of either convection or radiation.

Table 2.2 Summary of π Group Scaling Results [37]

Variable/Pi group	Dimensionless	Variable/Pi group	Dimensionless
T Temperature	$T \sim 1^0$	π_4 Wall Thickness	$\frac{\delta_w}{\alpha_w^{1/2}} \sim 1^{1/4}$
π_1 Reynolds number	Not explicitly preserved	π_5 Convection	$\dot{q}_c'' \sim 1^{1/5}$ $\dot{q}_c'' \sim 1^{1/2}$
π_2 Fire Power	$\dot{Q} \sim 1^{5/2}$	π_6 Radiation	$\dot{q}_r'' \sim 1^0$ $\dot{q}_r'' \sim 1^{1/2}$ $\dot{q}_r'' \sim 1^1$
π_3 Conduction	$k\rho c_w \sim 1^{3/2}$ $\dot{q}_k'' \sim 1^{1/2}$	π_7 Species	$y_i \sim 1^0$

The correlations obtain for the before extinction case [37]:

$$\frac{h_c}{\rho_\infty c_p gl^{1/2}} = \begin{cases} 2.03 \times 10^{-3} & \frac{\Delta T}{T_\infty} < 2 \\ 16 \times 10^{-3} \frac{\Delta T}{T_\infty} & \frac{\Delta T}{T_\infty} \geq 2 \end{cases} \quad 2.40$$

and for the after extinction case the correlation:

$$\frac{h_c}{\rho_\infty c_p gl^{1/2}} = 9.87 \times 10^{-3} \frac{\Delta T}{T_\infty} \quad 2.41$$

The results obtained from this study are shown in Figure 2.5 - 2.13. It is seen that the conservation laws are valid.

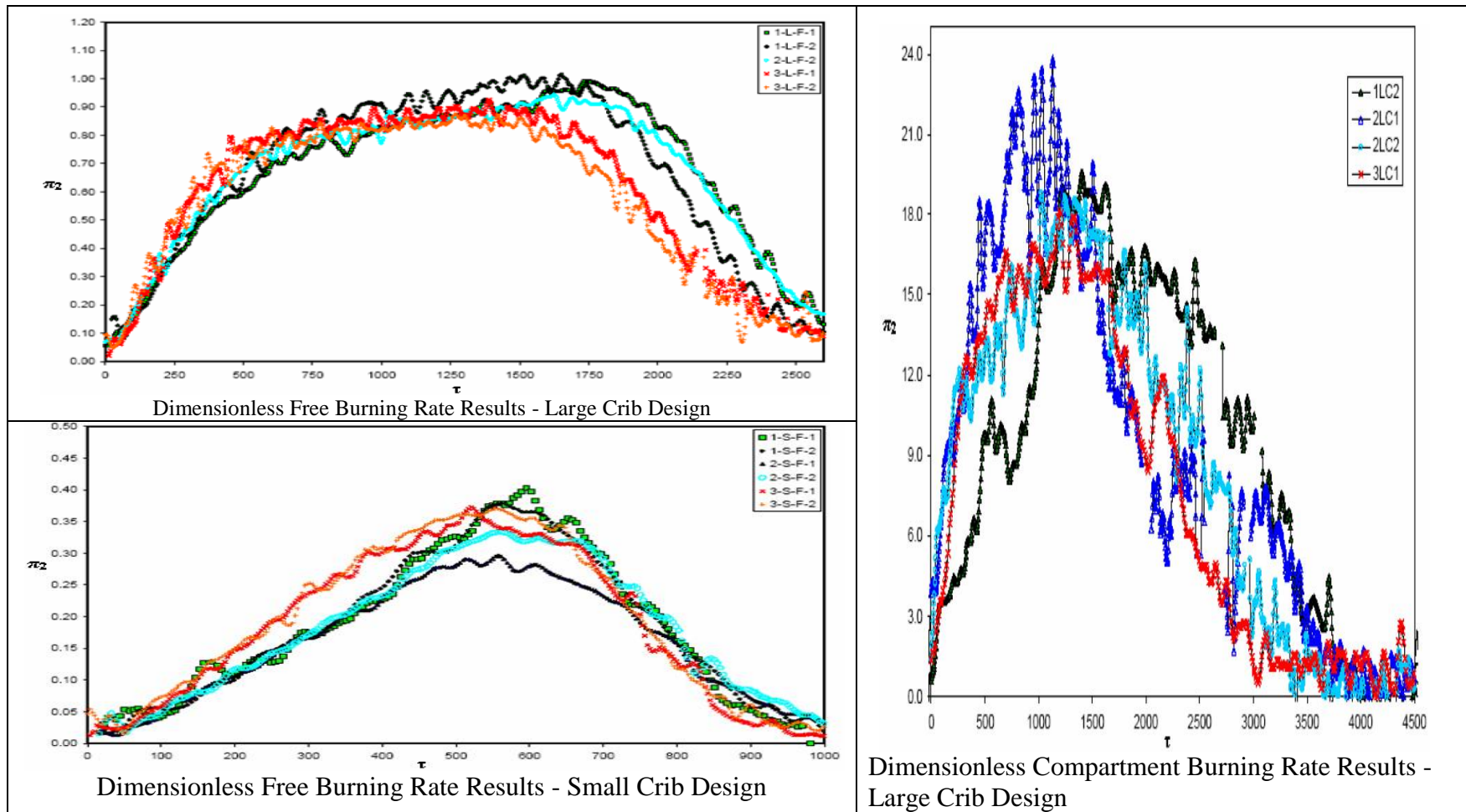


Figure 2.5 The Scaled Burning Rate for Wood Cribs [37]

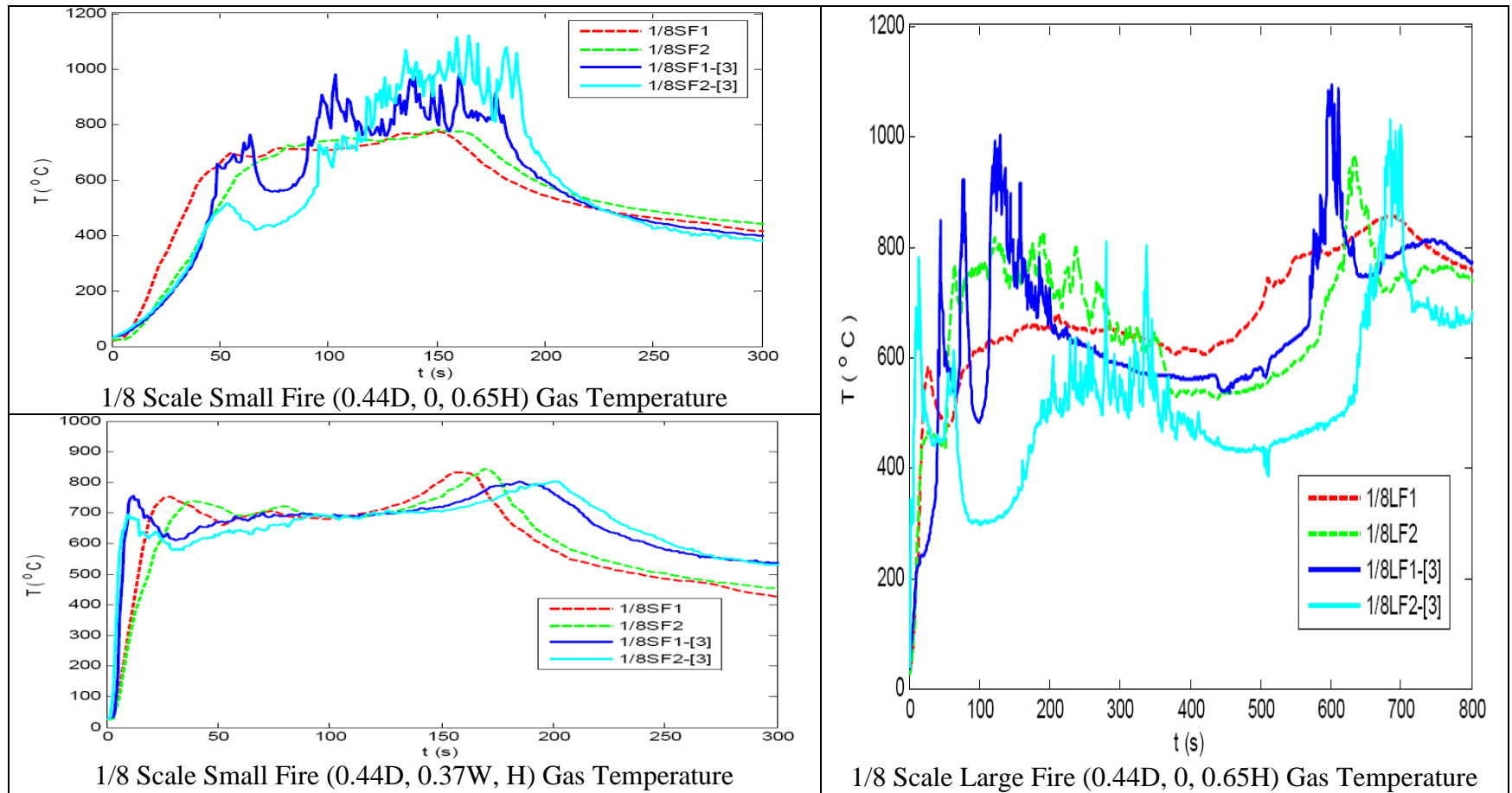


Figure 2.6 Gas Temperature for Wood Cribs 1/8 Scale at Different Locations [37]

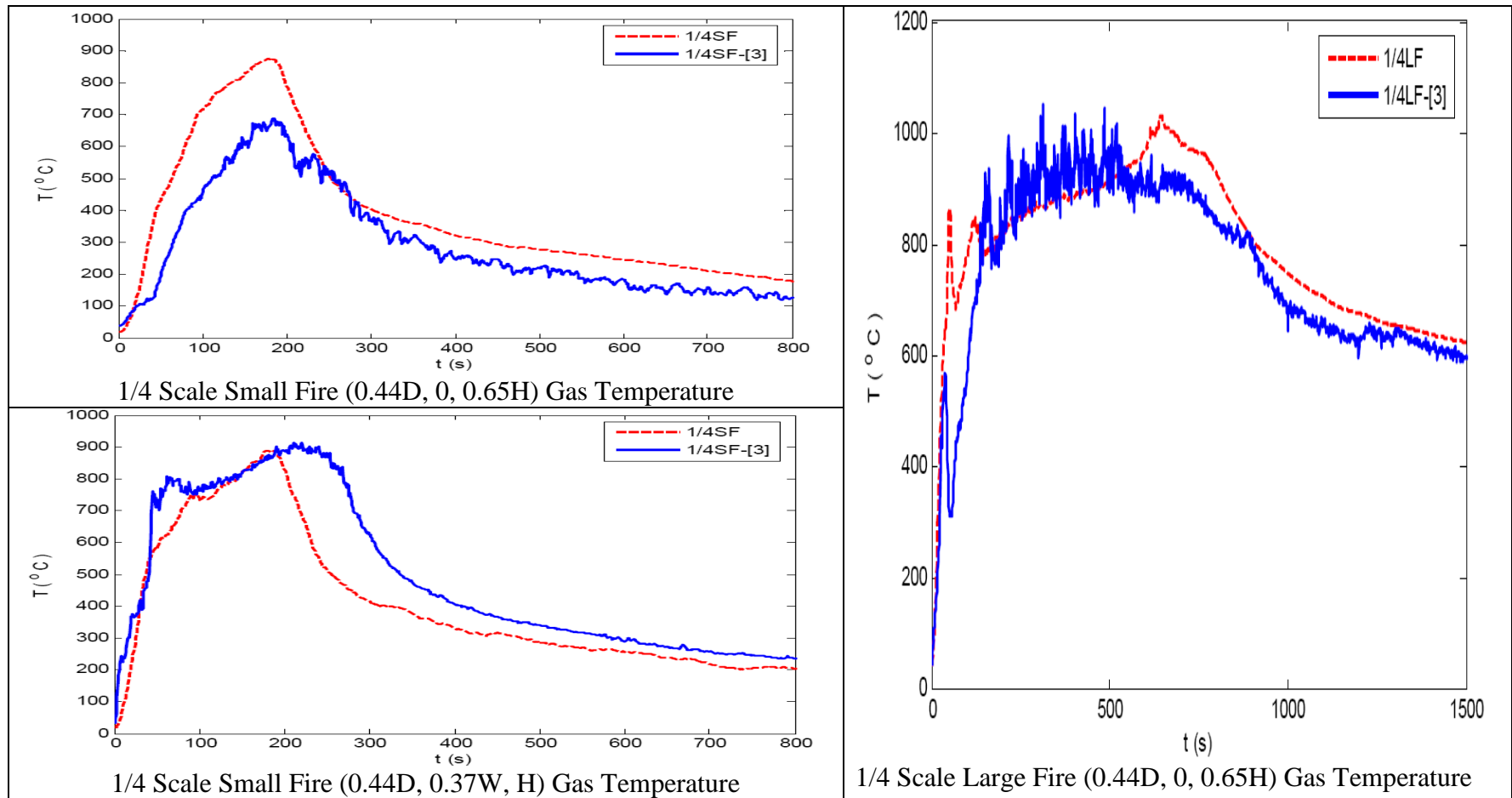


Figure 2.7 Gas Temperature for Wood Cribs 1/4 Scale at Different Locations [37]

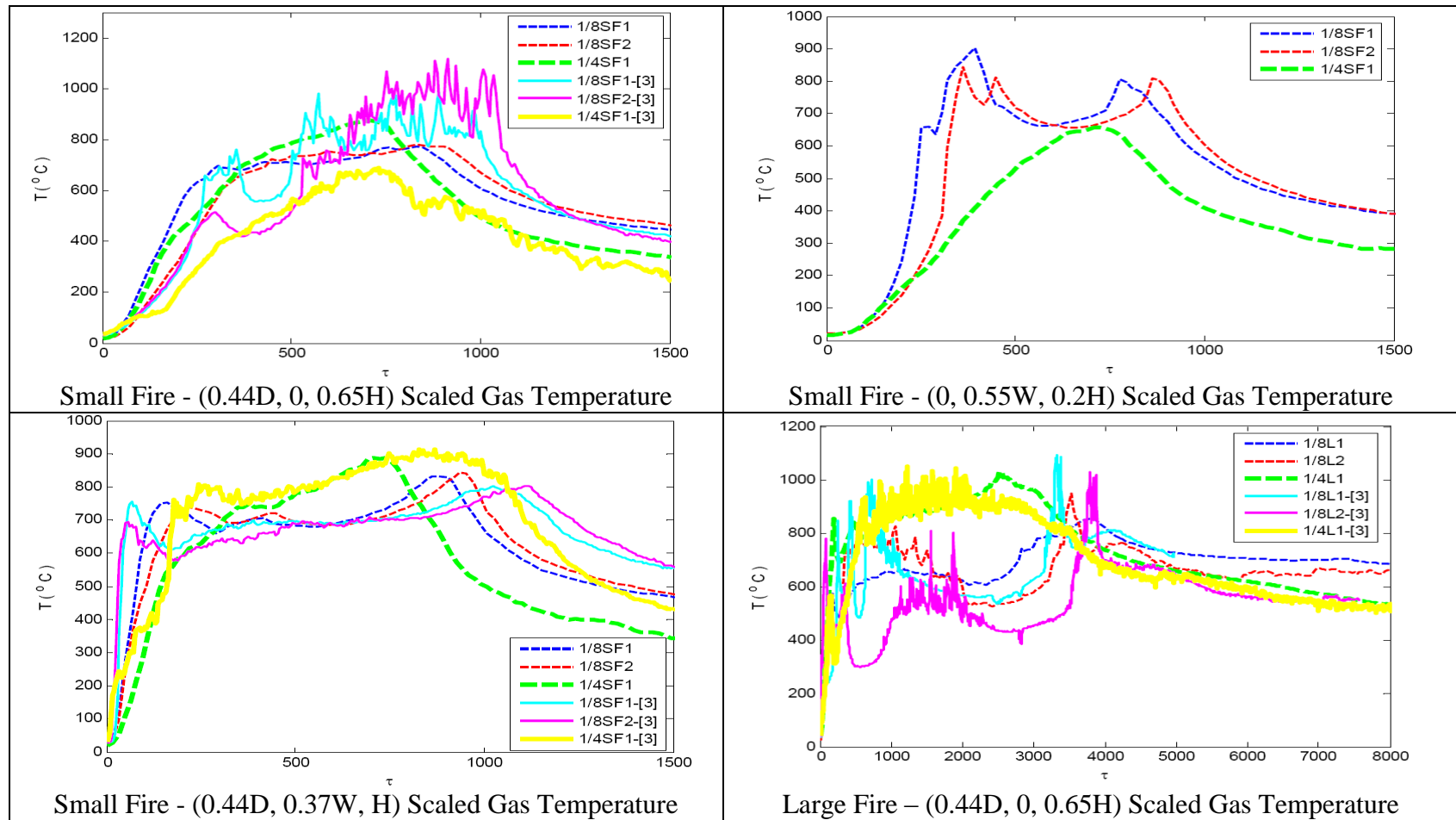


Figure 2.8 Gas Temperature for Wood Cribs for Scaled Fire at Different Locations [37]

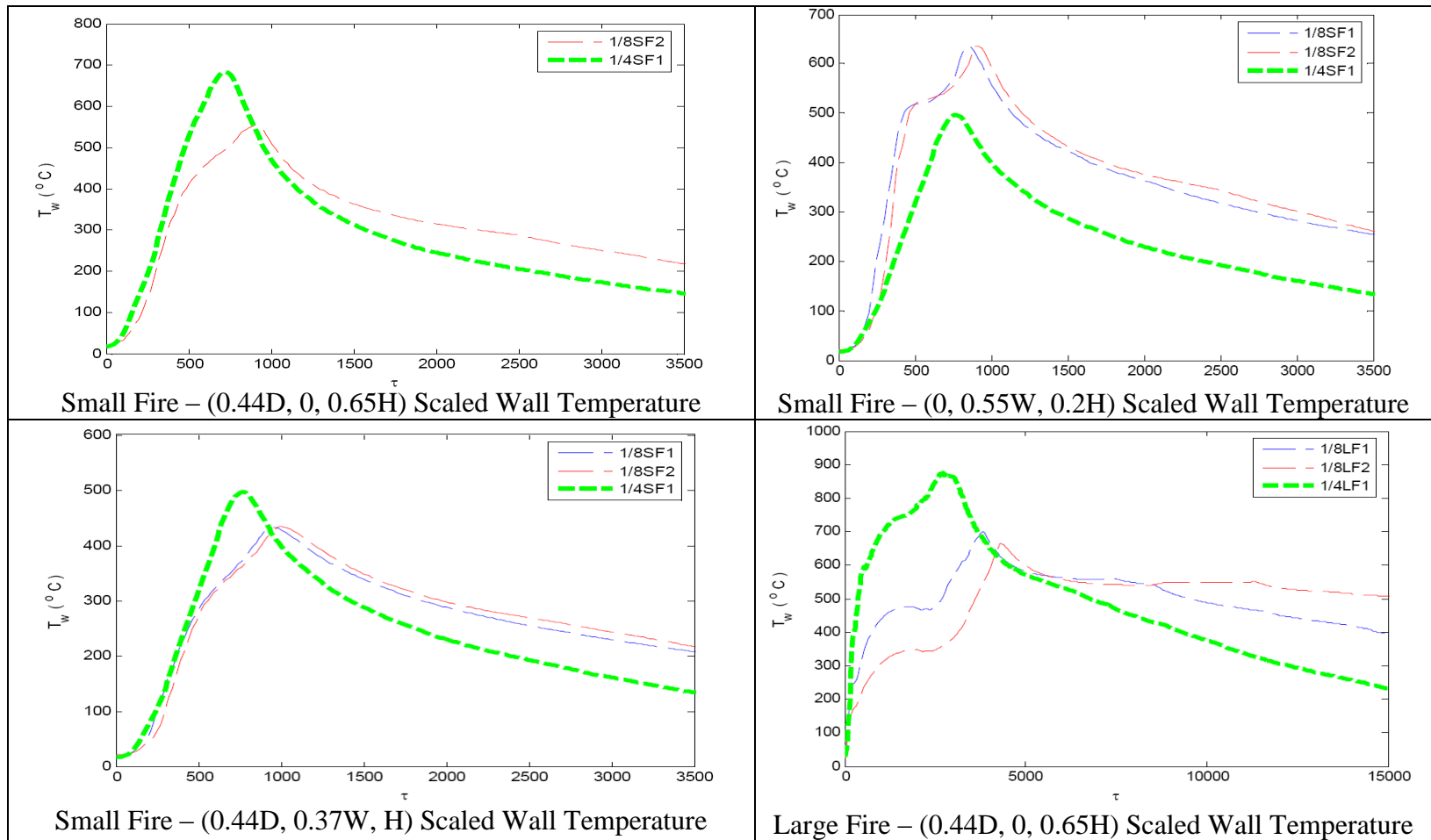


Figure 2.9 The Wall Temperature for Wood Cribs for Scaled Fire at Different Locations [37]

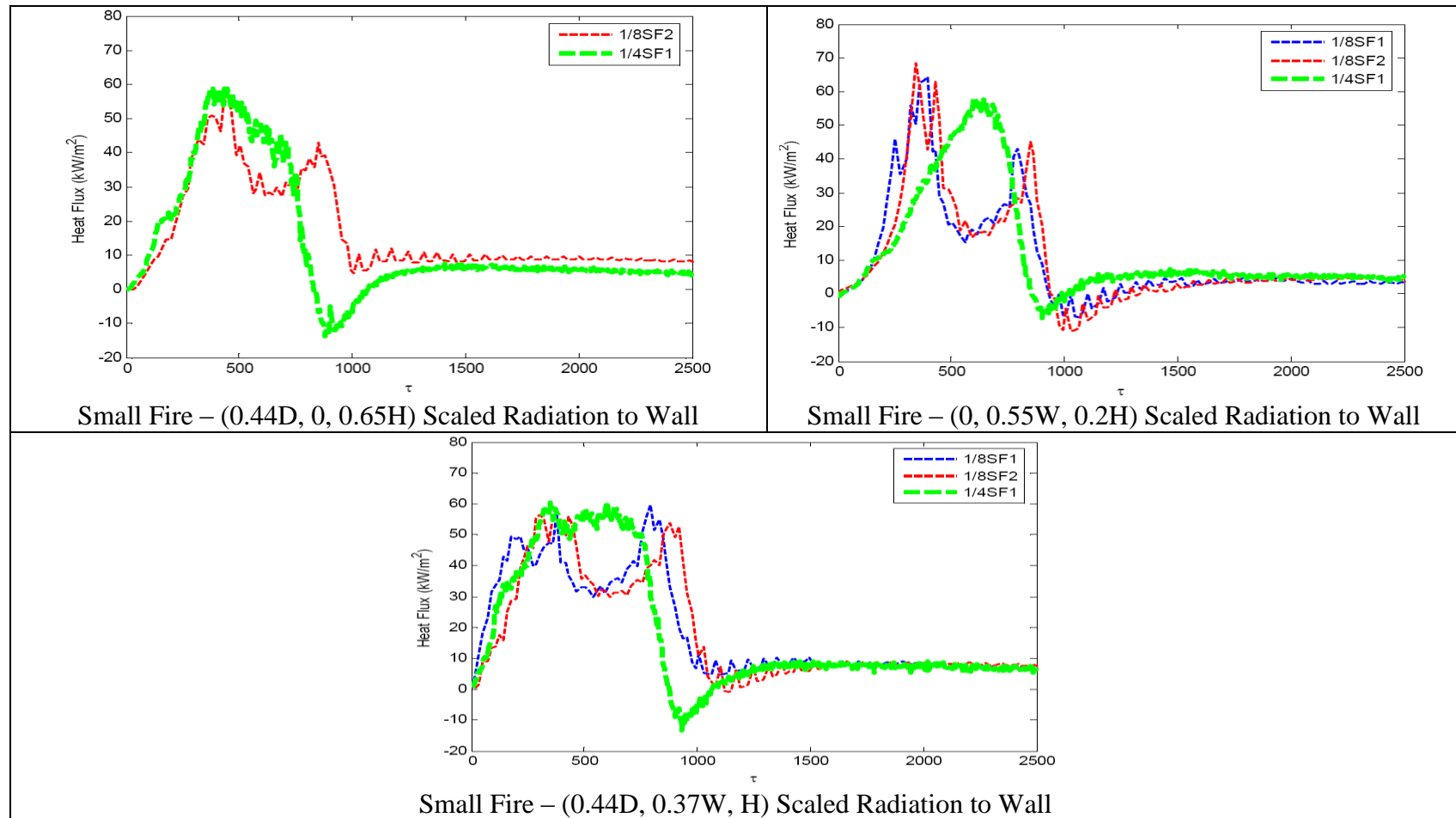


Figure 2.10 Scaled Radiation Heat Flux for Wood Cribs for Scaled Fire at Different Locations [37]

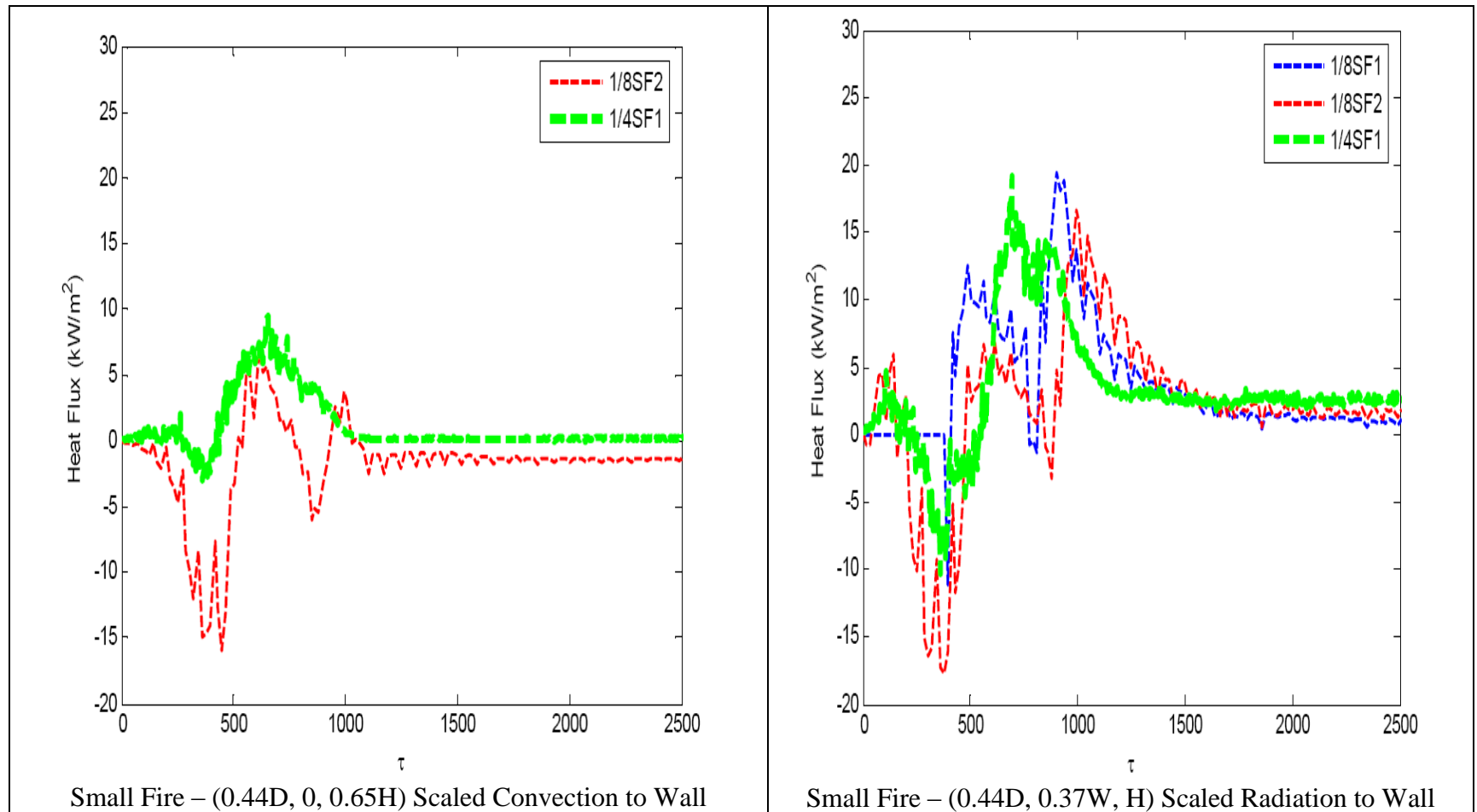


Figure 2.11 Scaled Convection Heat Flux for Wood Cribs for Scaled Fire at Different Locations [37]

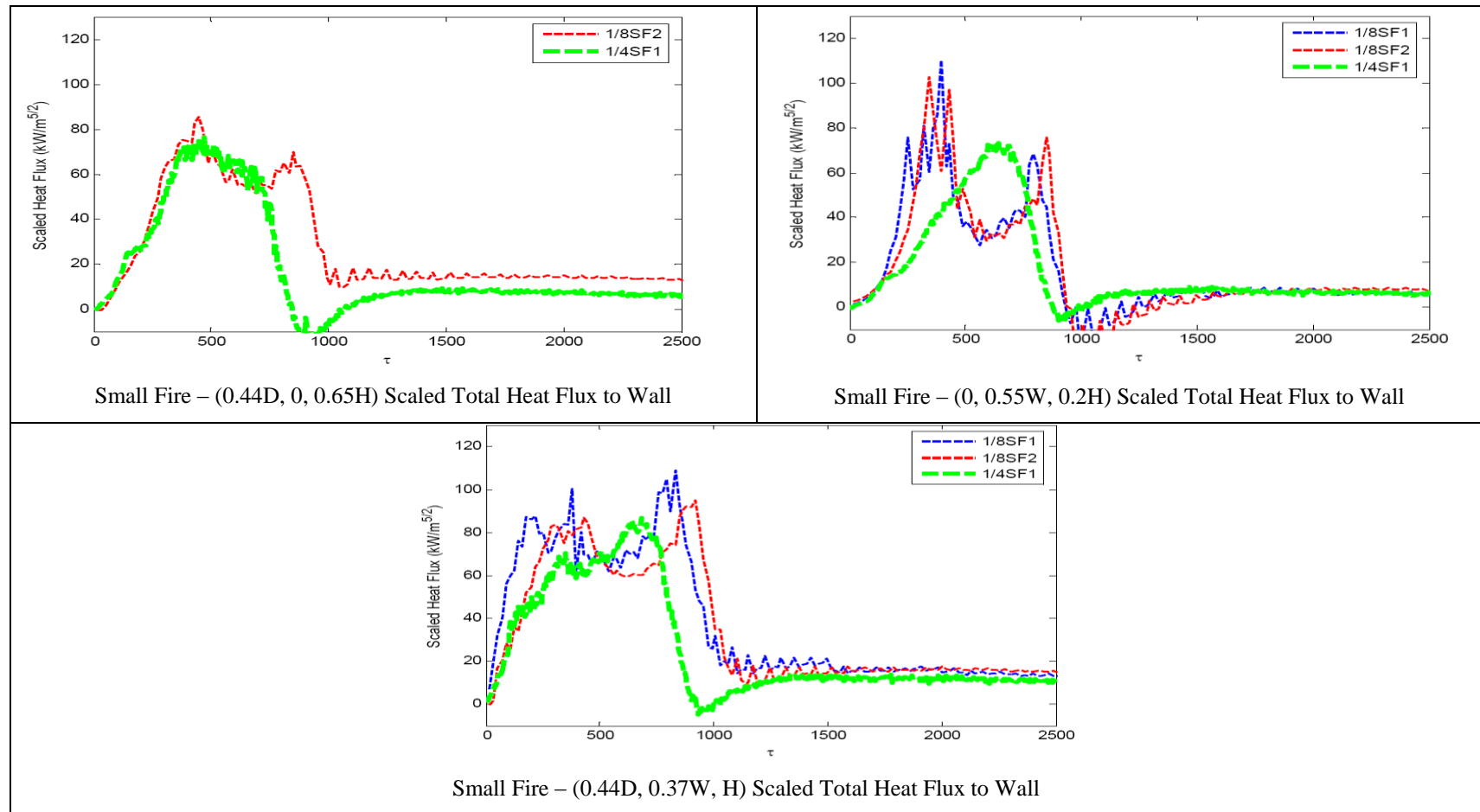


Figure 2.12 The Results of the Scaled Conduction for Each of the Small Fires [37]

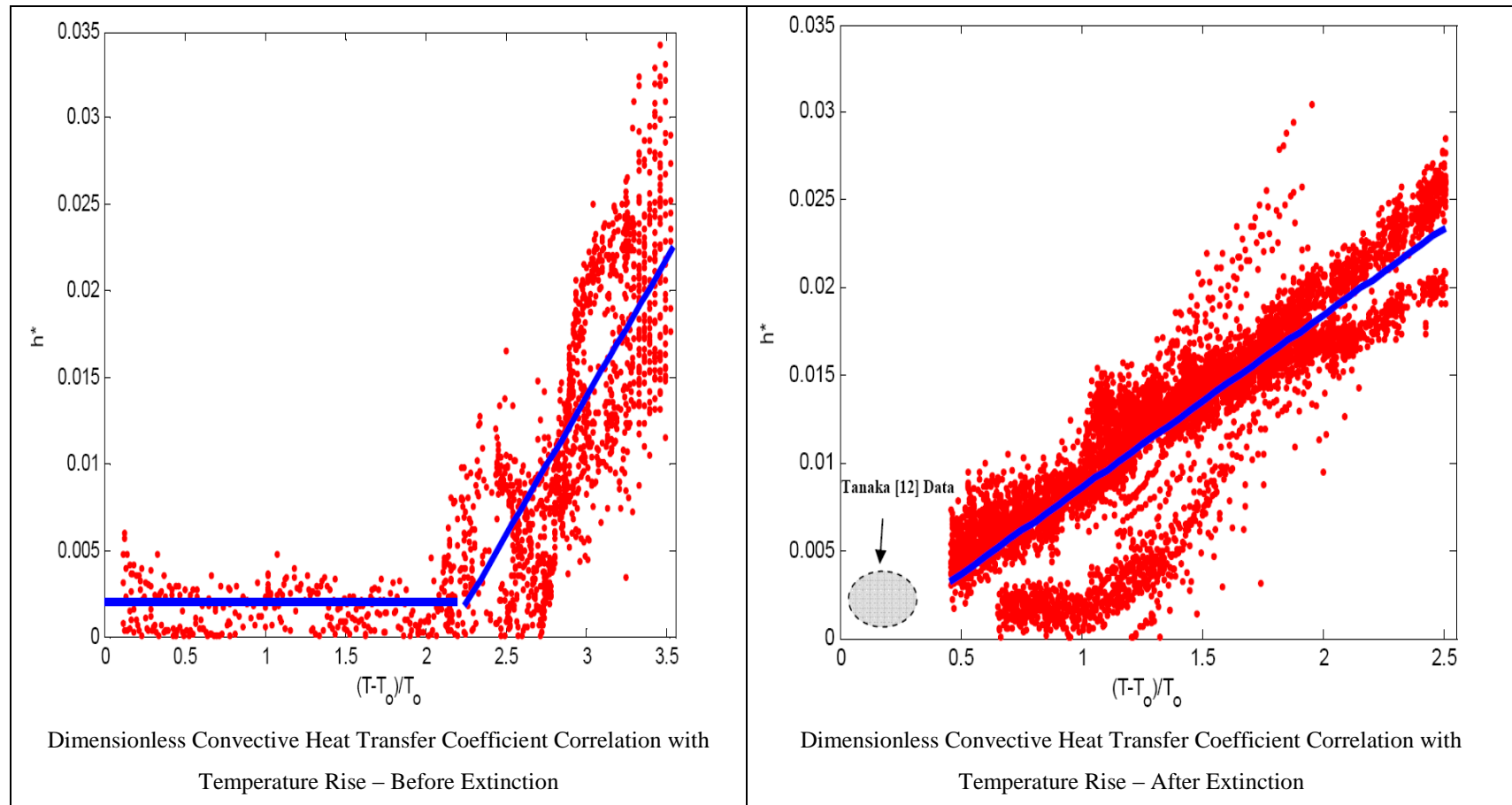


Figure 2.13 Dimensionless Convective Heat Transfer Coefficient Correlation with Temperature Rise [37]

2.5 Wood Cribs as A Burning Item

In this study, wood materials are burned. There are several reasons for this selection.

The reasons are the following:

1. The difficulties of scaling down the model vehicle materials are due to the fact that a large variety of materials are used in the vehicles. To simplify the tests, the variety of materials are limited to a single material, pine wood.
2. In the literature , the known heat release rate is scaled down, but few studies are available with vehicle fire.
3. The geometrical configurations of vehicles modelled are different for different cases. It is difficult to obtain the same configuration with different scale ratios. It is better to simplify the problem by testing the parameter in the design with an easily constructed vehicle configuration. This study investigates the vehicle configuration especially its cross sectional area to tunnel cross sectional ratio (blockage ratio) on heat release rate in case of different tunnel ventilation when it is constructed from a material with the same burning properties.
4. Wood is an easily obtainable material. The wood cribs with different configuration are investigated in the previous studies and the burning regime of the structure of wood cribs is known. When its porosity is higher than 0.5, the burning rate normalized with its configuration gives the constant burning rate.
5. The repeatability and conservation of scaling parameter in case of wood crib fire in enclosure are given in the literature.

6. In full scale tunnel tests, wood cribs are used. The total energy of the vehicles is simulated by an amount of wood of the same energy content in the tunnel.

2.5.1 Description of Wood Crib Configuration

The wood crib configuration has a square base and the sticks can be arranged as shown in Figure 2.14. Number of sticks in a single layer (n) is same for every layer.

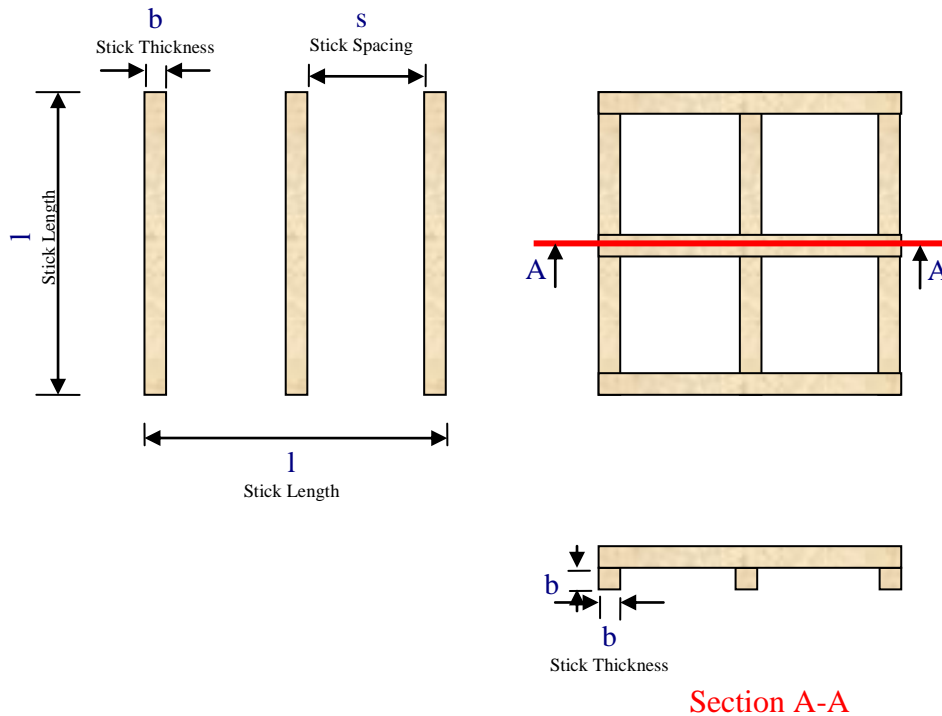


Figure 2.14 Wood Crib Structure [38]

The burning rate of the wood cribs is represented in graphical form (Figure 2.15).

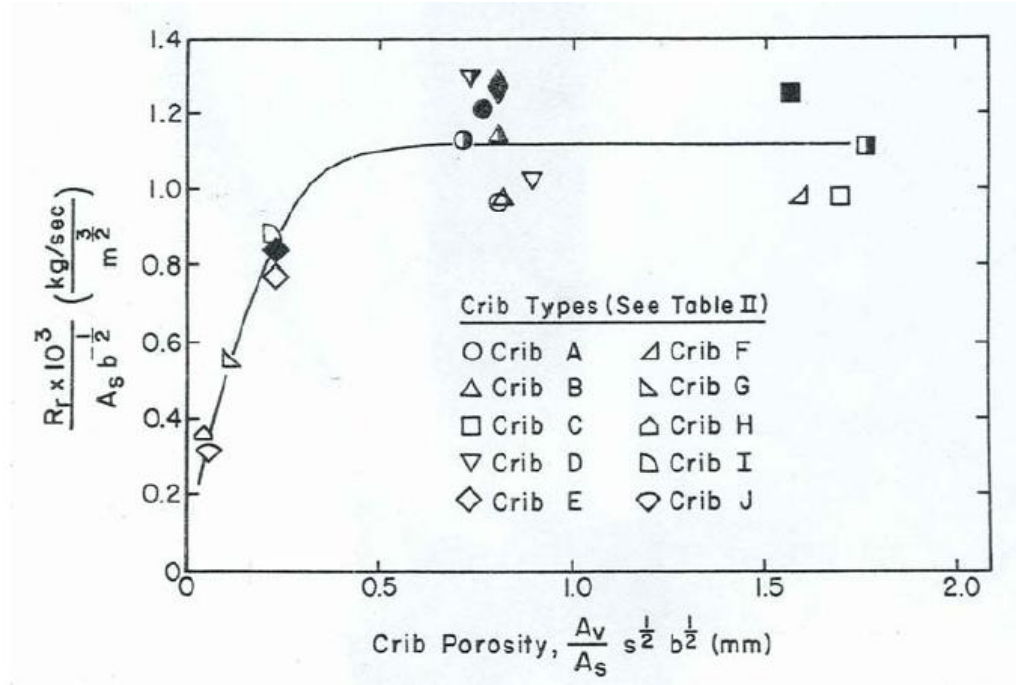


Figure 2.15 Free-Burn Model for Croce's Wood Crib Designs[37]

In Figure 2.15, exposed surface area of crib (A_s), total cross-sectional area of vertical crib shafts (A_v), crib porosity (P) and spacing between sticks (s) are calculated as

$$A_s = 4blNn \left(1 - \frac{b}{2l} \left(n - 1 - \frac{n}{N} \right) \right) \quad 2.40$$

$$A_v = l - nb^2 \quad 2.41$$

$$P = \frac{A_v}{A_s} s^{\frac{1}{2}} b^{\frac{1}{2}} \quad 2.42$$

$$s = l - nb / n - 1 \quad 2.43$$

where N , n , l , b represents number of layers, number of sticks per layer, stick length and stick thickness, respectively.

Figure 2.15 demonstrates the burning region of the wood crib structure in case of enclosure fire without ventilation. The wood crib structure with a porosity greater than 0.5 will not be affected from the ventilation much, but in the region of smaller porosity the ventilation effect is dominant for combustion growing.

CHAPTER 3

EXPERIMENTAL SETUP & INSTRUMENTATION

3.1 Experimental Setup

Experimental setup is constructed to have 1/13 scale down model of a bored tunnel in Istanbul Metro system. The full scale drawing of the tunnel is shown in Figure 3.1. It has a diameter of 520 cm and cross-sectional area of 20.75 m².

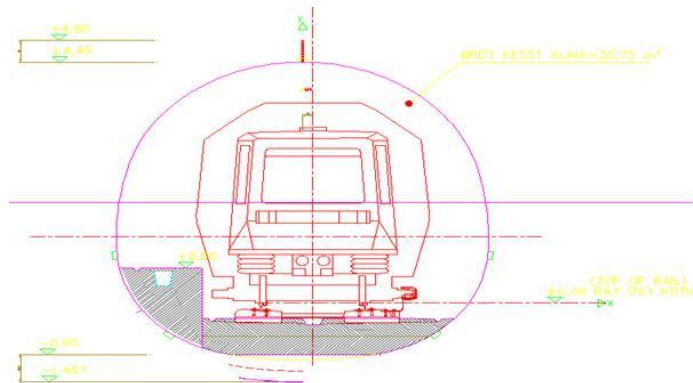


Figure 3.1 Prototype tunnel

The tunnel is scaled down without sidewalk based on the previous study and ease of construction purpose. This scaling ratio is compared with the scaling ratio of the

studies in the literature. As a result, it is confirmed that there is no conflict on the scaling ratio. The scaled tunnel drawing is shown in Figure 3.2.

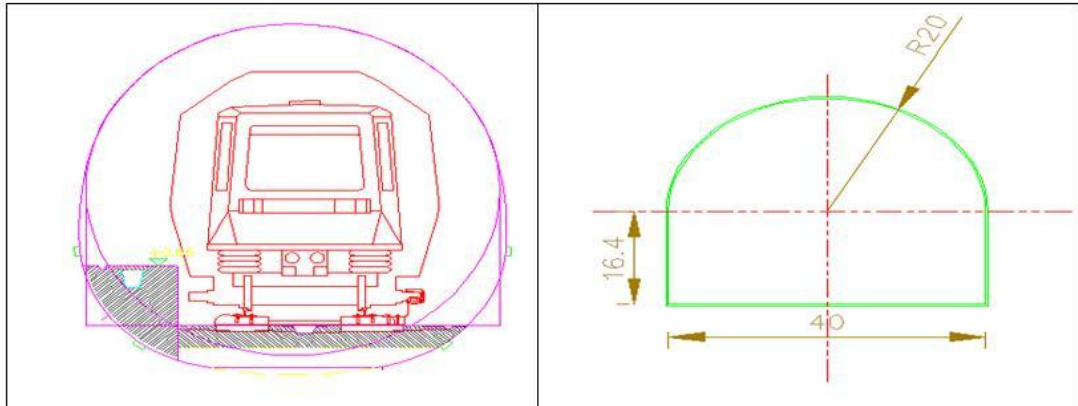


Figure 3.2 Model Tunnel

The four separate model tunnels with a length of 150 cm are manufactured. The model dimensions are represented in Figure 3.3. The four modules are assembled at the open laboratory area of the fluid mechanics laboratory used as “fire studies laboratory”.

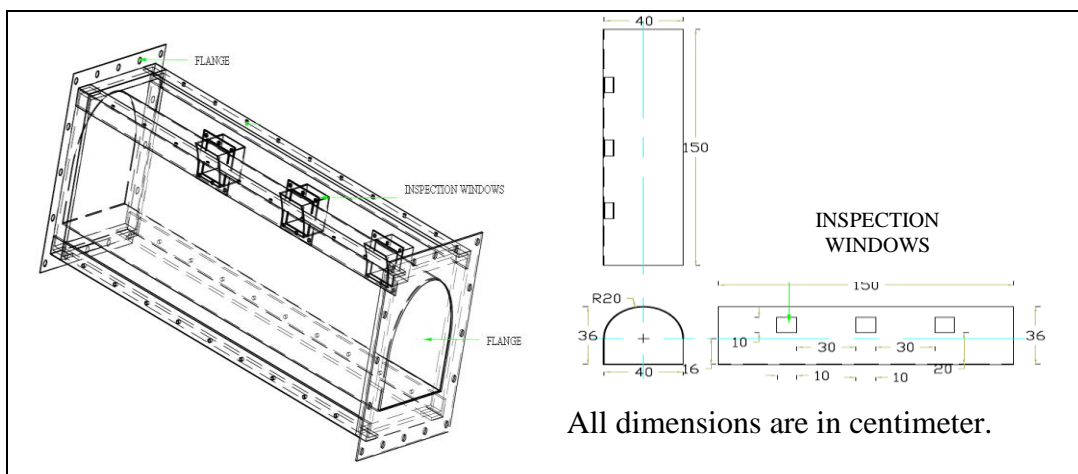


Figure 3.3 Tunnel Model Dimensions

The tunnel is supplied by the axial compressor in the laboratory for the longitudinal ventilation in the tunnel. The flow driven system and its mounting to the model tunnel are shown in Figure 3.4. The multi stage axial compressor takes the air from the inside of the laboratory. The discharge of the compressor is connected to plenum (settling chamber) in the laboratory, and then to the setup outside the laboratory for the tunnel fire simulation. The speed of the compressor is adjusted by using speed controller in front of the motor connection. Therefore, it is possible to control the ventilation velocity easily. The duct (20 cm x 20 cm rectangular cross-section) connected to the exit of the plenum is transferred the air to the model tunnel (Figure 3.4).



Figure 3.4 Flow Driven System and Auxiliary Connections

The exit connection of the plenum is too high with respect to the tunnel setup. Therefore, the auxiliary duct with 38 cm x 40 cm cross-section has been built with two 90° turns. After the auxiliary duct, the flow straightener is mounted (Figure 3.5). As a result, the large eddies due to turbulence and turns are to be eliminated. The uniformity of velocity distribution inside the model tunnel is checked and verified.



Figure 3.5 Flow Straightener

After duct alignment units (90° bends), flow straighteners are used. This is followed by the combustion section (Figure 3.6). The side section of the combustor is disassembled in each test to upload the burning materials to the test section of the setup. There are three inspection windows on the combustor section of the experimental setup and at least one inspection window exists on other modules. The total length of the experimental setup is 650 cm without chimney connection (Figure 3.6). The model tunnel's walls are enclosed with rock wool to isolate the system from extraneous effects.



Figure 3.6 Experimental Setup

3.2 Instrumentation

3.2.1 Combustion Gas Concentration Measurement

The carbon monoxide and oxygen gas concentration are measured by TESTO 350S gas analyzer (Figure 3.7). The technical specifications of the instruments are given in Appendix C.3. The sampling rate of gas concentration measurements is adjusted to 1 second.



Figure 3.7 TESTO 350S gas analyzer

The oxygen consumption is used to calculate the rate of heat release from a limited number of gas concentration measurements. It is possible to calculate the heat release on the basis of oxygen consumption because the quantity of heat released per unit mass of oxygen consumed is approximately constant and independent of fuel at 13.1 MJ/kg. Oxygen consumption calorimetry uses the following equation [39].

$$\dot{Q} = \left[\phi - \left(\frac{E'' - E'}{E'} \right) \left(\frac{1 - \phi}{2} \right) \frac{X_{CO}^A}{X_{O_2}^A} \right] \cdot E' X_{O_2}^o \dot{V}_A \quad 3.1$$

where

E' net heat release of combustion per unit volume of oxygen consumed referred to 25 °C ($E' = 17.2 \text{ MJ/m}^3$) assuming carbon goes to carbon dioxide.

E'' net heat release of combustion per unit volume of oxygen consumed referred to 25 °C ($E'' = 23.1 \text{ MJ/m}^3$) in the burning of carbon monoxide.

X_{CO}^A measured mole fraction of carbon monoxide in the exhaust flow

$X_{O_2}^A$ measured mole fraction of oxygen in the exhaust flow

$X_{O_2}^o$ actual mole fraction of oxygen in the incoming air (Eq. 3)

\dot{V}_e the volumetric gas flow in the duct

ϕ oxygen depletion factor representing representing the fraction of incoming air that is fully depleted from oxygen. It can be calculated from Equation 3.2.

$$\phi = \frac{X_{O_2}^o - X_{O_2}^A \frac{1 - X_{CO_2}^o - X_{H_2O}^o}{1 - X_{CO_2}^A - X_{CO}^A}}{X_{O_2}^o \left[1 - X_{O_2}^A / 1 - X_{CO_2}^A - X_{CO}^A \right]} \quad 3.2$$

X_{xxx}^A measured mole fraction of species in the exhaust flow by analyzer

$X_{xx}^{A^o}$ measured mole fraction of species in the system before the combustion by analyzer

$X_{H_2O}^o$ mole fraction of water vapor in the incoming air. (Eq. 3.5)

$$X_{O_2}^o = X_{O_2}^{A^o} \frac{1 - X_{H_2O}^o}{1 - X_{H_2O}^o} \quad 3.3$$

$$X_{CO_2}^o = X_{CO_2}^{A^o} \frac{1 - X_{H_2O}^o}{1 - X_{H_2O}^o} \quad 3.4$$

$$X_{H_2O}^o = \frac{P_{sat @ T_{ambient} \text{ of } H_2O}}{P_{atmosphere}} \frac{\text{Relative Humidity}(\%)}{100} \quad 3.5$$

3.2.2 Temperature Measurement and Data Acquisition System

Thermocouples are the most commonly used sensors to measure temperature in fire tests. In this study, “the mineral insulated “K” type thermocouples” with 0.5 mm thickness are used (Figure 3.8).



Figure 3.8 K Type Thermocouple

Thermocouple rakes (“trees”) can be attached so that the temperature distribution outside the combustor can be measured correctly. At the exit of the combustor section, 16 thermocouples are mounted (Figure 3.10). The temperature distribution along the model tunnel axis is also important. The temperature at the downstream of the construction can be measured. High temperature at the downstream increases the possibility of failure of the ventilation fan and tunnel material (concrete) spalling when the required ventilation velocity is not available. The thermocouple locations are represented in Figure 3.10. The three thermocouples are attached to the ceiling to measure the smoke temperature at 2.5 cm below the ceiling. The wall thermocouple piles are used to obtain the wall temperature on the ceiling (Figure 3.10).

The thermocouple readings are digitized and stored to the computer by Omega OMB-DAQ-3005 with QMB-PDQ 30 Expansion Module (Figure 3.9). Thirty two thermocouples are connected to this data acquisition system. The technical specification of data acquisition system is listed in Appendix C.2.



Figure 3.9 Omega OMB-DAQ-3005 with QMB-PDQ 30 Expansion Module

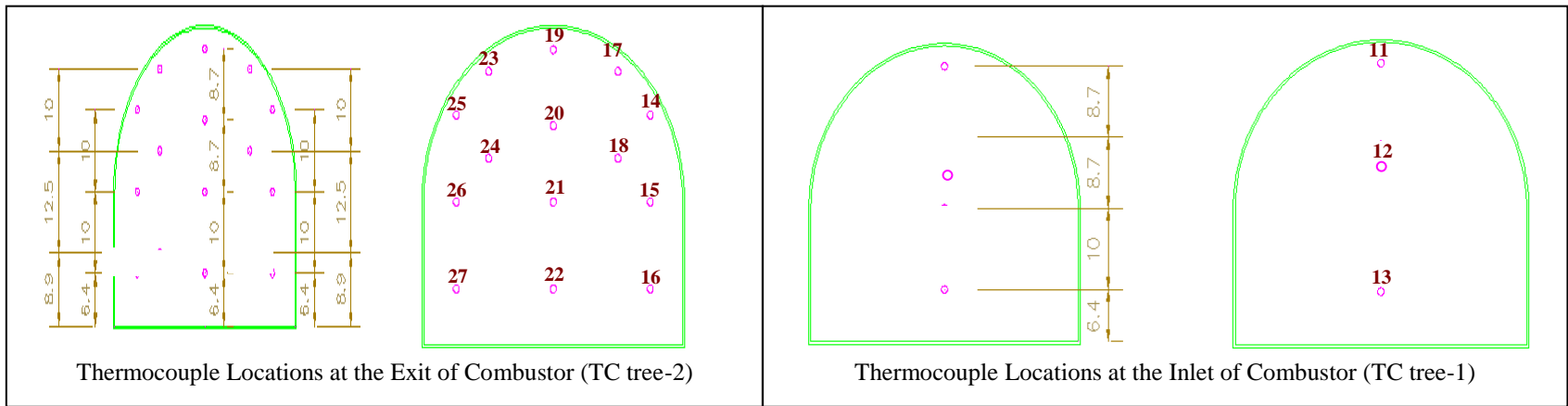
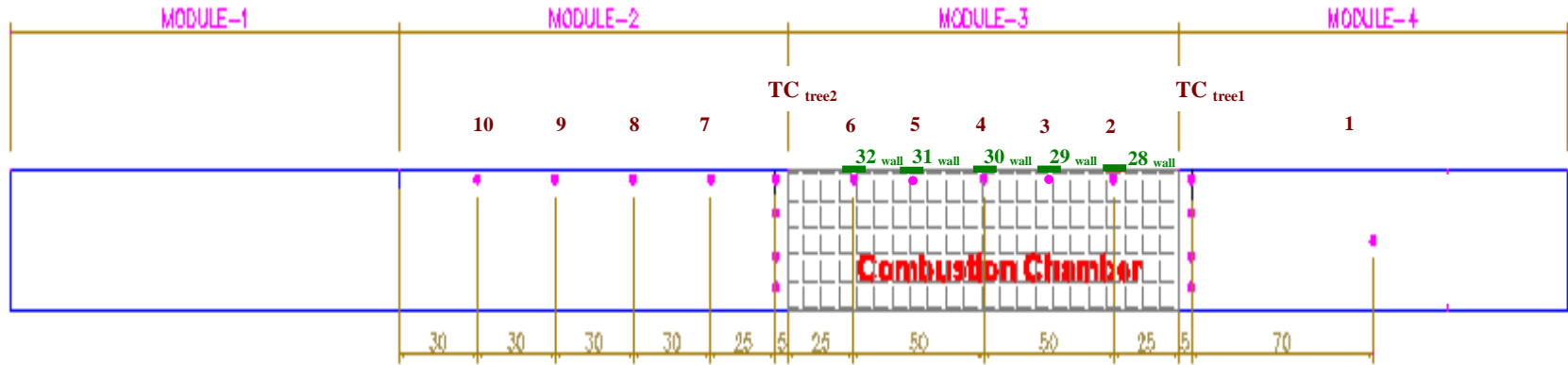


Figure 3.10 Temperature Measurement Points

3.2.3 Mass Loss Rate of Burning Specimen

The mass of a burning object is measured by A&D GF 20 K High Precision Industrial Balance. This balance measure the weight up to 20 kg with a precision of 0.1 gr. The data taken from the balance are transferred to computer by RS232 cable connection and stored in every 1 second. The technical specifications of the instruments are given in Appendix C.1.



Figure 3.11 A&D GF20K Balance

The mass loss rate can be estimated by sliding a window of n data points along the mass versus time curve and by calculating the time derivative of a polynomial of degree $n-1$ that goes through the n data points inside the window. It is very common to use window that consists of five data points ($n=5$). This leads to the following five point Formula [7]

$$-\left[\frac{dm}{dt}\right]_i = \frac{-m_{i-2} + 8m_{i-1} - 8m_{i+1} + m_{i+2}}{12\Delta t} \quad (1)$$

where m =specimen mass (g), t = time (s), i = data scan number.

3.2.4 Velocity Measurement

The ventilation velocity in model tunnel can be determined by measuring the differential pressure of a Pitot tube. The velocity can be calculated as follows:

$$v = \sqrt{\frac{2\Delta p}{\rho}} \quad 3.6$$

where v = velocity of the gas (m/s), Δp = differential pressure between the inner and outer tubes (Pa), ρ = density of the gas (kg/m^3). The pitot tube rake (Figure 3.12) are mounted to the duct with a width of 28 cm and height of 25 cm after the settling chamber. The pitot tube measurements are checked with hotwire anemometer and their measurements are verified. The verification experiment results are given in Appendix A. The dynamic pressure is measured by using Aschcroft CXLdp differential pressure transducer (Appendix C.3).

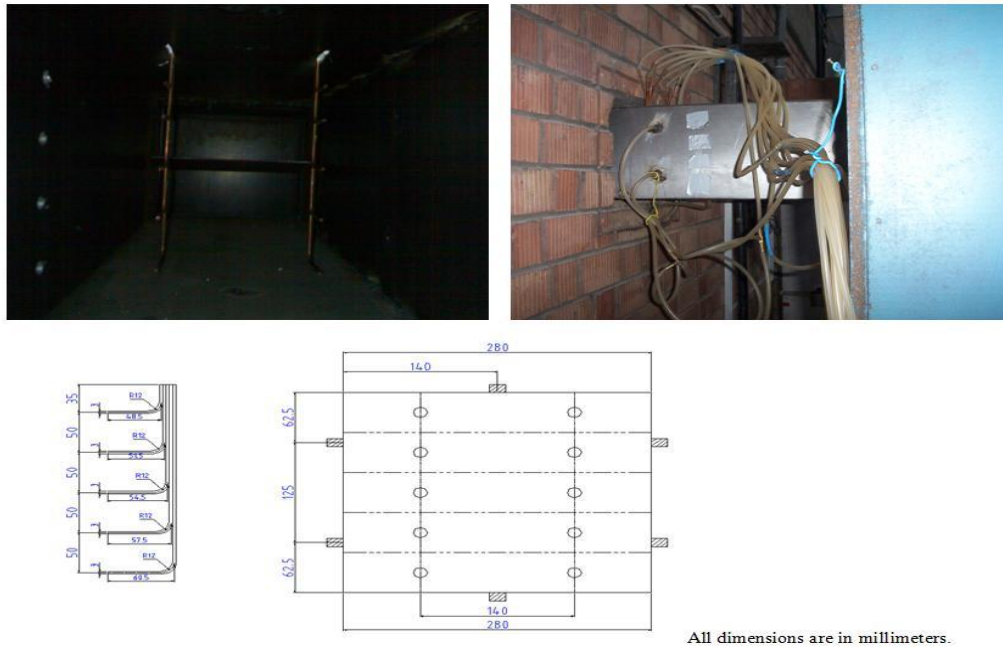


Figure 3.12 Pitot Tube Rakes Orientation

3.2.5. Measurement Chain

In this part of the study, the measured data and instruments for measurements are summarized. Table 3.1 shows the physical quantities measured and types of instruments use for measurement. Also, the schematic representation of measurement chain of the experimental setup is shown in Figure 3.13.

Table 3.1 List of Measured Quantities and Data Acquisition System

Measured Quantity	Instrument	Sampling Rate (Sample /second)
Ventilation Velocity by Pitot tube rake	Ashcroft CXLdp Differential Pressure Transducer	Adjusted before the experiment
Temperature by 32 thermocouples	Omega OMB-DAQ-3005 with QMB-PDQ 30 Expansion Module	1
Oxygen and Carbon monoxide Concentration by Electrochemical Sensors	Testo 350 S	1
Mass of Burning Specimen by Hybrid Sensor	A&D GF20 K	1

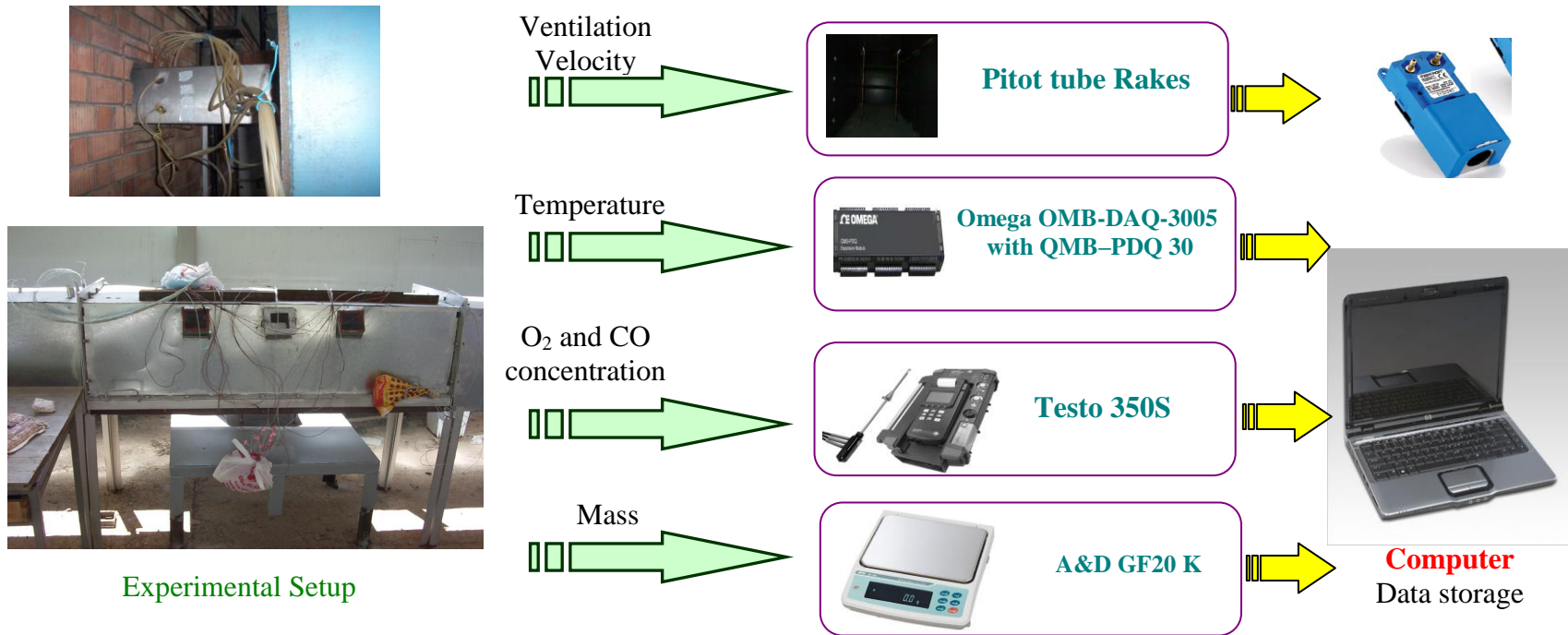


Figure 3.13 Measurement Chain of the Setup

CHAPTER 4

EXPERIMENTAL PROCEDURE

4.1 Experimental design parameters

The model vehicles are constructed as a wood crib structure. In chapter 2, the scaling laws and the properties of wood crib structure are given. It is better to decide the dimension of burning items. The wood crib's dimensions can be adjusted by selecting the length of the sticks, spacing between the sticks, number of sticks per layer, thickness of the sticks and height of burning items. A large number of combinations of wood cribs are built by varying the mentioned parameters.

In this study, the length and width of the mock-up models changes from 10 cm to 30 cm depending the model tunnel dimensions. The number of sticks per layer is selected as three. The heights of the mockup model vehicles are 12 , 18 and 24 cm. The thickness of the sticks are selected 1 cm, 2 cm and 3 cm for easy construction. The variety of length, thickness and height symbolizes the vehicles with different dimensions and different energy content. The wood crib configurations for different lengths are shown in Figure 4.1. The ventilation velocity inside model tunnel is the another design independent parameters. In the experimental study, three different ventilation velocities (1 m/s, 2 m/s and 3 m/s) are tested. Design parameters and their values are listed in Table 4.1

Length=Width	Model Tunnel and Vehicle Layout	Wood Crib Model
30 cm		<p style="text-align: center;">1 cm x 1 cm</p> <p style="text-align: center;">2 cm x 2 cm</p> <p style="text-align: center;">3 cm x 3 cm</p>
20 cm		<p style="text-align: center;">1 cm x 1 cm</p> <p style="text-align: center;">2 cm x 2 cm</p> <p style="text-align: center;">3 cm x 3 cm</p>
10 cm		<p style="text-align: center;">1 cm x 1 cm</p> <p style="text-align: center;">2 cm x 2 cm</p> <p style="text-align: center;">3 cm x 3 cm</p>

Figure 4.1 Dimensions of Model Vehicles and Their Layout inside tunnel

Table 4.1 Experimental Design Parameters

Design Parameters	Values
Stick Dimensions ($b \times b$)	1 cm x 1 cm
	2 cm x 2 cm
	3 cm x 3 cm
Length of Sticks (L) (Length = Width)	10 cm
	20 cm
	30 cm
Height of the Wood cribs (H)	12 cm
	18 cm
	24 cm
Ventilation velocity (V)	1 m/s
	2 m/s
	3 m/s
Number of Sticks per Layer	3

The total number of experiments for studying 4 design parameters with 3 level for each is $3^4 = 81$. This is called full factorial design of experiments. In full factorial design, researchers study all possible combinations of the levels of design parameters in the experiments.

Table 4.2 Full Factorial Design Table

#	Velocity (m/s)	Height (cm)	Length (cm)	Thickness (cm)
1	1	24	10	3
2	1	12	20	1
3	3	12	10	3
4	1	12	10	1
5	3	12	30	3
6	3	18	20	3
7	1	18	10	3
8	1	12	30	3
9	3	18	10	3
10	1	12	10	3
11	2	12	30	3
12	1	24	30	2
13	1	18	20	1
14	3	24	10	2
15	2	24	10	3
16	2	24	20	3
17	1	18	20	2
18	1	24	20	3
19	1	24	10	2
20	2	12	20	2
21	3	18	30	1
22	3	18	10	1
23	2	18	20	2
24	3	24	30	3
25	1	24	10	1
26	2	12	30	2
27	1	12	20	3
28	2	18	20	3
29	3	18	30	2
30	3	24	30	2
31	3	12	30	2
32	2	18	10	2
33	2	24	30	3
34	2	12	10	3
35	2	18	30	1
36	2	18	30	2
37	1	18	10	2
38	1	18	30	3
39	3	24	30	1
40	2	24	30	2
41	3	24	10	1

#	Velocity (m/s)	Height (cm)	Length (cm)	Thickness (cm)
42	1	18	30	1
43	2	12	20	1
44	2	12	10	1
45	1	24	30	1
46	1	18	30	2
47	2	24	10	2
48	3	24	20	2
49	2	24	30	1
50	1	18	10	1
51	2	12	10	2
52	3	24	20	1
53	1	24	20	2
54	1	12	30	2
55	3	18	20	1
56	2	24	20	2
57	2	12	20	3
58	2	24	20	1
59	1	18	20	3
60	3	12	10	1
61	3	12	10	2
62	1	24	30	3
63	3	12	20	1
64	2	18	20	1
65	1	12	20	2
66	3	18	20	2
67	1	24	20	1
68	2	24	10	1
69	3	12	20	3
70	3	24	10	3
71	2	18	10	3
72	1	12	30	1
73	2	12	30	1
74	3	12	20	2
75	3	18	30	3
76	1	12	10	2
77	2	18	10	1
78	3	12	30	1
79	2	18	30	3
80	3	24	20	3
81	3	18	10	2

4.2 Fractional Factorial Design

It is not usually possible to carry out a full factorial set of experiments due to time, budget and resources. Fractional factorial experiments are widely used in such circumstances. According to reference [43], “A fractional factorial experiment is the variation of the basic design factor in which only a subset of the runs are made.” Experiments with many factors are done as fractional factorial to estimate the important factor effects and low-order interactions. One-factor-at-a-time experiments, which vary only one factor or variable at a time while keeping others fixed, are often performed. However, statistically designed experiments which vary several factors simultaneously are more efficient when studying two or more factors and their interactions with each other.

Table 4.3 Experiment design matrix (L=W)

Experiment No:	Design Code	Velocity (m/s)	Height (cm)	Length (cm)	Thickness (cm)
1	0000	1 m/s	12	10	1 cm
2	0012	1 m/s	12	20	3 cm
3	2221	3 m/s	24	30	2 cm
4	0101	1 m/s	18	10	2 cm
5	0110	1 m/s	18	20	1 cm
6	0021	1 m/s	12	30	2 cm
7	1100	2 m/s	18	10	1 cm
8	0211	1 m/s	24	20	2 cm
9	0122	1 m/s	18	30	3 cm
10	1002	2 m/s	12	10	3 cm
11	1011	2 m/s	12	20	2 cm
12	0220	1 m/s	24	30	1 cm
13	0202	1 m/s	24	10	3 cm
14	1112	2 m/s	18	20	3 cm
15	1020	2 m/s	12	30	1 cm
16	1201	2 m/s	24	10	2 cm
17	1210	2 m/s	24	20	1 cm
18	1121	2 m/s	18	30	2 cm
19	2001	3 m/s	12	10	2 cm
20	2010	3 m/s	12	20	1 cm
21	1222	2 m/s	24	30	3 cm

Table 4.3 Continued

Experiment No:	Design Code	Velocity (m/s)	Height (cm)	Length (cm)	Thickness (cm)
22	2102	3 m/s	18	10	3 cm
23	2111	3 m/s	18	20	2 cm
24	2022	3 m/s	12	30	3 cm
25	2200	3 m/s	24	10	1 cm
26	2212	3 m/s	24	20	3 cm
27	2120	3 m/s	18	30	1 cm

The notation of experiments is shown in Figure 4.2. The first number in the design code number represents the level of velocity. “0”, “1”, “2” represents velocity level of 1 m/s , 2 m/s and 3m/s respectively. The second number in the design code represents the level of height of the wood cribs in the experiments. The height level varies from 12 cm (“ 0 ”), 18 cm (“ 1 ”) and 24 cm (“ 2 ”). The third and fourth number in the design code shows the levels of length of the wood cribs and thickness of the wood cribs.

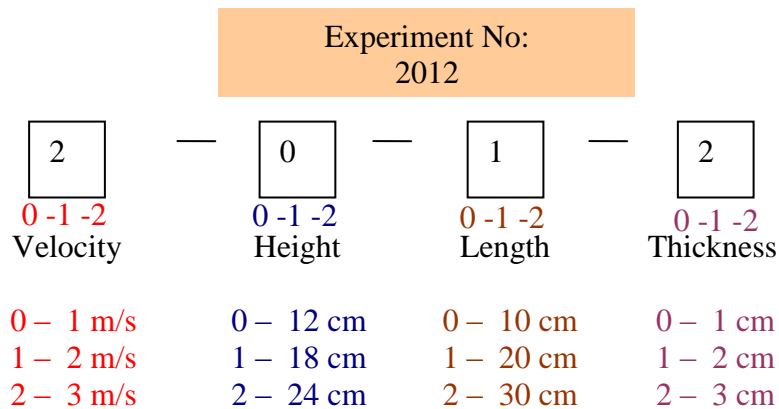


Figure 4.2 Description of Experiment Notation (L=W)

Also, the models with different length and width are tested. The reasons for this is that the face areas of the models with the square floor area except the top and floor areas are same. Therefore, it is necessary to check the dependence of the fire heat release rate on the burning object's length and width. The velocity in the model tunnel changes from 1 m/s and 3 m/s. The length and width of the wood structures change from 10 cm to 30 cm, respectively. 1 cm x 1cm and 3 cm x 3 cm square sticks with three number of sticks per layer are burned. Description of experimental notation for the tests when the wood structures have different length and width are shown in Figure 4.3

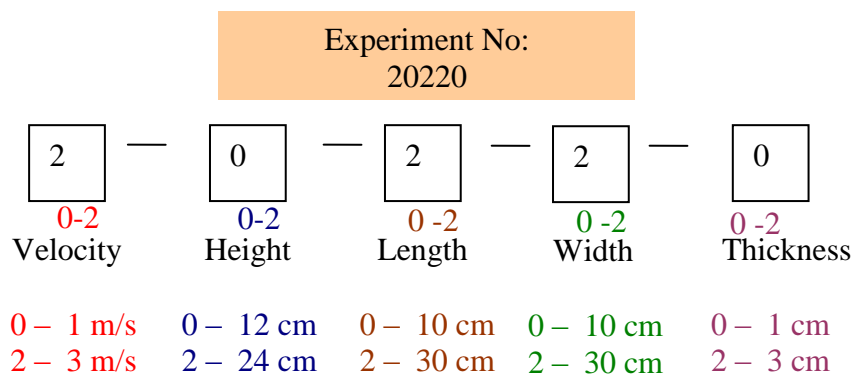


Figure 4.3 Description of Experiment Notation (L is not equal to W)

The tests are not performed in full factorial. The number of tests in full factorial design are $2^5 = 32$. The half-fraction of a full factorial experiment is done. Experimental design matrix for this case is listed in Table 4.4

Table 4.3 Experiment Design Matrix (Length is not equal to Width)

Experiment No:	Design Code	Velocity (m/s)	Height (cm)	Length (cm)	Width (cm)	Thickness (cm)
1	20220	3	12	30	30	1
2	02220	1	24	30	30	1
3	22200	3	24	30	10	1
4	02000	1	24	10	10	1
5	02022	1	24	10	30	3
6	22222	3	24	30	30	3
7	20022	3	12	10	30	3
8	00002	1	12	10	10	3
9	02202	1	24	30	10	3
10	00200	1	12	30	10	1
11	20000	3	12	10	10	1
12	22002	3	24	10	10	3
13	22020	3	24	10	30	1
14	20202	3	12	30	10	3
15	00222	1	12	30	30	3
16	00020	1	12	10	30	1

4.3 Steps of the Experimental Procedure

The experiments are performed as follows:

1. The woods are assembled with staples to form a wood crib. The weight of the wood before and after assembled are recorded.
2. The woods are put into an oven at 100 °C for 10 hours period to extract the humidity inside.
3. The weight of the wood after drying is also recorded.
4. The temperature, pressure and relative humidity values of the atmosphere are noted.
5. The scale and gas concentration device are initialized and zeroed.
6. The wood cribs are put on the scale platform and the model tunnel ventilation is adjusted according to the weather conditions.

7. The 100 ml of ethanol is poured on the scale platform and ignited.
8. The temperature, weight of the wood cribs and gas concentrations are stored into the computer every second.
9. The storage of data is stopped when there is no significant change in the weight of the burning substances.
10. The gas concentration data and ventilation velocity are utilized to calculate the fire heat release rate. Mass loss rate is obtained by using the mass data in the duration of experiment. The temperature inside tunnels is evaluated from the temperature readings at different location along the tunnel.

CHAPTER 5

EXPERIMENTAL RESULTS

5.1 Introduction

The experimental results are given in a graphical form. For each experiment, the mass loss rates, heat release rate variation with time are given. The temperature variations with time are given in Appendix-D. The results obtained from the experiments are maximum mass loss rate and maximum heat release rate. These are given in a tabular form with geometrical configurations of the wood cribs.

5.2 Results of Fire Tests

The experimental results of burning specimen are given in Figure 5.1 - 5.34. The results obtained from the experiments are listed in Table 5.1.

In Figure 5.1 and 5.2, the results of the model vehicle fire, which has a length of 10 cm, width of 10 cm, height of 12 cm and thickness of 1 cm, are given. Tests are carried out at different ventilation velocities. The blockage ratio of this burning specimen is 9.3 %. In each test, the mass loss rate reaches the maximum value almost after 60 seconds. When the ventilation velocity increases, the mass loss rate is not

affected up to 2 m/s but it decreases beyond 3 m/s. In Figure 5.2, the heat release rate increases from 16.44 kW to 42.2 kW as the velocity inside model tunnel changes from 0.5 m/s to 2 m/s. The heat release rate reaches to 41.2 kW at 3 m/s. As the ventilation velocity increases, the probability to mix with oxygen and burning material is also increases. It is known that the concentration of oxygen in the combustion significantly affects the combustion of the solid items. It seems that the cooling effect of the ventilation is dominant up to a certain velocity limit. With the increasing velocity, it is seen that the deflection of flames towards the ventilation direction is increasing. The highest temperature location is also transferred towards the ventilation direction due to ventilation. Due to higher ventilation velocity, the temperature levels decrease. These experiments are conducted twice in order to check the uncertainty of the measured variables. In this case, they are mass loss rate and heat release rate. The results of these trials are shown in Figure 5.1 and Figure 5.2. The maximum mass loss rate varies ± 0.5 g/s, but the maximum heat release rate varies between ± 5 kW if the results are examined. This variation can be tolerated as there are unforeseen difficulties to obtain the same combustion reaction at different ambient conditions (extraneous variable).

The results of the model vehicle, which has the same length, width and height as the previous one but with a thickness of 3 cm, are shown in Figure 5.3 and 5.4. The fire reaches to maximum heat release rate (HRR) earlier when the velocity is higher. In other words, the duration of time to reach the maximum mass loss rate is much smaller at 2 m/s than at 1 m/s. Models constructed from thicker sticks release less heat. The HRR increases from 9.1 kW to 13.7 kW as the velocity changes from 1 m/s to 2 m/s. It is seen that the velocity causes an increase in the HRR. The ventilation influences the mass loss rate value based on Figure 5.3. Also, the fully developed period of fire in higher ventilation level is larger. From these tests, one may conclude that higher velocities are necessary to reach the HRR value of same model with 1 cm thick sticks. The temperature levels inside the tunnel in these tests are lower than the values obtained with smaller thickness sticks.

In Figure 5.5 and 5.6, the height of the model vehicle is 18 cm, the width and the length are 10 cm and the sticks have the thickness of 2 cm. The blockage ratio of the model is 14 %. As the ventilation velocity varies from 0.5, 1 and 3 m/s and the maximum mass loss rate is 1.5, 1.6 and 2 g/s, respectively. It can be interpreted that the velocity increases the burning rate as the velocity is increasing between 0.5 m/s to 3 m/s. The same trend is observed if the maximum HRR values are considered. The highest temperature location is also transferred towards the ventilation. In experiment (-1)101, the highest temperature is 479 °C at thermocouple 5 location. In experiment 0101, the highest temperature is 375 °C at thermocouple 18 location. In experiment 2101, the highest temperature is 283 °C at thermocouple 26 location. Due to higher ventilation velocity, the temperature values inside the tunnel are decreasing.

The results of experiments with the models (24 cm height, 10 cm length, 10 cm width and 1 cm thickness) are represented in Figure 5.7 and 5.8. The blockage ratio of the model is 18.7 %. The velocity variation causes an increase in HRR. The maximum temperature values inside the tunnels vary from 759 °C (Exp. 02000), 583 °C (Exp.1200) and 500 °C (Exp.2200). The temperatures inside the tunnels decrease when the ventilation velocity increases. As the model is compared with the higher versions, the HRR is directly proportional to the height of the model vehicle with same length, width and thickness.

The mass loss rate and heat release rate variation of the model fire with 20 cm square base and 12 cm height with different stick thickness are presented in Figure 5.9 and 5.10. The blockage ratio of the model is 18.7 %. The increase of HRR results from increase in velocity. The flame spread characteristics vary due to stick thickness. As a result, the fire HRR is inversely proportional to stick thickness. On the other hand, maximum mass loss rate is not significantly affected from ventilation. It seems ventilation adversely affects the burning rate. The duration of fire is longer when the stick thicknesses are increasing.

The HRR is not affected from ventilation when the model with 20 cm square base, 18 cm height and 1 cm thickness are tested (Figure 5.11 – 5.12). It is emphasized that the ventilation decreases the HRR and mass loss rate. These models have a blockage ratio of 28 %. A faster burning occurs when the ventilation velocity increases. In the same figures, the results of model with square base, 24 cm height and 2 cm thickness are also shown. The ventilation is directly proportional to HRR and mass loss rate. Also, the fire duration is getting longer due to the increase in ventilation velocity.

In Figures 5.13-5.14, the models with same length (30 cm), height (12 cm) and width (30cm) are burned. There, the thicknesses of the sticks are different. The HRR increases as the ventilation velocity is higher as seen in the results of Experiment No: 1020-20220, but there is a decrease in maximum mass loss rate value. As the velocity increases, the duration of fire is getting shorter due to fast burning. It is seen that the variation of the sticks affect the flame spread characteristics.

In Figure 5.15-5.16, the models' blockage ratios are 18.7 %. The ventilation enhances the burning rate and HRR. The thickness of the sticks is inversely proportional to HRR.

In Figure 5.17 and 5.18, the height of models is 12 cm, but the length and width of the object are changed from 10 cm to 30 cm. These models do not have a square cross-sectional base. As the width of the object and the ventilation velocity increases, the burning rate and HRR also increases. However, the length of the object is inversely proportional to HRR and mass loss rate. This probably occurs due to decrease in the distance between the walls of the tunnel and the burning item. This result is similar to Carvel's study [16] . An increase in the ventilation causes an increase in HRR and mass loss rate.

In Figure 5.19 and Figure 5.20, the experimental results conducted with model with a blockage of 18.7 % are presented. According to these results, the velocity increase enhances the maximum burning rate and HRR.

In Figure 5.21- 5.22, the models which have blockage ratios of 56.1% and 42 % are presented. In Experiment No: (-1)2221 and 2221, the increase in velocity cause a decrease in HRR and mass loss rate. The cooling effect is dominant when the ventilation velocity reaches a certain value. In Figure 5.22, it can be said that it needs a long time to catch a fully developed fire at higher ventilation velocities.

In Figure 5.23 and 5.24, the experiments are conducted with the models which have blockage ratios of 42 %. The ventilation affects the HRR positively; however, the thickness of the sticks affects the HRR inversely.

The results obtained from models with a blockage ratio 14%, 28 % and 9.3% are presented in Figure 5.25 and Figure 5.26. These can be compared with the other models with same configuration. Based on the given figures, it can be seen that the variation of height affects the burning rate and HRR (Exp. No: 2102, 1100, 2001).

The results obtained from models with a blockage ratio 56.1% are presented in Figure 5.27 and Figure 5.28. The ventilation causes an increase in the burning rate and HRR up to a certain velocity limit.

In Figure 5.29 and Figure 5.30, the results of Exp. No: 2010 , 1210 and 2212 are given. As the results are compared in pairs, the variation of height of the model with same length, width and thickness enhances the burning rate and HRR. The thickness adversely affects the burning rate.

The length and width of the models are changed in the tests given in Figure 5.31 and Figure 5.32. For longer width, a higher HRR and maximum burning rate are obtained. This may occur due to the decrease in the distance between the walls of the tunnel and the burning item. This result is similar to Carvel's results [16]. An increase in the ventilation causes a increase in HRR and mass loss rate.

In Figure 5.33 and Figure 5.34 the models with a height of 24 cm, length of 10 cm and width of 30 cm are burned. The increase in velocity increases the burning rate. The spread of flame is affected by the thickness of the sticks.

In conclusion, the HRR and burning rate reach to high values in most of the experiments as the ventilation velocity increases during the experiments. The thicknesses of the sticks are inversely proportional to mass loss rate and HRR. The variation of blockage ratio is affected by HRR and mass loss rate. Its effect is positive or negative depending on the value of ventilation velocity.

Table 5.1 Experimental Result Table

Design Code	V (m/s)	H (cm)	L (cm)	W (cm)	T (cm)	Mass (g)	Blockage Ratio (%)	P _{ambient} (kPa)	T _{ambient} (°C)	Rel. Hum. (%)	M (g/s)	Q (kW)
(-1)000	0,5	12	10	10	1	158,2	9,3	92,8	18,4	55	2	16,44
0000	1	12	10	10	1	160,3	9,3	92,5	21,7	34,7	2,25	20,8
1000	2	12	10	10	1	159,5	9,3	91,4	24,1	31,1	2	42,2
20000	3	12	10	10	1	157,8	9,3	90,3	27,7	22,1	2,5	41,3
00002	1	12	10	10	3	452,7	9,3	91,8	20,4	53,4	0,47	9,1
1002	2	12	10	10	3	418,6	9,3	89,55	34	21,5	0,5	13,7
(-1)101	0,5	18	10	10	2	496,8	14,0	92,8	17,6	51,3	1,5	7,81
0101	1	18	10	10	2	369,2	14,0	90,9	25,6	28,9	1,6	15,7
2101	3	18	10	10	2	470,8	14,0	91,4	30,8	22,7	2	52,6
02000	1	24	10	10	1	352,6	18,7	90,7	33,3	20,7	3,8	45,5
1200	2	24	10	10	1	325,3	18,7	90,4	29,8	41,6	3,5	87,0
2200	3	24	10	10	1	332	18,7	91,4	29,7	28	3,84	98,5
0202	1	24	10	10	3	885,2	18,7	89,5	37,3	18,3	0,97	15,3
22002	3	24	10	10	3	848,1	18,7	90,8	19,3	47,8	1,4	42,8
1201	2	24	10	10	2	665,7	18,7	92	21,7	47,8	2,49	56,7
(-1)011	0,5	12	20	20	2	686,3	18,7	91,8	29,4	30,2	2,4	18,7
1011	2	12	20	20	2	643,4	18,7	91	25	46,6	2,1	39,2
(-1)012	0,5	12	20	20	3	905,5	18,7	91,3	23,1	45	1,75	15,62
0012	1	12	20	20	3	847,1	18,7	91	19,9	51,9	1,5	22,4
(-1)120	0,5	18	20	20	1	475	28,0	91,3	25,1	38,5	8,5	86,61
0110	1	18	20	20	1	486	28,0	91,4	28,9	41,2	6,55	85,4
(-1)211	0,5	24	20	20	2	1216,2	37,4	91,8	28	32	5,25	31,6
0211	1	24	20	20	2	1320,5	37,4	91,4	21,5	36,4	6	71,8
1020	2	12	30	30	1	475,5	28,0	91,4	27,5	37,8	5	105,0
20220	3	12	30	30	1	517,8	28,0	91,4	19,8	53,5	4,51	117,5
0021	1	12	30	30	2	942,7	28,0	91	19,2	51,4	3,85	69,7
(-1)021	0,5	12	30	30	2	1020,1	28,0	91,7	17,6	59,8	3	24,79
(-1)122	0,5	18	30	30	3	2045,8	42,1	91,8	24,3	41,6	4,35	39,7
0122	1	18	30	30	3	1944,8	42,0	91	26,2	39,7	-	94,2
(-1)121	0,5	18	30	30	2	1111,7	42,1	91,7	21,4	45,8	-	74,47
1121	2	18	30	30	2	1503,3	42,0	91,4	31,7	38,8	4,42	113,1
(-1)221	0,5	24	30	30	2	2011,3	56,1	91,3	26,2	37,6	9,5	105,2
2221	3	24	30	30	2	2058,3	56,1	91,4	32,6	37,8	2,0	78,9
0220	1	24	30	30	1	998,9	56,1	91,4	26,8	49,9	10	184,2
02220	1	24	30	30	1	1007,8	56,1	920	23	41,4	12,4	223,5
2120	3	18	30	30	1	742,4	42,0	91,4	33,7	34,5	5,1	136,1
(-1)222	0,5	24	30	30	3	2781	56,1	91,3	26,8	38	-	67,96
1222	2	24	30	30	3	2757,5	56,1	91	28,6	45	6,8	150,5
22222	3	24	30	30	3	2752,8	56,1	90,8	21,3	44	5,8	142,7
2102	3	18	10	10	3	676,3	14,0	92	33,6	25,2	1,2	41,7
1100	2	18	10	10	1	260,4	14,0	91,4	28,9	41,2	2,25	52,8
1112	2	18	20	20	3	1375,1	28,0	91,4	31,8	38,7	1,4	30,9

Table 5.1 Continued

Design Code	V (m/s)	H (cm)	L (cm)	W (cm)	T (cm)	Mass (g)	Blockage Ratio (%)	P _{ambient} (kPa)	T _{ambient} (°C)	Rel. Hum. (%)	M (g/s)	Q (kW)
2001	3	12	10	10	2	310,7	9,3	90,4	26,4	50	1,5	30,3
1210	2	24	20	20	1	677,5	37,4	91,4	27,2	45,3	7,51	148,3
2010	3	12	20	20	1	349	18,7	91,4	33,1	35,2	2,6	57,7
2212	3	24	20	20	3	1827	37,4	91,4	25	52	4,49	90,0
(-1)111	0,5	18	20	20	2	801,9	28,0	92,9	18,8	42,4	2,75	17,93
2111	3	18	20	20	2	1047,77	28,0	91	24,8	45,2	1,85	35,8
2022	3	12	30	30	3	1285,7	28,0	91,4	23,7	58	2,35	53,5
00222	1	12	30	30	3	1290,7	28,0	90,7	27,6	29,8	2,5	36,8
(-1)2200	0,5	24	30	10	1	628,4	18,7	92,8	19,8	43,6	12	43,4
22200	3	24	30	10	1	636,5	18,7	91,4	21,6	49,7	8,5	214,6
(-1)2202	0,5	24	30	10	3	638,2	18,7	92,8	23,3	35,6	2,25	10
02202	1	24	30	10	3	1799,8	18,7	92	19,6	65,6	2,31	36,1
20022	3	12	10	30	3	853,6	28,0	91,4	31,4	23,6	1,46	32,2
00020	1	12	10	30	1	309,9	28,0	90,7	20,8	50,1	4,28	68,2
20202	3	12	30	10	3	878,1	9,3	91,4	30,8	31	1,3	24,3
00200	1	12	30	10	1	318,6	9,3	90,7	25,8	32,7	3,75	50,2
(-1)2020	0,5	24	10	30	1	632,5	56,1	92,8	26,4	23,3	8	59,51
22020	3	24	10	30	1	642	56,1	91,4	25,6	35,1	-	215,1
02022	1	24	10	30	3	1674,3	56,1	92	18,9	52,7	2,77	40,0

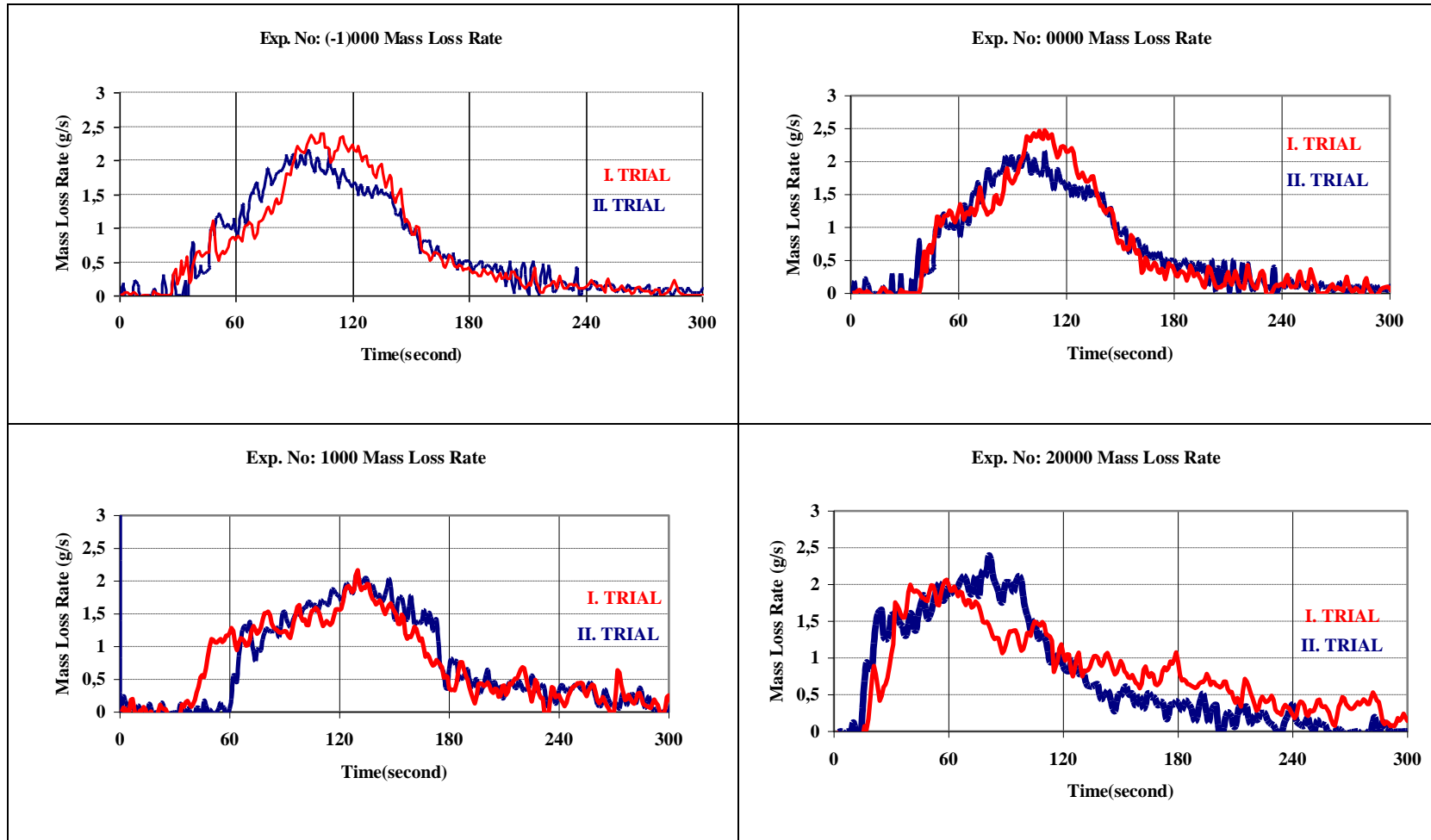


Figure 5.1 Mass Loss Rate versus Time Variation of Experiment No: (-1)000 - 0000 - 1000 - 20000 (Table 5.1 pg.86)

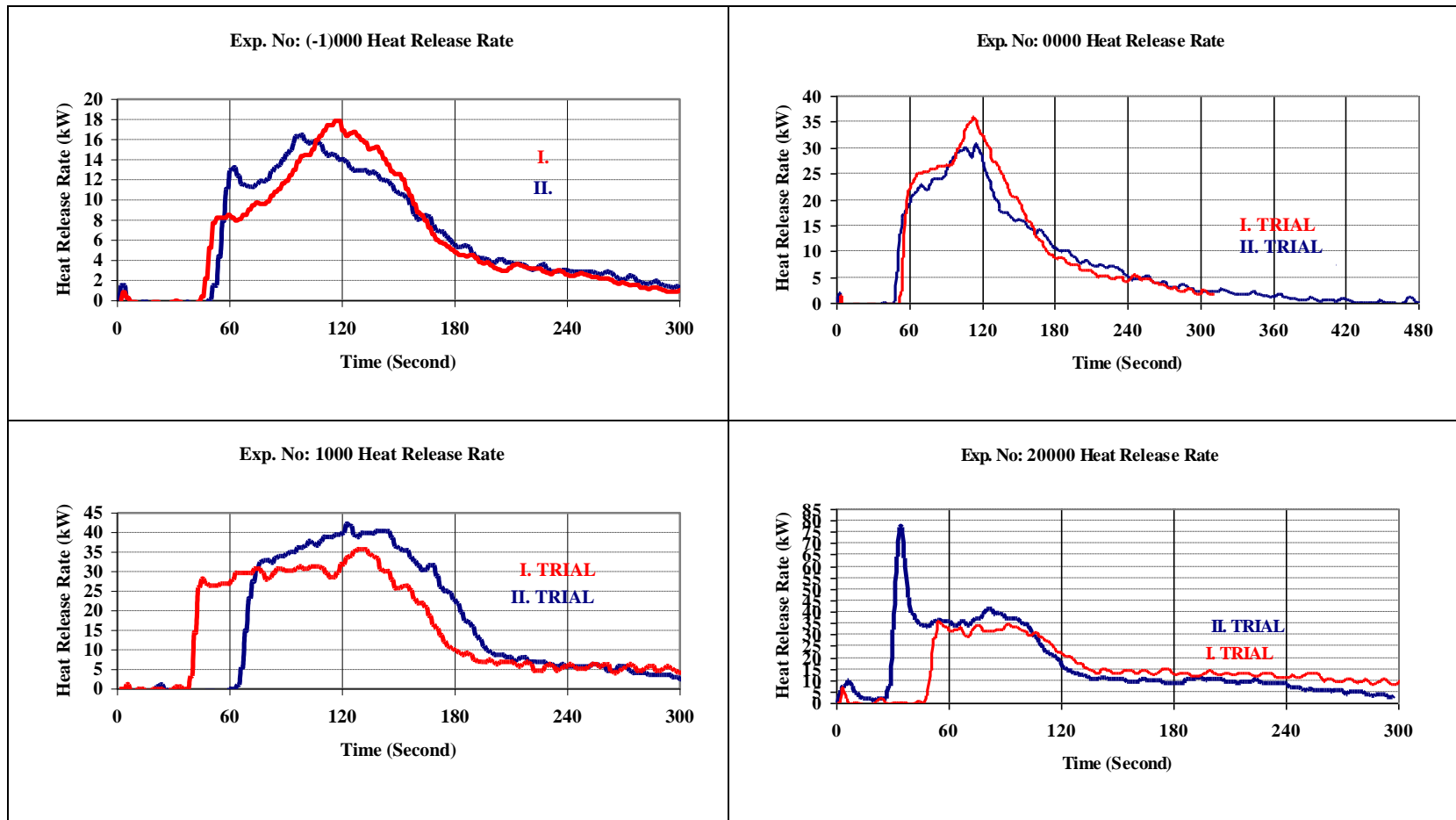


Figure 5.2 Heat Release Rate versus Time Variation of Experiment No: (-1)000 - 0000 - 1000 - 20000 (Table 5.1 pg.86)

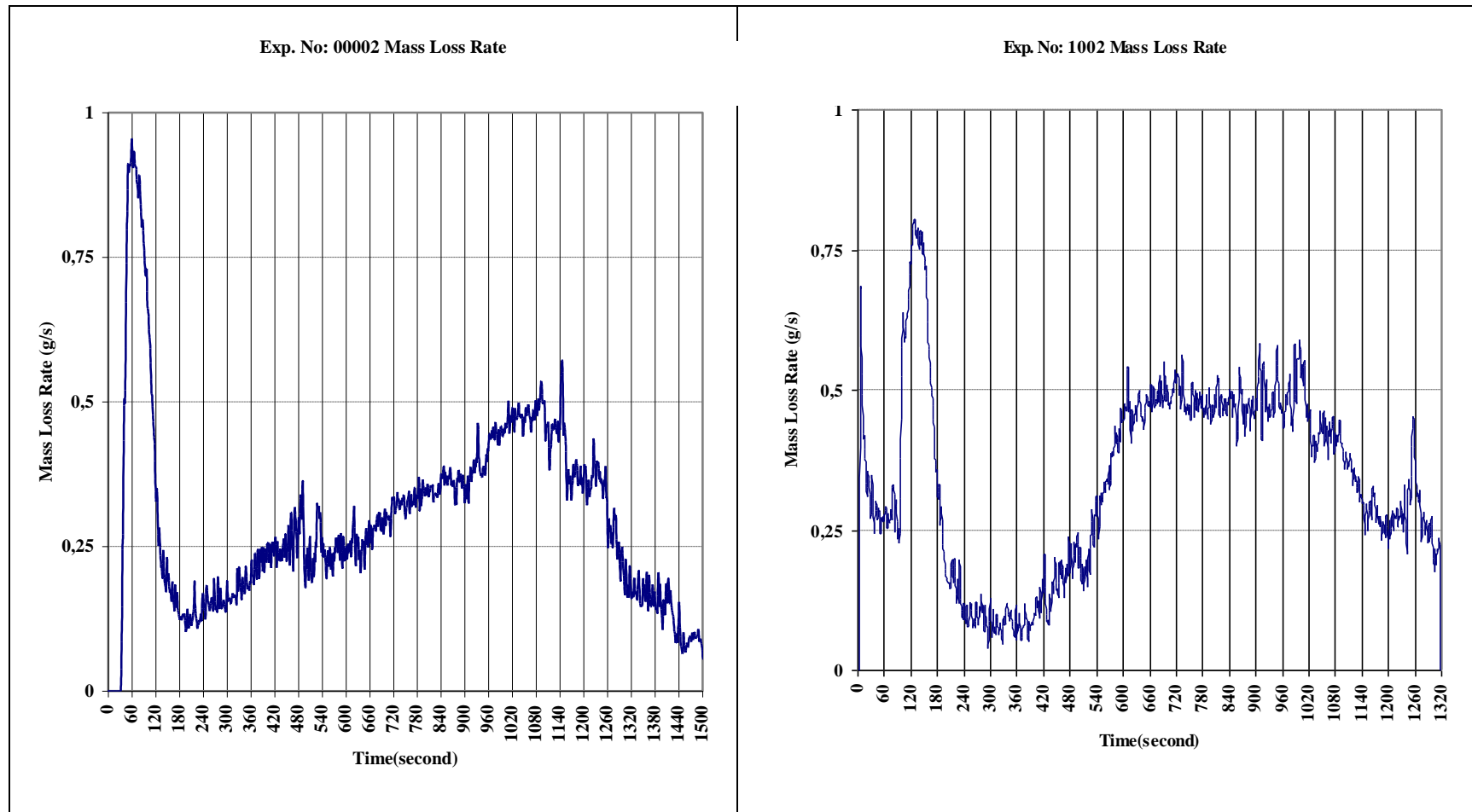


Figure 5.3 Mass Loss Rate versus Time Variation of Experiment No: 00002 - 1002 (Table 5.1 pg.86)

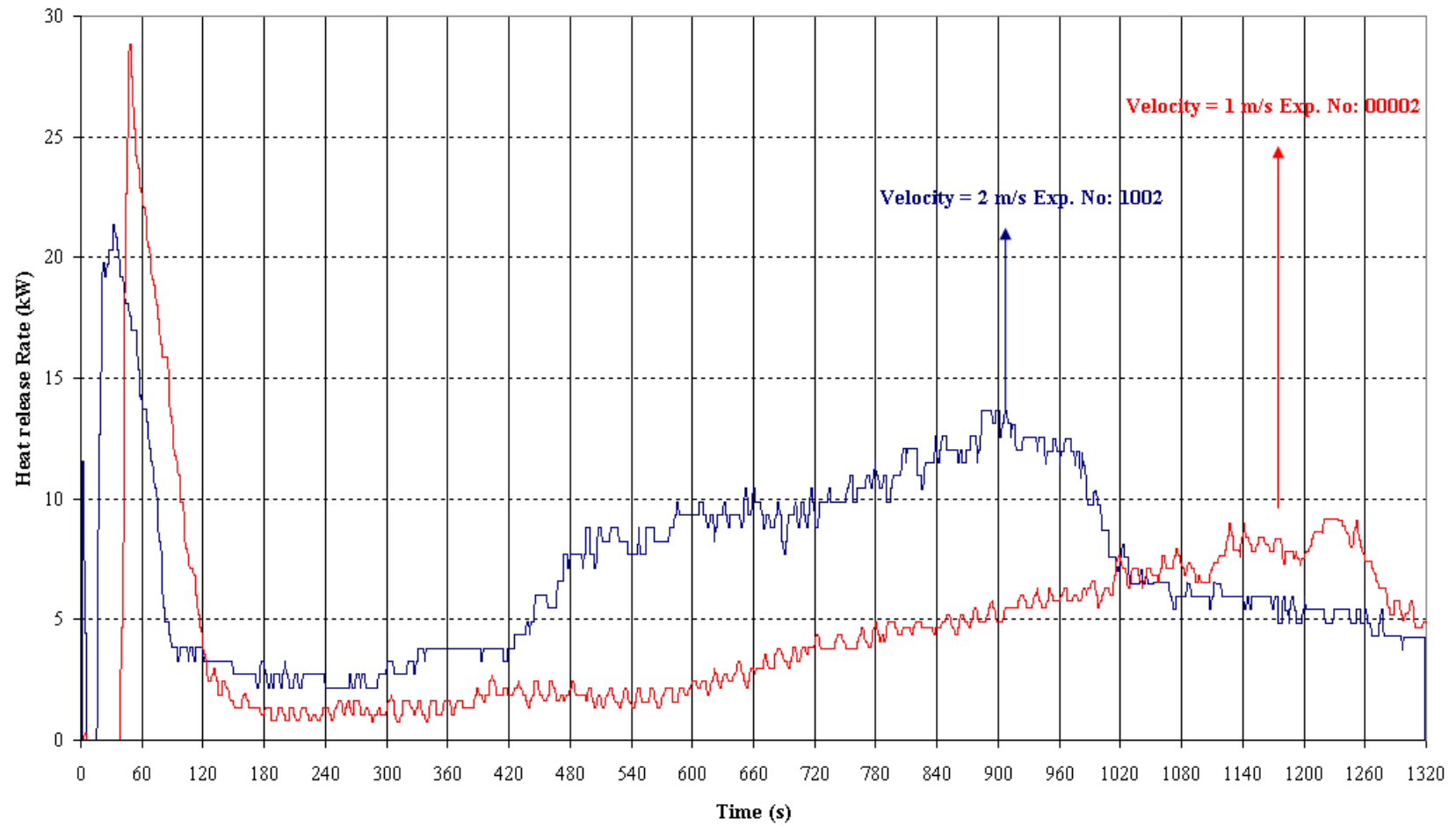


Figure 5.4 Heat Release Rate versus Time Variation of Experiment No: 00002 - 1002 (Table 5.1 pg.86)

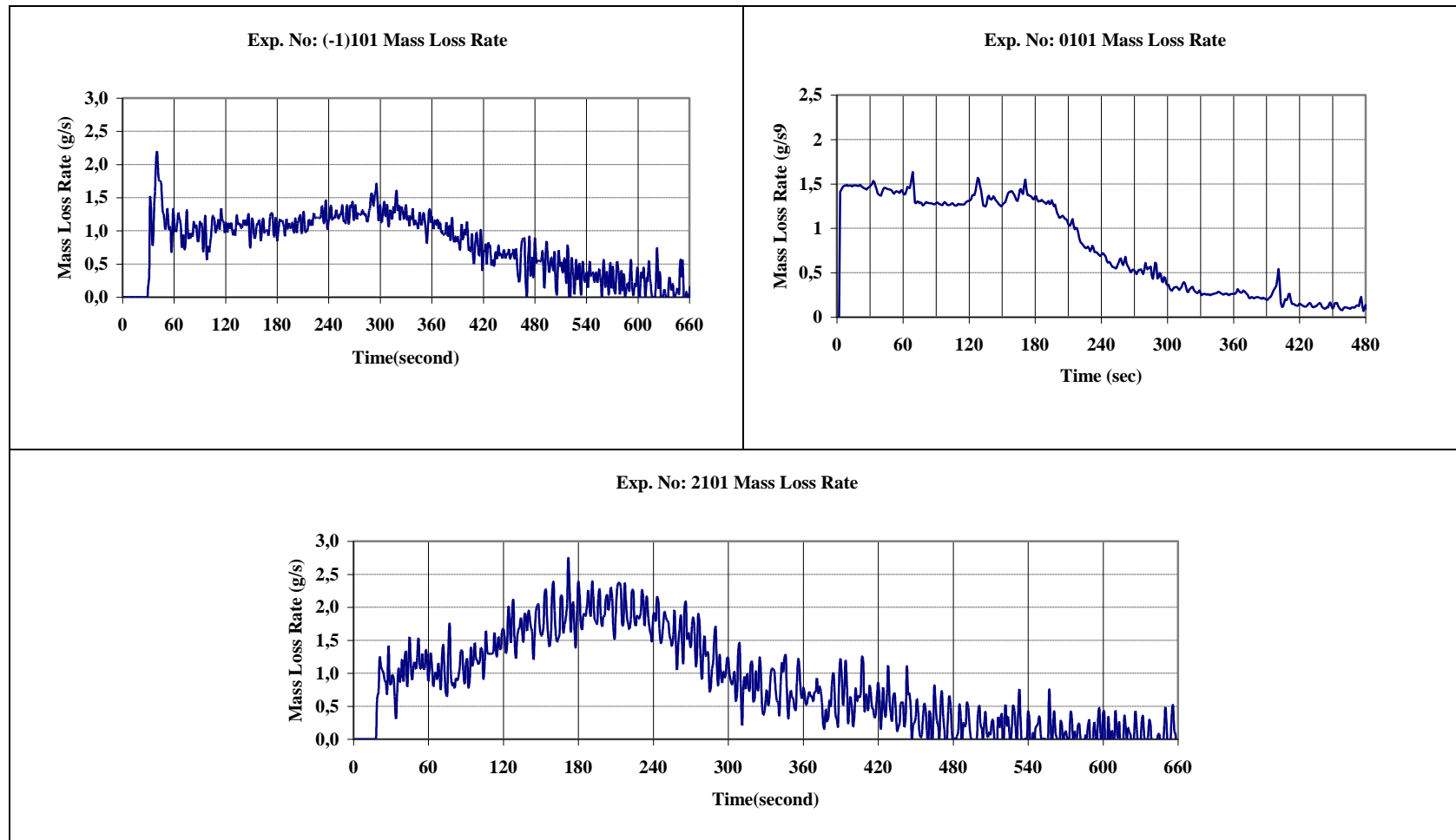


Figure 5.5 Mass Loss Rate versus Time Variation of Experiment No: (-1)101 - 0101 - 2101 (Table 5.1 pg.86)

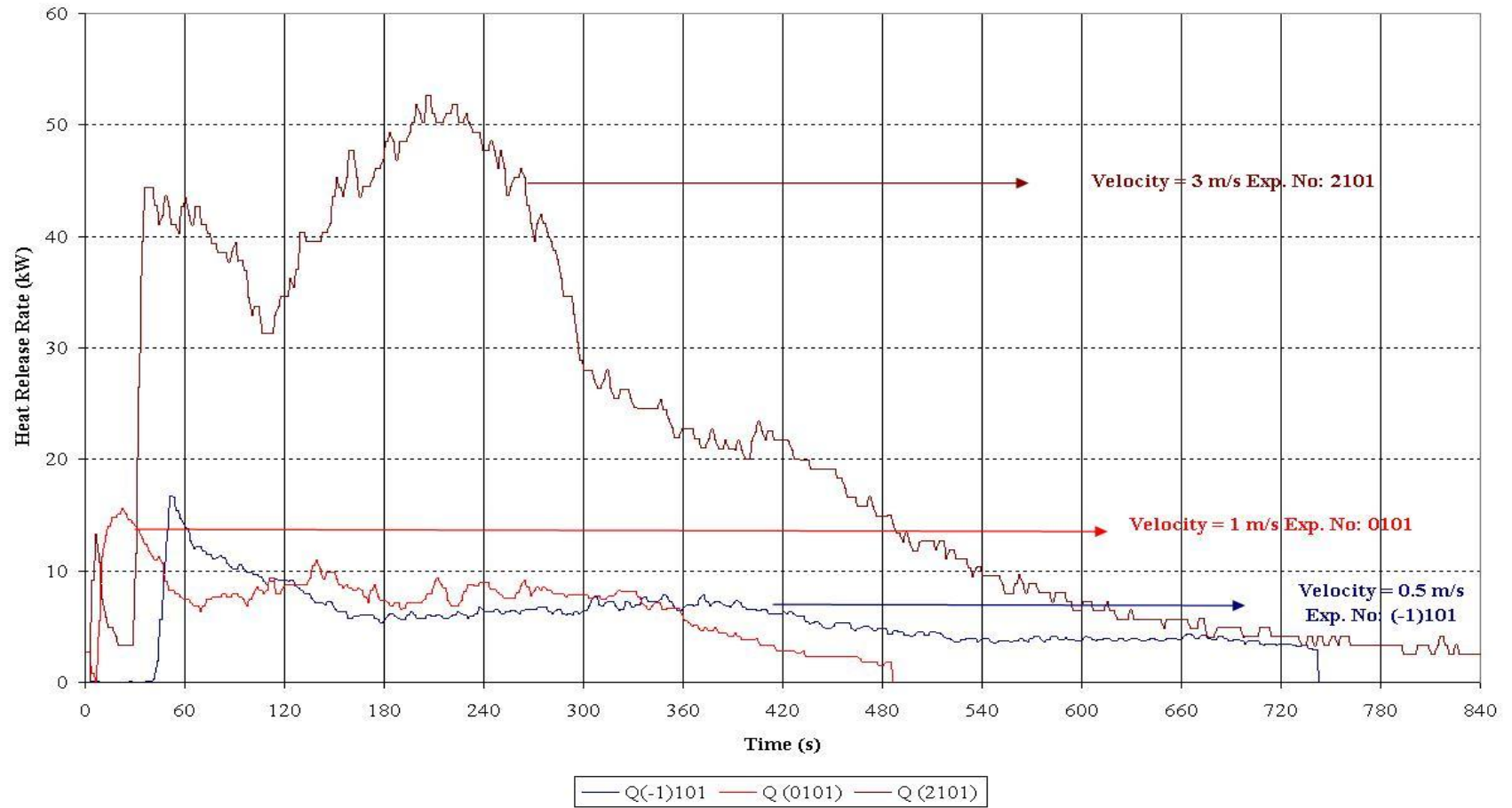


Figure 5.6 Heat Release Rate versus Time Variation of Experiment No: (-1)101 - 0101 - 2101(Table 5.1 pg.86)

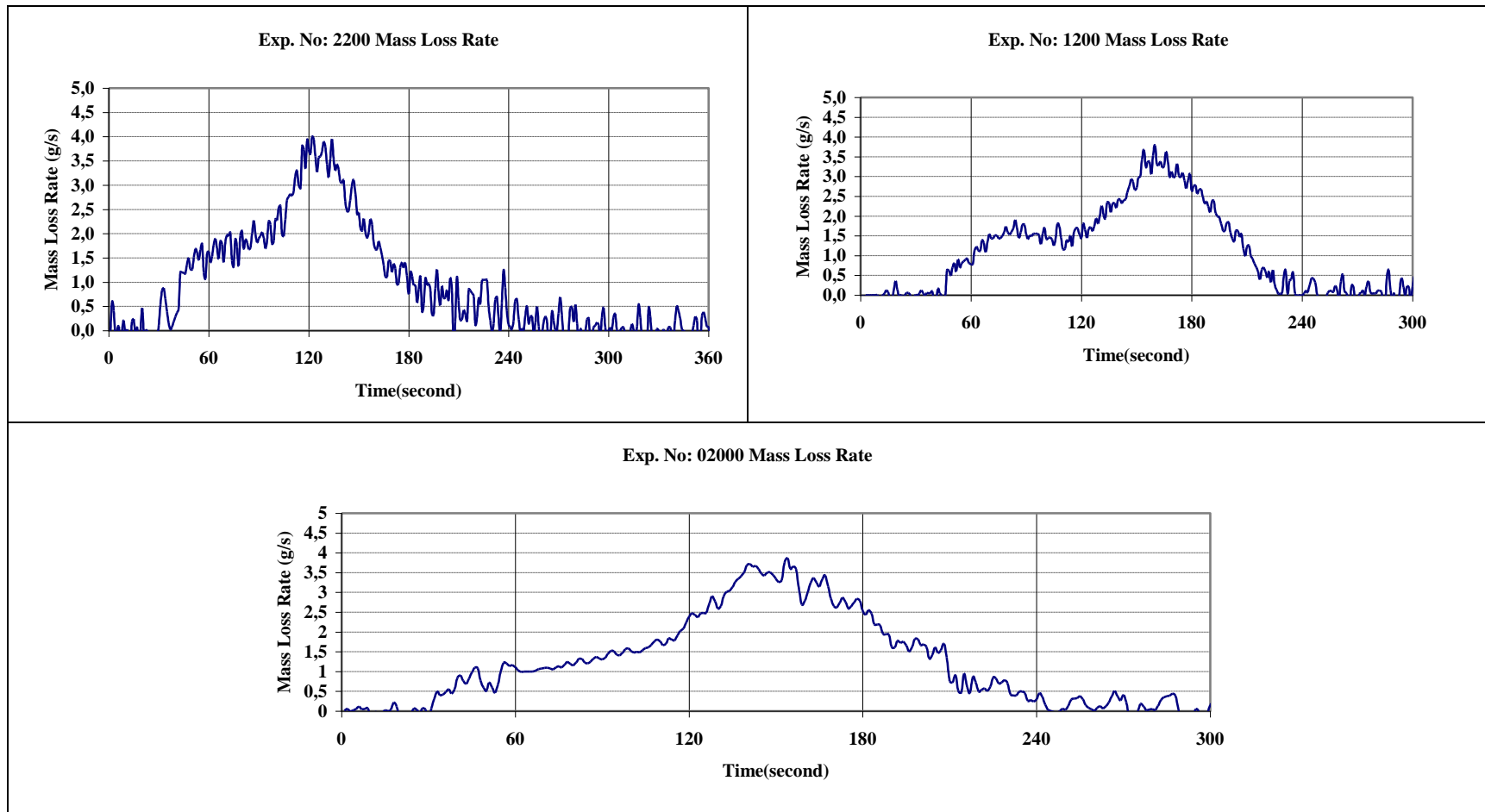


Figure 5.7 Mass Loss Rate versus Time Variation of Experiment No: 02000 - 1200 - 2200 (Table 5.1 pg.86)

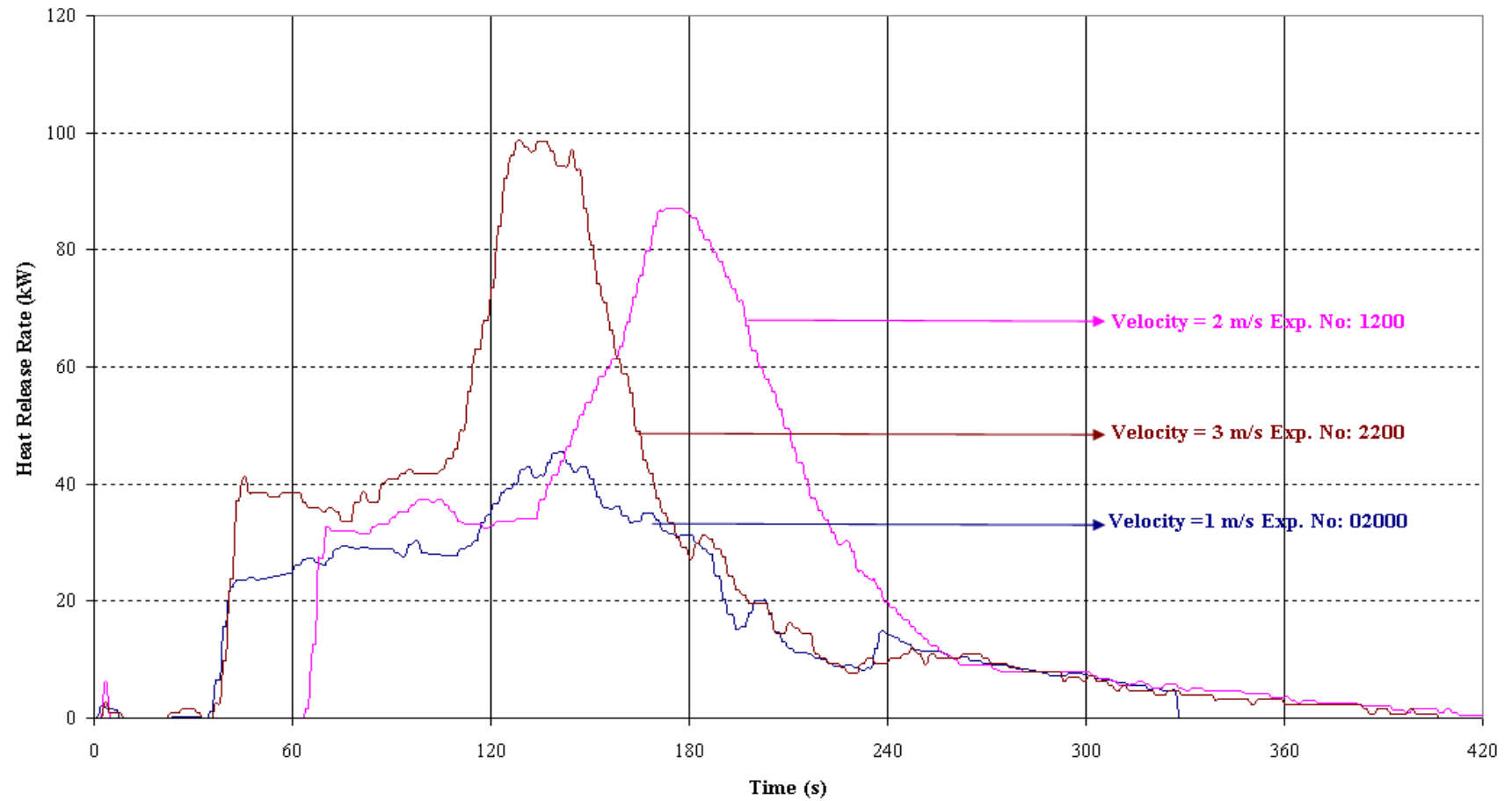


Figure 5.8 Heat Release Rate versus Time Variation of Experiment No: 02000 - 1200 - 2200 (Table 5.1 pg.86)

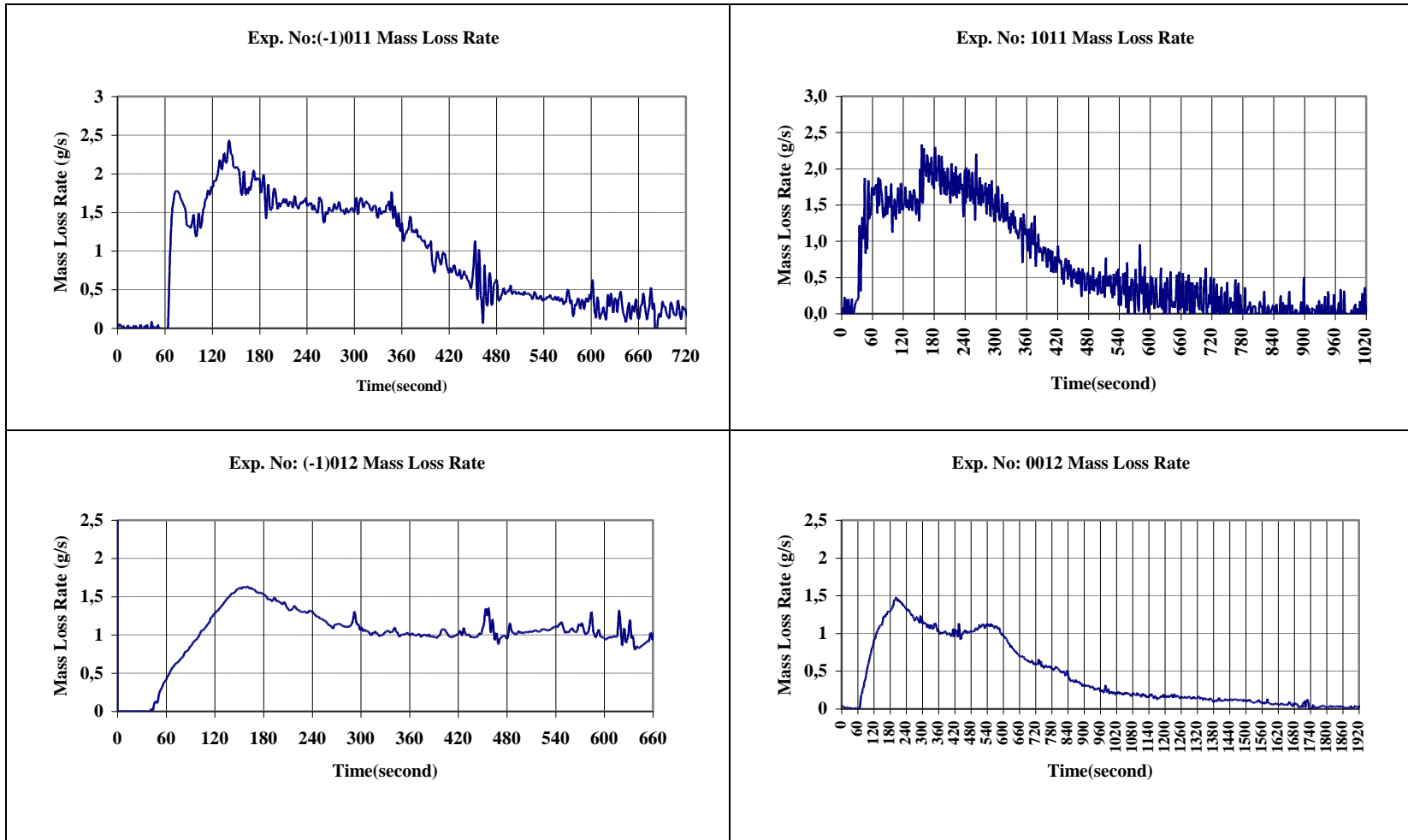


Figure 5.9 Mass Loss Rate versus Time Variation of Experiment No: (-1)011 - 1011 - (-1)012 - 0012 (Table 5.1 pg.86)

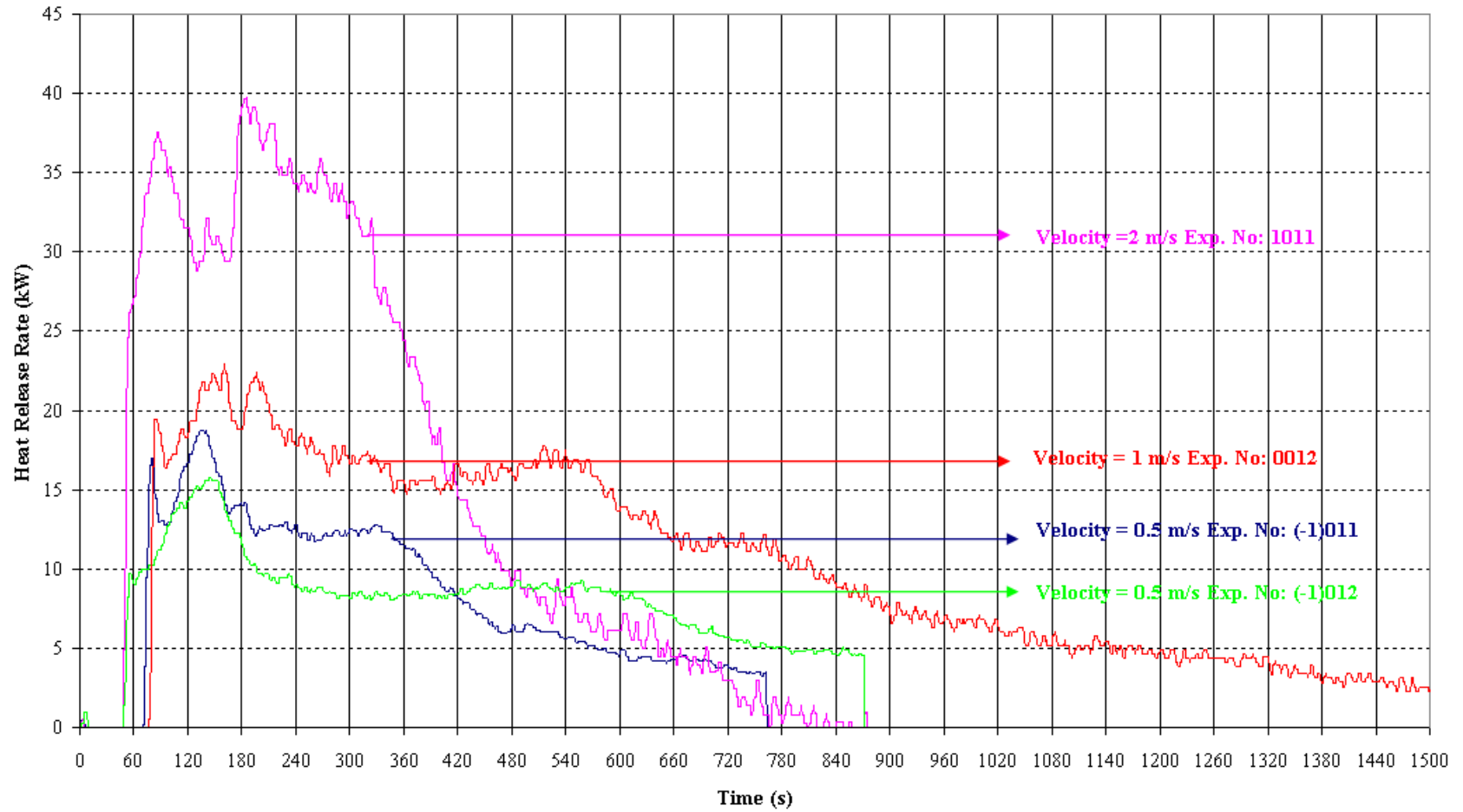


Figure 5.10 Heat Release Rate versus Time Variation of Experiment No: (-1)011 - 1011 - (-1)012 - 0012 (Table 5.1 pg.86)

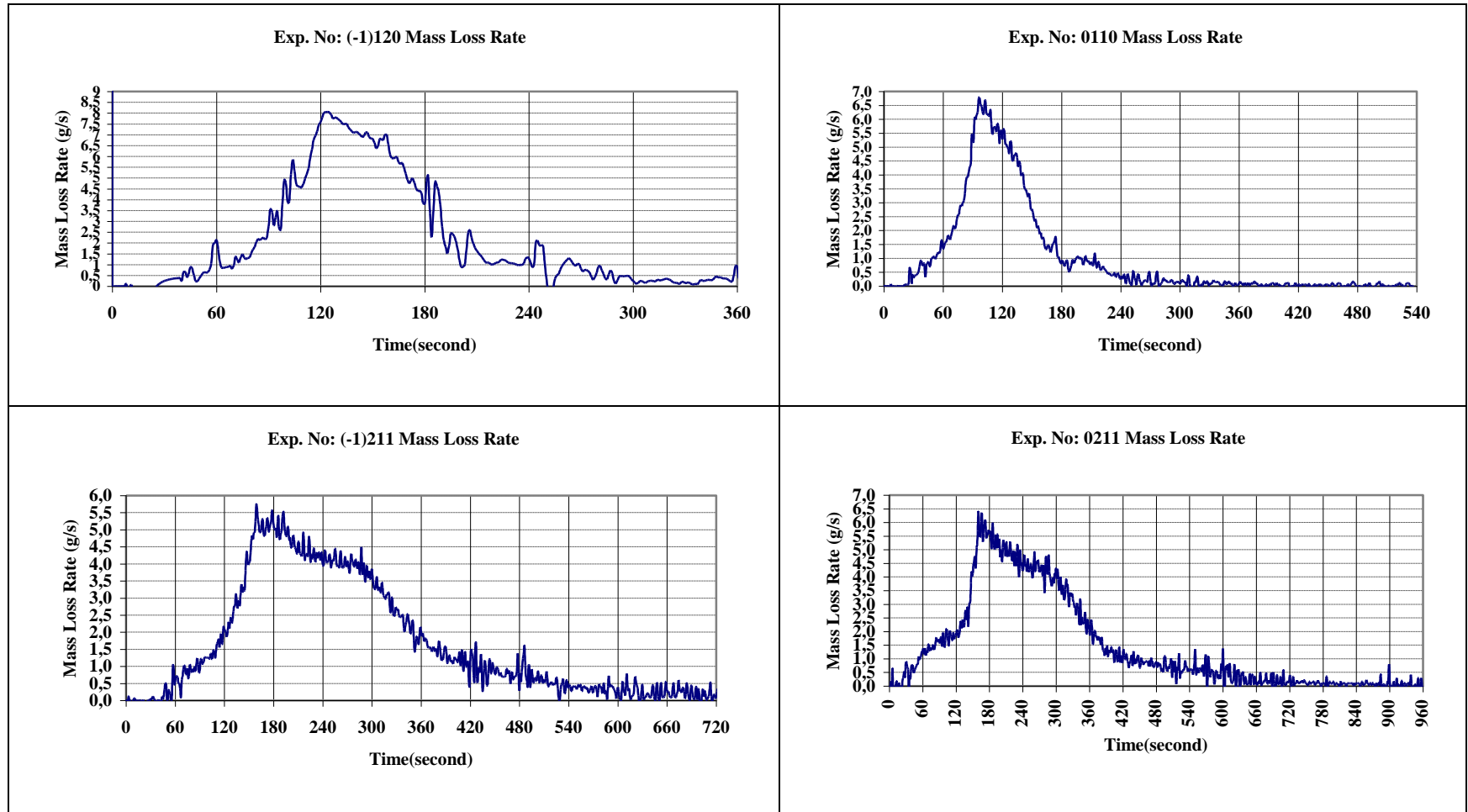


Figure 5.11 Mass Loss Rate versus Time Variation of Experiment No: (-1)120 - 0110 - (-1)211 - 0211 (Table 5.1 pg.86)

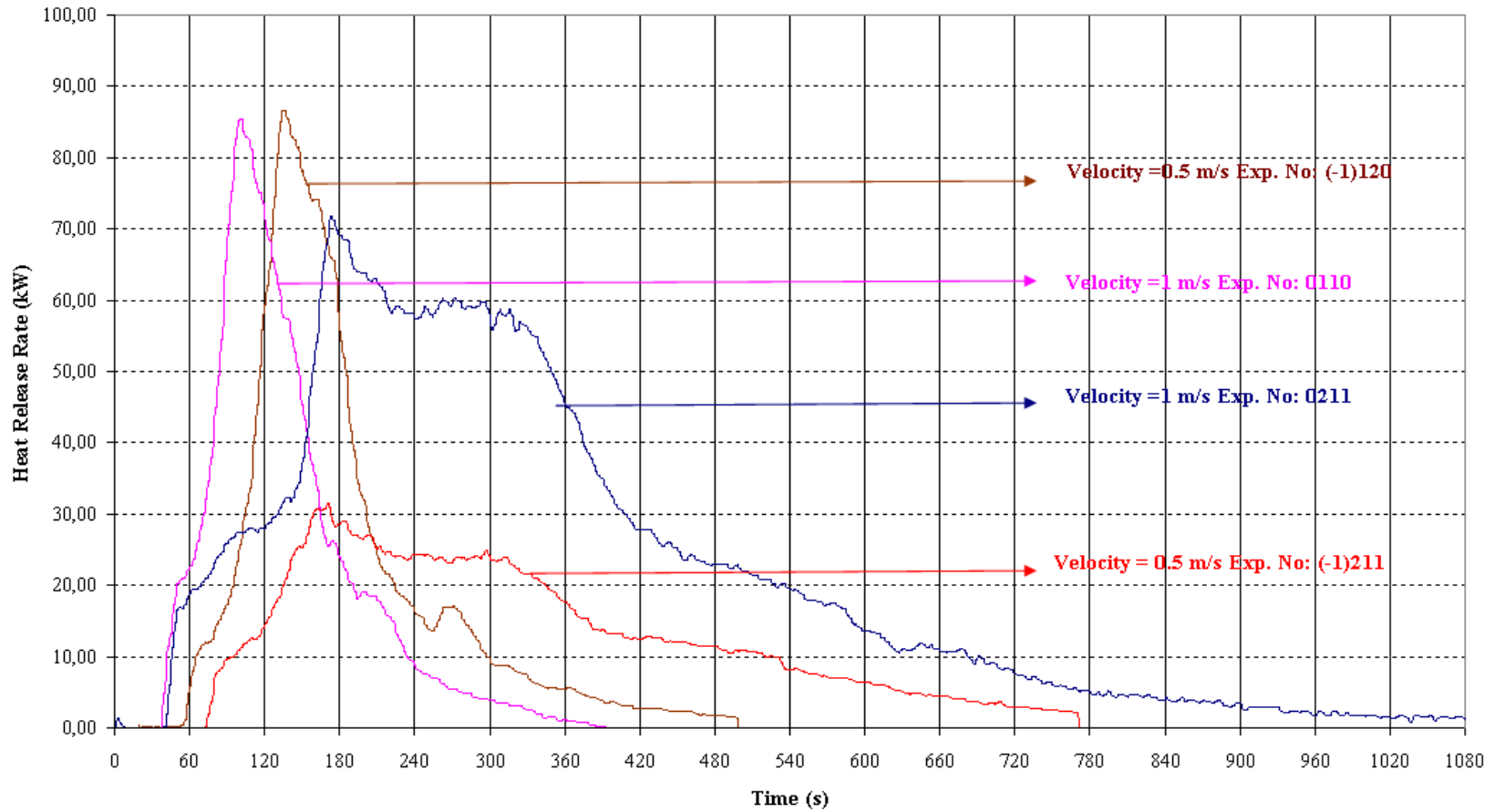


Figure 5.12 Heat Release Rate versus Time Variation of Experiment No: (-1)120 - 0110 - (-1)211 - 0211 (Table 5.1 pg.86)

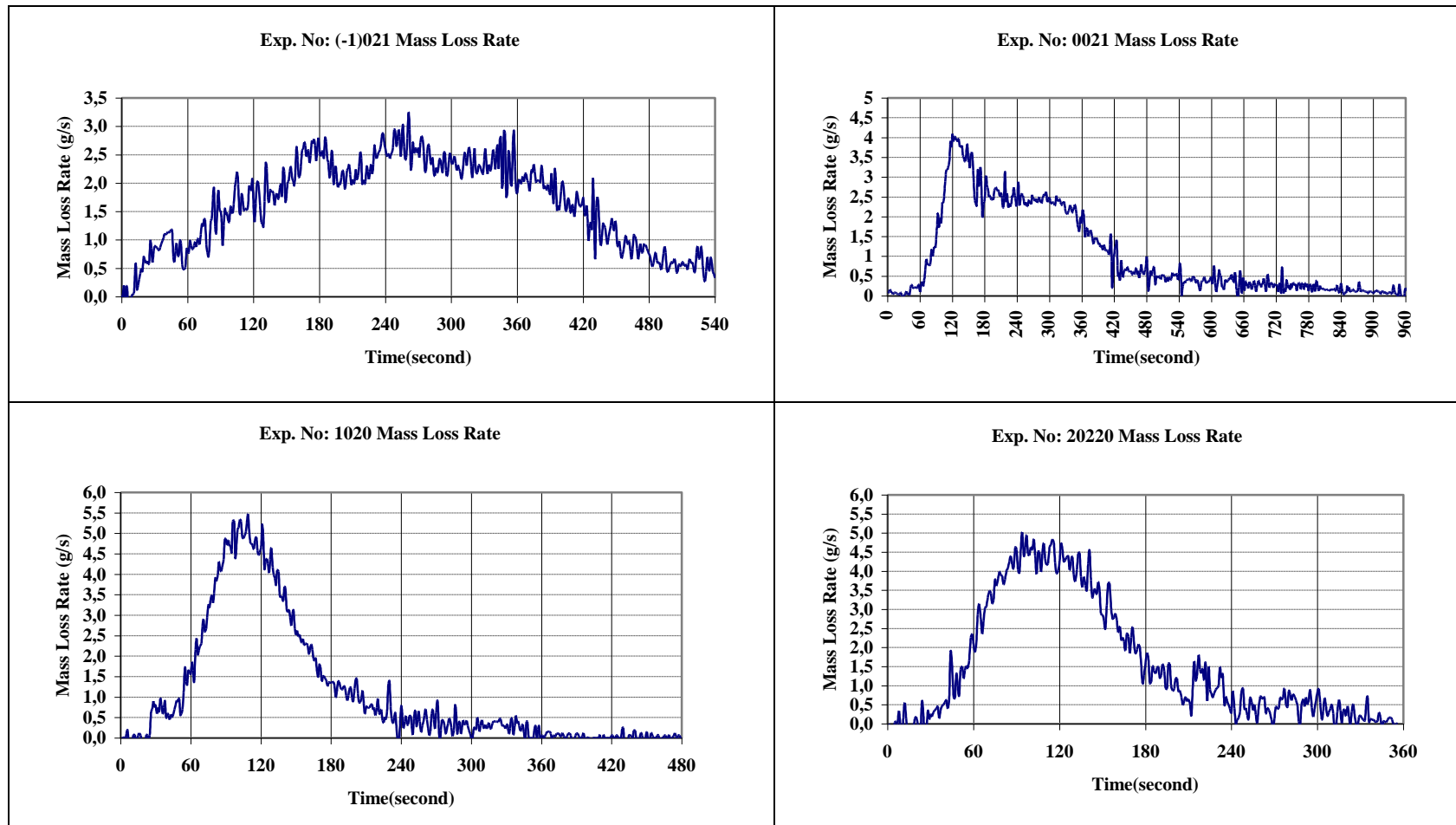


Figure 5.13 Mass Loss Rate versus Time Variation of Experiment No: (-1)021 - 0021 - 1020 - 20220 (Table 5.1 pg.86)

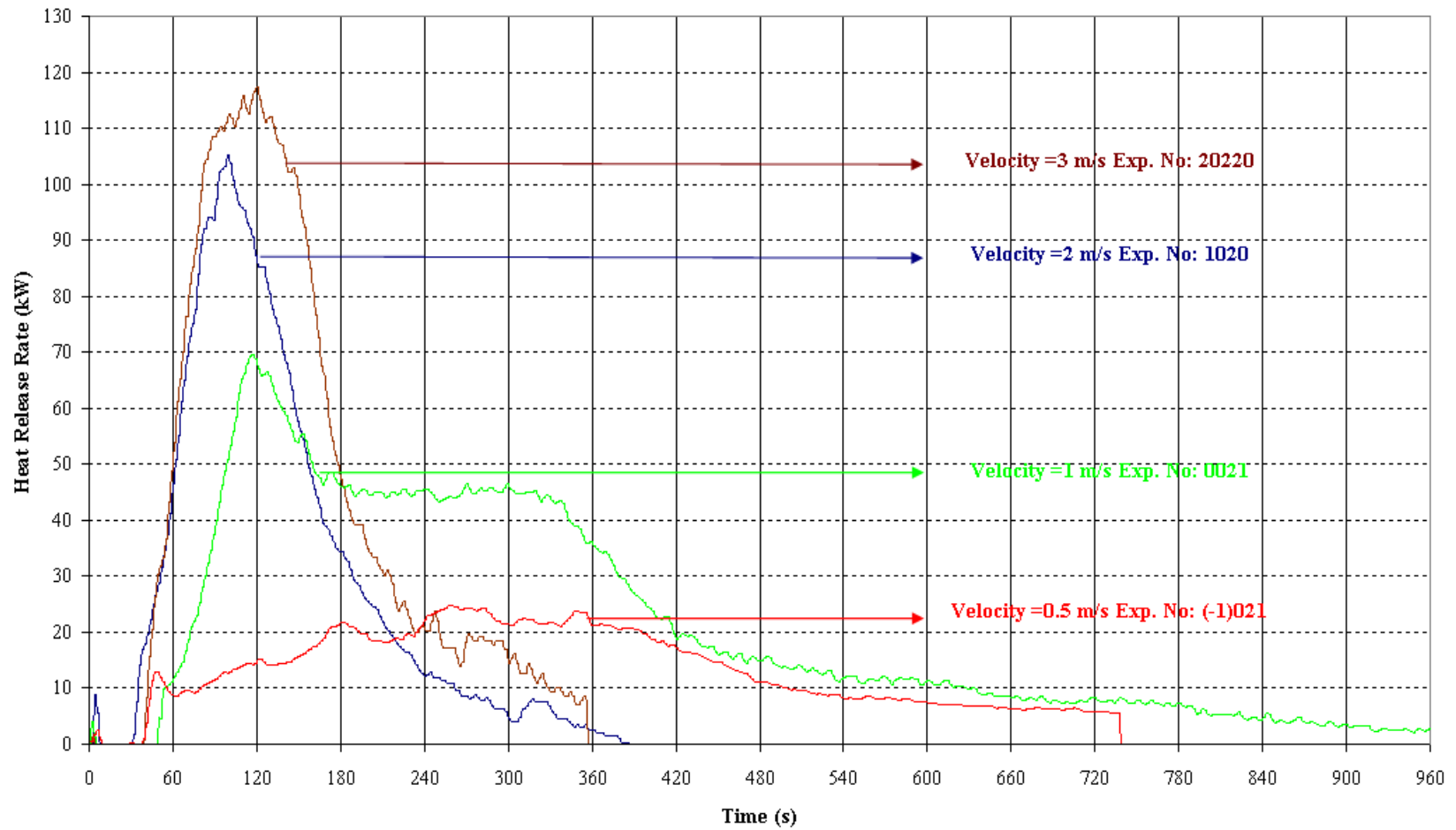


Figure 5.14 Heat Release Rate versus Time Variation of Experiment No: (-1)021 - 0021 - 1020 - 20220 (Table 5.1 pg.86)

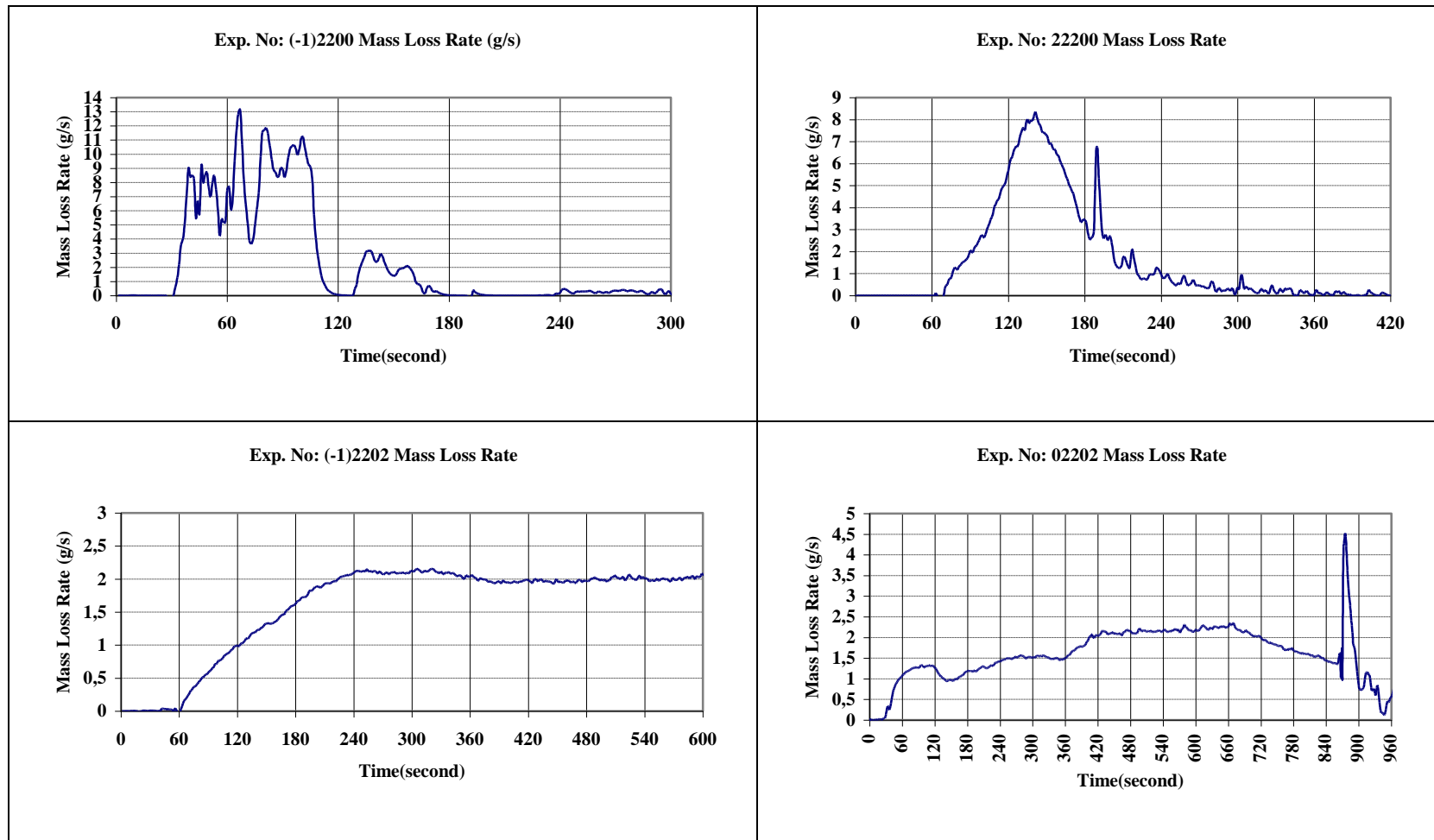


Figure 5.15 Mass Loss Rate versus Time Variation of Experiment No: (-1)2200 - 22200 - (-1)2202 - 02202 (Table 5.1 pg.86)

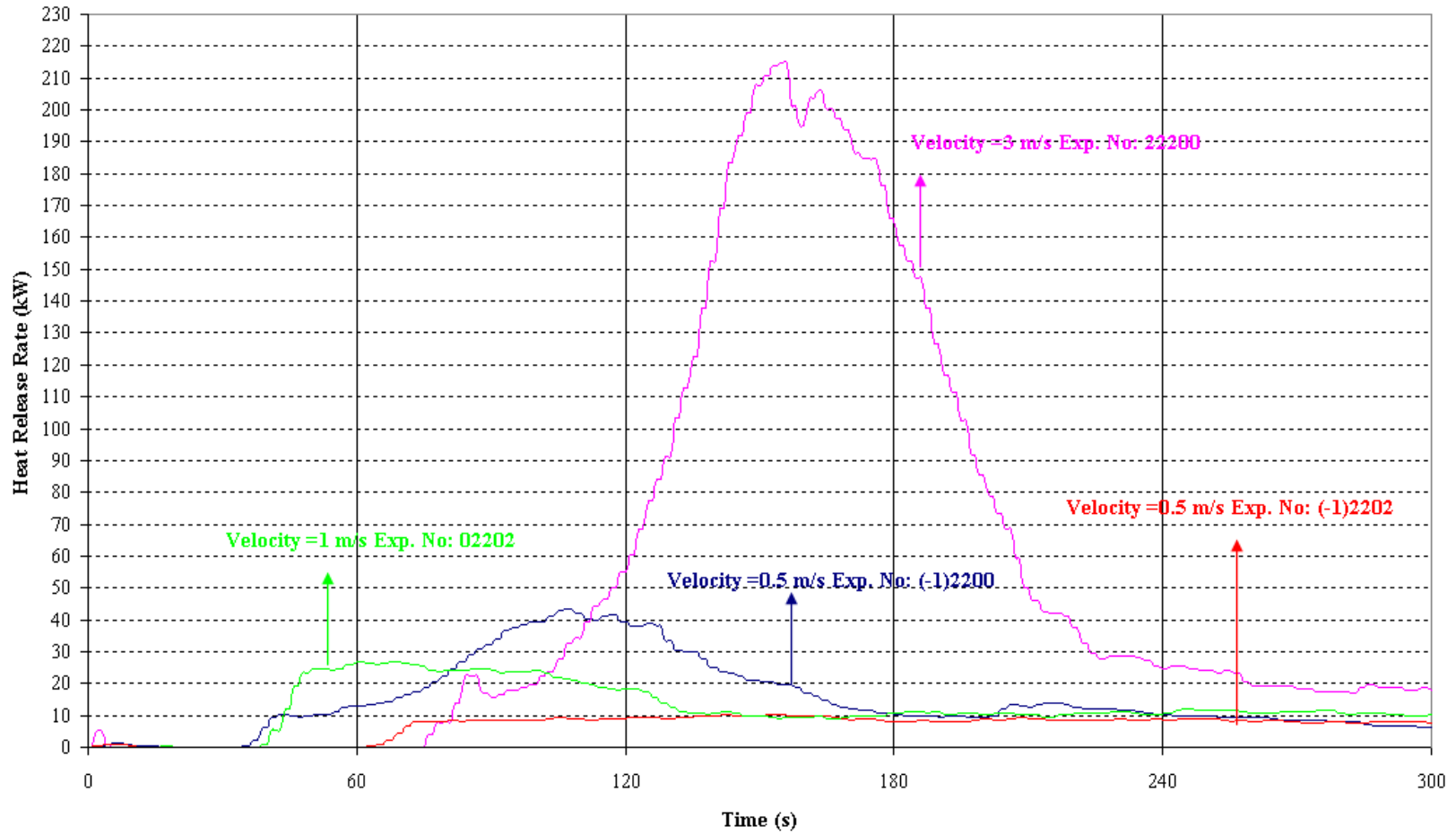


Figure 5.16 Heat Release Rate versus Time Variation of Experiment No: (-1)2200 - 22200 - (-1)2202 - 02202 (Table 5.1 pg.86)

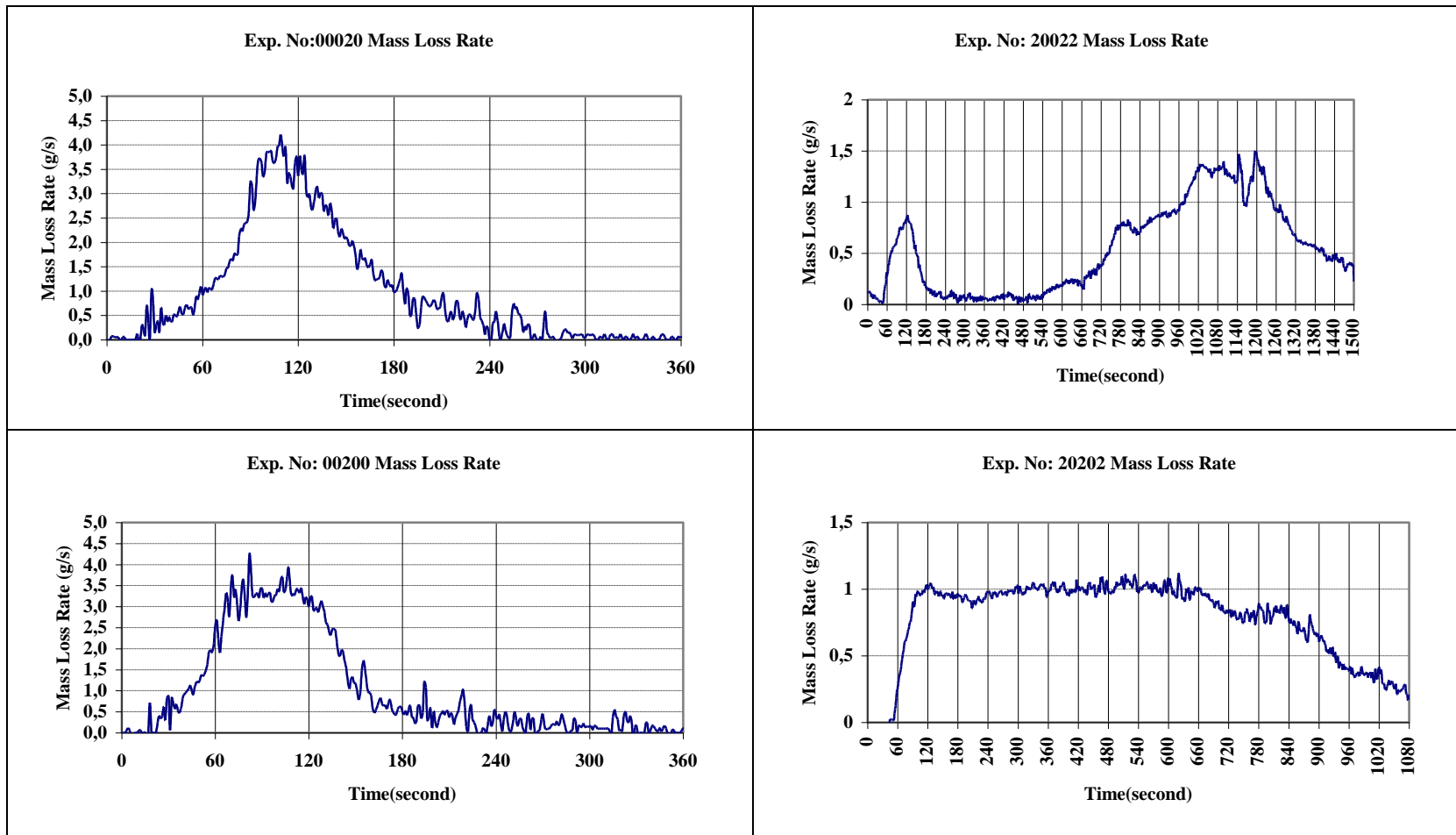


Figure 5.17 Mass Loss Rate versus Time Variation of Experiment No: 20022 - 00020 - 20202 - 00200 (Table 5.1 pg.86)

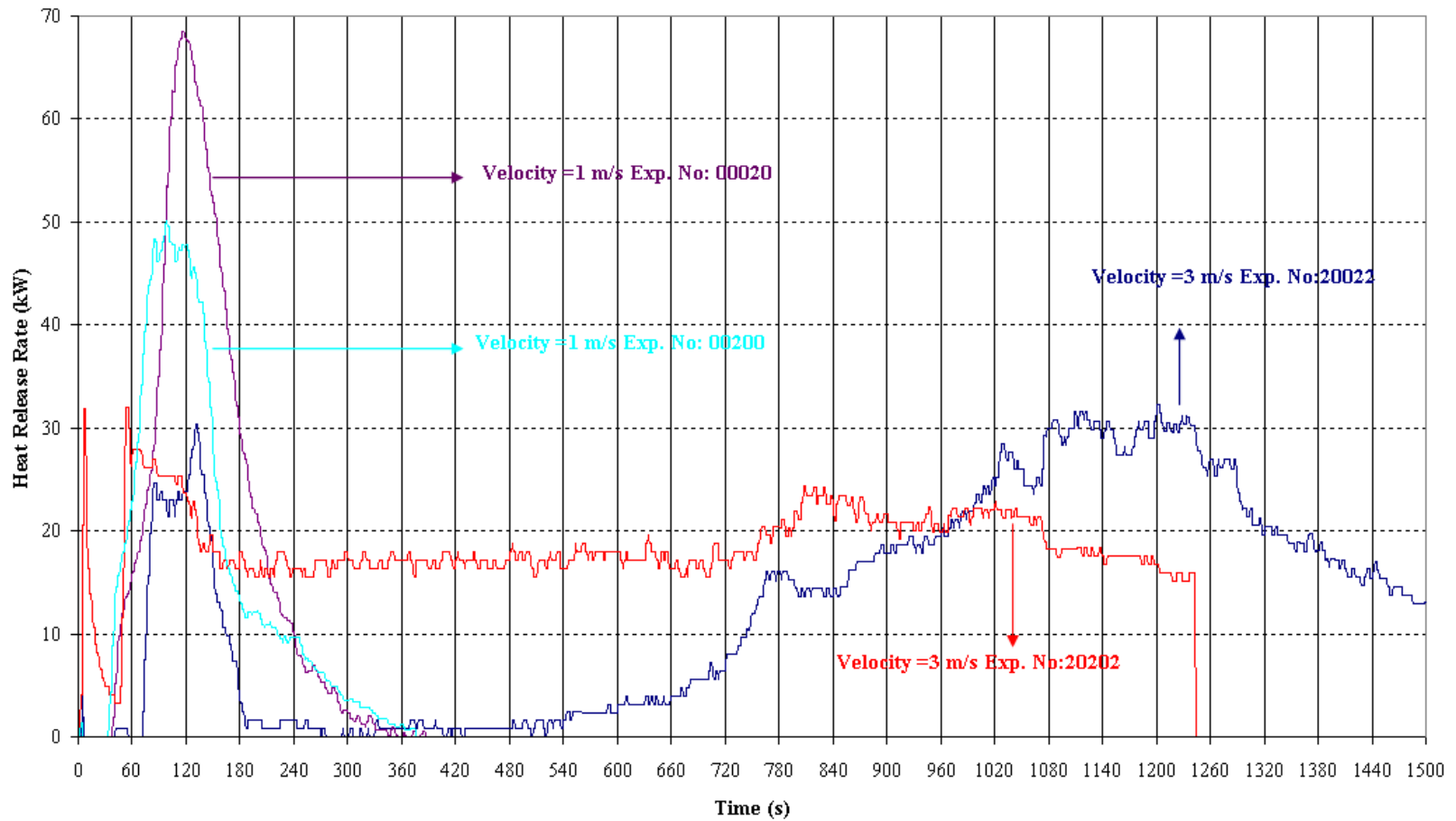


Figure 5.18 Heat Release Rate versus Time Variation of Experiment No: 20022 - 00020 - 20202 - 00200 (Table 5.1 pg.86)

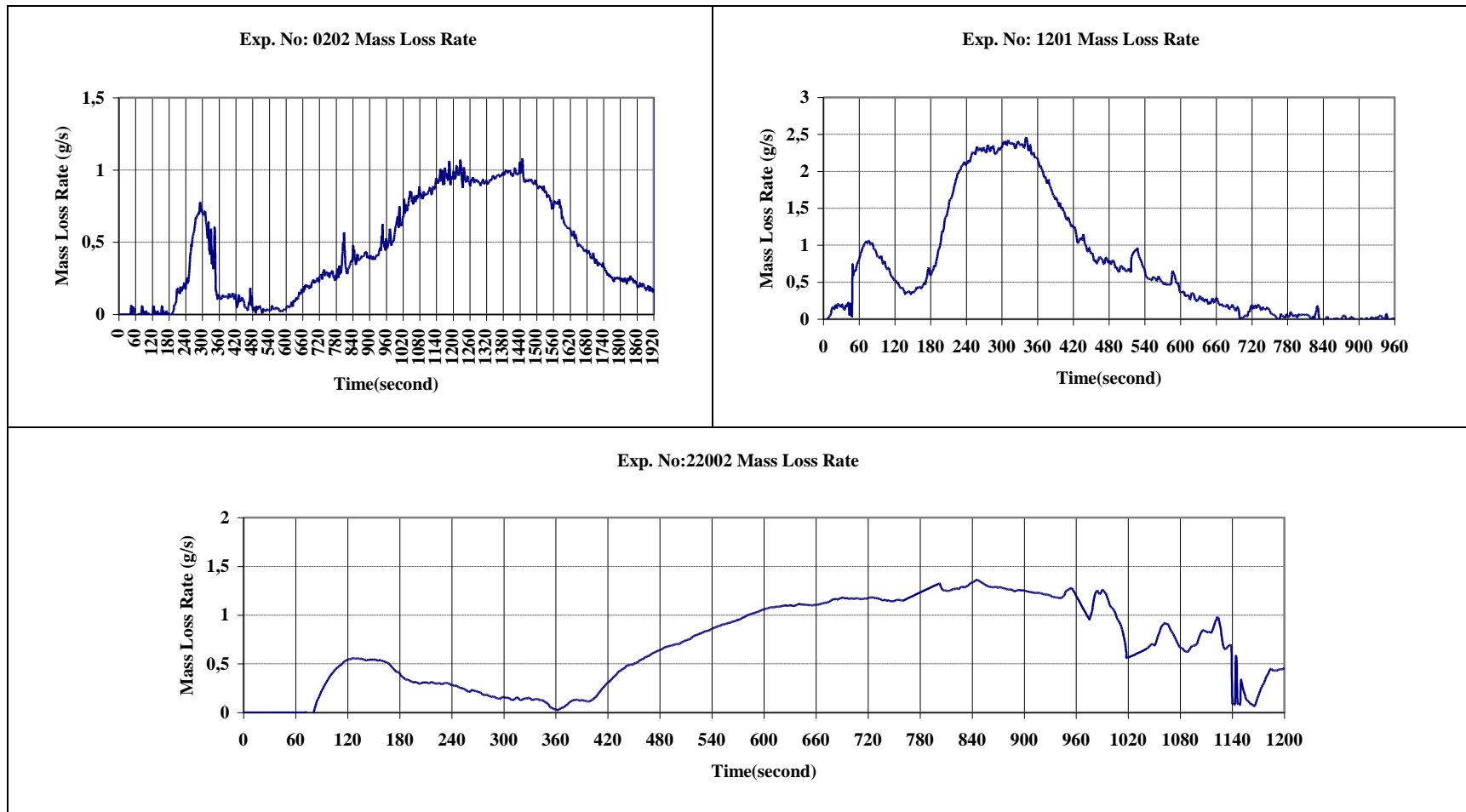


Figure 5.19 Mass Loss Rate versus Time Variation of Experiment No: 0202 - 22002 - 1201 (Table 5.1 pg.86)

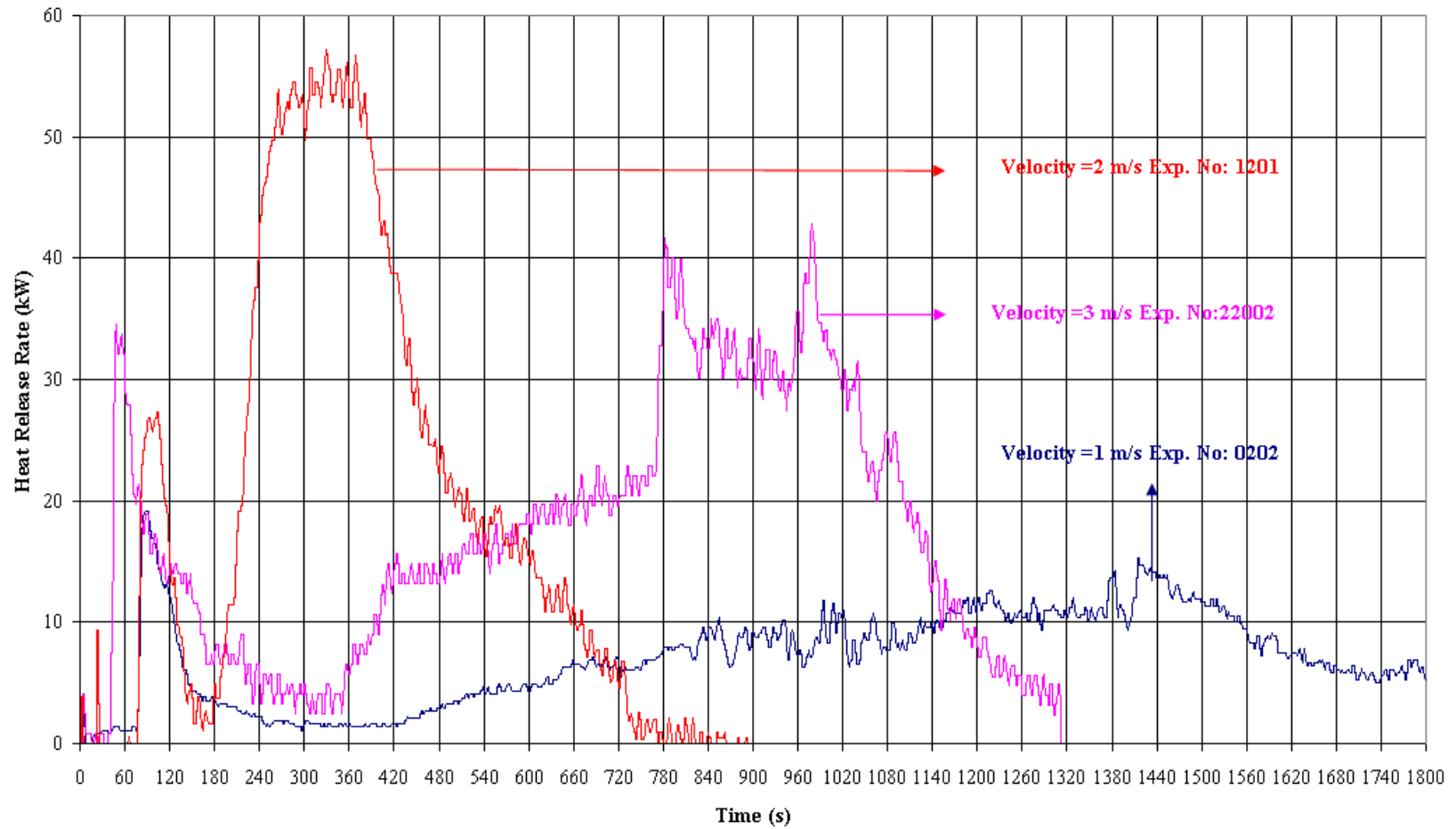


Figure 5.20 Heat Release Rate versus Time Variation of Experiment No: 0202 - 22002 - 1201 (Table 5.1 pg.86)

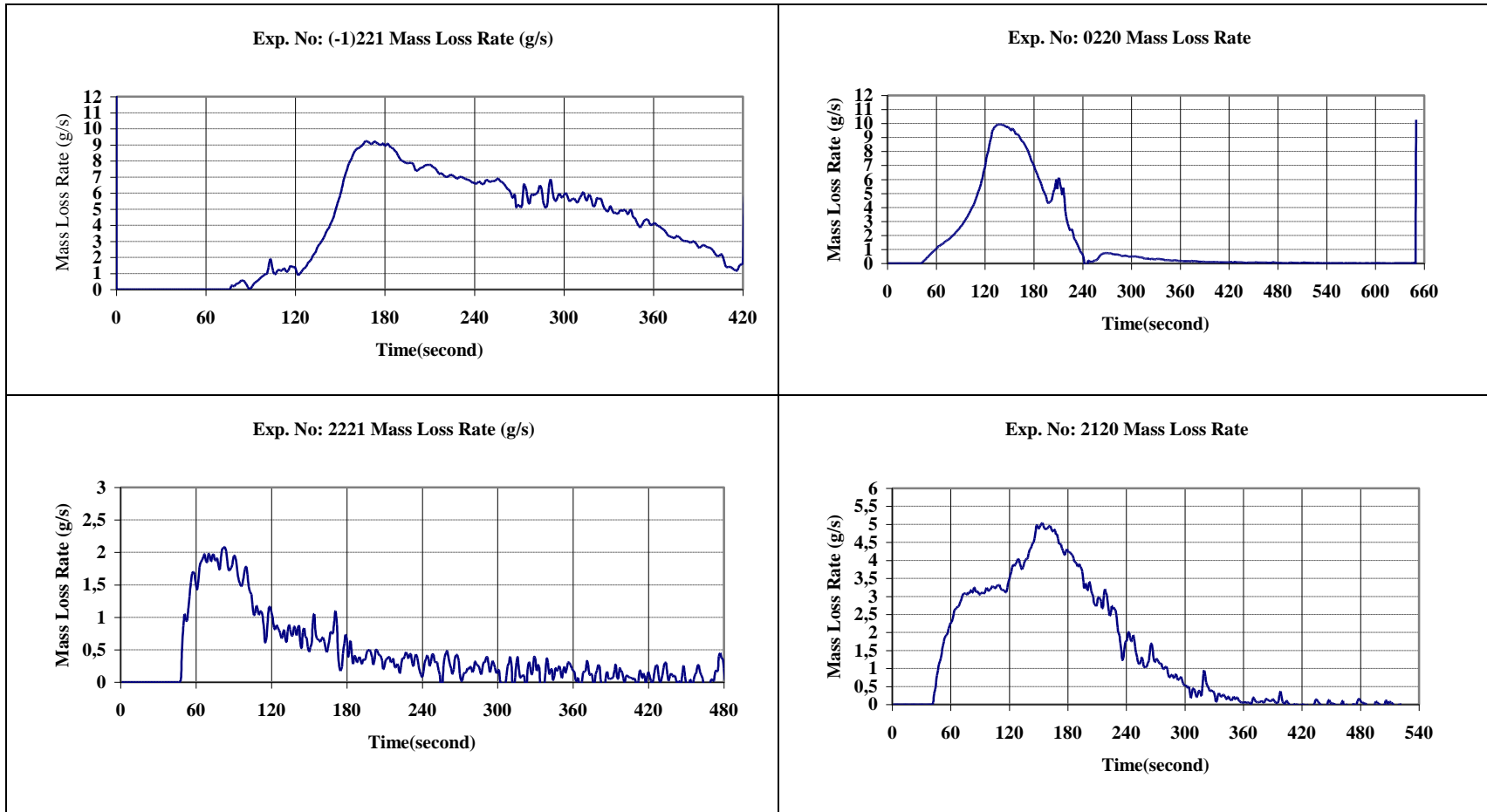


Figure 5.21 Mass Loss Rate versus Time Variation of Experiment No: (-1)221 - 2221 - 0220 - 2120 (Table 5.1 pg.86)

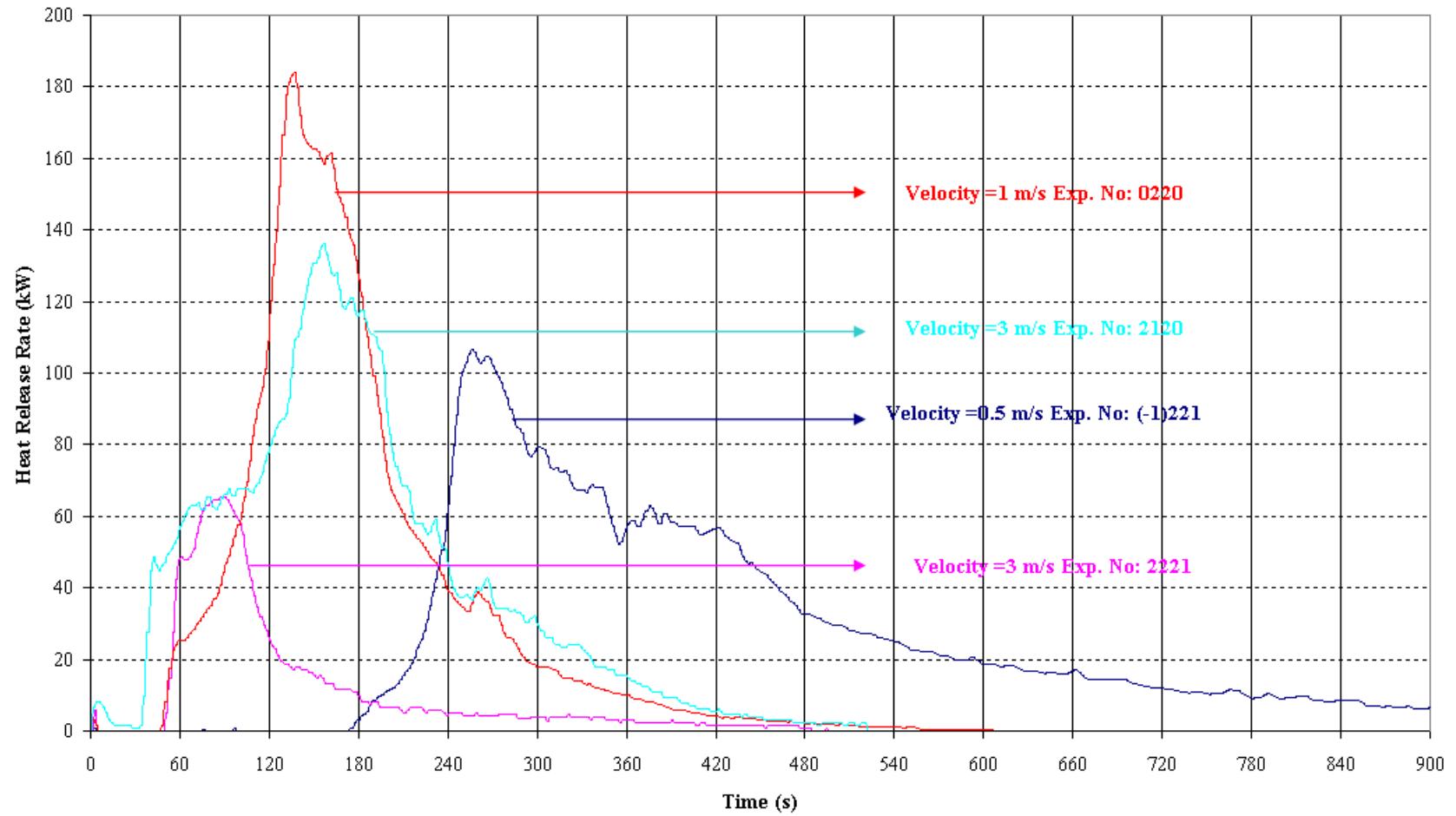


Figure 5.22 Heat Release Rate versus Time Variation of Experiment No: (-1)221 - 2221 - 0220 - 2120 (Table 5.1 pg.86)

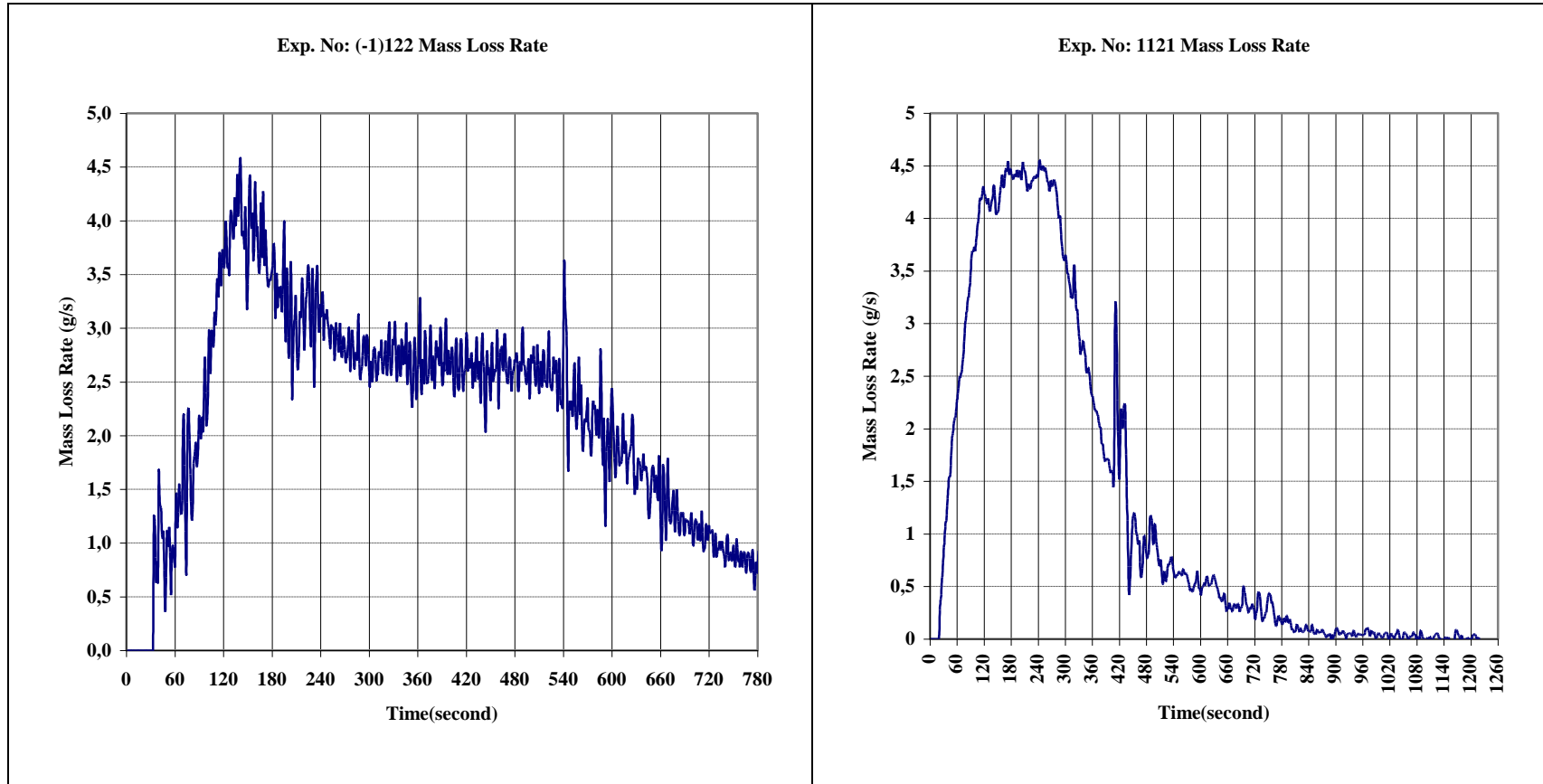


Figure 5.23 Mass Loss Rate versus Time Variation of Experiment No: (-1)122 - 1121 (Table 5.1 pg.86)

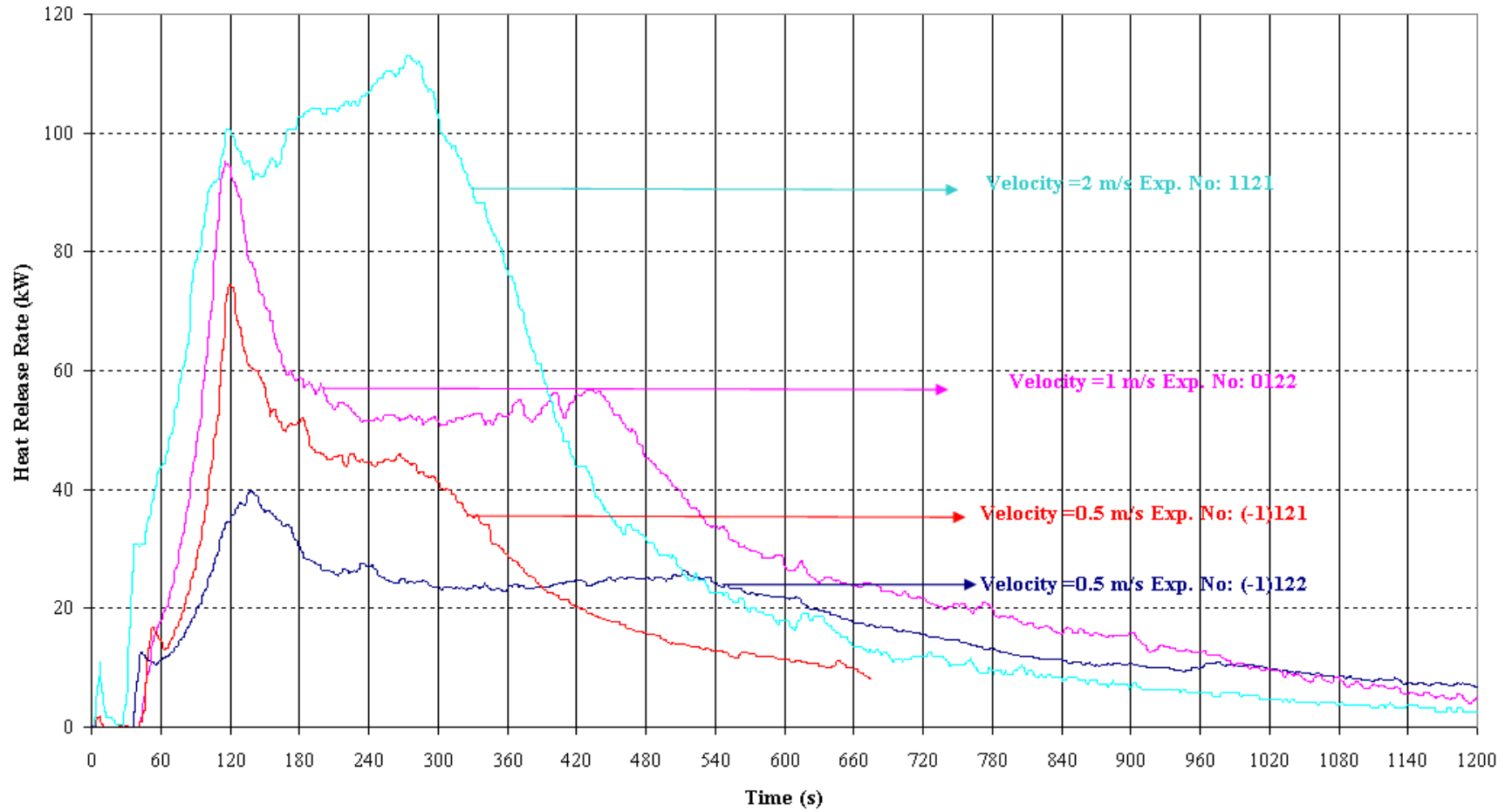


Figure 5.24 Heat Release Rate versus Time Variation of Experiment No: (-1)122 – 1121 – 0122 - (-1)1121 (Table 5.1 pg.86)

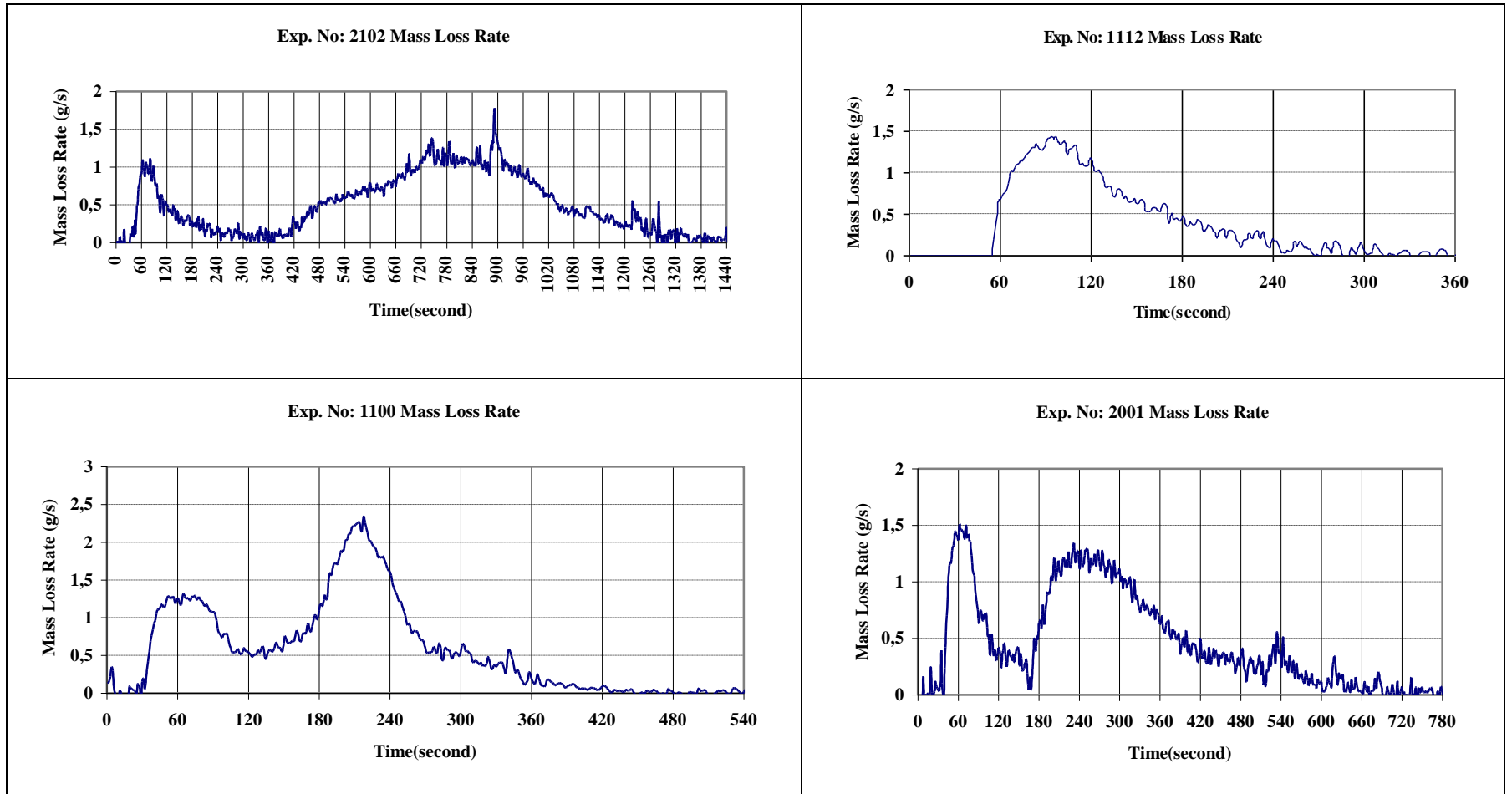


Figure 5.25 Mass Loss Rate versus Time Variation of Experiment No: 2102 – 1112 – 1100 - 2001(Table 5.1 pg.86)

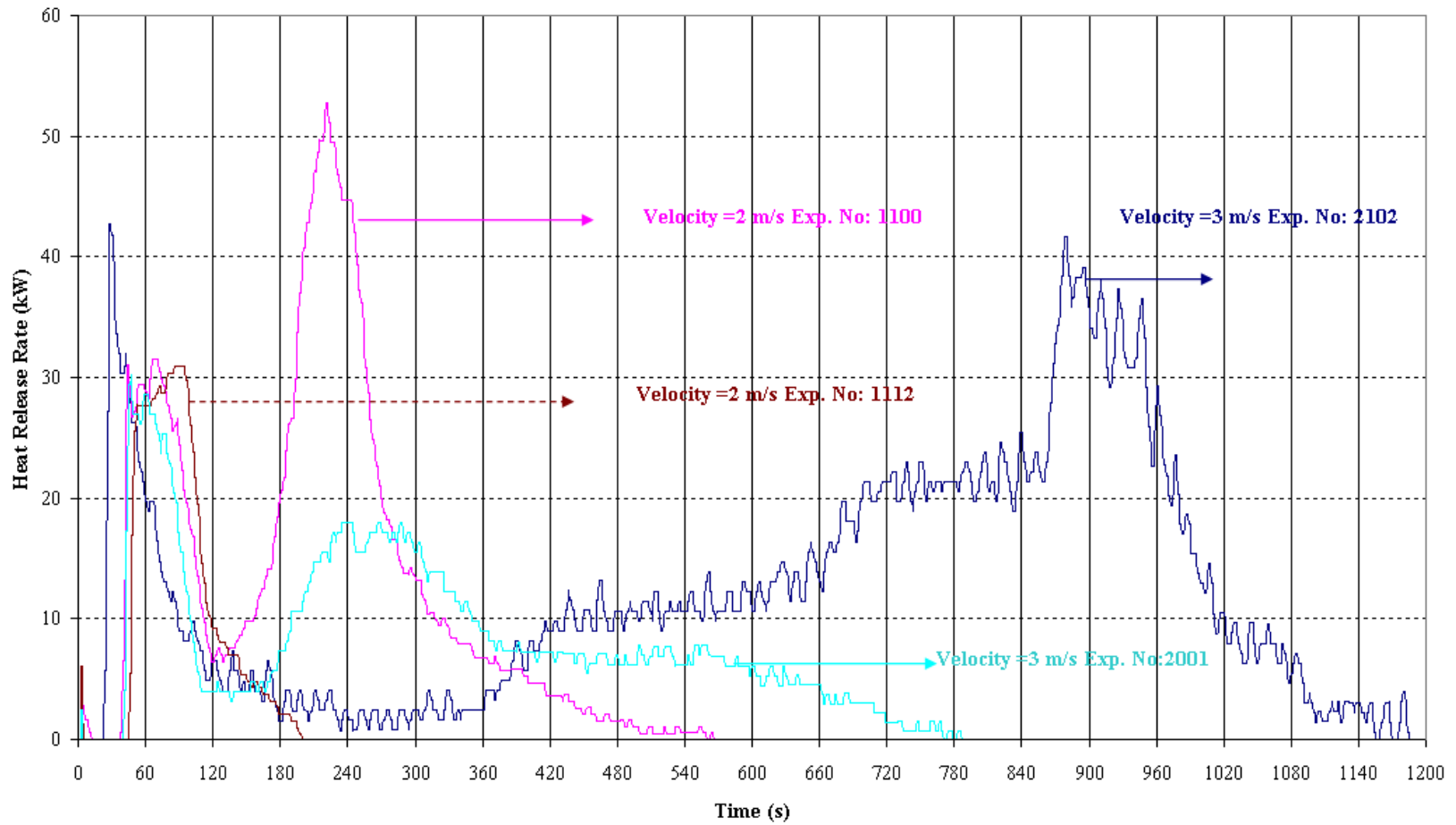


Figure 5.26 Heat Release Rate versus Time Variation of Experiment No: 2102 - 1112 - 1100 - 2001 (Table 5.1 pg.86)

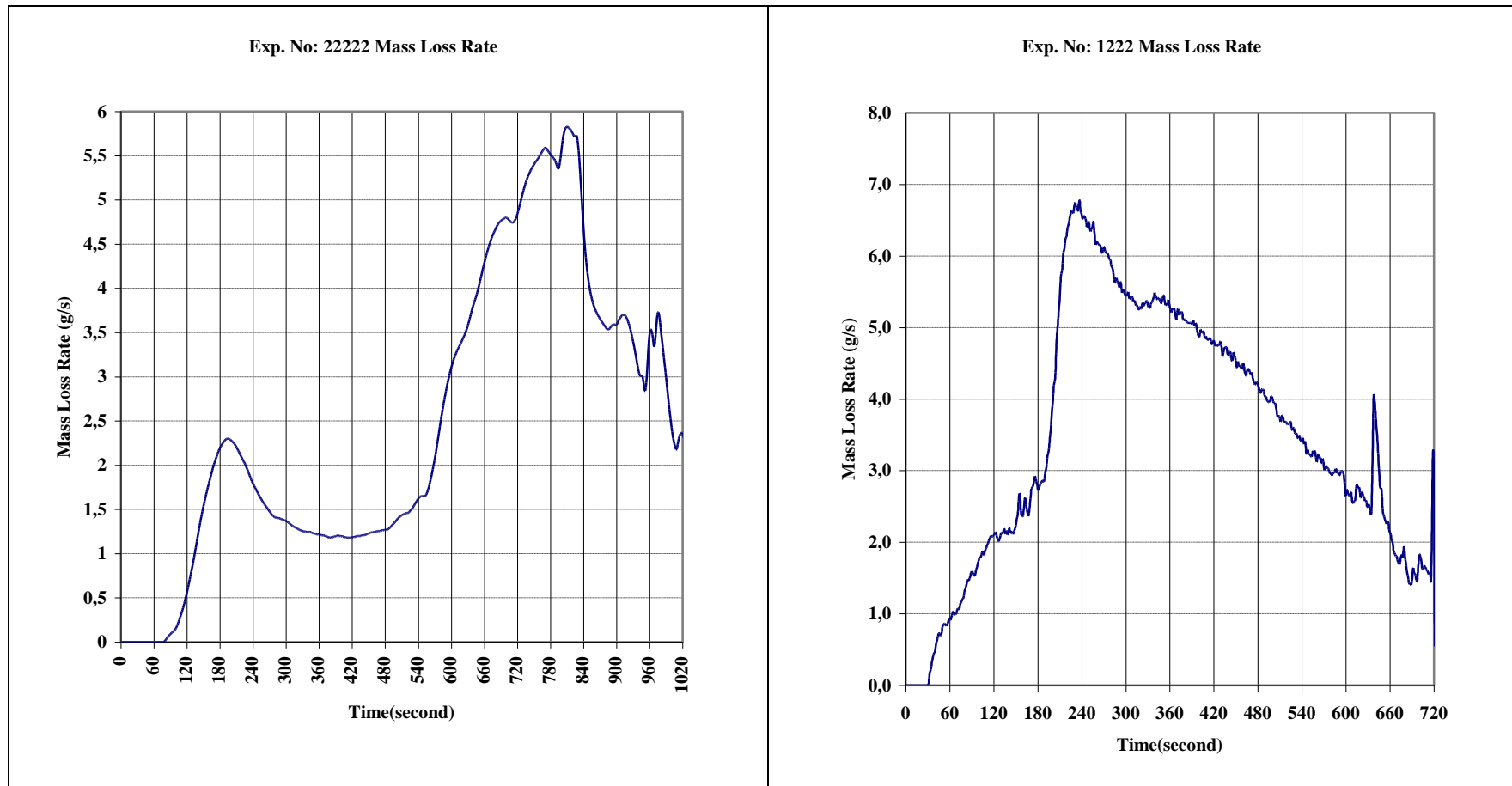


Figure 5. 27 Mass Loss Rate versus Time Variation of Experiment No: 1222 - 22222 (Table 5.1 pg.86)

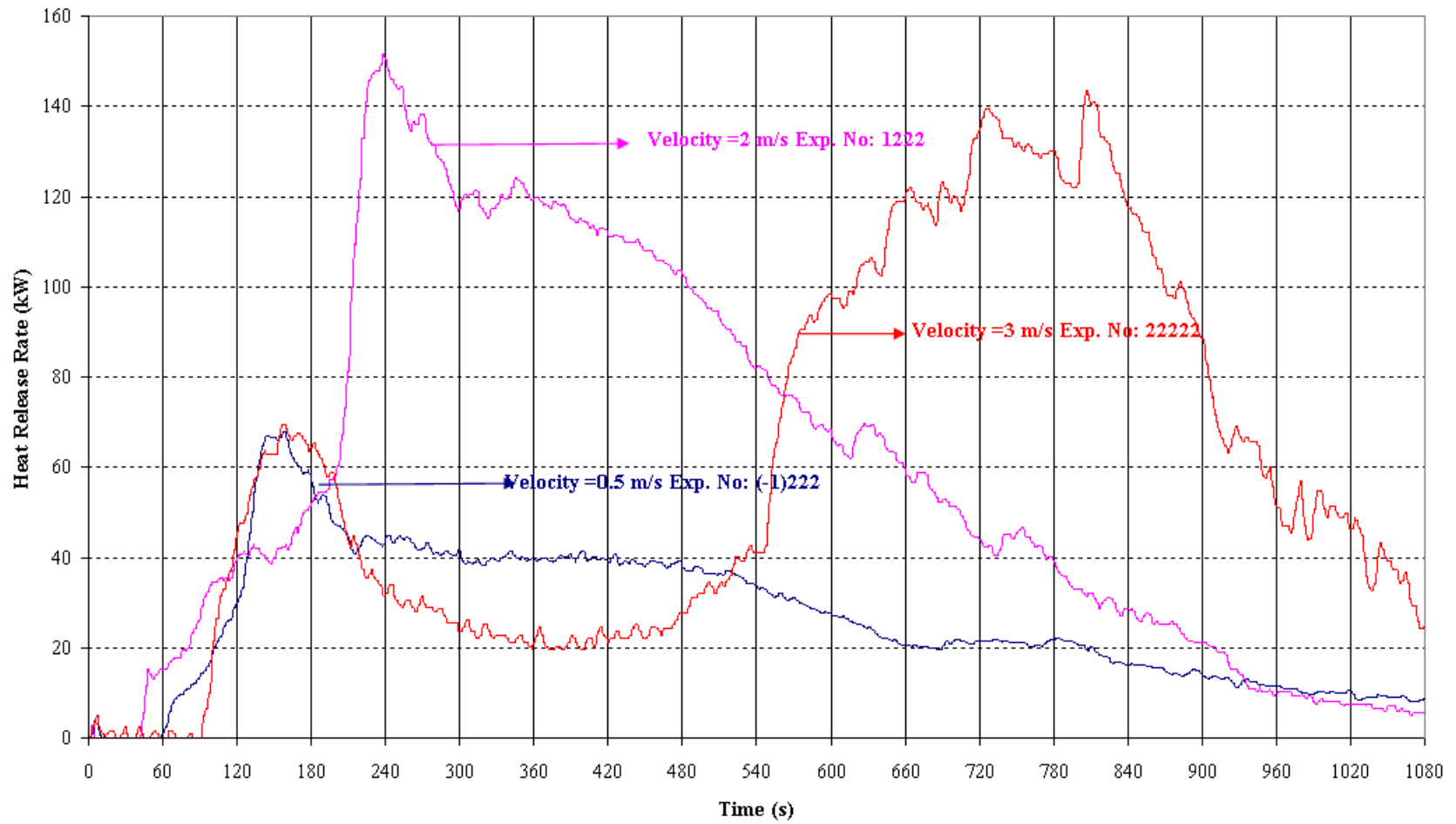


Figure 5.28 Heat Release Rate versus Time Variation of Experiment No: (-1)222 - 1222 - 22222 (Table 5.1 pg.86)

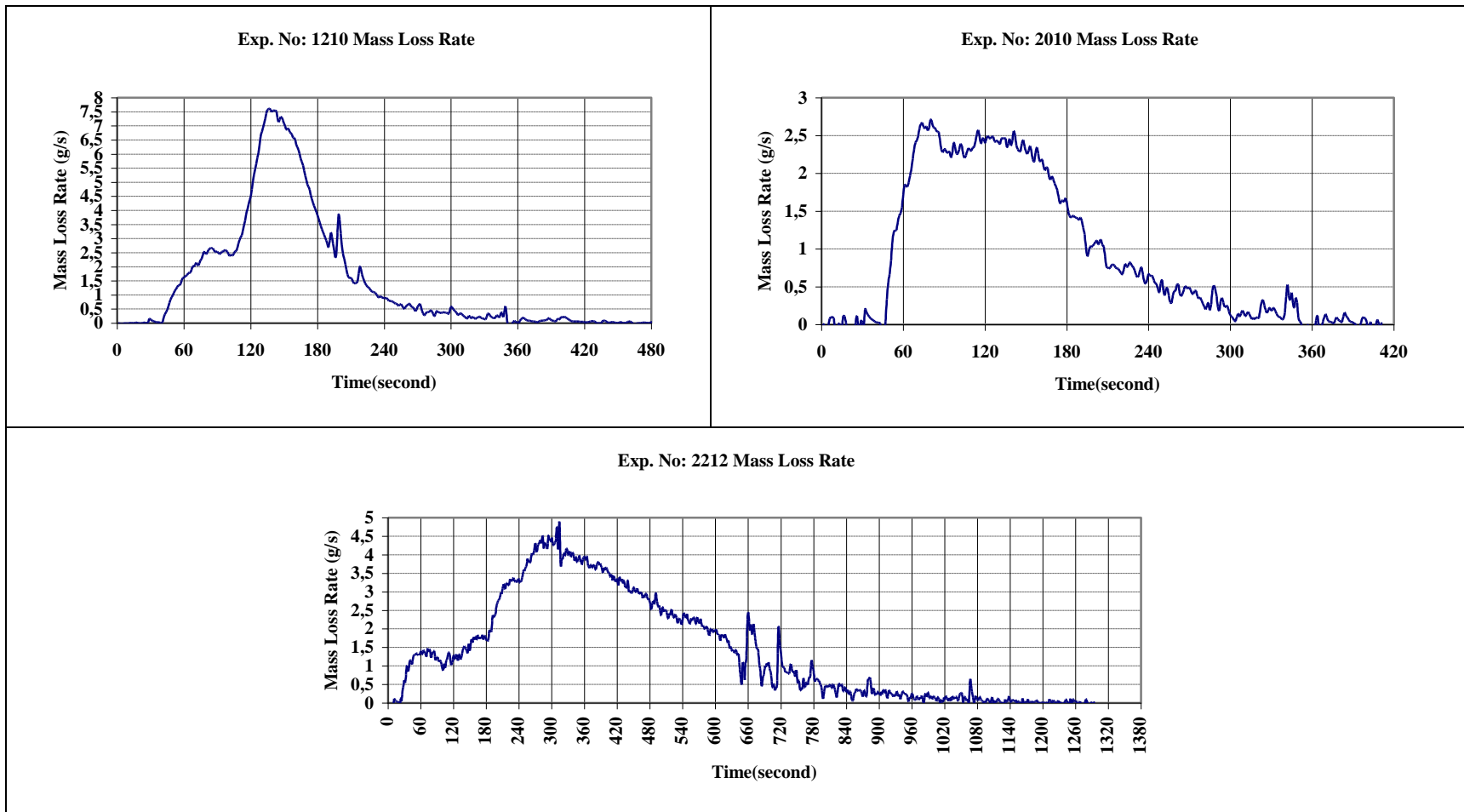


Figure 5.29 Mass Loss Rate versus Time Variation of Experiment No: 1210 - 2010 - 2212 (Table 5.1 pg.86)

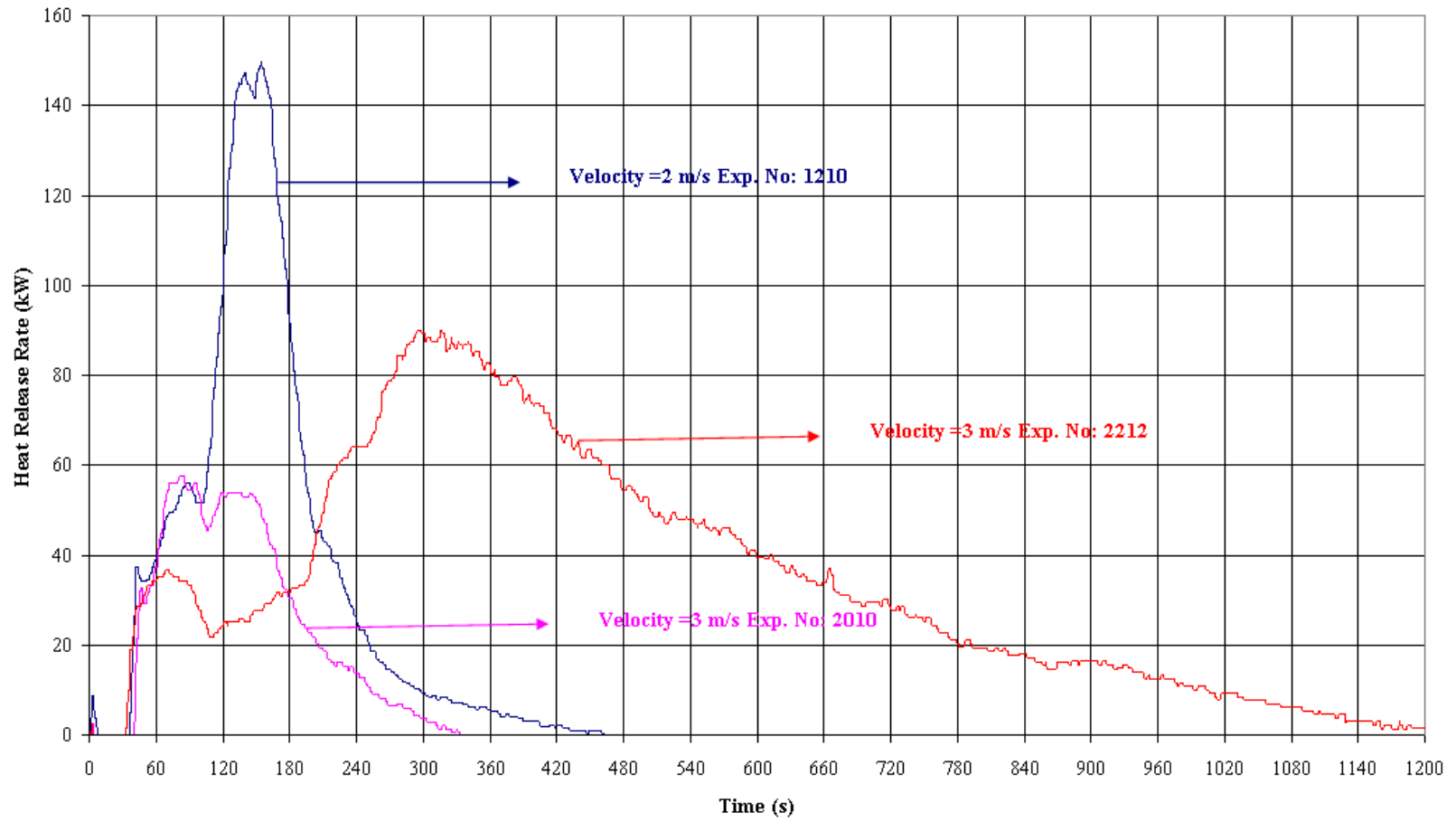


Figure 5.30 Heat Release Rate versus Time Variation of Experiment No: 1210 - 2010 - 2212 (Table 5.1 pg.86)

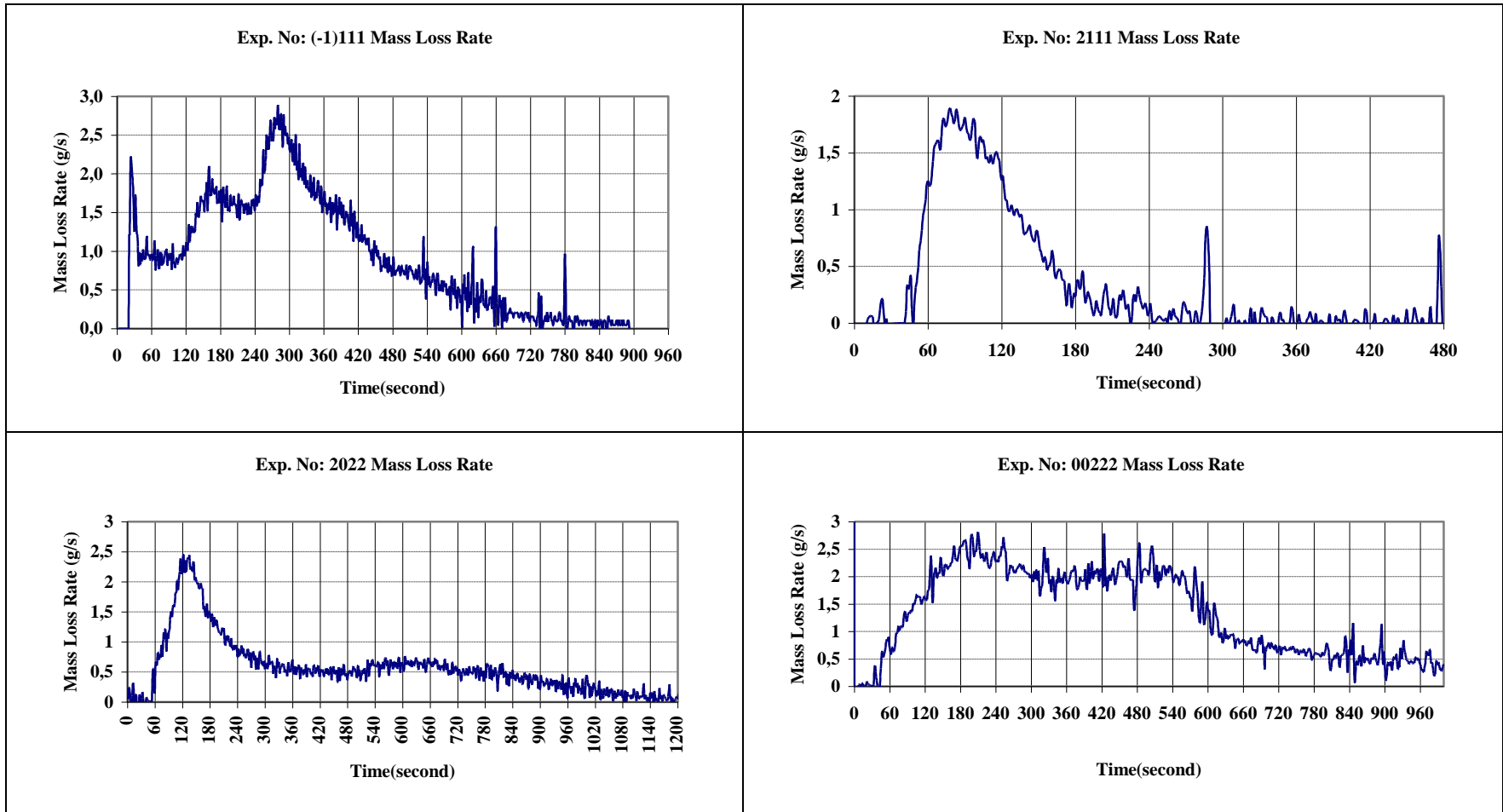


Figure 5.31 Mass Loss Rate versus Time Variation of Experiment No: (-1)111 - 2111 - 2022 - 00222 (Table 5.1 pg.86)

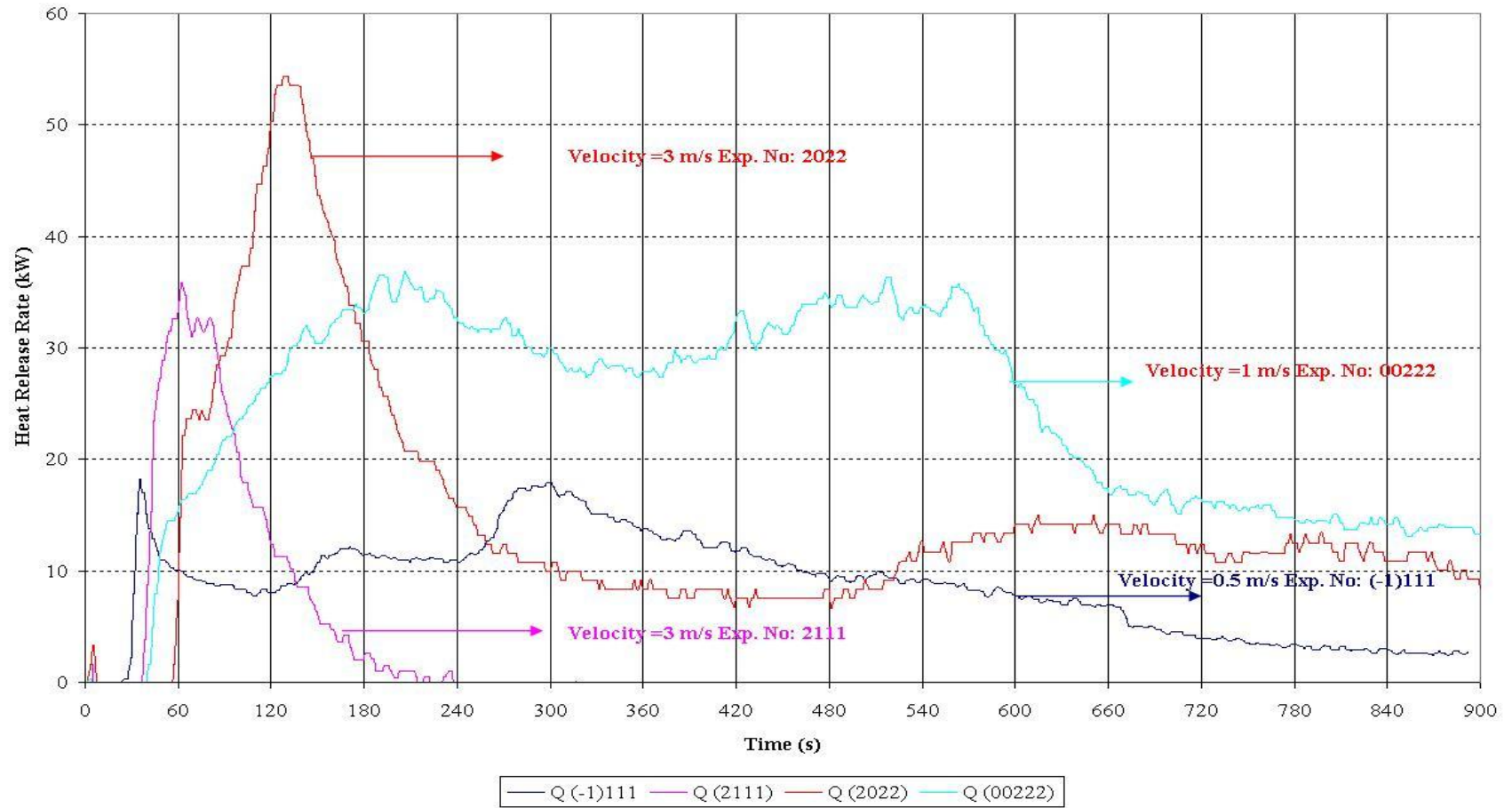


Figure 5.32 Heat Release Rate versus Time Variation of Experiment No: (-1)111 - 2111 – 2022 - 00222 (Table 5.1 pg.86)

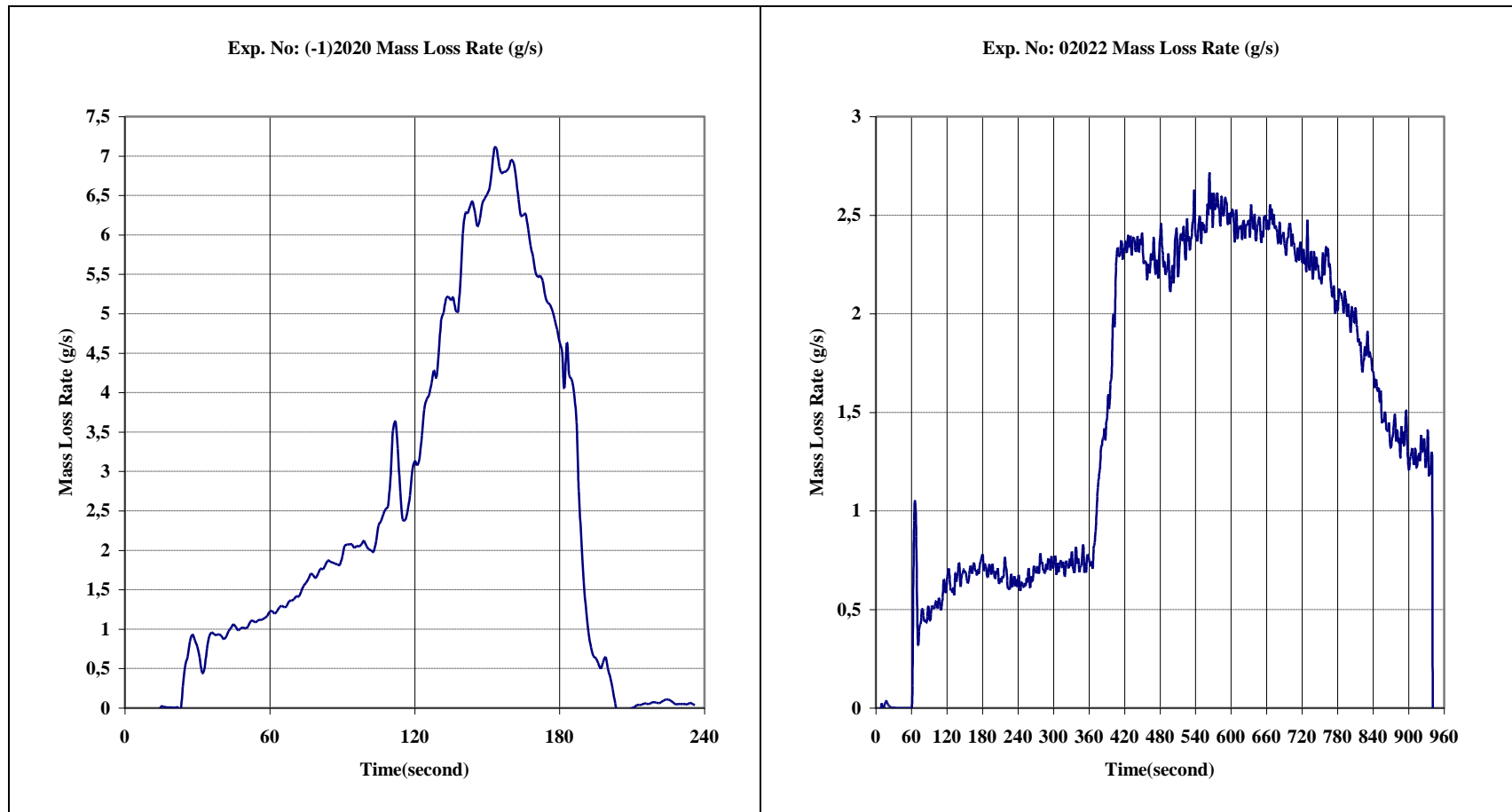


Figure 5.33 Mass Loss Rate versus Time Variation of Experiment No: (-1)2020 - 02022 (Table 5.1 pg.86)

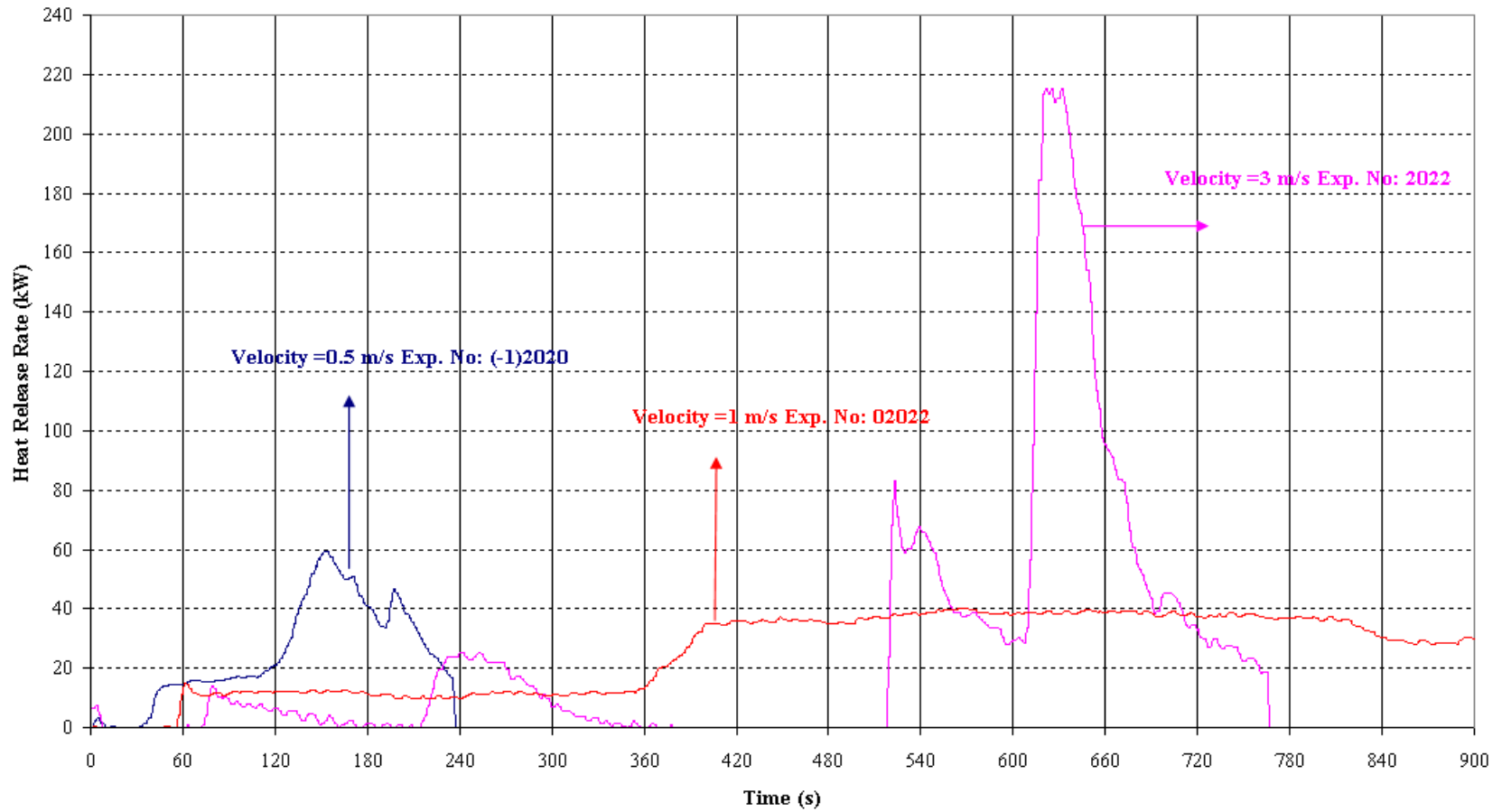


Figure 5.34 Heat Release Rate versus Time Variation of Experiment No: (-1)2020 – 22020 - 02022 (Table 5.1 pg.86)

CHAPTER 6

STATISTICAL ANALYSIS - ANALYSIS OF VARIANCE

6.1 Introduction

Analysis of Variance (ANOVA) is a collection of statistical models which is used to analyze the effect of factors on a response. This method explains the variation in the response by using the predetermined factors. The following conclusions can be reached by using ANOVA [52]

- a) which factors have a significant effect on the response, and/or
- b) how much of the variability in the response variable is attributable to each factor.

According to reference [43], ANOVA was developed by the English statistician, R.A. Fisher (1890-1962). He used this methodology to deal with agricultural data, but today ANOVA is applied to many other fields for data analysis. The types of ANOVA mentioned in this study are as follows;

- 1) One-Way ANOVA is used when there is only a single factor with several levels and multiple observations at each level. One-way ANOVA can be used if there are statistically significant differences among the level means.

- 2) Multifactor ANOVA is used when the researchers want to study the effects of two or more factors. Both main effects and interactions between the factors may be estimated.
- 3) General Linear Models are used whenever there are both crossed and nested factors, when some factors are fixed and some are random, and when both categorical and quantitative factors are present.

“The name analysis of variance is derived from a partitioning of total variability into its component parts” according to reference [43]. In this study, One-way ANOVA is mentioned briefly. Detailed information for the other methods can be obtained from reference [43]. Suppose the researcher investigates effect of one factor on the response and do experiments for each factor level. The data taken from the experiments with total number of observation for each factor level ($N=an$) as listed in Table 6.1.

Table 6.1 Typical Data for Single Factor Experiments

Level	Observations	Total $y_{i.} = \sum_{j=1}^n y_{ij}$	Averages $\bar{y}_{i.} = y_{i.} / n$
1	y ₁₁ y ₁₂ y _{1n}	y _{1.}	$\bar{y}_{1.}$
2	y ₂₁ y ₂₂ y _{2n}	y _{2.}	$\bar{y}_{2.}$
·			
·			
·			
A	y _{a1} y _{a2} y _{an}	y _{a.}	$\bar{y}_{a.}$
		$y_{..} = \sum_{i=1}^a \sum_{j=1}^n y_{ij}$	$\bar{y}_{..} = y_{..} / N$

The total variability in the data is calculated from the data set called as the total sum of squares by Equation 6.1.

$$SS_T = \sum_{i=1}^a \sum_{j=1}^n y_{ij} - \bar{y}_{..}^2 \quad \text{Eq. 6.1}$$

This equation can be rewritten as in the following form

$$SS_T = n \sum_{i=1}^a \bar{y}_{i.} - \bar{y}_{..}^2 + \sum_{i=1}^a \sum_{j=1}^n y_{ij} - \bar{y}_{i.}^2 \quad \text{Eq. 6.2}$$

First term and second term in Eq. 6.2 are represented as the sum of squares of the differences between the level averages and the total average (measure of differences due to level mean) and a sum of squares of the differences of observations within the levels from the level average (random error). Finally, sum of squares terms can be expressed as

$$SS_T = SS_{Level} + SS_{Error} \quad \text{Eq. 6.3}$$

SST has N-1 degree of freedom. SS_{level} has a-1 degrees of freedom and error has N-a degree of freedom. The variation mean squares can be calculated

$$MS_{Level} = \frac{SS_{Level}}{a-1} \quad \text{Eq. 6.4}$$

$$MS_{Error} = \frac{SS_{Error}}{N-a} \quad \text{Eq. 6.5}$$

The test procedure is summarized in Table 6.2. There are different in the factor means if $F_o > F_{\alpha, a-1, N-a}$ (percentage points of F distribution) where α means level of significance. Another decision can be made from p-value approach. According to D. Montgomery [43], the P-value is the smallest level of significance that would lead to verify the occurrence of differences. In a nutshell, when the p-value is smaller than the level of significance, the data variation is significant.

Table 6.2 The Analysis of Variance Table for the Single Factor, Fixed Effect Model

Source of variation	Sum of Squares	Degrees of freedom	Mean Square	F _o
Between Levels	$SS_{Levels} = n \sum_{i=1}^a \bar{y}_i - \bar{y}_{..}^2$	a-1	$MS_{Level} = \frac{SS_{Level}}{a-1}$	$F_o = \frac{MS_{Level}}{MS_E}$
Error	$SS_{Error} = SS_T - SS_{Level}$	N-a	$MS_{Error} = \frac{SS_{Error}}{N-a}$	
Total	$SS_T = \sum_{i=1}^a \sum_{j=1}^n y_{ij} - \bar{y}_{..}^2$	N-1		

6.2 Statistical Analysis of Experimental Results

The continuous variables have to be tested to show whether there is a relation between them. The statistical evaluation is performed by comparing the Pearson's correlation and p-values for the hypothesis test of the correlation coefficient being zero. Pearson's correlation coefficient (r) assesses whether two continuous variables are linearly related. The coefficient will fall between -1 and +1. The closer the absolute correlation is to 1, the more tightly the data points fall on a line. A correlation close to 0 indicates no linear relationship. The p-value tells if the correlation coefficient is significantly different from 0. If the p-value is less than or equal to your level of significance (α -value), then it can be concluded that the correlation is different from zero. If the p-value is greater than the α -level, then one can not conclude that the correlation is different from zero. One must select an α -level before conducting the test. It is possible to choose any value that is greater than 0.0 and less than 1.0. The 0.05 α -level is commonly used.

Table 6.3 Evaluation of Correlation Between Continuous Variables

		Height (cm)	Length (cm)	Thickness (cm)
Length(cm)	Pearson correlation	-0,000		
	P-Value	1.000		
Thickness(cm)	Pearson correlation	0.000	0,089	
	P-Value	1.000	0,634	
Wood Weight(gr)	Pearson correlation	0,410	0,656	0,580
	P-Value	0,003	0,000	0,694
Blockage Ratio	Pearson correlation	0,515	0,827	0,074
	P-Value	0,003	0,000	0,694
		Blockage Ratio	Porosity	
Porosity	Pearson correlation	0.539		
	P-Value	0.002		
As	Pearson correlation	0.879	0.520	
	P-Value	0.000	0.003	
Weight	Pearson correlation	0.799		
	P-Value	0.000		

From Table 6.3, it is not possible to perform a model with weight and blockage ratio, porosity and blockage ratio, length and height with blockage ratio, weight with length and height.

The first ANOVA is performed on the data used in order to investigate the importance of the main effects. The main effects are velocity, length, thickness, width, height. The analysis are performed from the experimental data taken from Experiment No: 00222, 20000, 00002, 02000, 22002, 20220, 02220, 22222, (-1)2200, 22200, (-1)2202, 02202, 20022, 00020, 20202, 00200, (-1)2020, 22020, 02022. ANOVA is performed by using Minitab 15.1 statistical analysis software. The variation of HRR and mass loss rate based on main effects are shown in Figure 6.1 and Figure 6.2.

According to Figure 6.1, the velocity, height, length and width are directly proportional to heat release rate. However, as the thickness of the sticks are increasing, the HRR is decreasing.

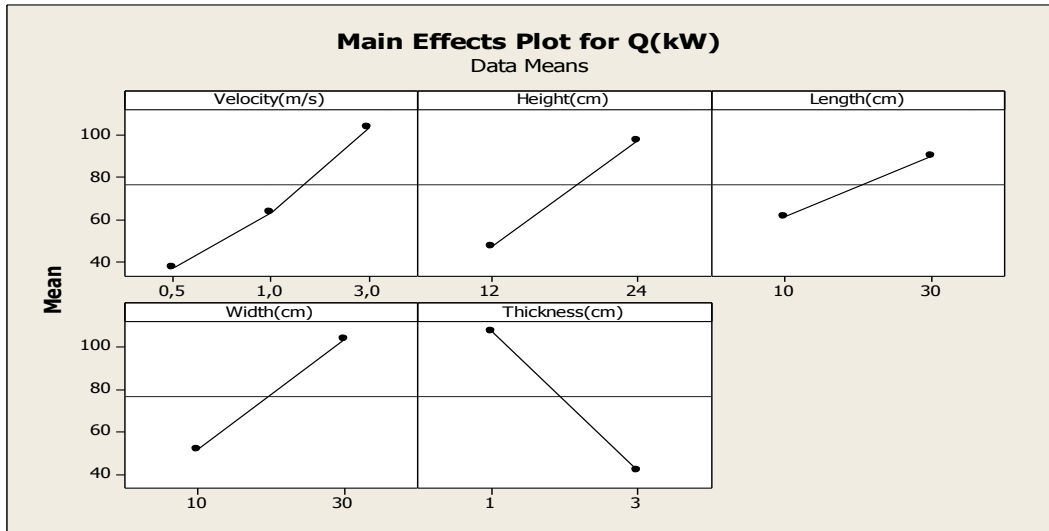


Figure 6.1 Main Effect Plots for Experiments in HRR ($L \neq W$)

According to Figure 6.2, the height, length and width are directly proportional to mass loss rate. However, the velocity seems that it has a negative influence on mass loss rate. This result is not so conservative due to the fact that the variation between the change in mass loss rate is only 0.5 g/s. Similar results for mass loss rate is obtained for the thickness variation as for the HRR.

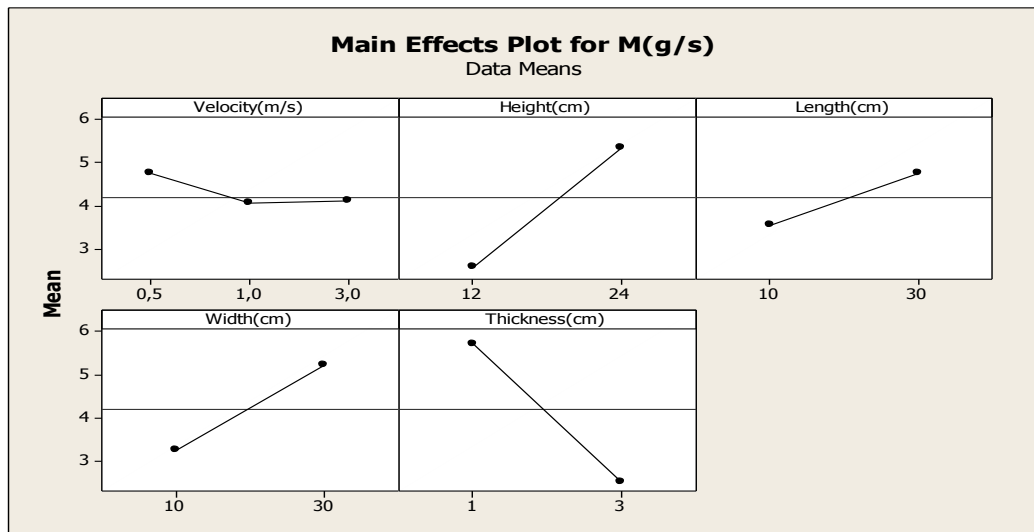


Figure 6.2 Main Effect Plots for Experiments in Mass Loss Rate ($L \neq W$)

The results obtained from Minitab software are shown in Figure 6.3. This figure is obtained as a result of test after choosing the significant parameters based on p-value in analysis table. If the p-value is less than or equal to the level of significance (α -value), then it can be concluded that the parameter affects the response in a significant way. In this analysis, the 0.05 α -level is used. This variation table represents 78.77 % of the variation of mass loss rate. This result is obtained from R-Sq(adj) value in the ANOVA result table.

General Linear Model: M(gr/s) versus Velocity(m/s); Thickness(cm); ...						
Factor	Type	Levels	Values			
Velocity(m/s)	fixed	3	0,5; 1,0; 3,0			
Thickness (cm)	fixed	2	1; 3			
Length (cm)	fixed	2	10; 30			
Width (cm)	fixed	2	10; 30			
Height (cm)	fixed	2	12; 24			
Analysis of Variance for M(gr/s), using Adjusted SS for Tests						
Source	DF	Seq SS	Adj SS	Adj MS	F	P
Pambient (kPa)	1	71,170	18,261	18,261	10,31	0,008
Velocity (m/s)	2	9,388	2,598	1,299	0,73	0,502
Thickness (cm)	1	23,429	28,407	28,407	16,04	0,002
Length (cm)	1	0,924	3,700	3,700	2,09	0,176
Width (cm)	1	6,407	8,529	8,529	4,81	0,051
Height (cm)	1	19,373	19,373	19,373	10,94	0,007
Error	11	19,486	19,486	1,771		
Total	18	150,178				
S = 1,33097 R-Sq = 87,02% R-Sq(adj) = 78,77%						

Figure 6.3 Minitab Output for ANOVA of Mass Loss Rate (L≠ W)

The percentage distribution of the variation in the data based on mass loss rate values is shown in Figure 6.4. The variation in mass loss rate is due to

- Height (23.8 %)
- Thickness (34.9 %)
- Width (10.5 %)
- Length (4.5 %)

- Velocity (1.6 %)
- Other (24.6 %)

It can be noted that the change in the width of the burning object is much higher than the length of the burning objects. As the height of the burning object increases, the mass loss rate increases due to the decrease in the distance between the ceiling and burning object. An increase in the width of the burning object causes an increase in the mass loss rate due to the decreasing of the distance between the tunnel wall and burning substances.

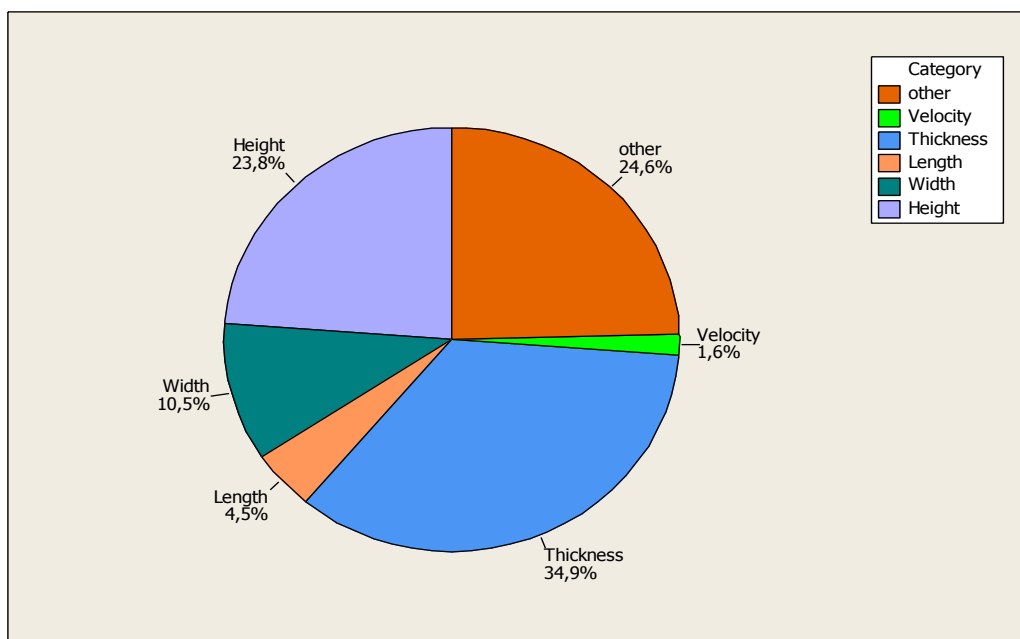


Figure 6.4 Pie Chart for a Cause of Variation in Mass Loss Rate ($L \neq W$)

The ANOVA result obtained from Minitab software is shown in Figure 6.5. This variation table represents 78.01 % of the variation of HRR. This result is obtained from R-Sq(adj) value in the ANOVA result table.

General Linear Model: Q(kW) versus Velocity(m/s); Thickness(cm); ...						
Factor	Type	Levels	Values			
Velocity(m/s)	fixed	3	0,5; 1,0; 3,0			
Thickness (cm)	fixed	2	1; 3			
Length (cm)	fixed	2	10; 30			
Width (cm)	fixed	2	10; 30			
Height (cm)	fixed	2	12; 24			
Analysis of Variance for Q(kW), using Adjusted SS for Tests						
Source	DF	Seq SS	Adj SS	Adj MS	F	P
Pambient (kPa)	1	22768	2567	2567	2,34	0,154
Velocity(m/s)	2	18253	24167	12083	11,04	0,002
Thickness (cm)	1	13419	17605	17605	16,08	0,002
Length (cm)	1	2174	5489	5489	5,01	0,047
Width (cm)	1	5767	7538	7538	6,88	0,024
Height (cm)	1	15190	15190	15190	13,87	0,003
Error	11	12043	12043	1095		
Total	18	89614				
S = 33,0883 R-Sq = 86,56% R-Sq(adj) = 78,01%						

Figure 6.5 Minitab Output for ANOVA of HRR Data (L ≠ W)

The percentage distribution of the variation in the data based on HRR values is shown in Figure 6.6. The variation in HRR is due to

- Height (25.1 %)
- Thickness (29.1 %)
- Width (12.4 %)
- Length (9.1 %)
- Velocity (19.9 %)
- Other (4.4 %)

It can be noted that the change in the width of the burning object is much higher than the length of the burning objects. It gives the impression that similar results are obtained based on the ANOVA results. The significant difference is at the velocity influence on heat release rate and mass loss rate. From the experimental result configuration, mass loss rate measurement may be influenced from other parameters (except velocity, height, width, length) more seriously than the heat release rate measurement. Also, the variation between the change in mass loss rate is only 0.5 g/s due to velocity change. It may lead to a wrong decision based on the analysis of mass loss rate data.

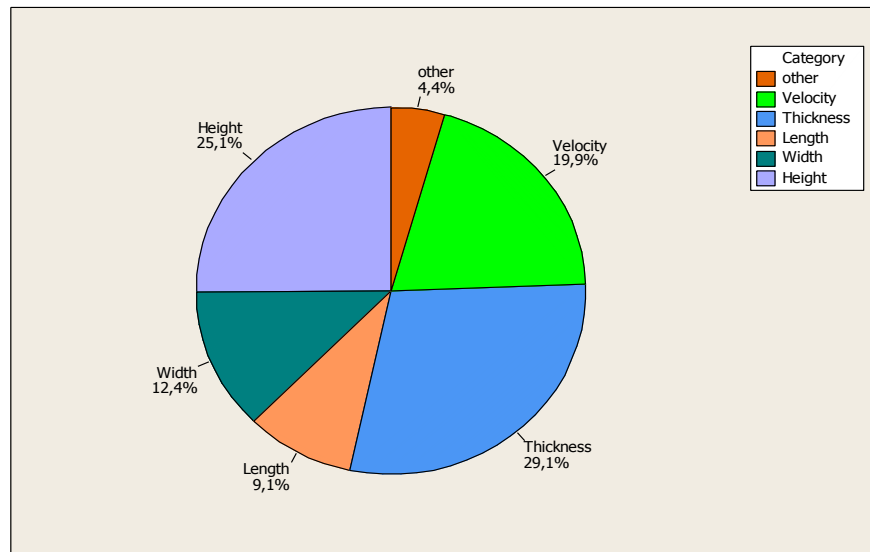


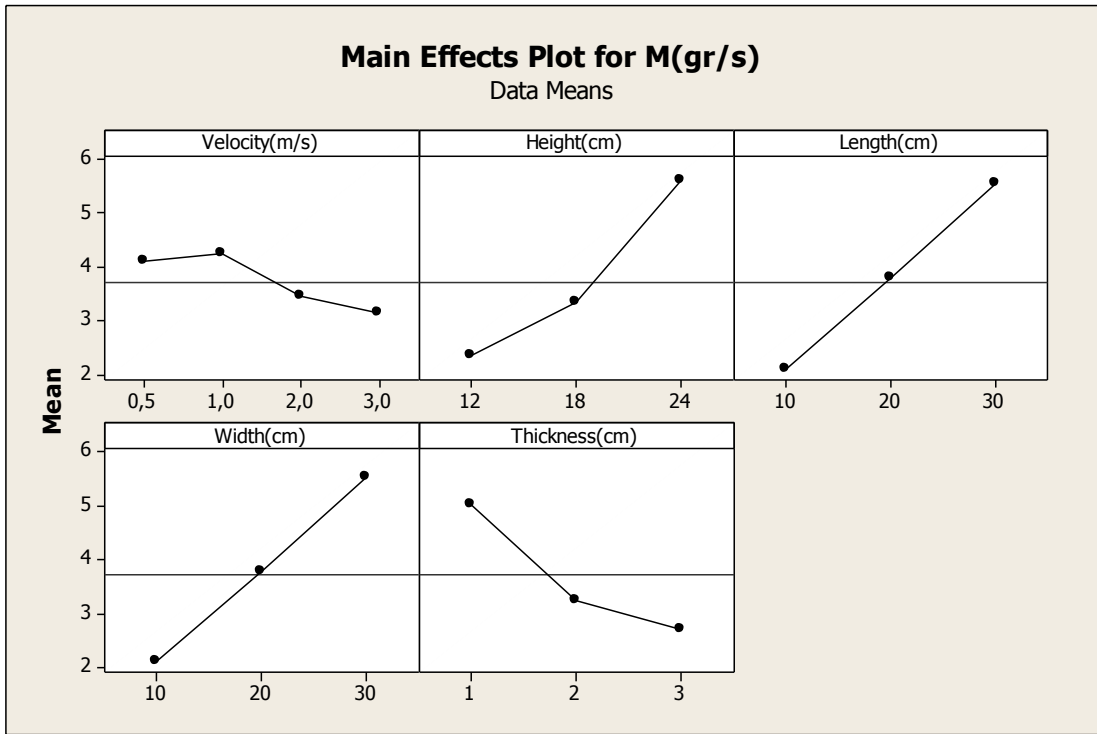
Figure 6.6 Pie Chart for a Cause of Variation in HRR ($L \neq W$)

The wood cribs with repeatable characteristics have a square floor area. The effect of blockage on heat release rate and mass loss rate is investigated based on the analysis performed on the experimental results where the burning object length and thickness are equal to each other. The design parameters variation and their interaction with each other can be represented in Figure 6.7 and Figure 6.8.

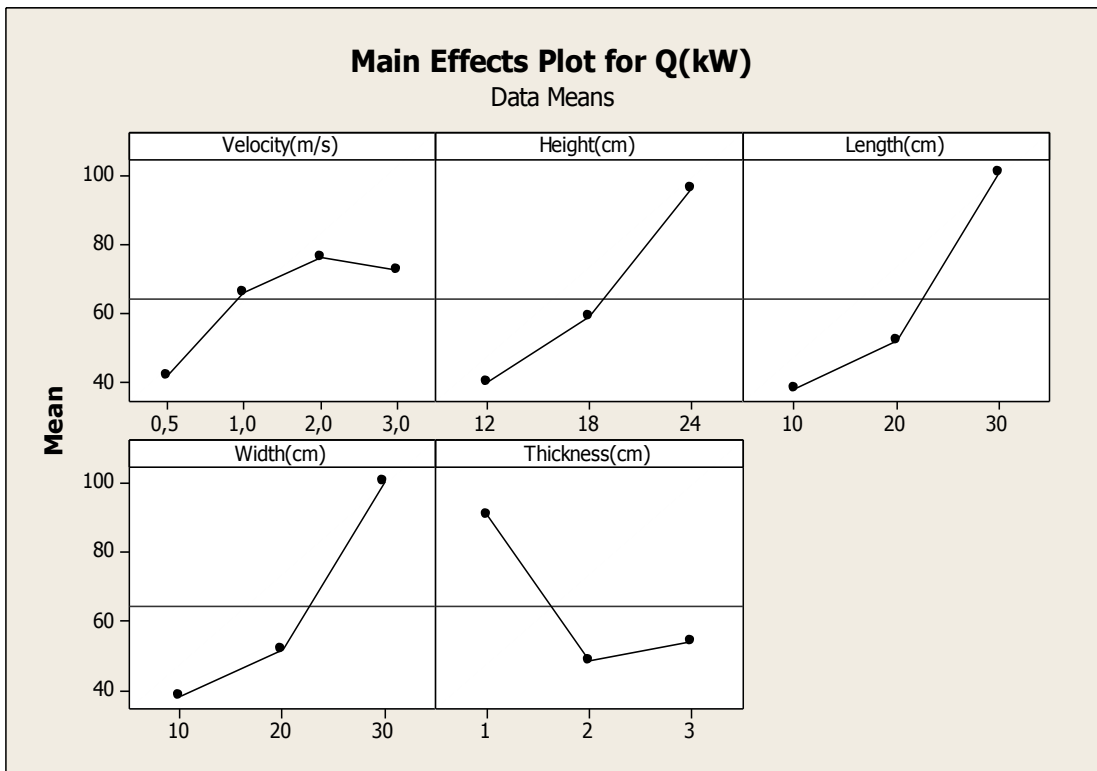
If Figure 6.7 is examined, the following conclusions can be reached:

1. The change in the height and width of the burning object causes an increase in mass loss rate and heat release rate.
2. The thickness increase causes a large change in heat release rate and mass loss rate up to 2 cm thickness. However, the variation of thickness between 2 cm to 3 cm causes an insignificant increase in HRR and small decrease in mass loss rate.

3. As the velocity changes from 0.5 m/s to 1 m/s, a slight increase can be observed in the mass loss rate data (Figure 6.7a). Beyond 1 m/s, the mass loss rate is decreasing. The variation in the average of the mass loss rate value obtained from the experiments is only 1 g. It is probably due to the sensitivity of the measuring instrument or its response to change in environmental conditions (extraneous effects). Based on heat release rate data (Figure 6.7b), velocity can significantly affect HRR change up to 2 m/s. It causes an increase in HRR. However, it seems that HRR decreases after 2 m/s probably. The cooling effect of ventilation is dominant in this region.



a) Mass Loss Rate



b) HRR

Figure 6.7 Main Effect Plots of Mass Loss Rate and HRR (L= W)

If Figure 6.8a is examined, the following conclusions can be reached:

1. From the velocity and height interaction graph, the higher object gives a higher mass loss rate value at fixed velocity. As the velocity and height increase together, the slight increase in mass loss rate is observed.
2. From width and velocity interaction, the wider the width of the object, the higher is the mass loss rate at constant velocity. At constant width, the mass loss rate tends to decrease as the velocity increases except at the low velocity (0.5 m/s).
3. From thickness and velocity interaction, the mass loss rate generally decreases as the velocity increases at constant thickness. The thinner sticks give a larger mass loss rate at the fixed velocity.
4. From height and width interaction, the increase in height and width causes an increase in mass loss rate.
5. From thickness and height interaction, the decrease in thickness and the increase in height give a higher mass loss rate. The variation seems very small at the thickness 2 cm and 3 cm.
6. From width and thickness interaction, the decrease in thickness and the increase in width give a higher mass loss rate. There is no significant change in mass loss rate as the thickness varies from 2 cm to 3 cm.

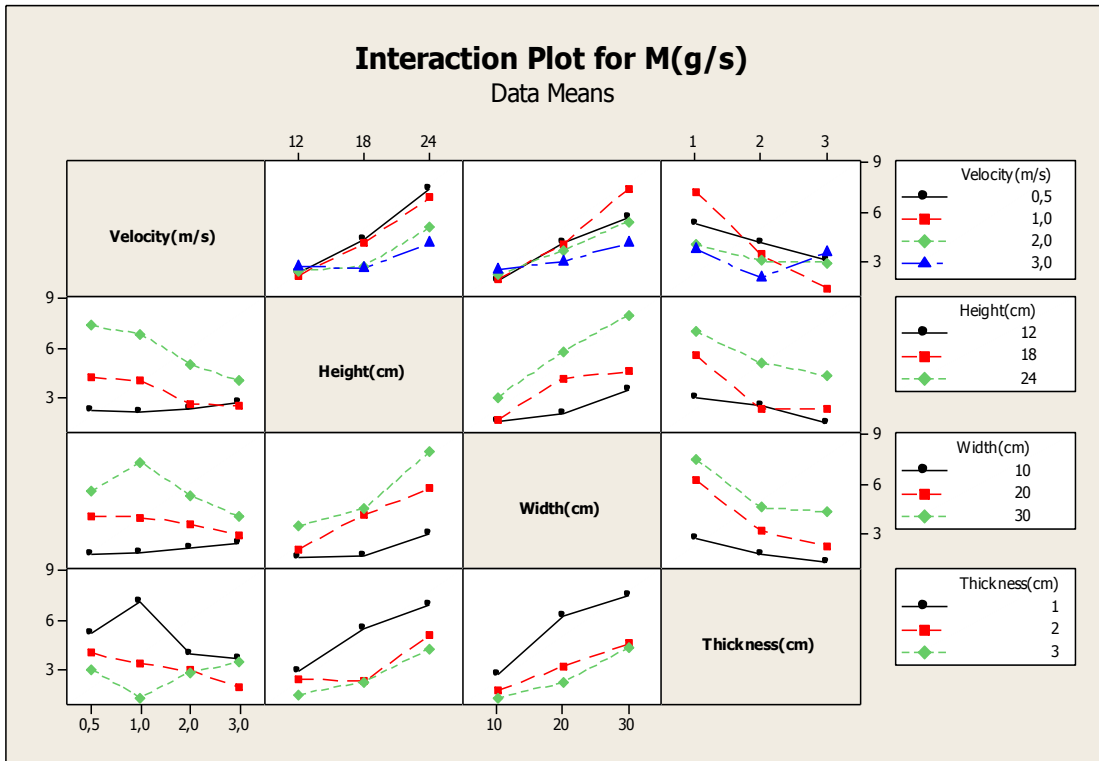
If Figure 6.8b is examined, the following conclusions can be reached:

1. From the velocity and height interaction graph, the higher object gives a higher HRR at fixed velocity. As the velocity and height increase together, the increase in HRR is observed up to 2 m/s. After 2 m/s, the change due to

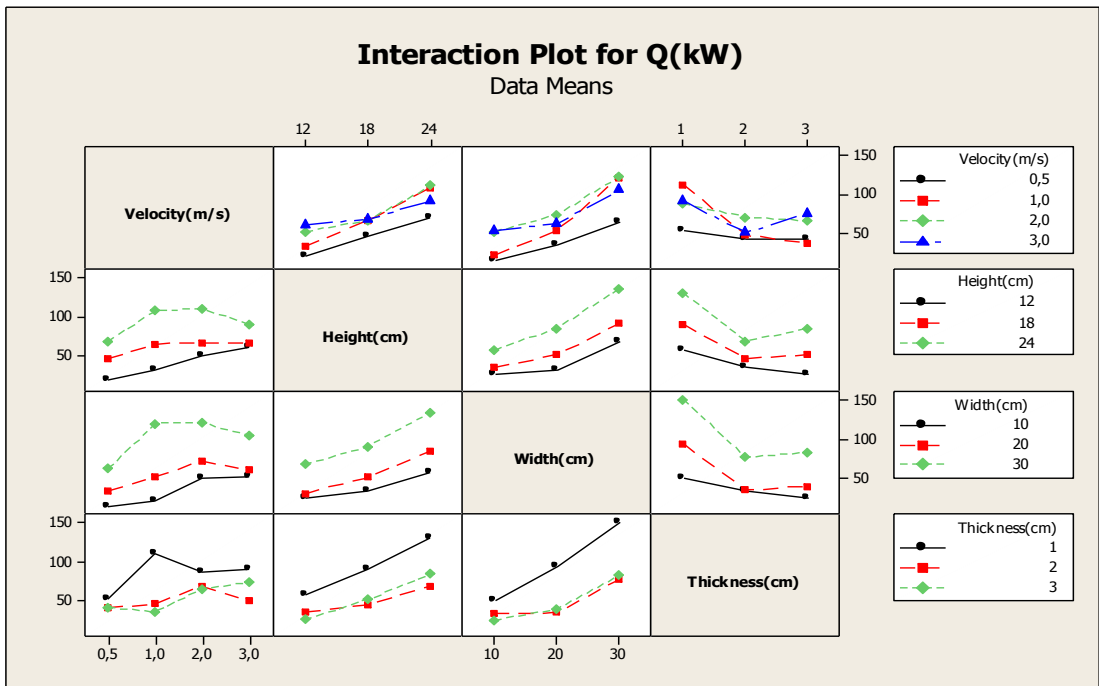
the increase in velocity and height is getting smaller at a height of 18 cm and 24 cm.

2. From width and velocity interaction, the wider the width of the object, the higher is the HRR at constant velocity up to 2 m/s. At constant width, the HRR tends to increase as the velocity increases. There is a slight decrease in HRR between ventilation velocity 2 m/s and 3 m/s when the width of the object is 20 cm and 30 cm.
3. From thickness and velocity interaction, the HRR generally increases as the velocity increases at constant thickness. The thinner sticks give a higher HRR at the fixed velocity.
4. From height and width interaction, the increase in height and width causes an increase in HRR.
5. From thickness and height interaction, the decrease in thickness and the increase in height give a higher HRR. The variation seems very small at the thickness 2 cm and 3 cm.
6. From width and thickness interaction, the decrease in thickness and the increase in width give a higher HRR. There is no significant change in mass loss rate as the thickness varies from 2 cm to 3 cm.

The importance of vehicle blockage effect is decided by using ANOVA. The parameters which are selected for this analysis are blockage ratio, ventilation velocity, thickness, ambient pressure, ambient temperature and relative humidity. The general linear model option is used in Minitab 15 software. In Figure 6.9, it is observed that the blockage ratio is proportional to mass loss rate and HRR. The results obtained from the full scale test show that the larger energy content of vehicle releases higher heat release rate in case of tunnel fire [6].

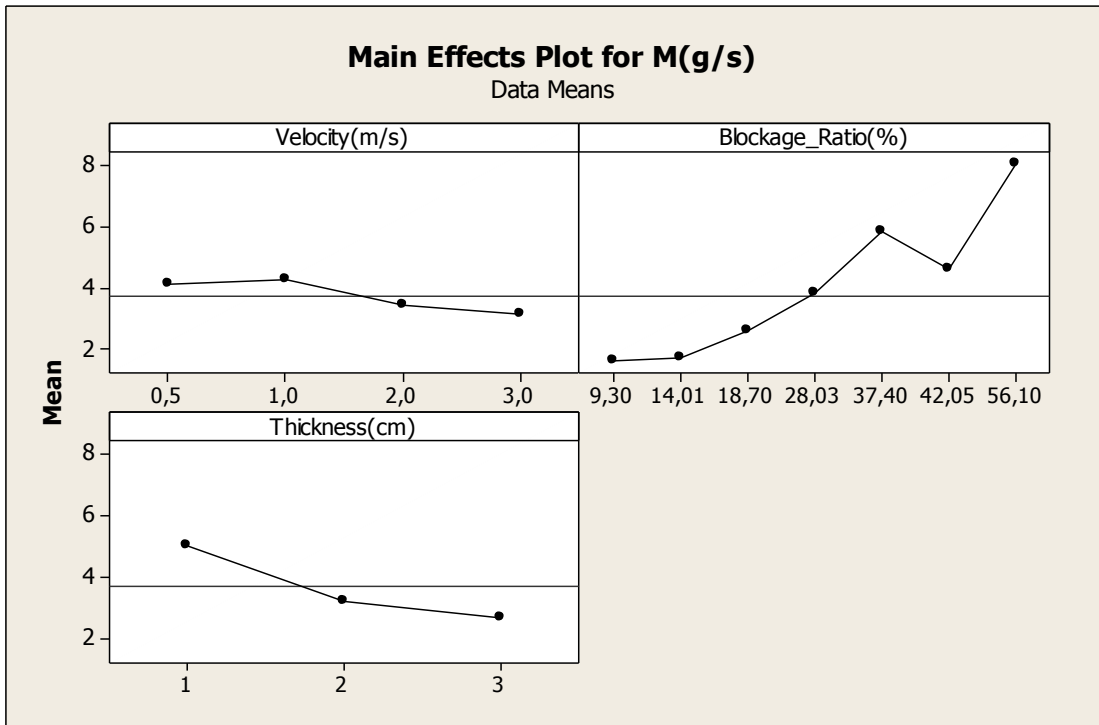


a) Mass Loss Rate

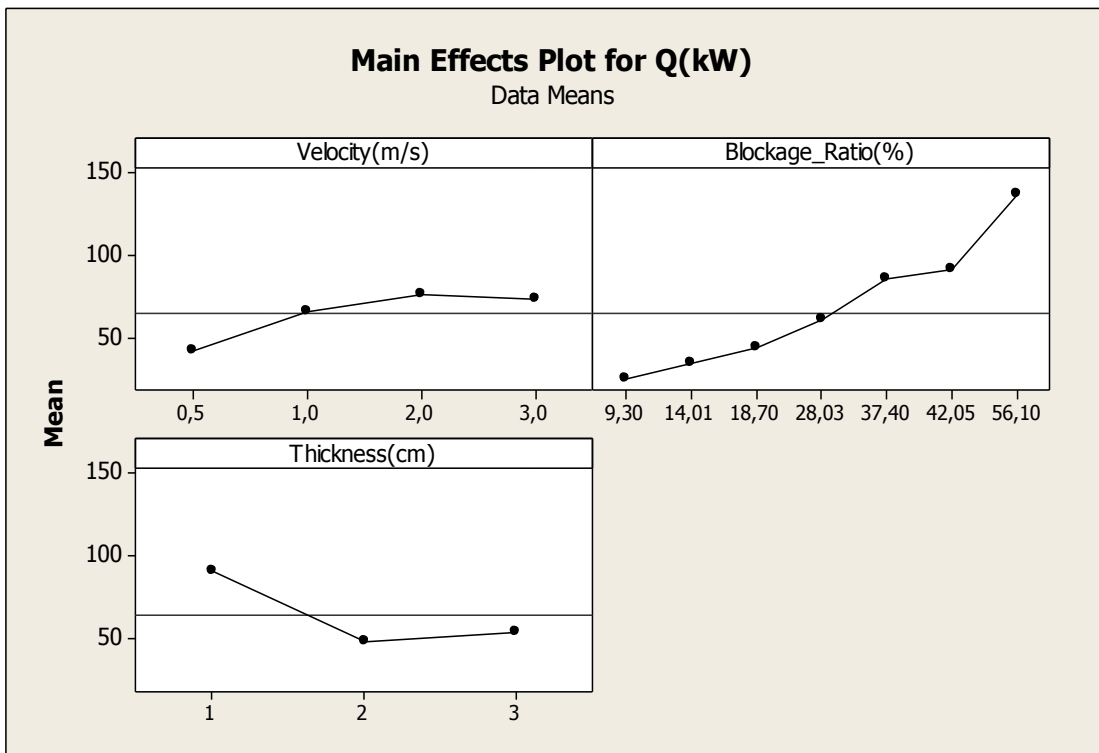


b) HRR

Figure 6.8 Interaction Plots of Mass Loss Rate and HRR (L= W)



a) Mass Loss Rate



b) HRR

Figure 6.9 Velocity, Thickness and Blockage Ratio Variation Plots of Mass Loss Rate and HRR (L= W)

The blockage ratio increases indirectly show the increase in energy content of the vehicle. The ANOVA result obtained from Minitab software is shown in Figure 6.10. This variation table represents 85.96 % of the variation of HRR. This result is obtained from R-Sq(adj) value in the ANOVA result table.

General Linear Model: Q(kW) versus Velocity(m/s); Thickness(cm)						
Factor	Type	Levels	Values			
Velocity(m/s)	fixed	4	0,5; 1,0; 2,0; 3,0			
Thickness(cm)	fixed	3	1; 2; 3			
Analysis of Variance for Q(kW), using Adjusted SS for Tests						
Source	DF	Seq SS	Adj SS	Adj MS	F	P
Pambient(kPa)	1	25722	3515	3515	10,74	0,002
Blockage_Ratio(%)	1	45214	59696	59696	182,38	0,000
Velocity(m/s)	3	15713	10049	3350	10,23	0,000
Thickness(cm)	2	15862	15862	7931	24,23	0,000
Error	43	14075	14075	327		
Total	50	116584				
S = 18,0918 R-Sq = 87,93% R-Sq(adj) = 85,96%						

Figure 6.10 Minitab Output for ANOVA of HRR Data (L=W)

The percentage distribution of the variation in the data based on HRR values is shown in Figure 6.10. The variation in HRR is due to

- Blockage Ratio (79.8 %)
- Thickness (10.6 %)
- Velocity (4.5 %)
- Ambient Conditions (4.7 %)
- Other (0.4 %)

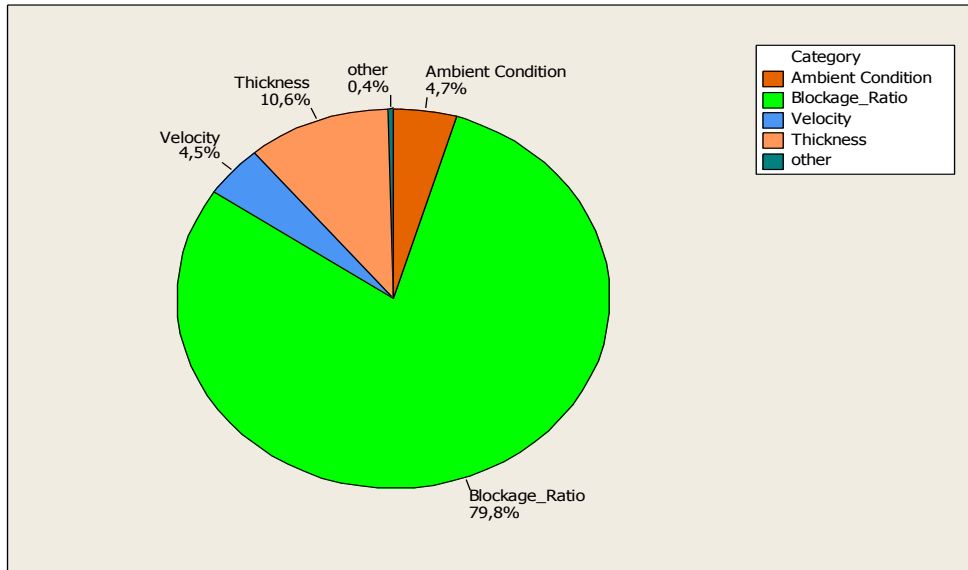


Figure 6.11 Pie Chart for a Cause of Variation in HRR (L=W)

Similarly, ANOVA result based on mass loss rate data obtained from Minitab software is shown in Figure 6.10. This variation table represents 79.24 % of the variation of mass loss rate.

General Linear Model: M(gr/s) versus Velocity(m/s); Thickness(cm)

Factor	Type	Levels	Values
Velocity(m/s)	fixed	4	0,5; 1,0; 2,0; 3,0
Thickness(cm)	fixed	3	1; 2; 3

Analysis of Variance for M(gr/s), using Adjusted SS for Tests

Source	DF	Seq SS	Adj SS	Adj MS	F	P
Pambient(kPa)	1	77,091	6,995	6,995	4,76	0,035
Blockage_Ratio(%)	1	138,732	159,928	159,928	108,92	0,000
Velocity(m/s)	3	5,995	9,222	3,074	2,09	0,116
Thickness(cm)	2	51,823	51,823	25,912	17,65	0,000
Error	40	58,730	58,730	1,468		
Total	47	332,372				

S = 1,21171 R-Sq = 82,33% R-Sq(adj) = 79,24%

Figure 6.12 Minitab Output for ANOVA of Mass Loss Rate Data (L=W)

The percentage distribution of the variation in the data based on mass loss rate data is shown in Figure 6.13. The variation in mass loss rate is due to

- Blockage Ratio (81 %)
- Thickness (13.1 %)
- Velocity (1.6 %)
- Ambient Conditions (3.5 %)
- Other (0.7 %)

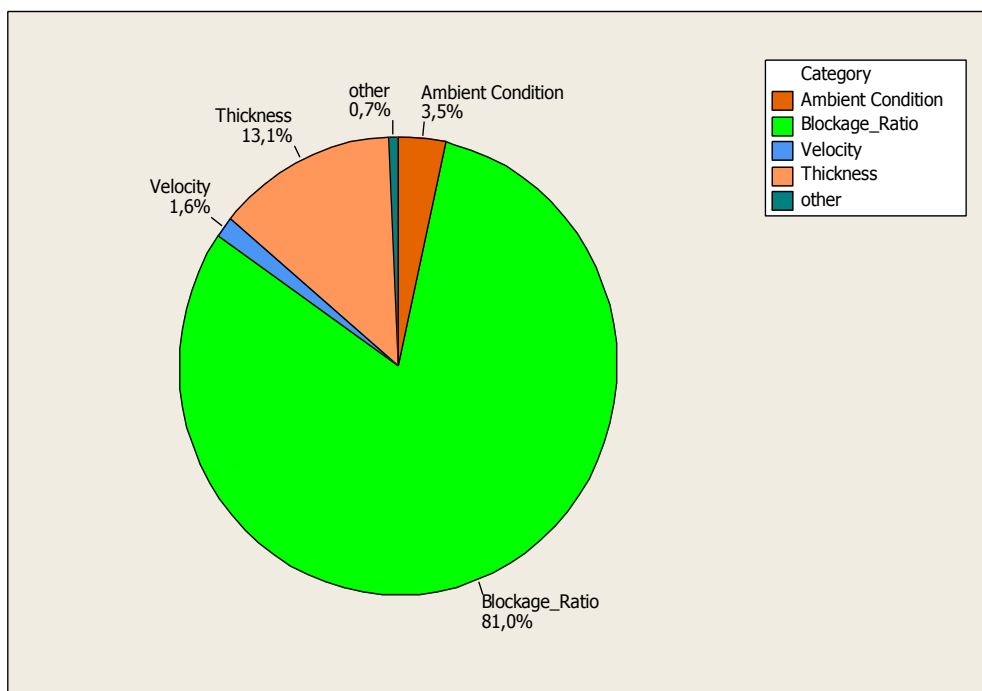


Figure 6.13 Pie Chart for a Cause of Variation in Mass Loss Rate (L=W)

CHAPTER 7

DISCUSSION AND CONCLUSION

7.1 Comments on the Experimental Results

The purpose of this research study is to investigate tunnel vehicle blockage effect and its configuration on heat release rate and temperature distribution inside tunnel with different ventilation velocities. 1/13 scale model tunnel configuration is constructed in the annex of Fluid Mechanics Laboratory of Mechanical Engineering Department, METU. A set of experiments is conducted with various configurations of burning substances and different ventilation velocities to achieve this purpose.

In this study, wood materials are burned. There are several reasons for this selection. Firstly, as a large variety of materials are used in the vehicles, it is difficult to scale down the model vehicle materials. To simplify the tests, the variety of materials are limited to a single material, pine wood. Secondly, it is difficult to obtain the same configuration of vehicle with different scale ratios. It is better to simplify the problem by testing the parameter in the design with an easily constructed vehicle configuration. This study investigates the vehicle configuration especially its cross sectional area to tunnel cross sectional ratio (blockage ratio) on heat release rate in case of different tunnel ventilation when it is constructed from a material with the same burning properties. Thirdly, the repeatability and conservation of scaling

parameter in case of wood crib fire in enclosure are given in the literature. Finally, wood cribs are used in full scale tunnel tests. Therefore, the total energy of the vehicles is simulated by an amount of wood of the same energy content in the tunnel.

According to the heat release rate results, ventilation velocity affects the heat release rate of vehicle positively. The ventilation causes an increase up to a certain limit of velocity (2 m/s). However, the increase in velocity inside tunnel does not affect the heat release rate after 2 m/s. This result is obtained from results of Analysis of Variance. The variations in height and width of the burning object are directly proportional to heat release rate. As the blockage ratio of the burning substances increase, the heat release rate increases. According to statistical analysis, the variation in heat release rate is composed of 79.8 % due to change in blockage ratio, % 4.5 due to change in velocity, % 10.6 due to change in thickness, the remaining percentage due to their interactions and the extraneous variables.

According to the mass loss rate results, ventilation velocity does not significantly affect the heat release rate of vehicle positively. As the blockage ratio of the burning substances increases, the heat release rate increases. According to the statistical analysis, the variation in heat release rate is composed of 81 % due to change in blockage ratio, 1.6 % due to change in velocity, 13.1 % due to change in thickness, the remaining percentage is due to their interactions and the extraneous variables.

As the ventilation velocity increases, the temperature inside the tunnel decreases and the heat release rate increases. The cooling effect of ventilation is observed as the ventilation velocity increases and if the same model is burned with a different ventilation velocity. According to E. Musluoğlu [34], “the ventilation of 2.5 m/s at tunnel cross section, the forced ventilation controls the development of fire and reduces the rate of heat released if the air-flows penetrate through the rolling stocks.” However, it is difficult to compare his result with the experimental results since all materials used in the train compartment are modelled in a computational domain in his research. Nevertheless, only single material is used in order to understand the

tunnel fire phenomena in this study. The fire development inside the train is affected from the arrangement of materials and their combustion characteristics. Also, the airflows penetrate into these model vehicles easily. However, the velocity positively affects the heat release rate in this study. In full scale experiments, the ventilation enhances the heat release rate.

In literature, the temperature and thickness of the hot layer and the temperature of the upper bounding surfaces thus have a considerable impact on the fire growth due to radiation toward the burning fuel. Wider burning substance gives a much higher energy release rate. This is due to decrease in the distance between the tunnel wall and burning substances. As a result, radiation from the walls to the burning object increases.

The heat transfer to the burning object will be greater when the fire is at an enclosure with a low ceiling. This results in a considerable increase in the feedback to the fuel and to other combustibles, and a very rapid fire growth. When the height of the object is increasing, the distance between the tunnel ceiling and burning object is decreasing. This is the result of increase of radiation emitted from the tunnel walls to the surface of the burning object.

The critical velocity calculation based on constant heat release rate cannot give the correct value. The heat release rate is affected by ventilation. Therefore, the heat release rate value used in the calculations can be adjusted based on the velocity inside the tunnel.

The results obtained from this study can be used to understand the vehicle's blockage effect in case of tunnel fire. The variations in the type of the materials in the vehicle are not taken into consideration. In addition, it is not possible to obtain same "opening configurations" such as windows and doors for the vehicle when it is scaled down. As a result, the result obtained from this study can only be used to investigate the burning object dimensions especially its cross sectional area. Heat release rate

data obtained this study can be scaled up by $\dot{Q}_{prototype} \rightarrow \dot{Q}_{model} / \text{scale ratio}^{5/2}$ based on Froude number modelling. In addition to this, the volume flow due to ventilation can be scaled up by $q_{prototype} \rightarrow q_{model} / \text{scale ratio}^{5/2}$. These results can simulate the conditions when the fire heat release rate and volume flow rate of ventilation are equal to scaled up value. However, these results cannot be used directly to calculate the heat release rate value of the original vehicle. This study gives an important finding about the effect of vehicle blockage on heat release rate in case of tunnel fire. With the increasing vehicle blockage ratio, the heat release rate is also increasing up to certain ventilation conditions. This depends on the ignition source type and amount. There are certain limitations in this study. Firstly, the model vehicle is always ignited from the bottom surface and it is only enclosed by tunnel walls. However, in same vehicle fire, the vehicle may catch on fire from the inside and vehicle boundary encloses the fire. Secondly, tunnel wall structure affects the fire development. The tunnel wall's thermal inertia influences the heat loss from the tunnel wall and also temperature inside the tunnel.

The results obtained from this study can be used to evaluate the burning of an object made up of single materials. The heat release rate can be converted to other materials. In enclosure fire, the rate of burning strongly depends on the combustibility ratio which is defined as the combustibility ratio (the ratio of heat of combustion to heat of gasification) [11]. If the net heat entering the surface is kept constant, heat release rate is directly proportional to combustibility ratio.

7.2 Recommendations for Future Work

- If the tunnel ventilation fans are started to operate in different instants, the effect of changing velocities on the heat release rate and mass loss rate is to be investigated.

- Tests will be conducted with combination of different materials.
- The material in the walls of the tunnel can affect the hot gas temperature considerably, and thereby the heat flux to the burning fuel and other combustible objects. By changing the materials on the wall of the tunnel, the effect of tunnel wall structure will be investigated. Insulating materials have a low thermal inertia ($k\rho c$); materials with relatively high thermal inertia, such as brick and concrete, allow more heat to be conducted into the construction, thereby lowering the hot gas temperatures.
- The larger aspect ratio of the burning object (length over width ratio) should be investigated.
- The effect of blockage ratio will be examined in the tunnel with downhill slope and uphill slope. Also, the experiments will be repeated in different tunnel geometry.
- The experiments will be conducted with different type of ignition source and energy.

REFERENCES

- [1] NFPA, NFPA 130-Standard for Fixed Guideway Transit System, National Fire Protection Association, 2003
- [2] The Handbook of Tunnel Fire Safety, Beard, A., Carvel, R., Thomas Telford Publishing , 2005
- [3] Enclosure Fire Dynamics, Karlsson, B.; Quintiere, J.G., CRC Press, 2000
- [4] An Introduction to Fire Dynamics, 2nd ed., Drysdale, D., John Wiley & Sons, 1999
- [5] PIARC Committee on Road Tunnels, “Fire and Smoke Control in Road Tunnels”, ref. 05.05.B, 1995
- [6] Lönnermark, A.,”On the Characteristics of Fires in Tunnels”, Ph.D. Thesis Lund University, 2005
- [7] Flammability Testing Of Materials Used In Construction, Transport And Mining, Apte, V. B., Woodhead Publishing Limited,2006

- [8] Li, J.S.M. , Chow, W.K., “Numerical Studies on Performance Evaluation of Tunnel Ventilation Safety System”, *Tunnelling and Underground Space Technology*, v.18, 2003, 435-452
- [9] “SFPE Handbook of Fire Protection Engineering”, 2nd Edition, Chapter 15“
- [10] NFPA, “Fire Protection Handbook”, Seventh Edition , 1991
- [11] Fundamentals of Fire Phenomena, Quintiere, J. G., Wiley, 2006
- [12] Kennedy, W. D.; Gonzales, J. A.; Sanchez, J. G.; “Derivation and Application of the SES Critical Velocity Equations”, *ASHRAE Transactions*, 3983
- [13] Kayılı, S., Köktürk,T., Eralp, O.C., “Design Criteria And Technical Issues On Emergency And Comfort Ventilation Of Underground Rail Transit (Urt) Systems, Focus On Turkey”, VIII. International HVAC+R Technology Symposium and Exhibition, 12-14 May 2008
- [14] Subway Environmental Design Handbook, V.1, Principles and Applications, 2nd ed., U.S. Department of Transportation, 1976
- [15] NFPA, NFPA 502 Standard for Road Tunnels, Bridges and other Limited Access highways, National Fire Protection Association, 2000
- [16] Carvel, R. O. “Fire Size in Tunnels”, Ph.D. Dissertations, Heriot-Watt University School of Built Environment Division of Civil Engineering , 2003
- [17] Vauquelin, O., “Experimental Simulations of Fire-Induced Smoke Control in Tunnels Using an “ air-helium reduced scale mode”’: Principle, Limitations,

Results and Future”, Tunnelling and Underground Space Technology, Volume 23, 2008, Pages 171-178

- [18] Roh, J. S., Yang, S. S., Ryou, H.S., Yoon, M.O., Jeong, Y. T., “An Experimental Study on the Ventilation Velocity on Burning Rate in Tunnel Fires-Heptane Pool Fire Case”, Building and Environment, Volume 43, Issue 7, July 2008, Pages 1225-1231
- [19] Roh, J. S., Ryou, D.H. , Kim, D.H. , Jung, W. S. , Jang, Y. J., “Critical Velocity and Burning Rate In Pool Fire During Longitudinal Ventilation”, Tunnelling and Underground Space Technology, Volume 22, Issue 3, May 2007, Pages 262-271
- [20] Ingason, H., “Model Scale Railcar Fire Tests”, Fire Safety Journal, Volume 42 ,2007 , Pages 271-282
- [21] Vauquelin, O. , Wu, Y., “Influence of Tunnel Width on Longitudinal Smoke Control”, Fire Safety Journal, Volume 41 ,2006 , Pages 420-426
- [22] Lee, S. R., Ryou, H. S., “ An Experimental Study of the Effect of the Aspect Ratio on the Critical Velocity in Longitudinal Ventilation Tunnel Fires”, Journal of Fire Sciences, vol 23, Pages 119- 138 , March 2005
- [23] Choi, J.S., Kim, M.B., Choi, D.H., “Experimental Investigation on Smoke Propagation in a Transversely Ventilated Tunnel”, vol. 23, Pages 469- 483, November 2005
- [24] Chiam, B. H., “ Numerical Simulation of a Metro Train Fire, Master of Engineering in Fire Engineering, University of Canterbury, June 2005

- [25] Carvel, R.O. , Beard, A.N., Jowitt, P.W. , Drysdale, D.D. , “The Influence of Tunnel Geometry and Ventilation on The Heat Release Rate of Fire” , Fire Technology, 40, Pages 5 - 26 ,2004
- [26] Kunsch, J. P., “Simple Model for Control of Fire Gases in a Ventilated Tunnel”, Fire Safety Journal v 37, 2002, p 67-81
- [27] Carvel, R. O.; Beard, A. N.; Jowitt, P. W.; Drysdale, D. D.; “Variation of Heat Release Rate with Forced Longitudinal Ventilation for Vehicle Fires in Tunnels”, Fire Safety Journal v 36, 2001, p 569-596
- [28] Wu, Y., Bakar, M. Z. A., “Control of Smoke Flow in Tunnel Fires Using Longitudinal Ventilation Systems – A Study of the Critical Velocity”, Fire Safety Journal v 35, 2000, p 363-390
- [29] Xue,H., Chew, T. C, Kay K. L.,Cheng Y. M, “Control of Ventilation Airflow for Tunnel Fire Safety”, Combustion Science Technology 2000; 152: Pages 179-96
- [30] Mégret, O.; Vauquelin, O.; “A Model to Evaluate Tunnel Fire Characteristics”, Fire Safety Journal v 34, 2000, p 393-401
- [31] Kennedy, W. D.; Gonzales, J. A.; Sanchez, J. G.; “Derivation and Application of the SES Critical Velocity Equations”, ASHRAE Transactions, USA, Ashrae Transactions, Vol 102, Pt 2, 1996
- [32] Atkinson, G. T.; Wu, Y.; “Smoke Control in Sloping Tunnels”, Fire Safety Journal v 27, 1996, p 335-341
- [33] Oka, Y.; Atkinson, G. T.; “Control of Smoke Flow in Tunnel Fires”, Fire Safety Journal v 25, 1995, p 305-322

- [34] Musluoğlu, E.; “ A Theoretical Analysis of Fire Development and Flame Spread in Underground Trains”, Ph.D. Dissertations, Middle East Technical University Mechanical Engineering Department, 2009
- [35] Musluoğlu, E.; “Simulation of A Fire Incidence in Underground Transportation Systems”, M. Sc. Thesis, Middle East Technical University Mechanical Engineering Department, 2003
- [36] Kayılı, S., “CFD Simulation of Fire and Ventilation in the Stations of Underground Transportation Systems”, M. Sc. Thesis, Middle East Technical University Mechanical Engineering Department, 2005
- [37] Veloo, P. S., Scale Modeling Of The Transient Behavior Of Heat Flux In Enclosure Fires, Masters Thesis, University of Maryland, Master of Science, 2006
- [38] Perricone, J. A., Scale Modeling Of The Transient Behavior Of Wood Crib Fires in Enclosures, Masters Thesis, University of Maryland, Master of Science, 2005
- [39] Parker, W. J., Calculations of the Heat Release Rate by Oxygen Consumption for Various Applications, Journal of Fire Sciences, Vol. 2, No. 5, 380-395, September/October 1984.
- [40] GX-K Series & GF-K Series High Resolution Industrial Balance, A&D Company Limited, 2004
- [41] OMB-DAQ-3000 Series 1 Mhz, 16 Bit USB Data Acquisition Modules User’s Manual (OMB-1136-0901 rev 1.1), Omega Engineering

- [42] Testo 350-S Control Unit in combination with Testo 350-S/ -XL Flue Gas Analyzer Instruction Manual, Testo AG
- [43] Design and Analysis of Experiments, Montgomery, D.C., John Wiley & Sons Inc. , 2001
- [44] Design and Analysis of Experiments, Dean, A., Voss, D., Springer-Verlag New-York, 1999
- [45] Applied Statistics and Probability for Engineers, Montgomery, D.C., Runger, G.C., 3rd Edition, John Wiley & Sons Inc. , 2002
- [46] Statistical Design and Analysis of Experiments with Application to Engineering Science and Science, Mason, R. L., Gunst, R. F., Hess, J. L. , 2nd Edition, John Wiley & Sons Inc. , 2003
- [47] Design of Experiments for Engineers and Scientists, Antony, J. Elsevier Butterworth-Heinemann, 2005
- [48] An Introduction to Design of Experiments: A Simplified Approach, Barrentine, L. B., ASQ Quality Press, 1999
- [49] Meet Minitab 15 for Windows, Minitab Inc., January 2007
- [50] Deney Düzenleri ve İstatistiksel Analizleri, Erbaş, S. O., Olmuş, H., Gazi Kitabevi, 2006
- [51] Deney Düzenlemede İstatistiksel Yöntemler, Hicks, C. R., Gazi Kitabevi, 2009
- [52] Statgraphs Centurion ,www.statgraphics.com, last visited on September 2009

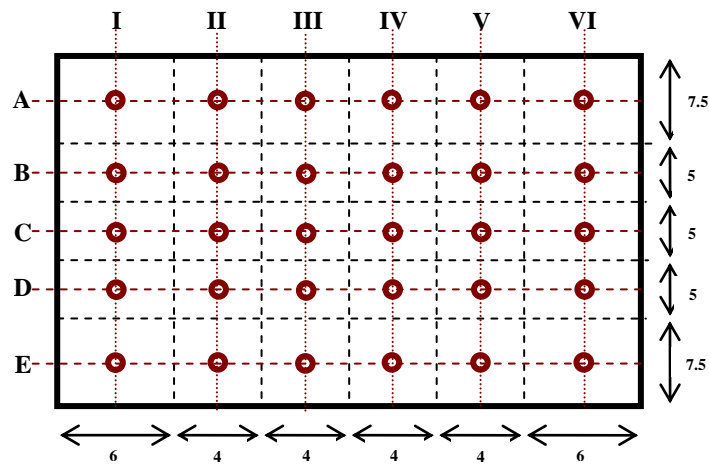
APPENDIX-A

VERIFICATION OF PITOT TUBE RAKE MEASUREMENT WITH HOT WIRE ANEMOMETER

Date: 08.01 .2009

Temperature : 14 °C

Pressure : 700 mm Hg



Method	Points	I	II	III	IV	V	VI
Hotwire Anemometer	A	2,16 /2,41	3,9 /3,09	4,38 /3,75	4,67 /3,2	4 /2,65	2,91 /1,97
	B	3,65 /3,33	4,47 /3,80	4,64 /3,95	4,72 /3,78	4,55 /3,80	4,18 /2,98
	C	4,13 /3,47	4,62 /3,91	4,65 /3,94	4,74 /4,01	4,53 /3,83	4,14 /2,98
	D	3,31 /3,05	4,2 /3,73	4,53 /3,73	4,56 /3,82	4,33 /3,73	3,57 /3,00
	Area Integration Velocity (m/s)						
Pitot Tube Rake	Average Velocity (m/s)						4,0 / 3,3

APPENDIX-B

TECHNICAL DRAWINGS & PHOTOS OF EXPERIMENTAL SETUP

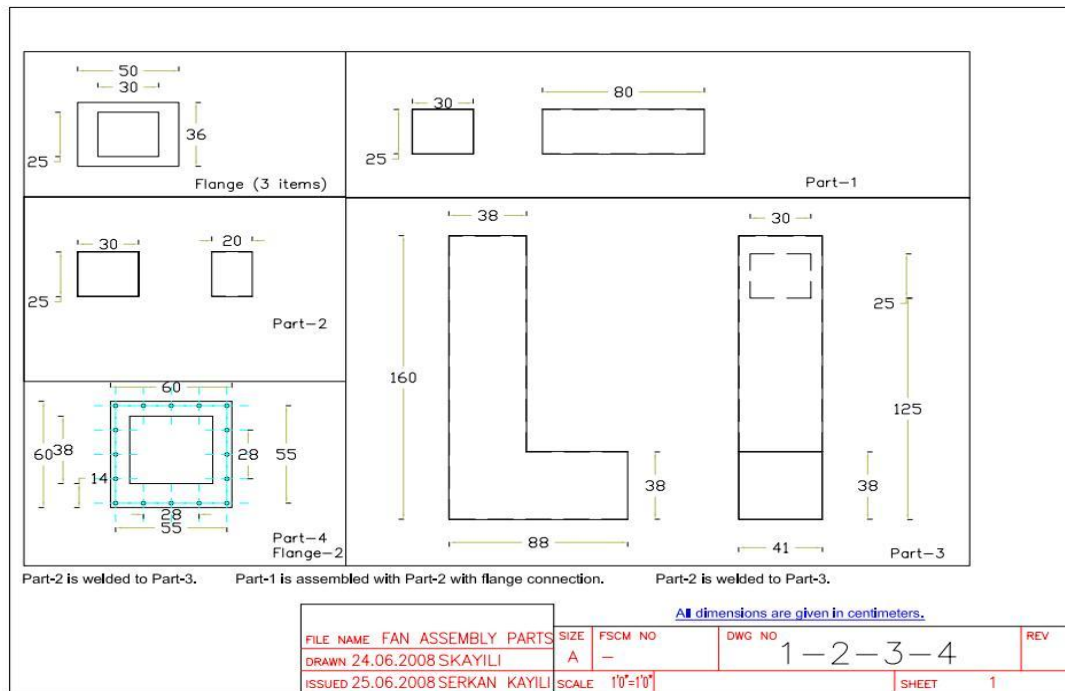


Figure B.1 Technical Drawings of Experimental Setup

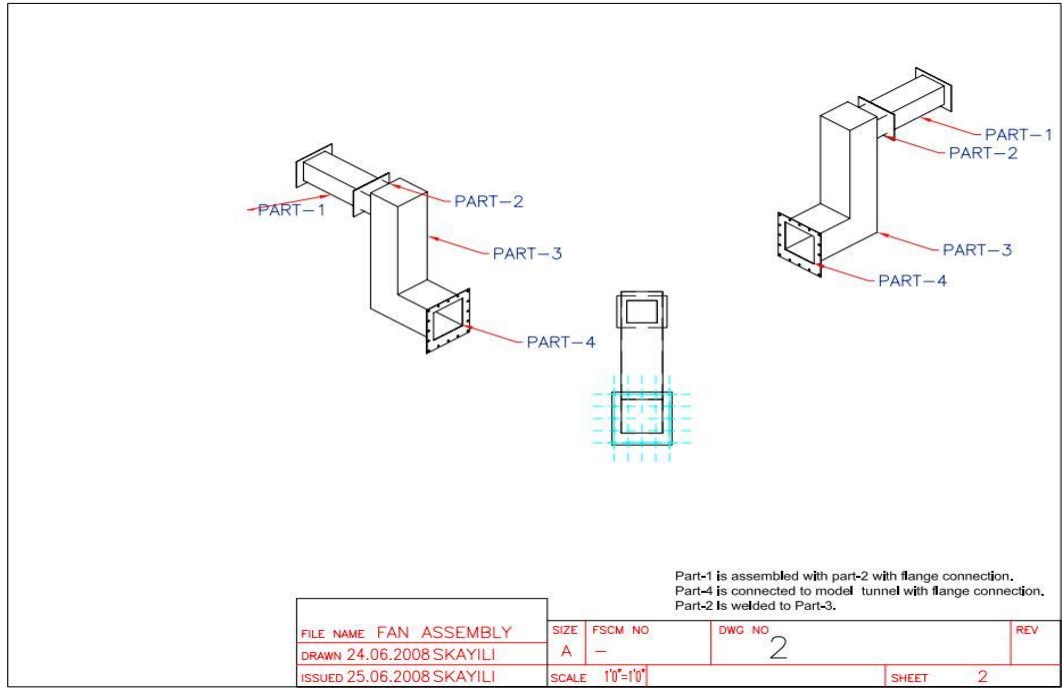


Figure B.1 Continued

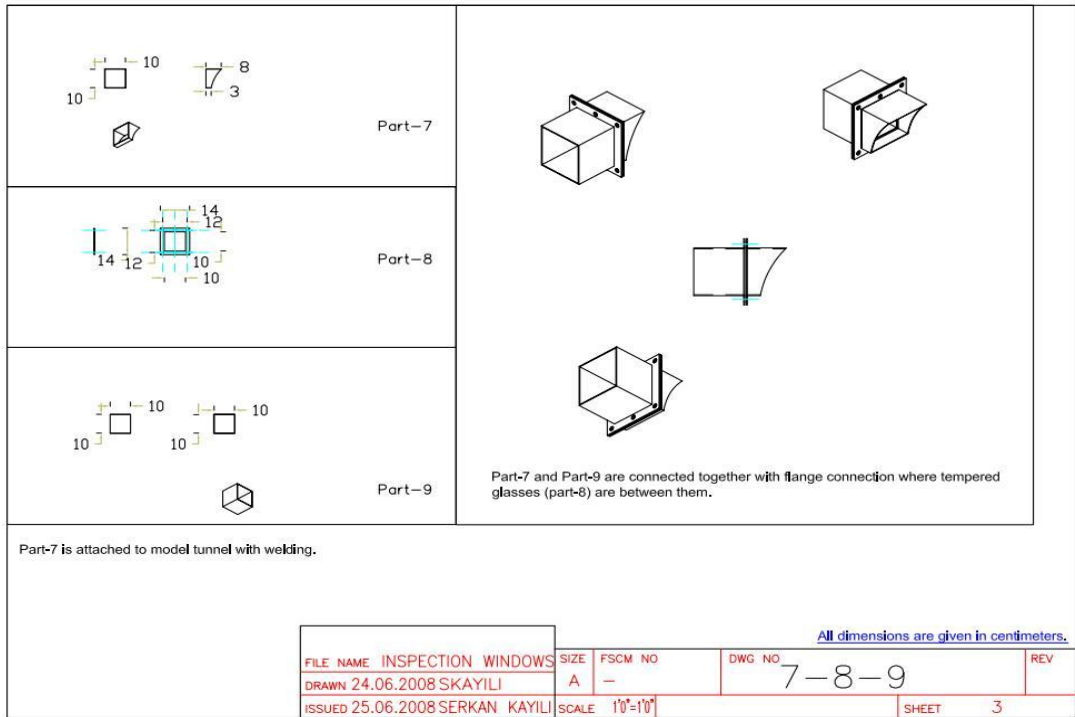


Figure B.1 Continued

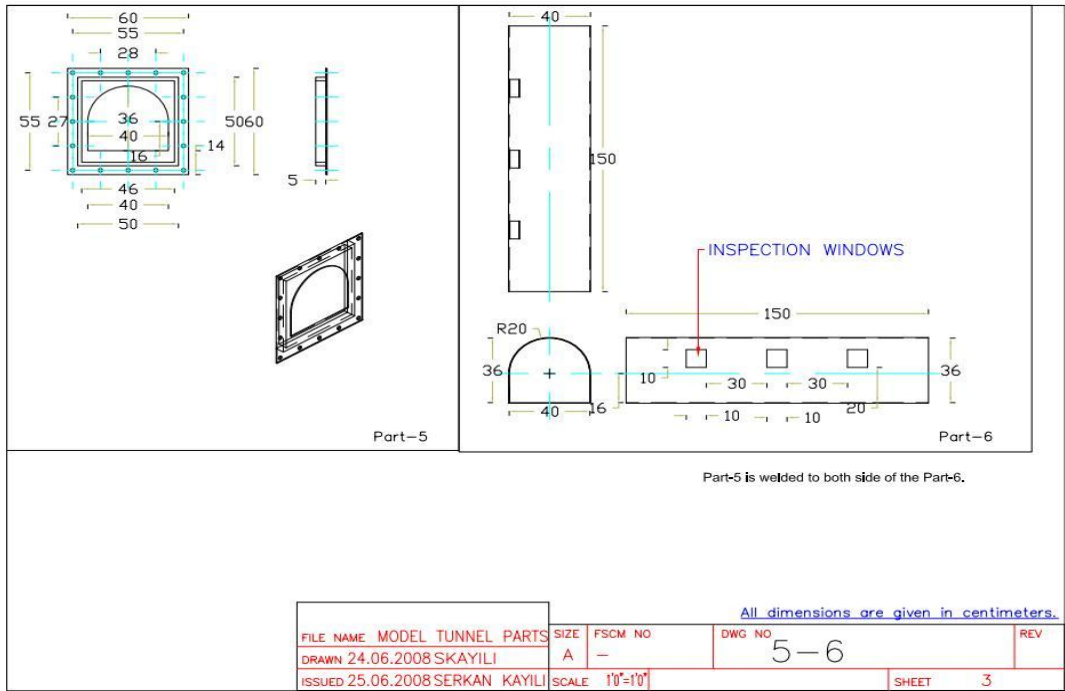


Figure B.1 Continued

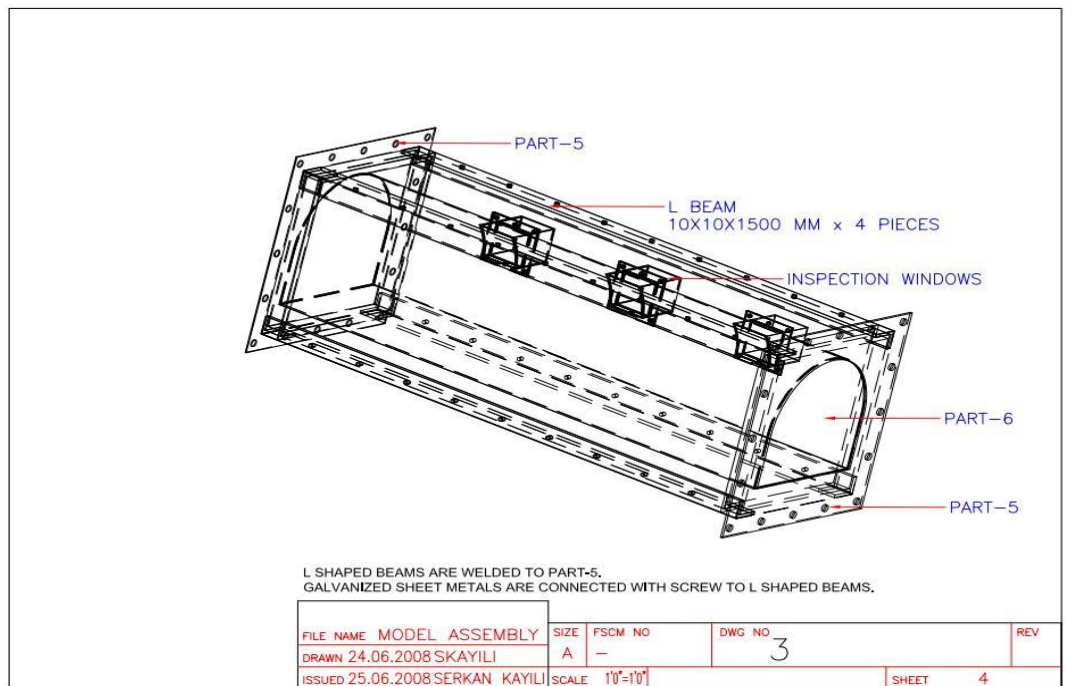


Figure B.1 Continued



Figure B.2 Experimental Setup Construction Procedure



Figure B.2 Continued

APPENDIX-C

TECHNICAL SPECIFICATIONS OF INSTRUMENTS

C.1 A&D Company GF 20 K High Precision Industrial Balance

Table C.1 Technical Specification of Industrial Balance

Manufactures		A&D Company, Limited /Japan
Model		GF 20 K
Weighing capacity		21 kg
Minimum weighing value (1 digit)		0.1 g
Repeatability(Standard deviation)		0.1 g
Linearity		±0.2 g
Stabilization time (Typical at FAST)		Approx. 1.5 seconds
Sensitivity drift, (10°C ~ 30°C / 50°F ~ 86°F)		±3 ppm/°C
Operating environment		5°C to 40°C, 85%RH or less (No condensation)
Display refresh rate		5 times/second or 10 times/second
Counting mode	Minimum unit mass	0.1 g
	Number of samples	10, 25, 50 or 100 pieces
Percent mode	Minimum 100% reference mass	10 g
	Minimum 100% display	0.01 %, 0.1 %, 1 % (Depends on the reference mass stored.)
Interface (Provided as standard)		RS-232C with Windows Communication Tools Software WinCT
Weighing pan		270 x 210mm
External dimensions		300(W) x 355(D) x 111(H) mm
Power supply & AC adapter type		Power consumption: Approx. 11VA (supplied to the AC adapter) Confirm that the adapter type is correct for the local voltage and power receptacle type.
Weight		Approx. 8.3kg



Figure C.1 Picture and External Dimensions of GF20K Balance

C.2 OMEGA Data Acquisition Modules

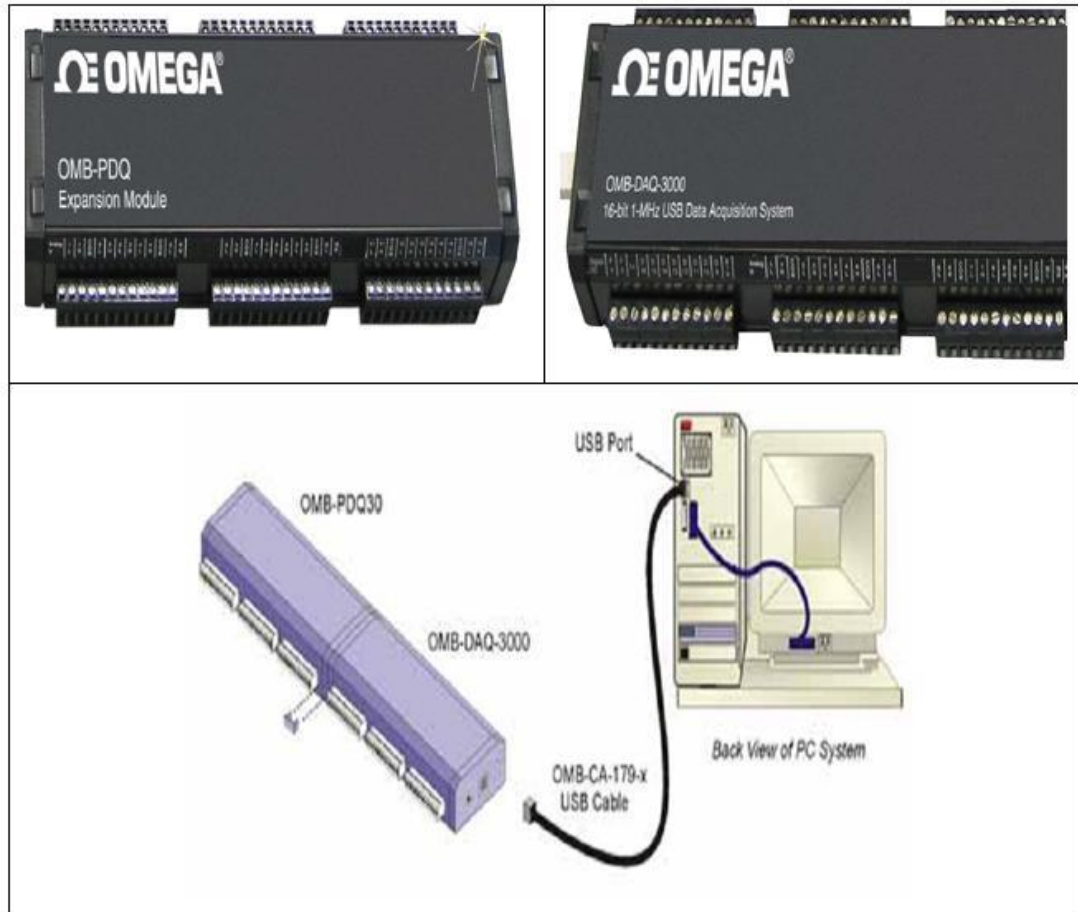


Figure C.2 Picture and Direct Connection of OMB-DAQ-3005 and QMB –PDQ

**Table C.2 Technical Specification of OMB-DAQ-3005 with QMB –PDQ 30
Expansion Module [41]**

ENVIRONMENT:
Operating Temperature: -30 to 70°C
Storage Temperature: -40 to 80°C
Relative Humidity: 0 to 95% non-condensing
Communications: USB 2.0 high-speed mode (480 Mbps), USB1.1 full-speed mode (12 Mbps)
Acquisition Data Buffer: 1 MSample
Signal I/O Connector: Removable screw-terminal blocks
EXTERNAL POWER
Weight: 431 g (0.95 lb)
Connector: Switchcraft# RAPC-712
Power Range: 6 to 16 VDC (used when USB port supplies insufficient power)
Over Voltage: 20 V for 10 seconds, max
Expansion Connector: 25-pin DSUB, female
Dimensions: 269 W x 92 D x 45 mm H (10.6 x 3.6 x 1.6")
ANALOG INPUTS
Channels: 16 single-ended or 8 differential OMB-DAQ-3005
Expansion: An additional 48 analog inputs per board (OMB-PDQ30 module) expansion channels have identical features as the main board channels
Expansion Connector: 25-pin, DSUB, female
Over-Voltage Protection: ± 30 V without damage
Voltage Measurement Speed: 1 μ s per channel
Ranges: Software or sequencer selectable on a per-channel basis, ± 10 V, ± 5 V, ± 2 V, ± 1 V, ± 0.5 V, ± 0.2 V, ± 0.1 V [J,K,T, E,R,S,N Types thermocouples]
Temperature Measurement Speed: Programmable from 100 μ s to 20 ms per channel
Input Impedance: 10M Ω single-ended; 20 M Ω differential
Total Harmonic Distortion: -80 dB typical for ± 10 V range, 1 kHz fundamental
Signal-to-Noise and Distortion: 72 dB typ for ± 10 V range, 1 kHz fundamental
Bias Current: 40 pA typical (0 to 35°C)
Crosstalk: -75 dB typical DC to 60 Hz; -65 dB typical @ 10 kHz
Common Mode Rejection: -70 dB typical DC to 1 kHz
A/D SPECIFICATIONS
Type: Successive approximation
Resolution: 16-bit
Maximum Sample Rate: 1 MHz
Nonlinearity (Integral): ± 2 LSB maximum
Nonlinearity (Differential): ± 1 LSB maximum
EXTERNAL ACQUISITION SCAN CLOCK INPUT
Maximum Rate: 1.0 MHz
Clock Signal Range: Logical zero 0 V to 0.8 V; logical one 2.4 V to 5.0 V
Minimum Pulse Width: 50 ns high, 50 ns low
INPUT SEQUENCER
Analog, digital and frequency inputs can be scanned synchronously
Scan Clock Sources: 2 [1. Internal, programmable 2. External, TTL level input]
Programmable Parameters per Scan: Channel (random order), gain
Depth: 512 locations
On-Board Channel-to-Channel Scan Rate: Analog - 1 MHz maximum Digital - 4 MHz if no analog channels are enabled, 1 MHz with analog channels enabled

Table C.2 Continued

DIGITAL I/O

Channels: 24 Ports: 3 x 8 bit, each port is programmable as input or output
Input Scanning Modes: 2 programmable
Input Characteristics: 220 Ω series resistor, 20 pF to common
Input Protection: ± 15 kV ESD clamp diodes
Input Levels: Low: 0 to 0.8 V; High: 2.0 V to 5.0 V
Output Levels: Low: <0.8 V; High: >2.0 V
Output Characteristics: Output 1.0 mA per pin
Sampling/Update Rate: 4 MHz max

PATTERN GENERATION OUTPUT

Two of the 8-bit ports can be configured for 16-bit pattern generation. The pattern can also be updated synchronously with an acquisition at up to 1 MHz.

COUNTER

Channels: 4 x 32 bit
Input Frequency: 20 MHz max
Input Signal Range: -15 V to 15 V
Input Characteristics: 10K Ω pull up, ± 15 kV ESD protection
Trigger Level: TTL
Minimum Pulse Width: 25 ns high, 25 ns low
Debounce Times: 16 selections from 500 ns to 25.5 ms; positive or negative edge sensitive; glitch detect mode or debounce mode
Time Base Accuracy: 50 ppm (0° to 50°C)
Five Programmable Modes: counter, period, pulsewidth, timing, Encoder
Multi-Axis Quadrature Encoder Inputs: 1 channel with A (phase), B (phase) and Z (index); 2 channel with A (phase) and B (phase); x1, x2 and x4 count modes; single-ended TTL

FREQUENCY/PULSE GENERATORS

Channels: 2 x 16-bit
Output Waveform: Square wave
Output Rate: 1 MHz base rate divided by 1 to 65,535 (programmable)
High-Level Output Voltage: 2.0 V min @ -1.0 mA; 2.9 V min @ -400 μ A
Low-Level Output Voltage: 0.4 V max @ 400 μ A

C.3 TESTO 350S Flue Gas Analyzer



Figure C.3 Picture of TESTO 350S Flue Gas Analyzer

Table-C.3 Technical Specification of TESTO 350S Flue Gas Analyzer[42]

Dimensions:	16" x 11" x 4"	Dewpoint calculation:	0 to 99 °C td
Weight:	4.08 kg	Maximum positive pressure/Flue gas:	20" H ₂ O
Storage temperature:	-4 to +49 °C	Maximum negative pressure:	80" H ₂ O
Operating temperature:	-5 to +45 °C	Pump flow:	0.5 - 1.2 l/min
Housing material:	ABS	Max. dust load:	20 g/m ³ dust in flue gas
Memory:	250,000 readings	Max. humidity load:	+70 °C Dewpoint temperature at sample gas inlet of analyzer box
Power supply:	Via built-in power supply (90 V to 260 V, 47 to 63 Hz) or exchangeable rechargeable batteries or external 12 V cables	Trigger input:	Voltage 5 to 12 Volt (rising or falling edge)
Electrical power consumption:	0.5 A (110 V AC), 0.3 A (230 V AC)	Pulse width:	> 1 s
Load:	5 V/max, 5 mA, 12 V/max. 40 mA	Communication with PC:	RS 232
Sensor Properties			
	O₂	CO	CO₂ (calculated)
Range	0 to 25% vol.	1. 0 to 10,000 ppm H ₂ comp.	0 - CO ₂ max vol. %
Accuracy	< 0.2% of m.v.	< 5 ppm 0 to 99 ppm < 5% of m.v. 100 to 2,000 ppm < 10% of m.v. 2,001 to 10,000 ppm	Calculated from O ₂
Resolution	0.1 vol. %	1 ppm	0.01 vol. %
Response Time	20 s (t95)	40 s (t90)	-
Type:	Electrochemical	Electrochemical	Electrochemical

C.4 ASHCROFT CXLdp Differential Pressure Transducer

Table C.4 Technical Specification ASHCROFT CXLdp Differential Pressure Transducer

	Reference Temperature	21 °C
	Accuracy Class	± 0.4 %
	Pressure Range	0 - 0.10'' Water Column
	Response Time	250 msec
	Warm-up Time	15 sec
	Storage Temperature Limit	-40 to 82 °C
	Operating Temperature Limit	-18 to 71 °C
	Compensated Temperature Range	2 to 54 °C
	Power supply	12 -36 VDC
	Output signal	4-20 mA
	Weight:	Approximately 71 g

APPENDIX-D

COMPLEMENTARY EXPERIMENTAL RESULTS

Exp. No:0000-1 Temperature Measurement

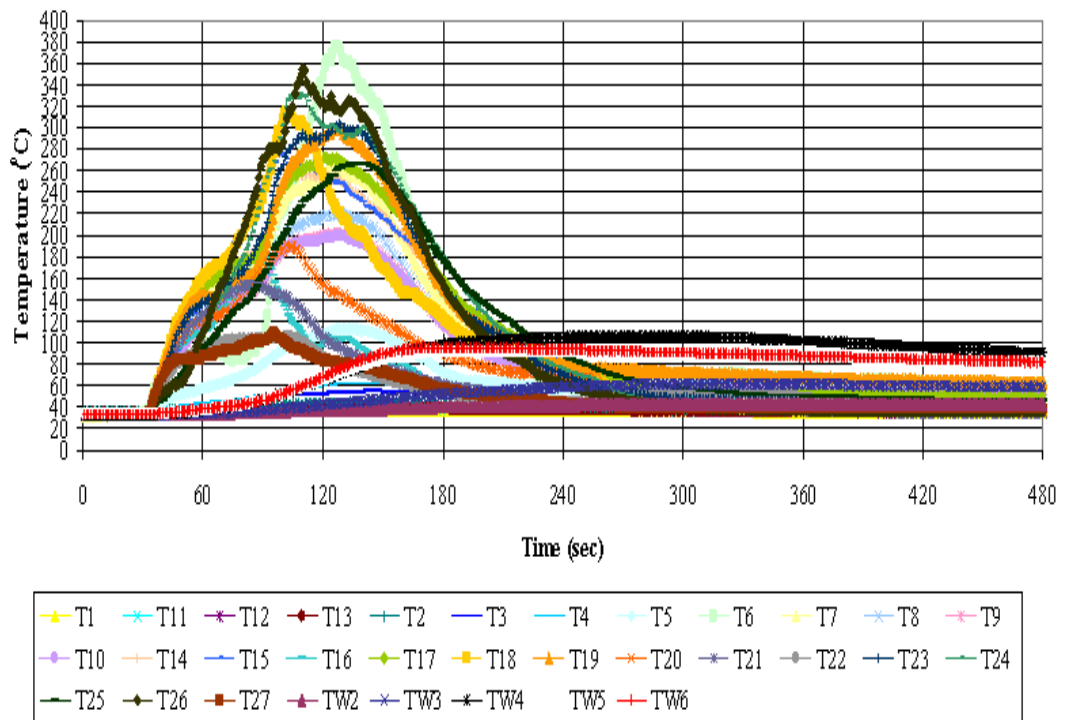


Figure D.1 Experiment No: 0000

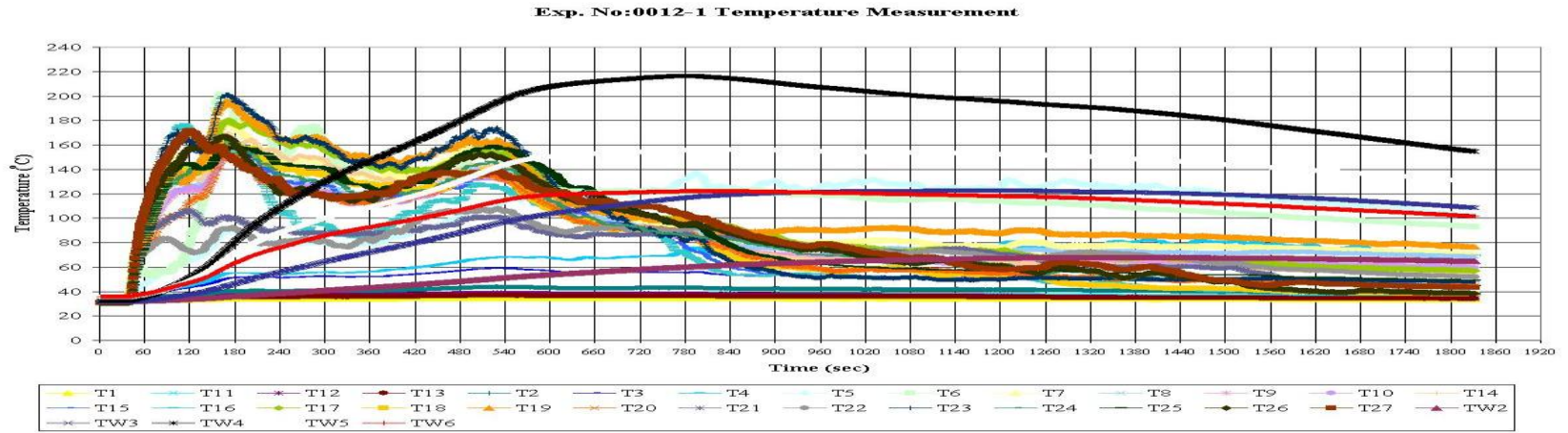


Figure D.2 Experiment No: 0012

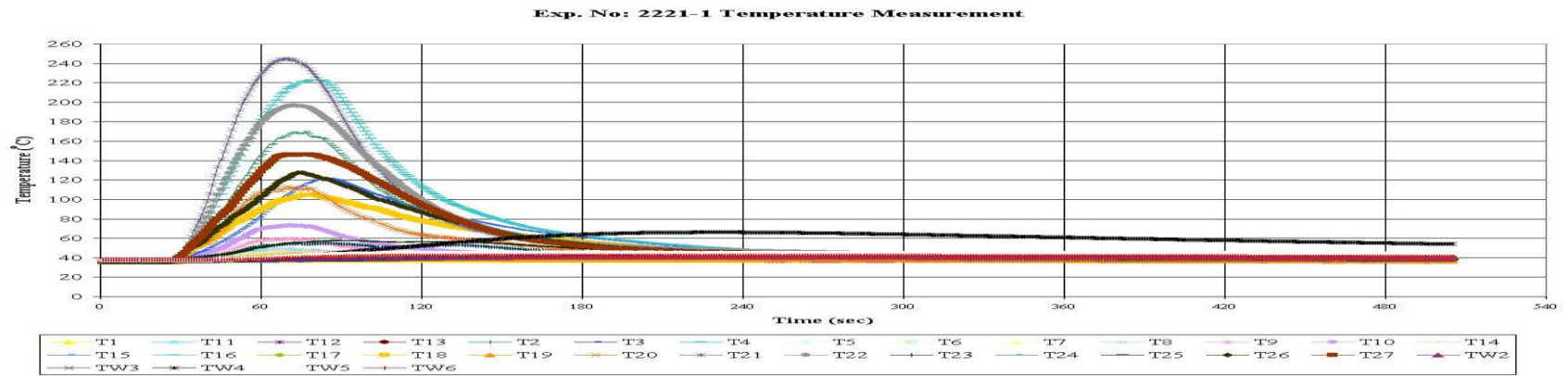


Figure D.3 Experiment No: 2221

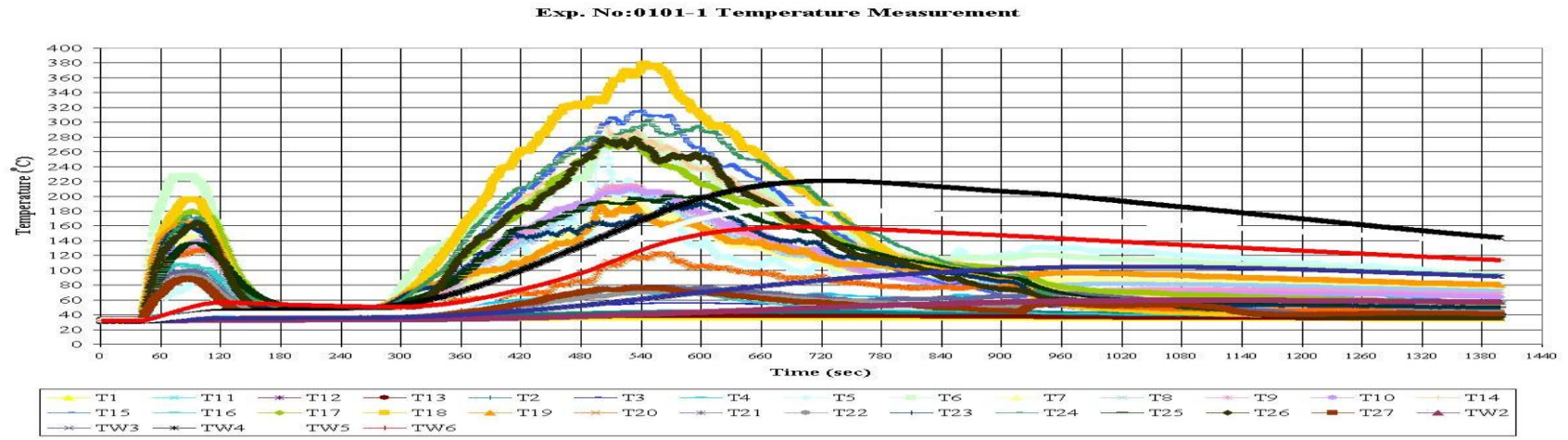


Figure D.4 Experiment No: 0101

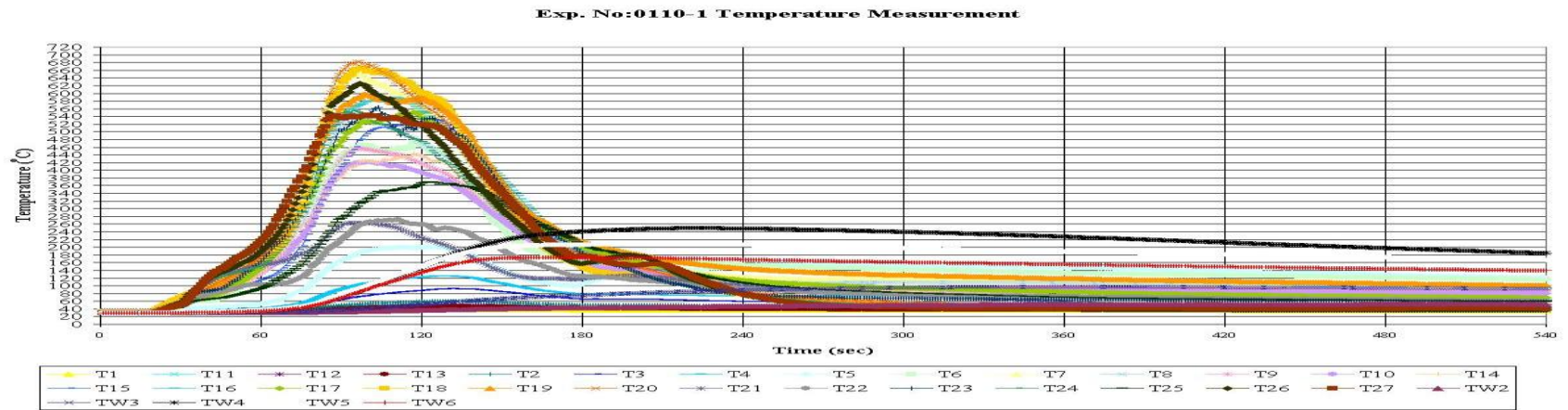


Figure D.5 Experiment No: 0110

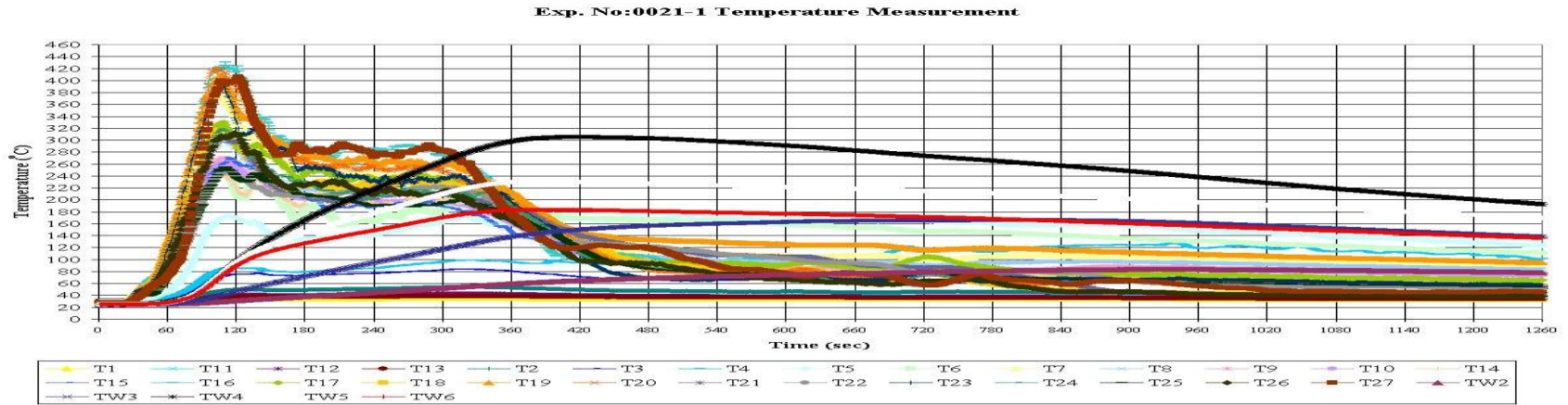


Figure D.6 Experiment No: 0021

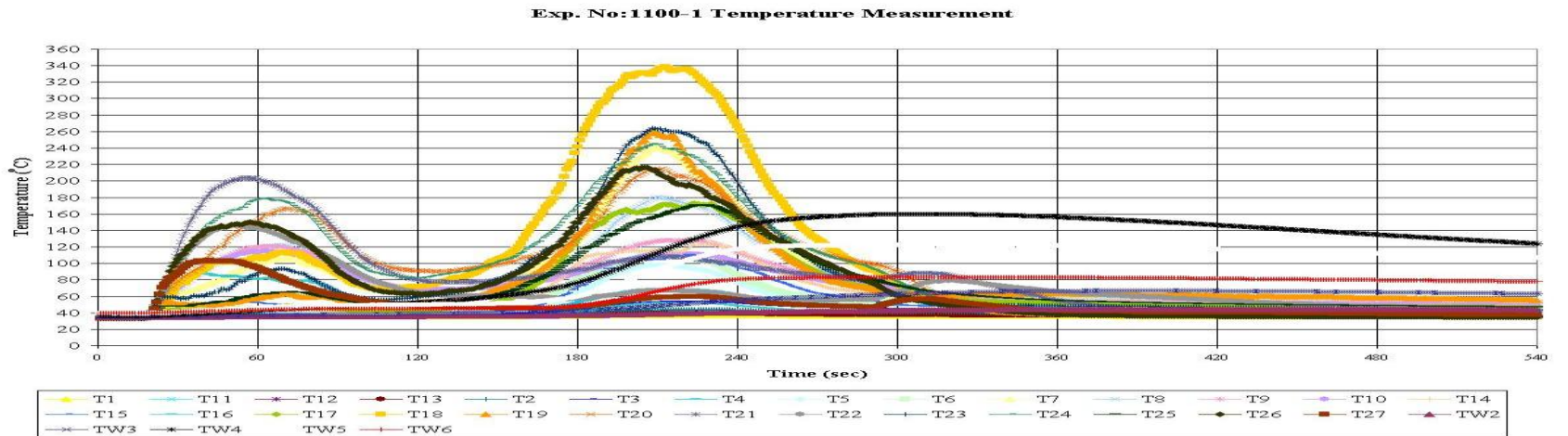


Figure D.7 Experiment No: 1100

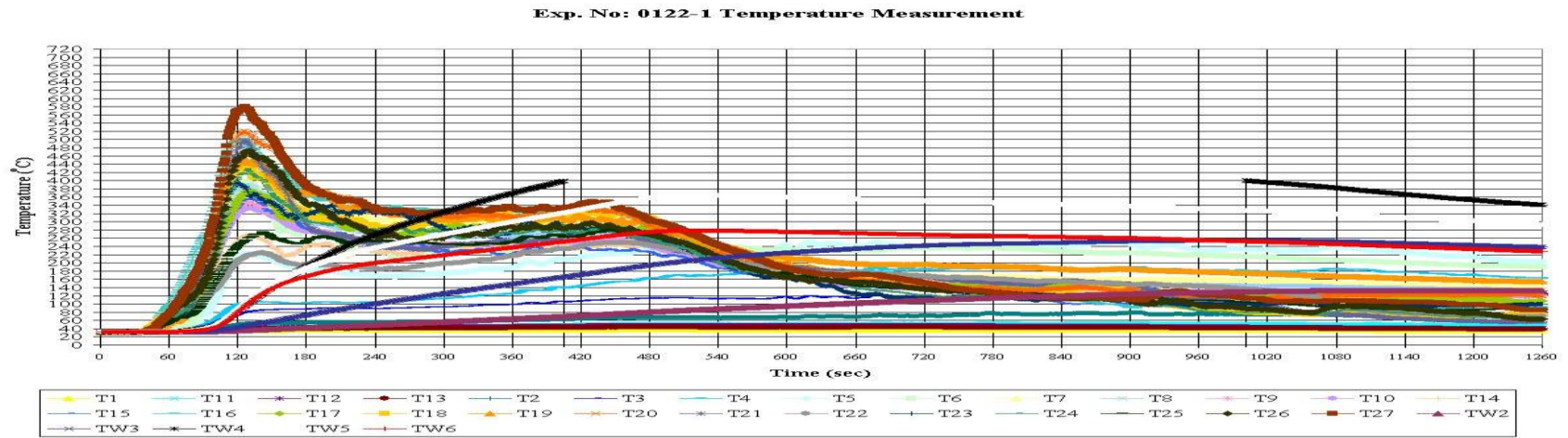


Figure D.8 Experiment No: 0122

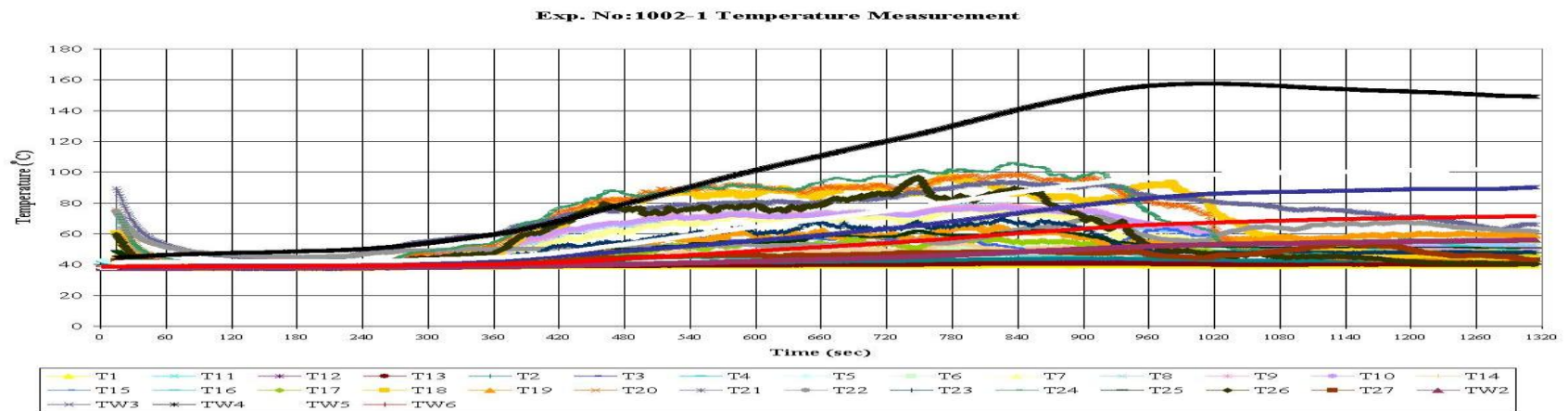


Figure D.9 Experiment No: 1002

Exp. No:1011-1 Temperature Measurement

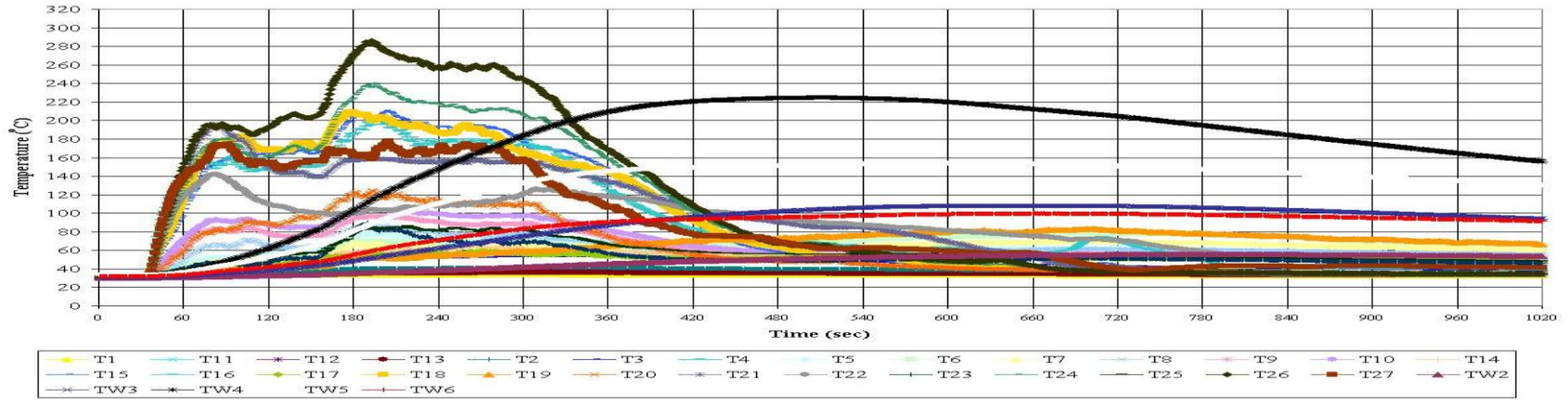


Figure D.10 Experiment No: 1011

Exp. No:0220-1 Temperature Measurement

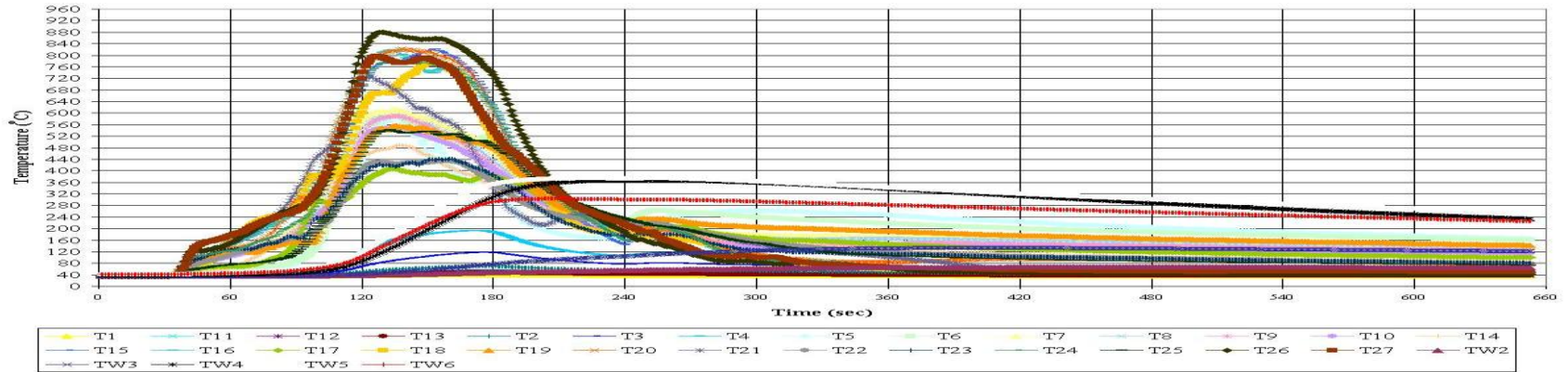


Figure D.11 Experiment No: 0220

Exp. No:0202-1 Temperature Measurement

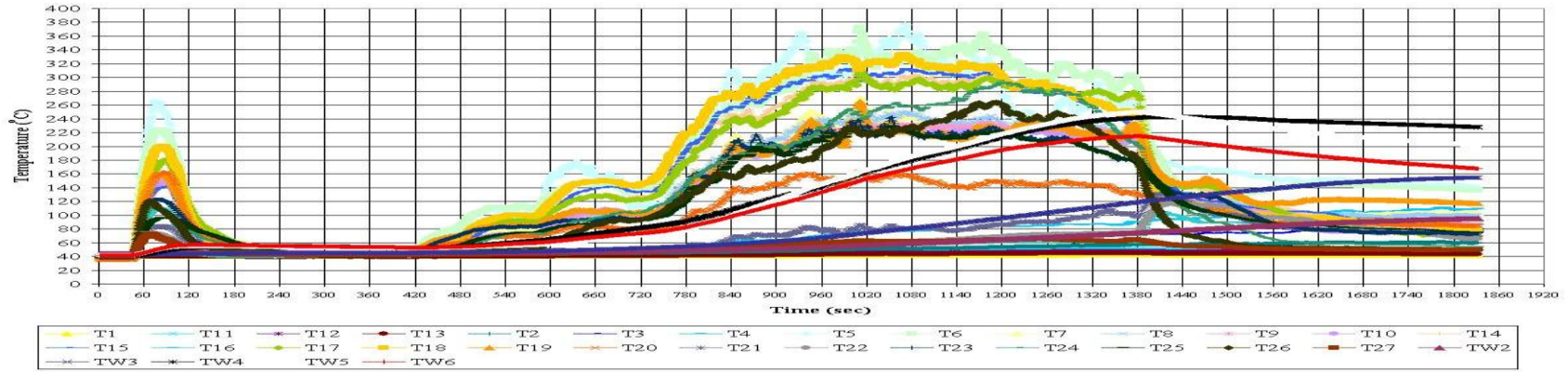


Figure D.12 Experiment No: 0202

Exp. No:1112-1 Temperature Measurement

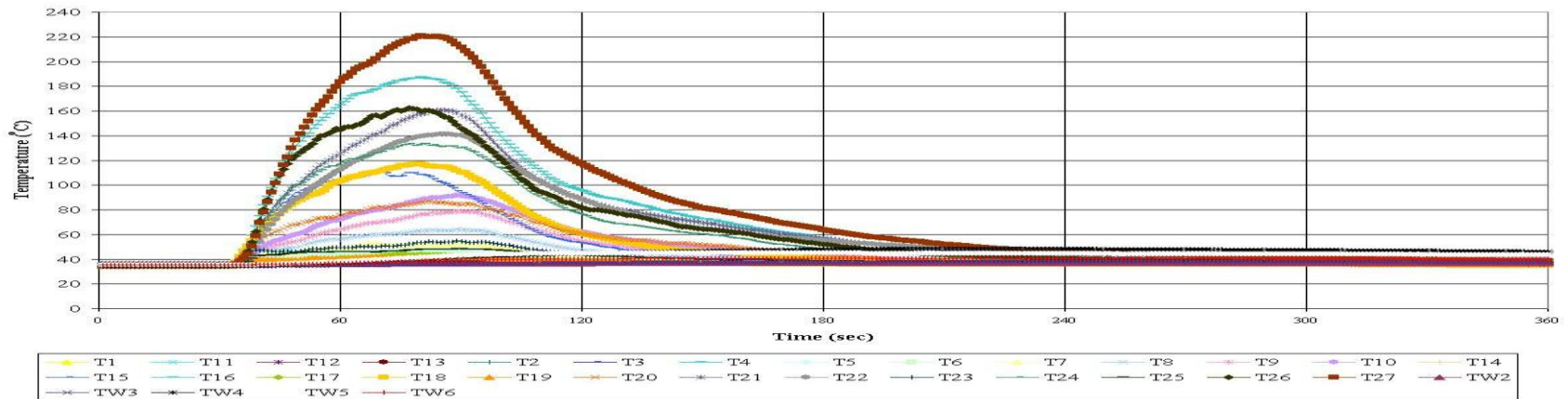


Figure D.13 Experiment No: 1112

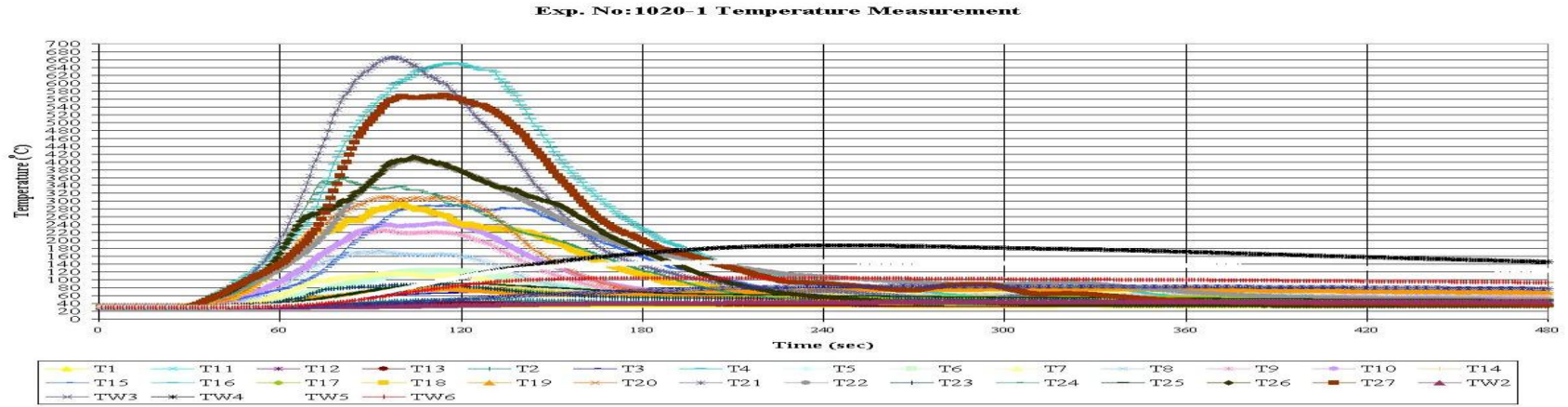


Figure D.14 Experiment No: 1020

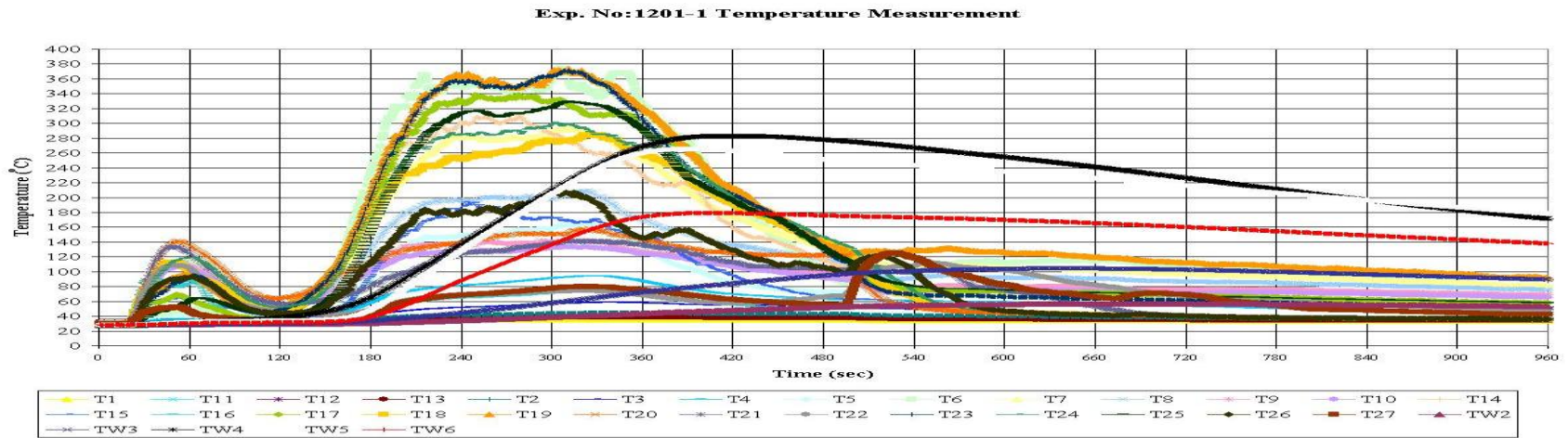


Figure D.15 Experiment No: 1201

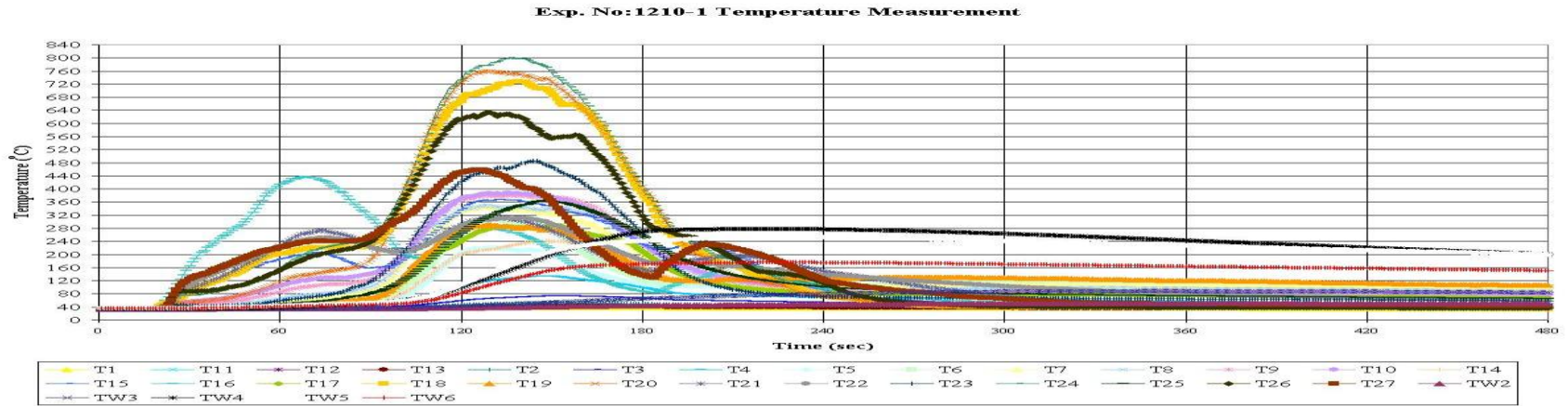


Figure D.16 Experiment No: 1210

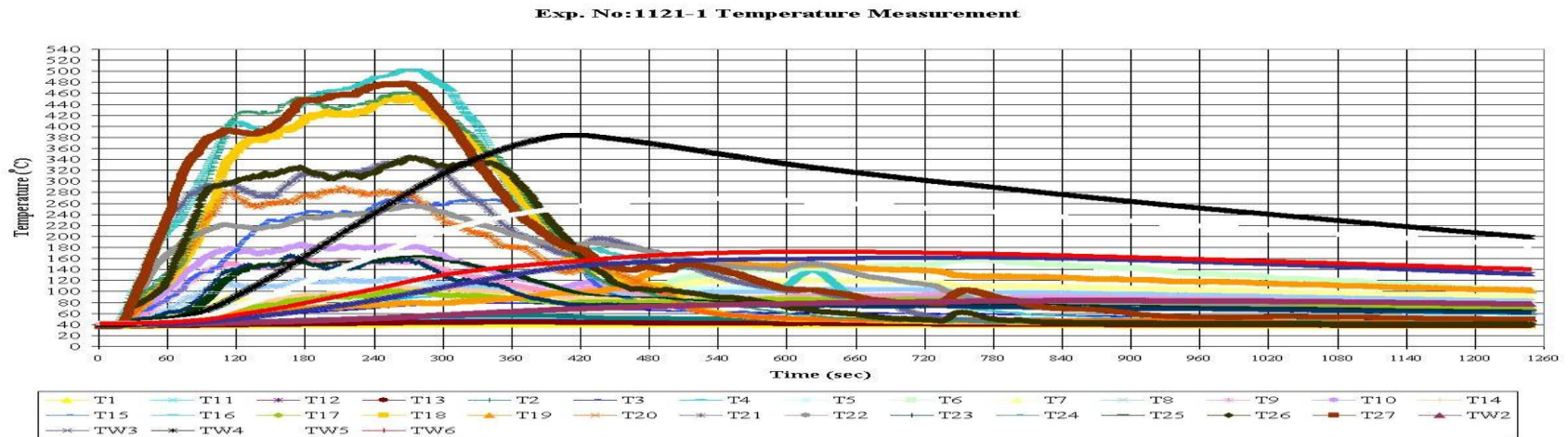


Figure D.17 Experiment No: 1121

Exp. No:2001-2 Temperature Measurement

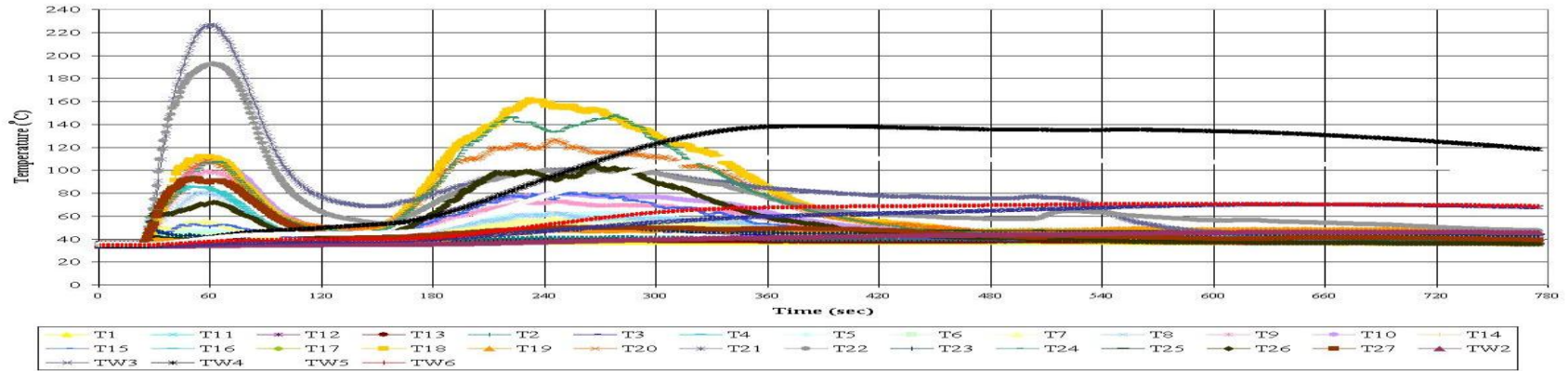


Figure D.18 Experiment No: 2001

Exp. No:2010-1 Temperature Measurement

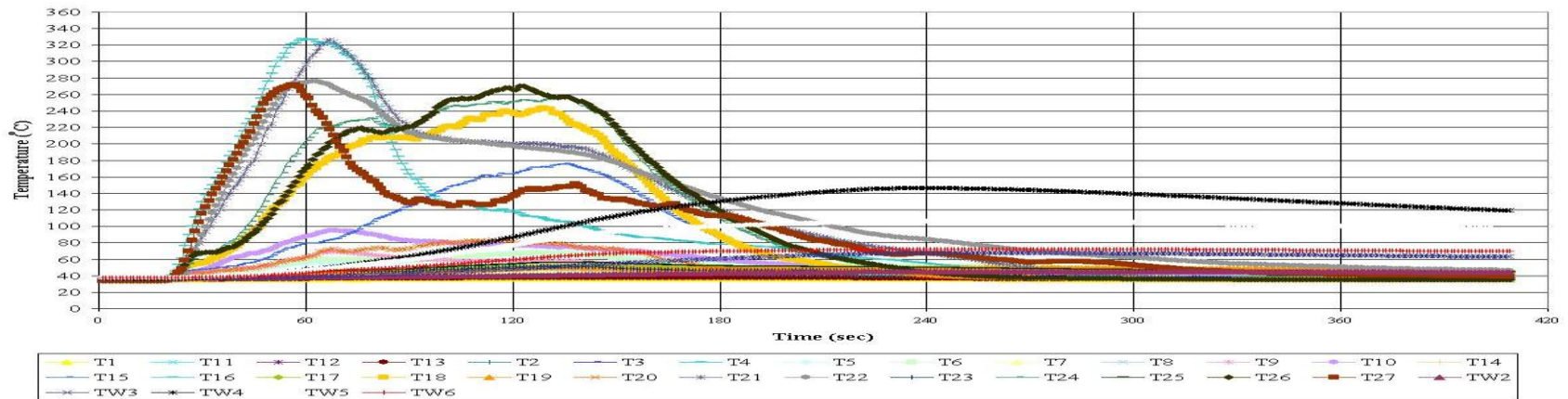


Figure D.19 Experiment No: 2010

Exp. No:1222-1 Temperature Measurement

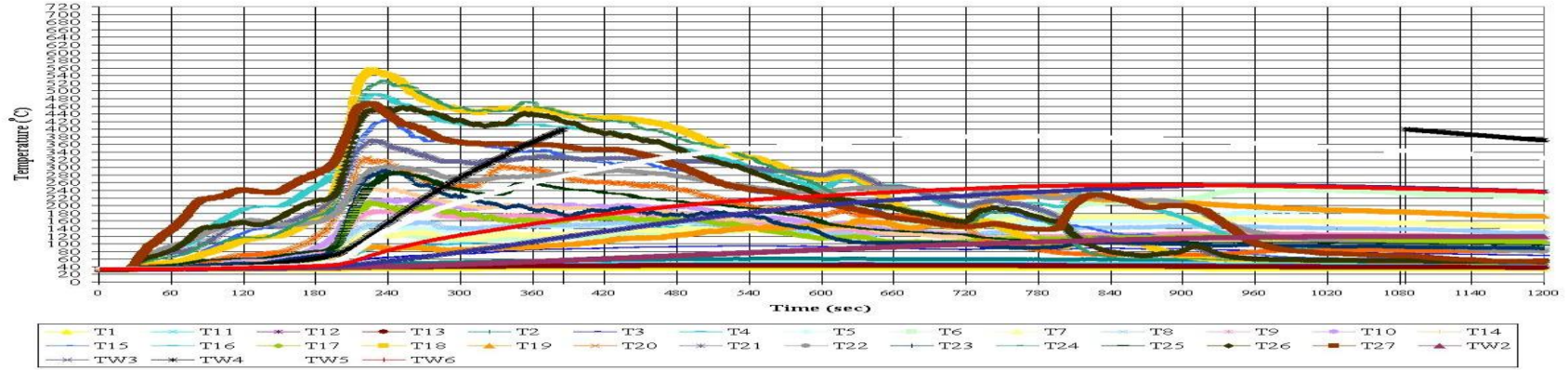


Figure D.20 Experiment No: 1222

Exp. No:2102-2 Temperature Measurement

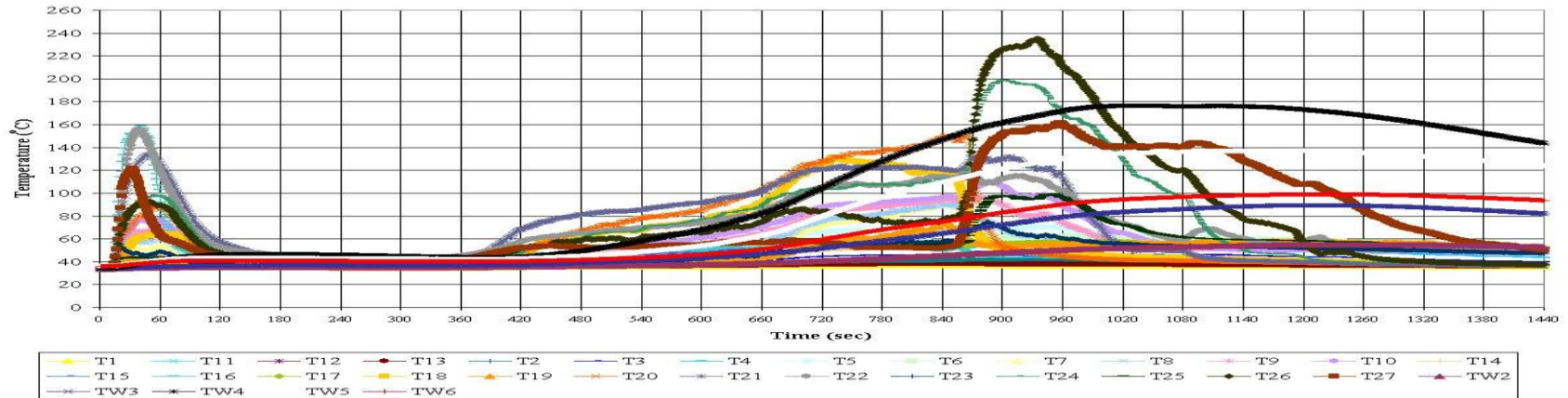


Figure D.21 Experiment No: 21002

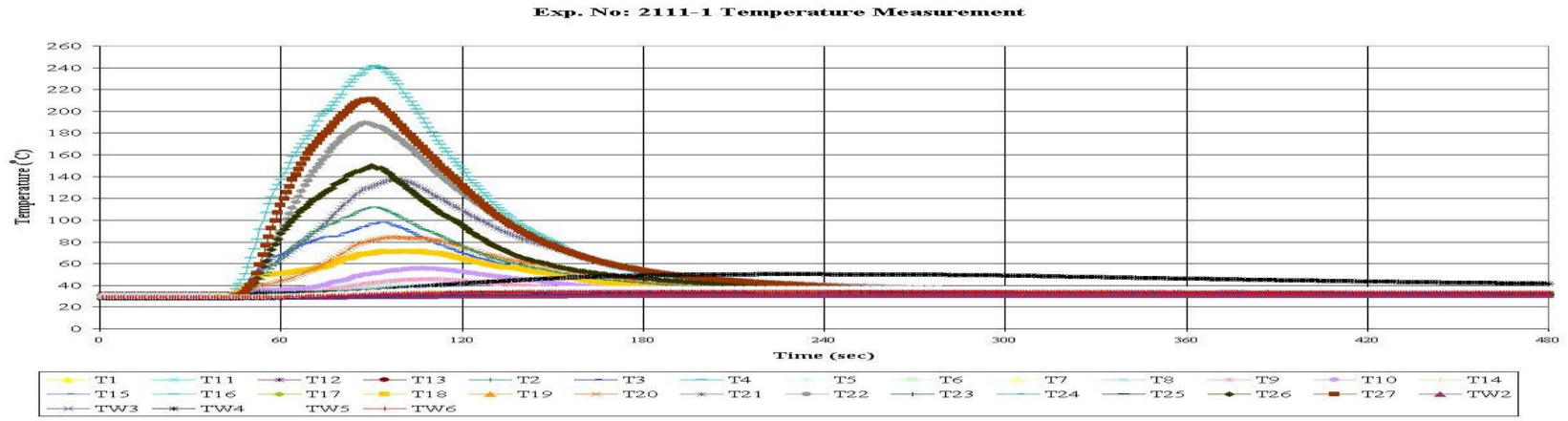


Figure D.22 Experiment No: 2111

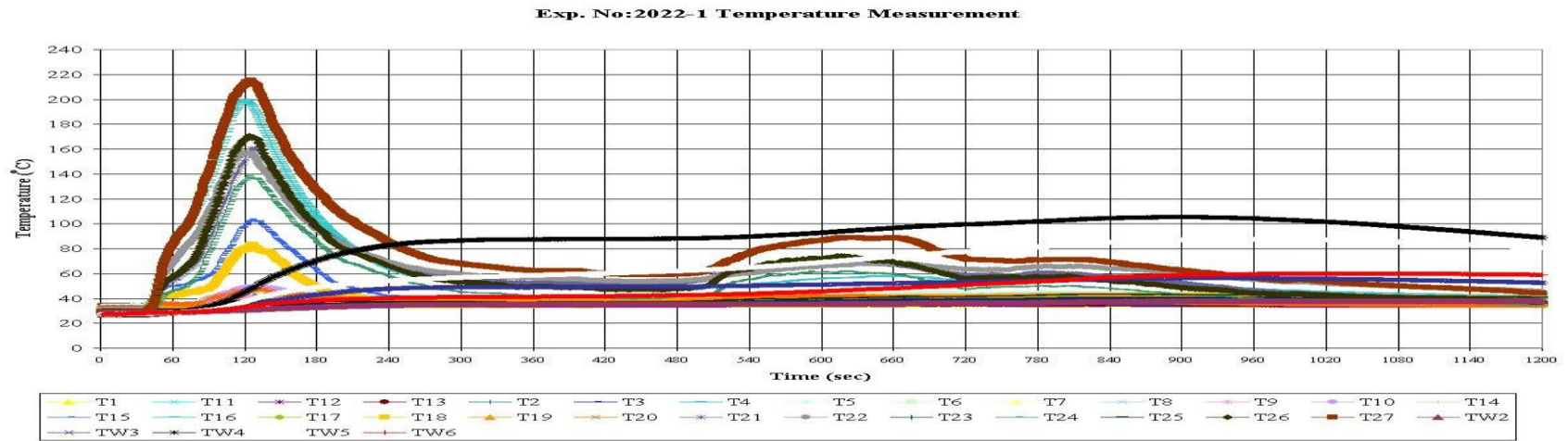


Figure D.23 Experiment No: 2022

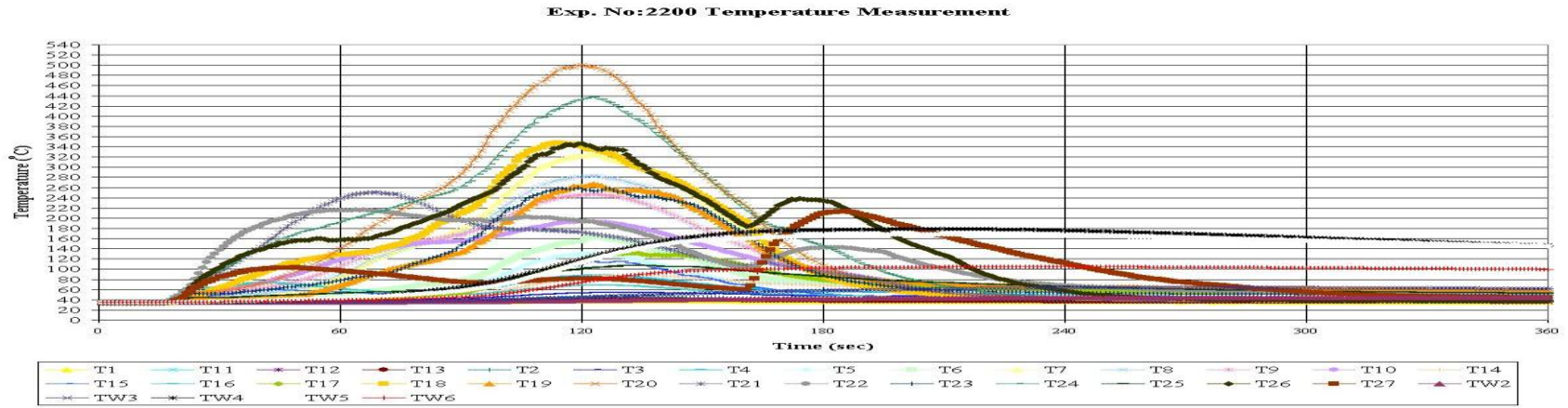


Figure D.24 Experiment No: 2200

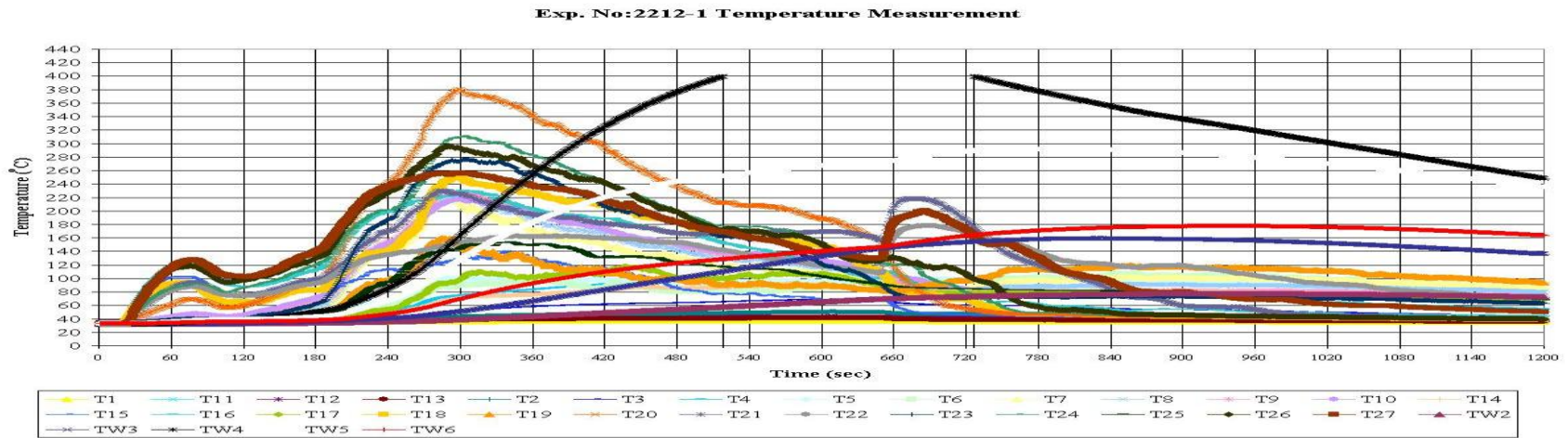


Figure D.25 Experiment No: 2212

Exp. No: 2120-1 Temperature Measurement

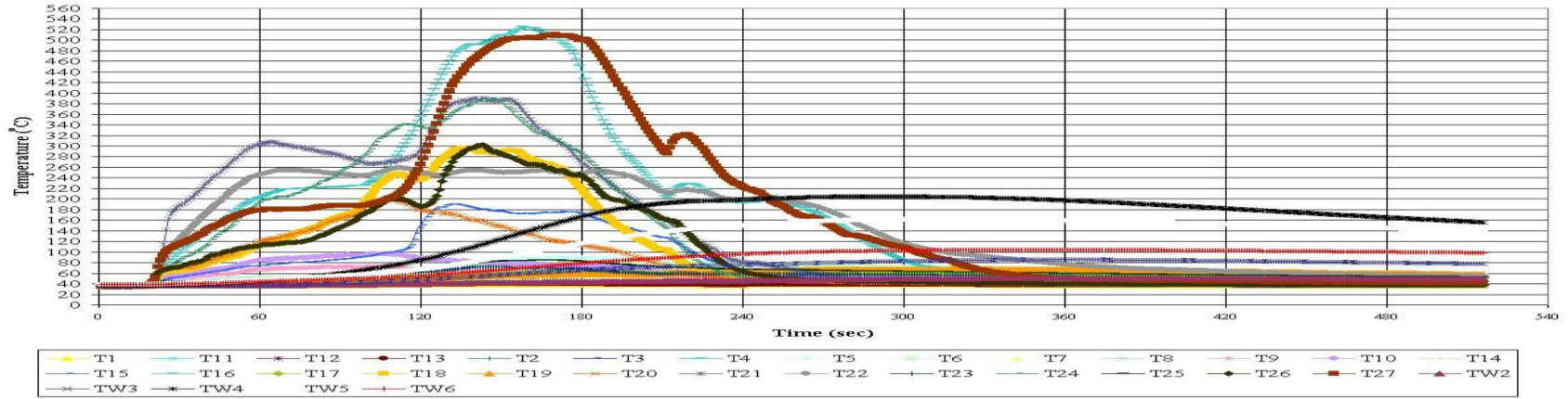


Figure D.26 Experiment No: 2120

Exp. No: 1000-1 Temperature Measurement

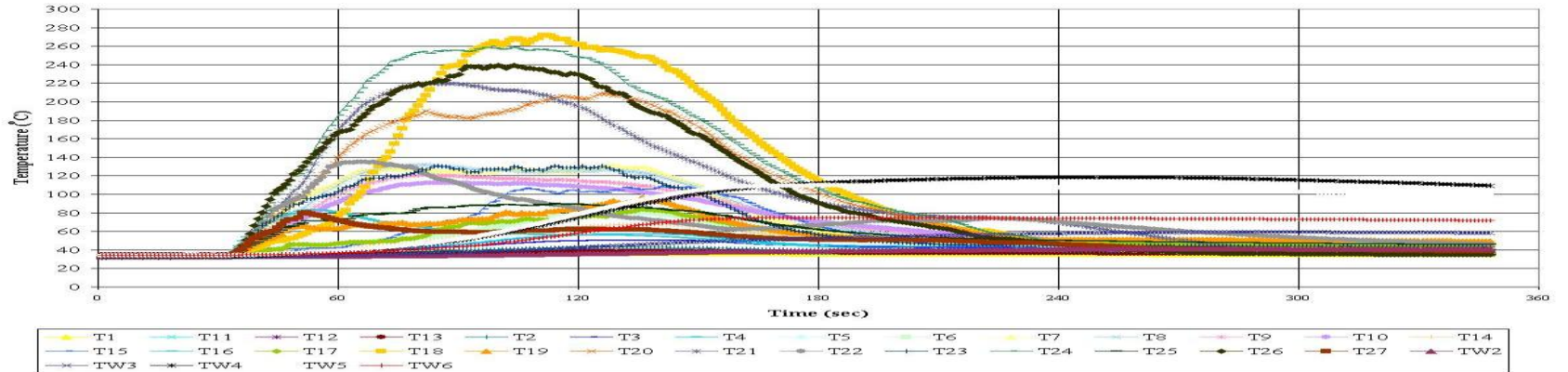


Figure D.27 Experiment No: 1000

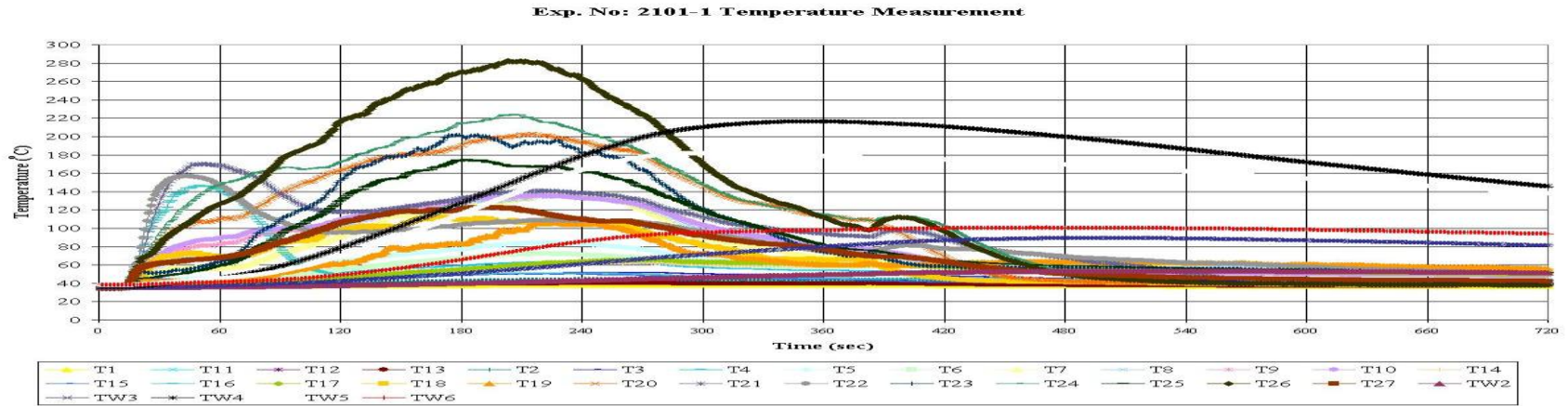


Figure D.28 Experiment No: 2101

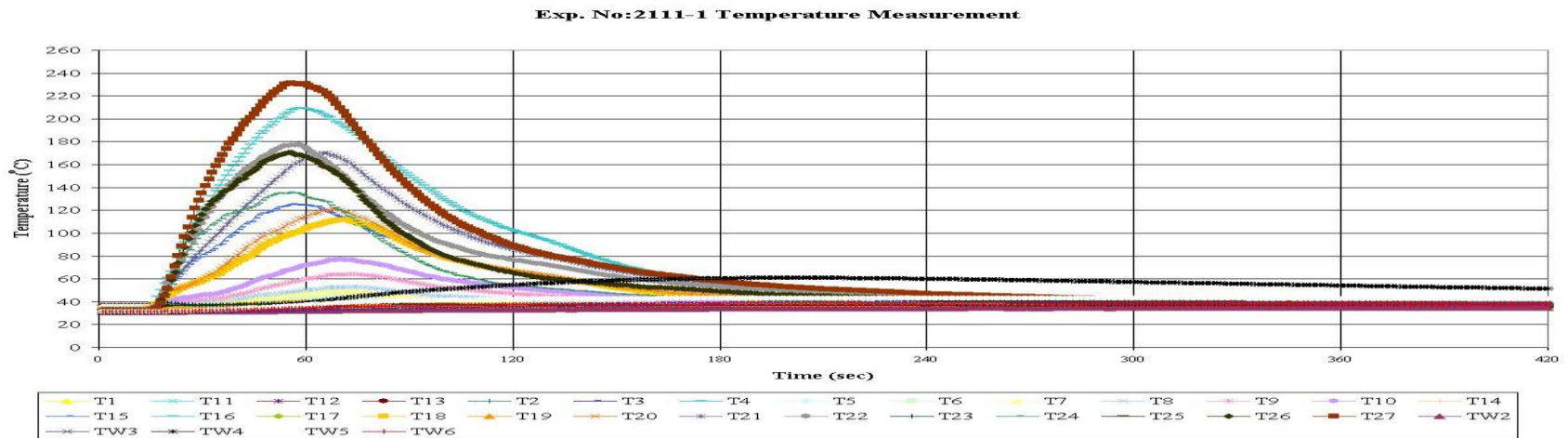


Figure D.29 Experiment No: 2111

Exp. No: 1200-1 Temperature Measurement

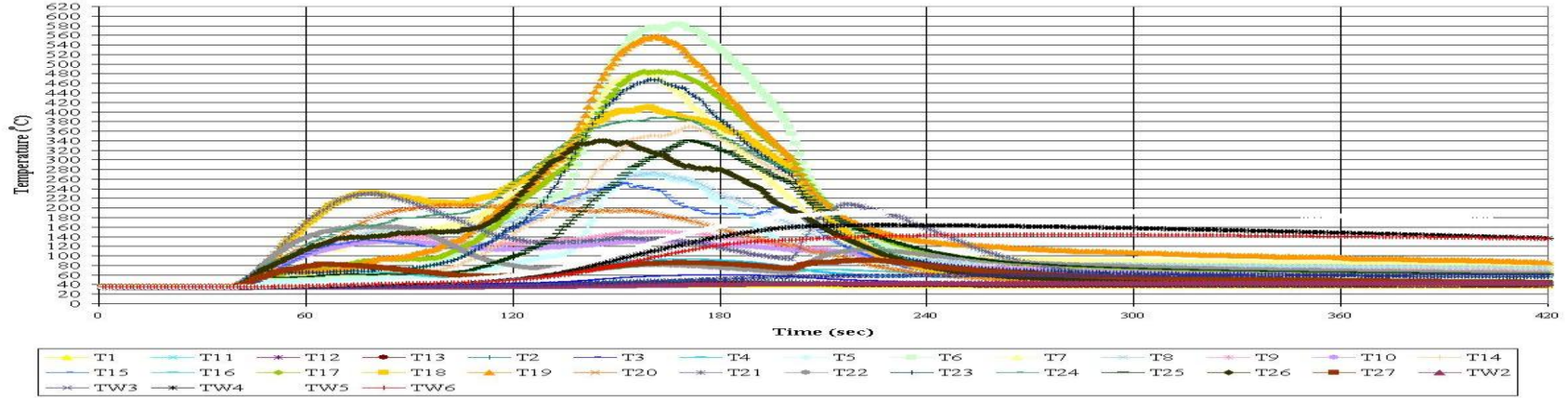


Figure D.30 Experiment No: 1200

Exp. No: 20220 Temperature Measurement

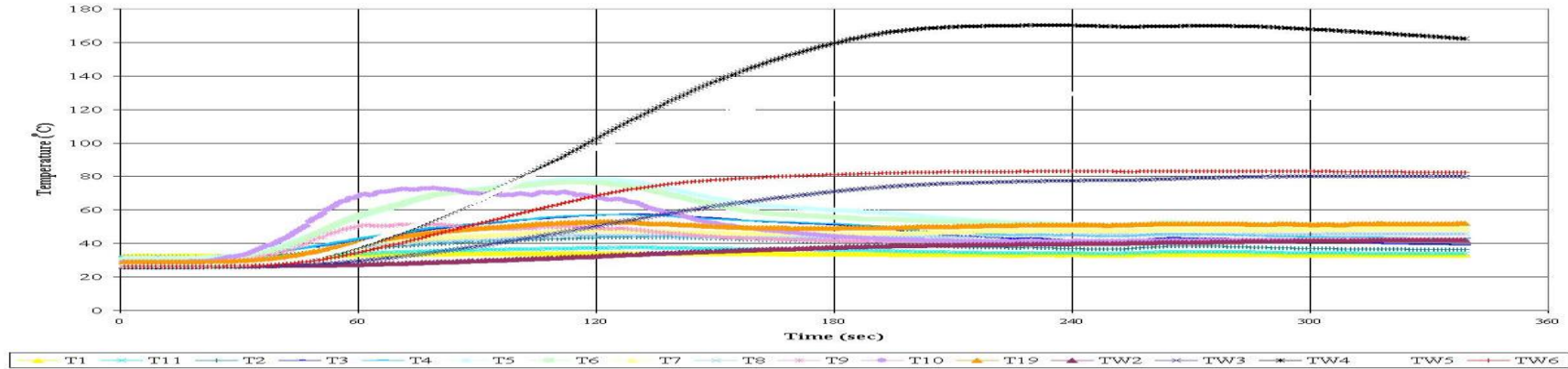


Figure D.31 Experiment No: 20220

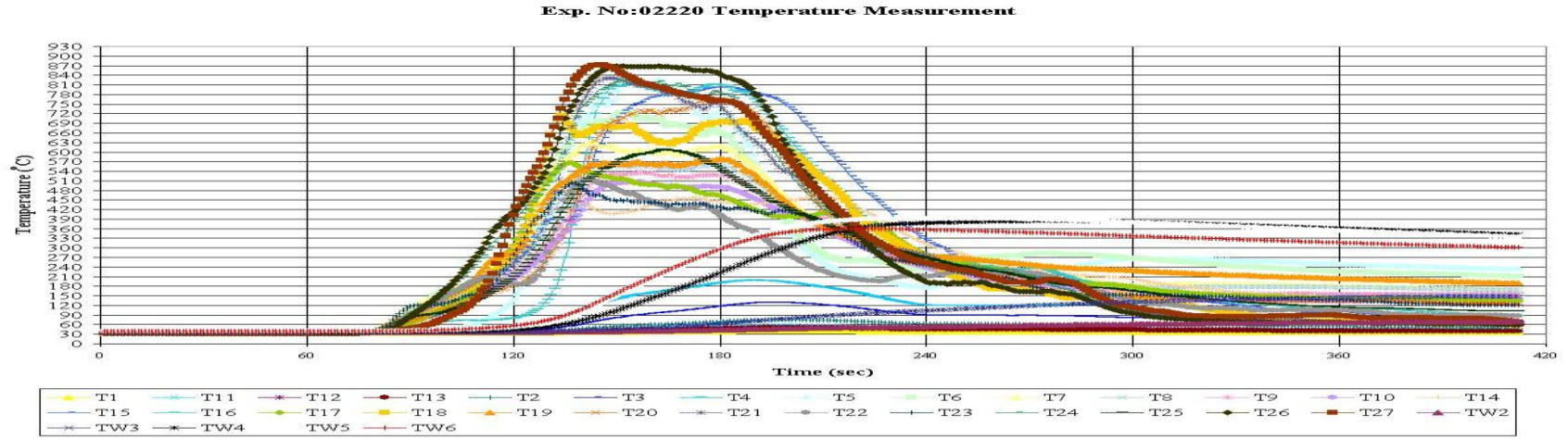


Figure D.32 Experiment No: 02220

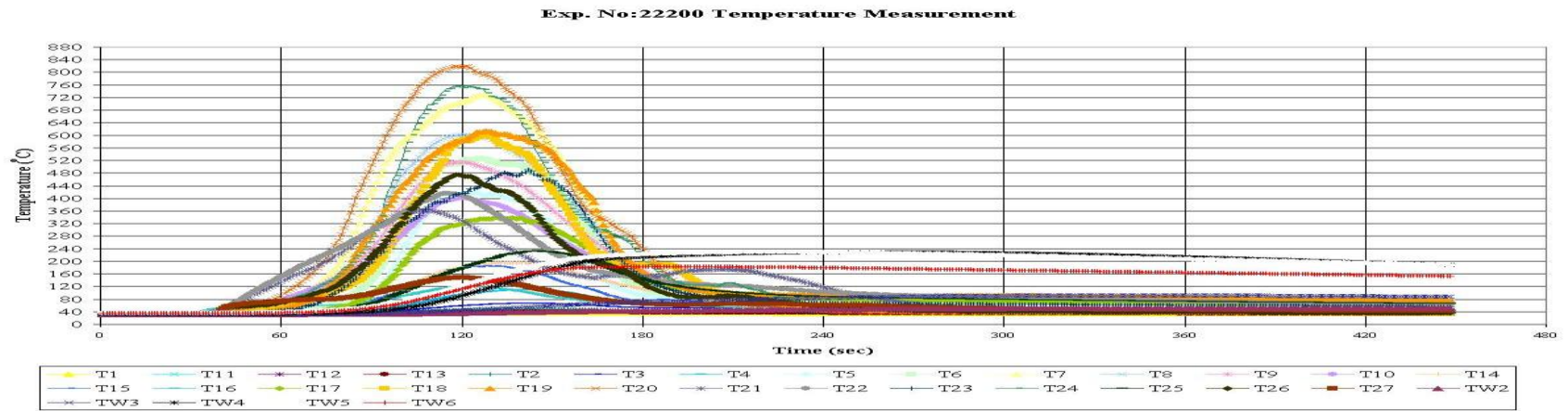


Figure D.33 Experiment No: 22200

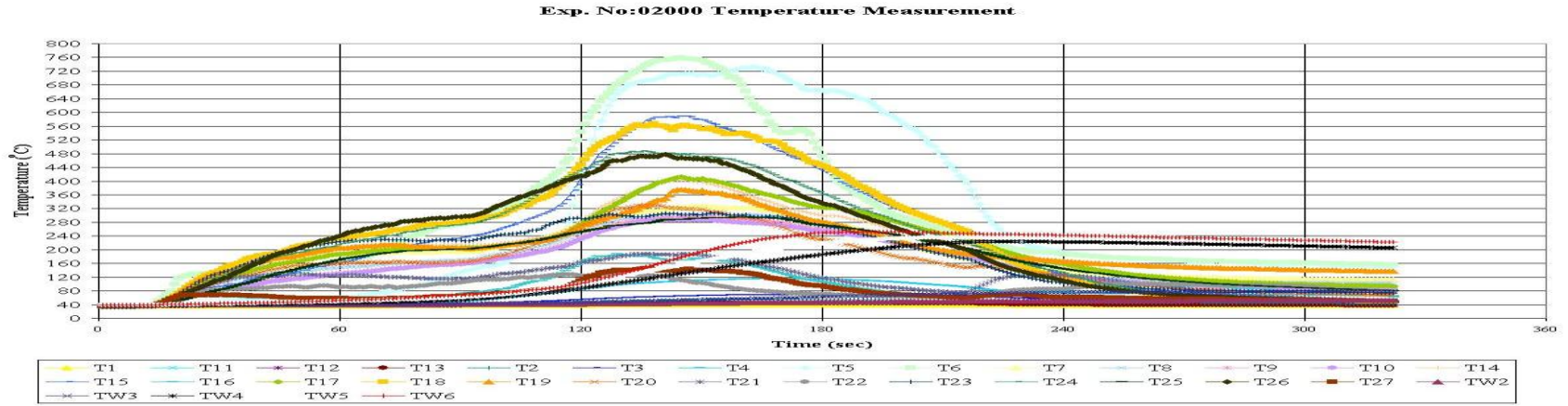


Figure D.34 Experiment No: 02000

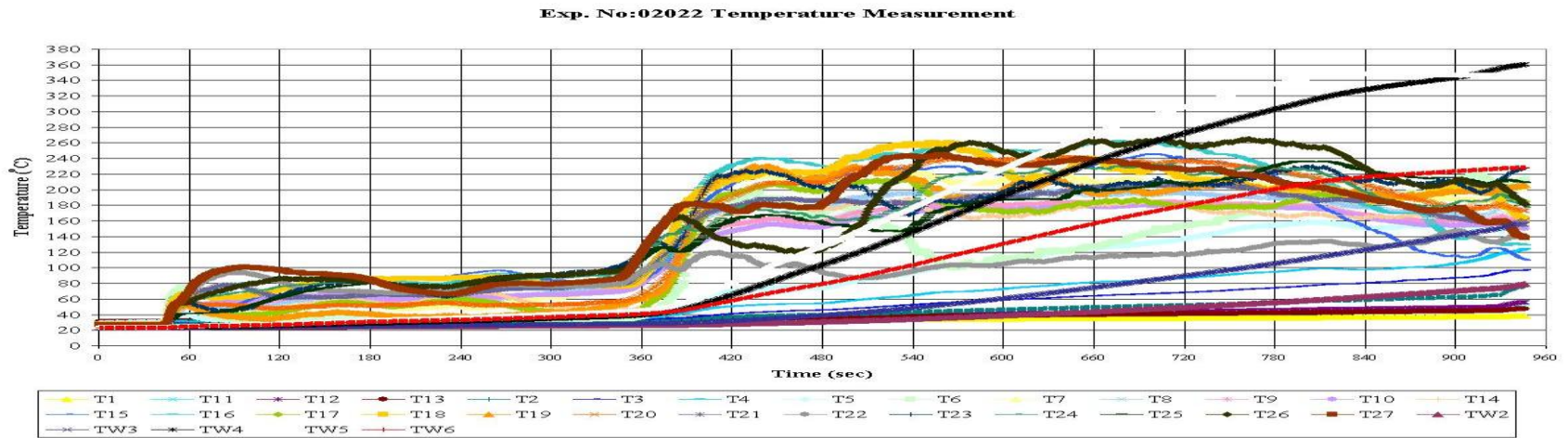


Figure D.35 Experiment No: 02022

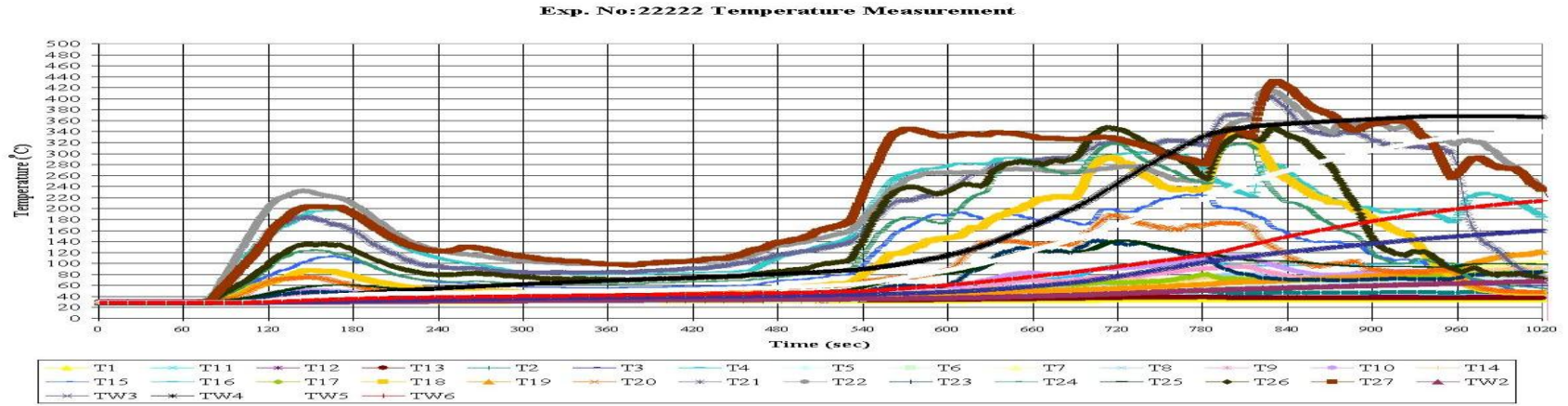


Figure D.36 Experiment No: 22222

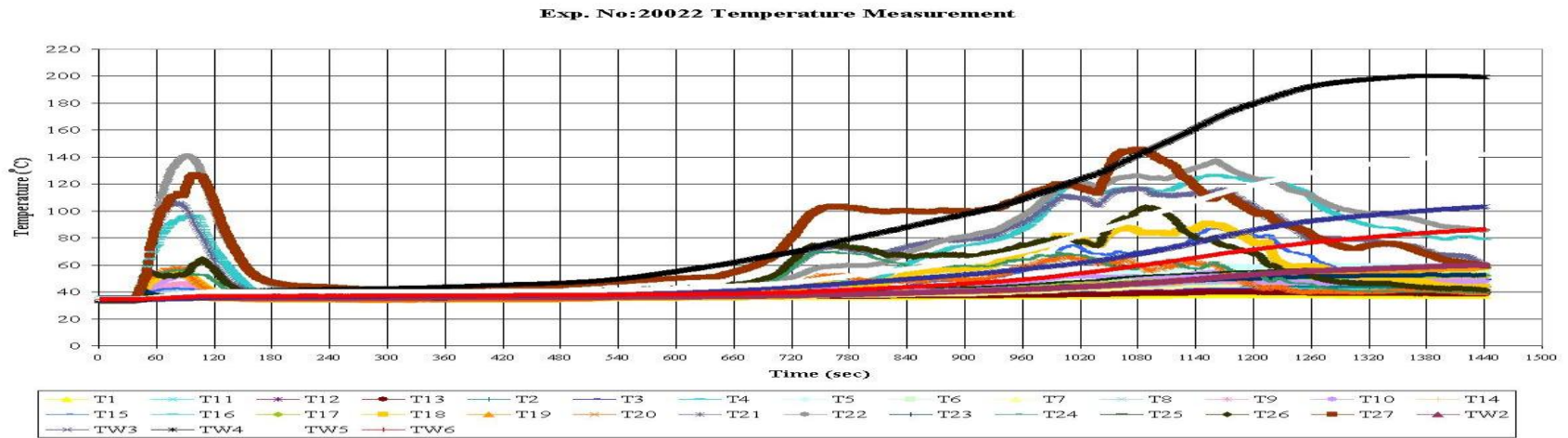


Figure D.37 Experiment No: 20022

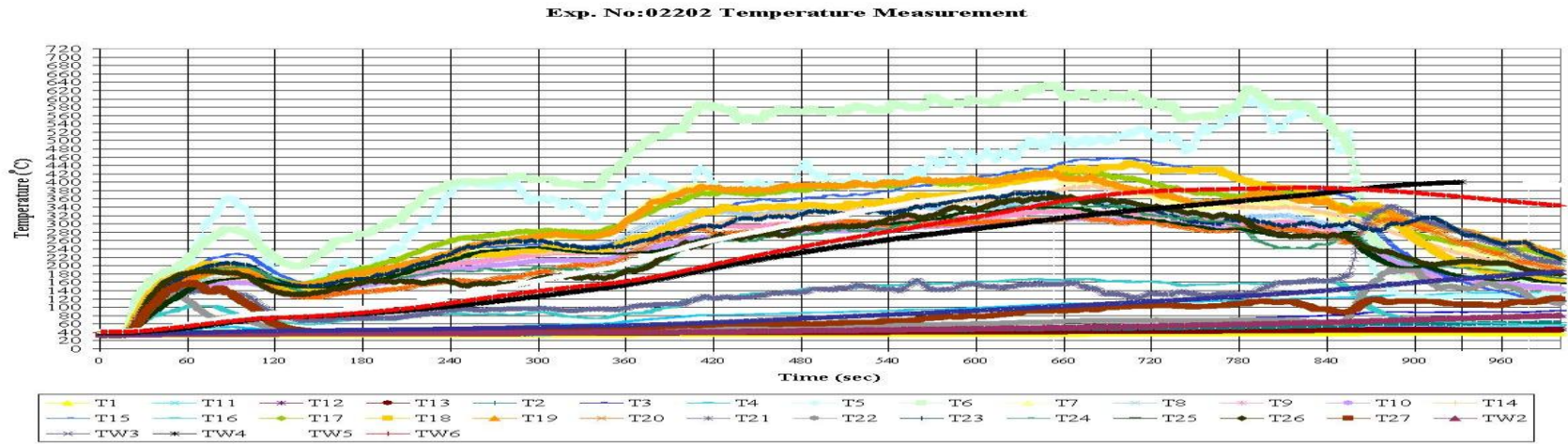


Figure D.38 Experiment No: 02202

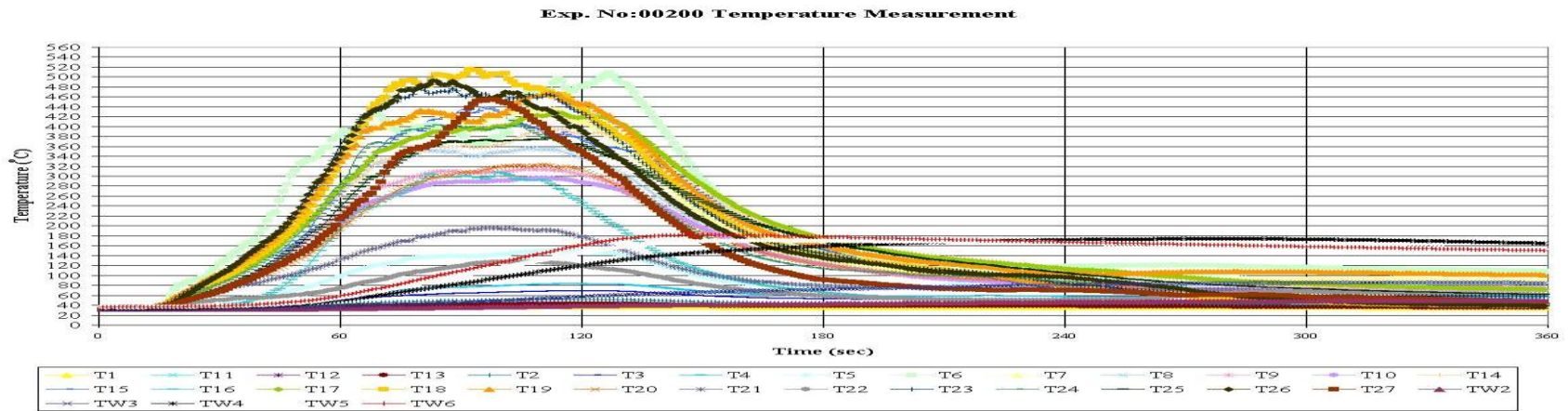


Figure D.39 Experiment No: 00200

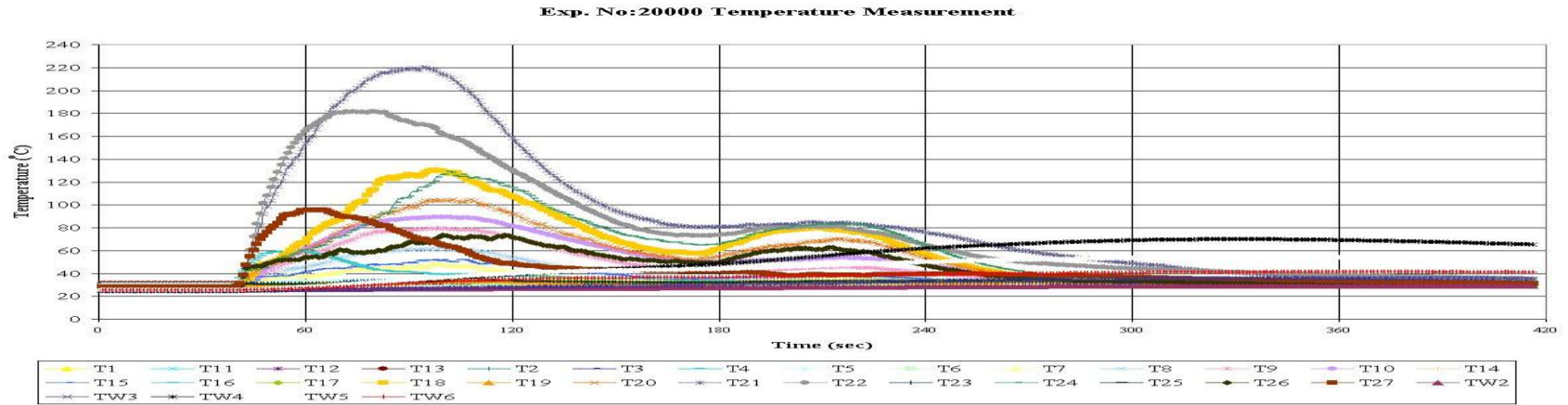


Figure D.40 Experiment No: 20000

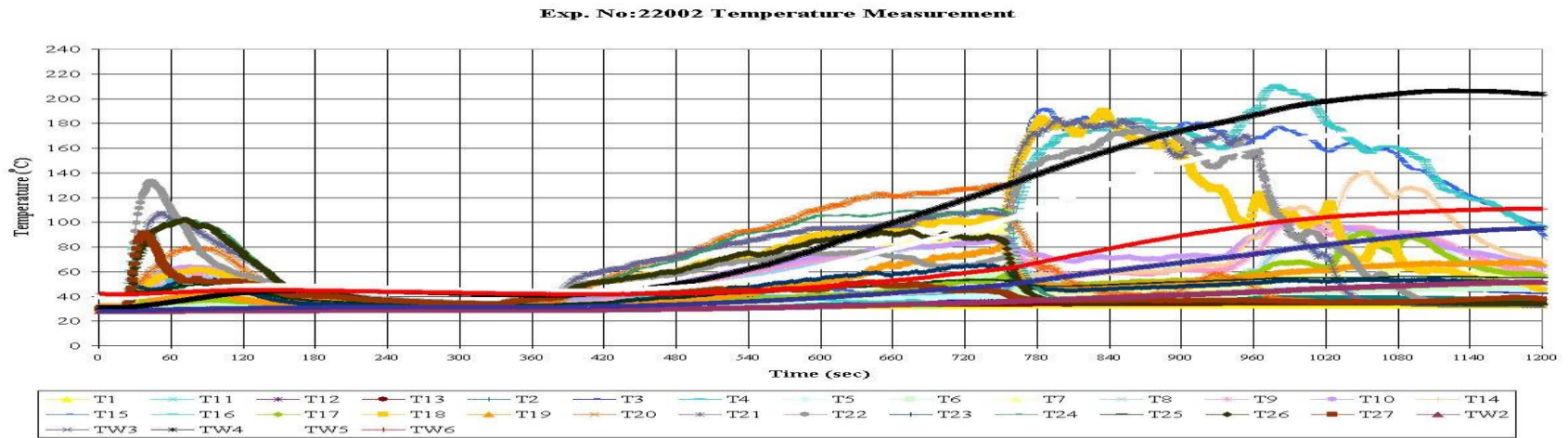


Figure D.41 Experiment No: 22002

Exp. No:22020 Temperature Measurement

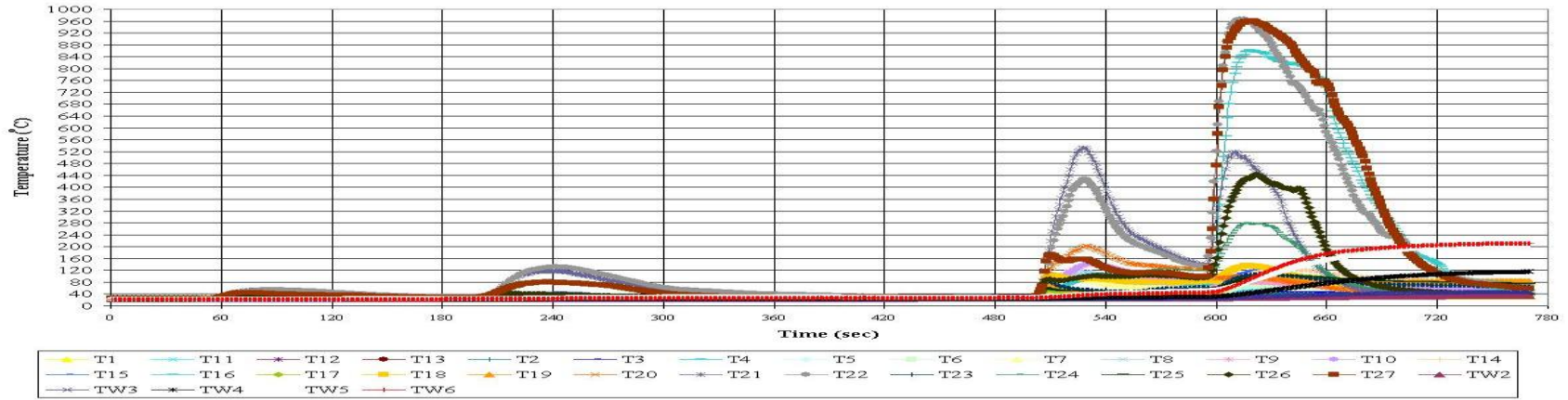


Figure D.42 Experiment No: 22020

Exp. No:20202 Temperature Measurement

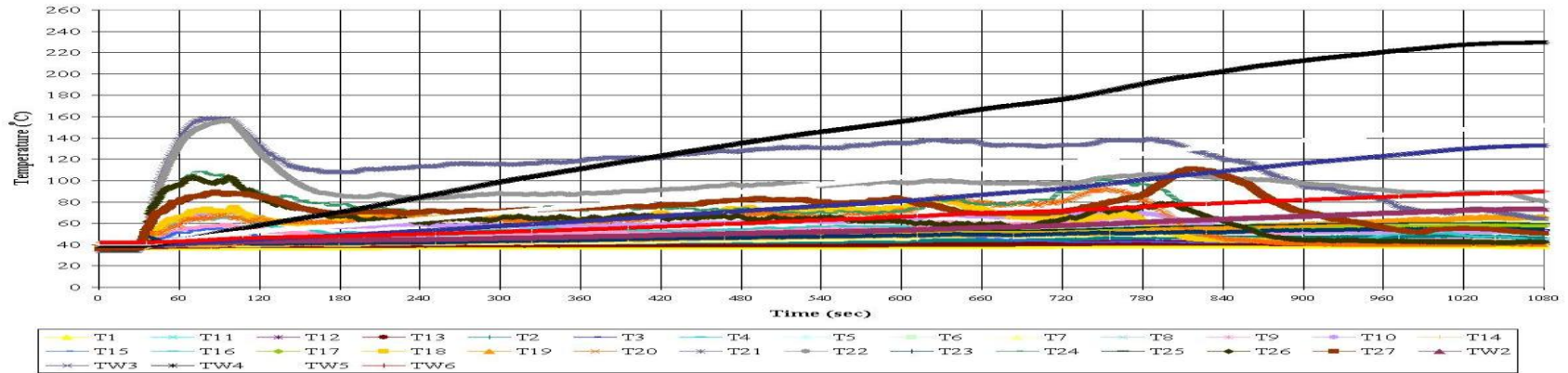


Figure D.43 Experiment No: 20202

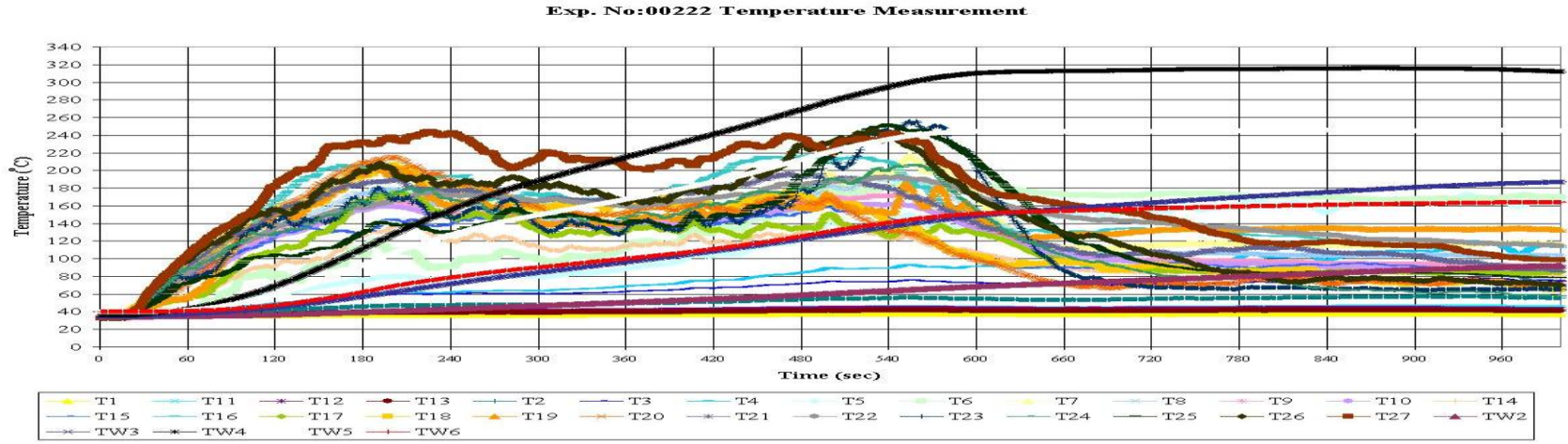


Figure D.44 Experiment No: 00222

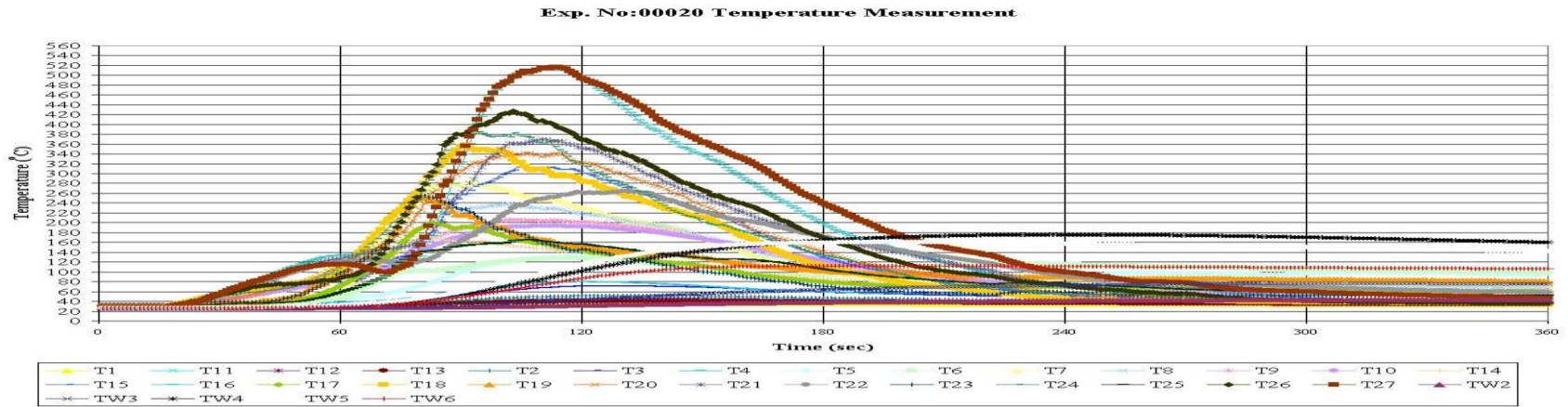


Figure D.45 Experiment No: 00020

Exp. No: (-1)122 Temperature Measurement

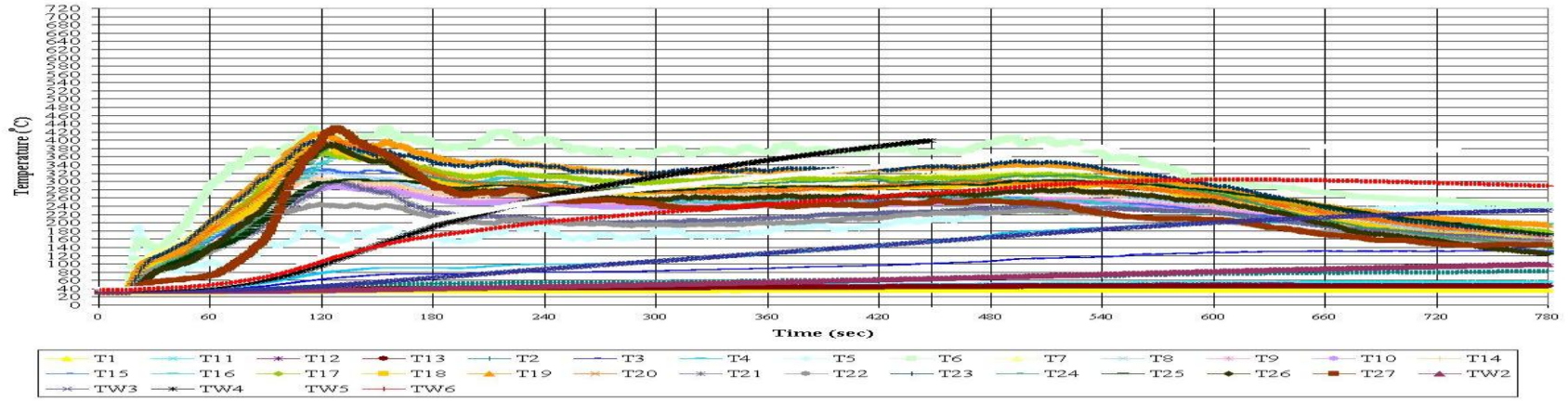


Figure D.46 Experiment No: (-1)122

Exp. No: (-1)011 Temperature Measurement

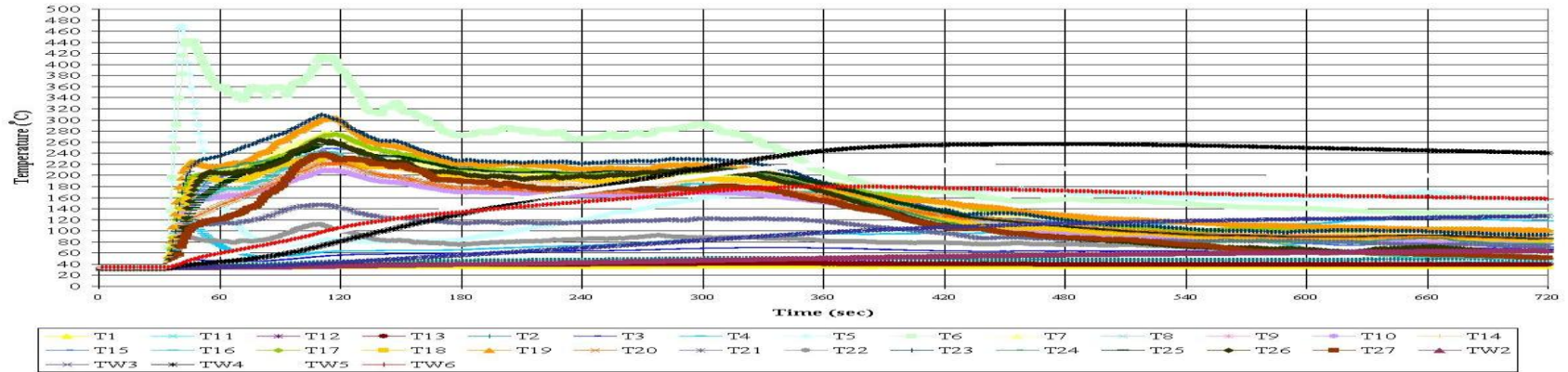


Figure D.47 Experiment No: (-1)011

Exp. No: (-1)211 Temperature Measurement

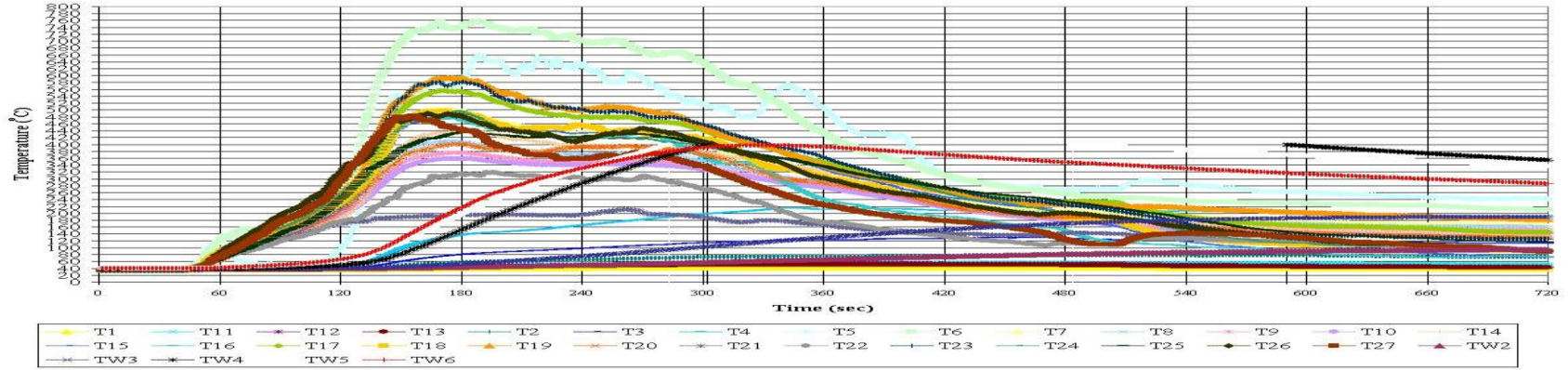


Figure D.48 Experiment No: (-1)211

Exp. No: (-1)012 Temperature Measurement

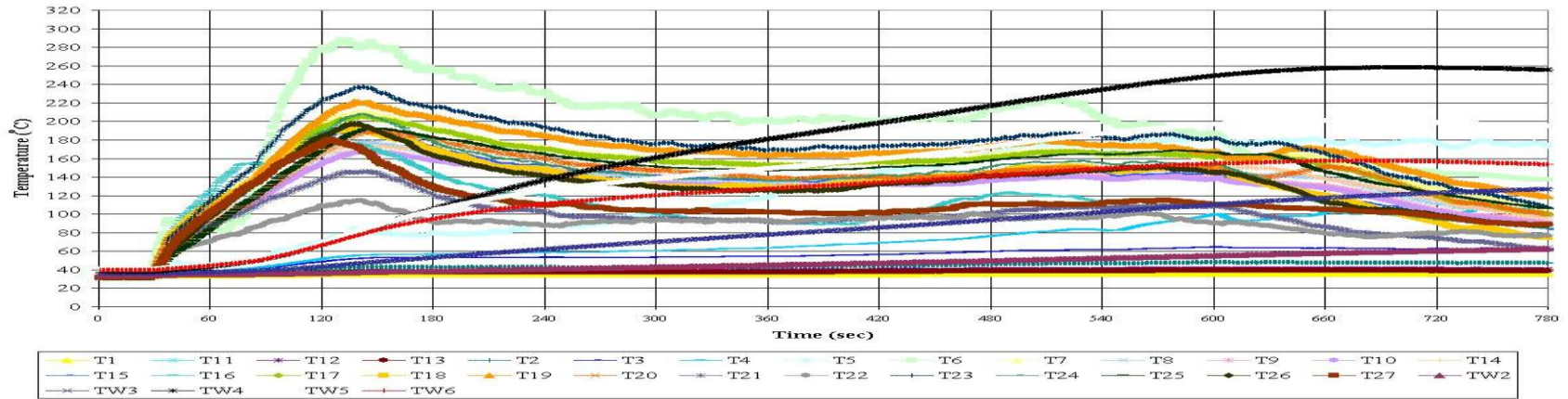


Figure D.49 Experiment No: (-1)012

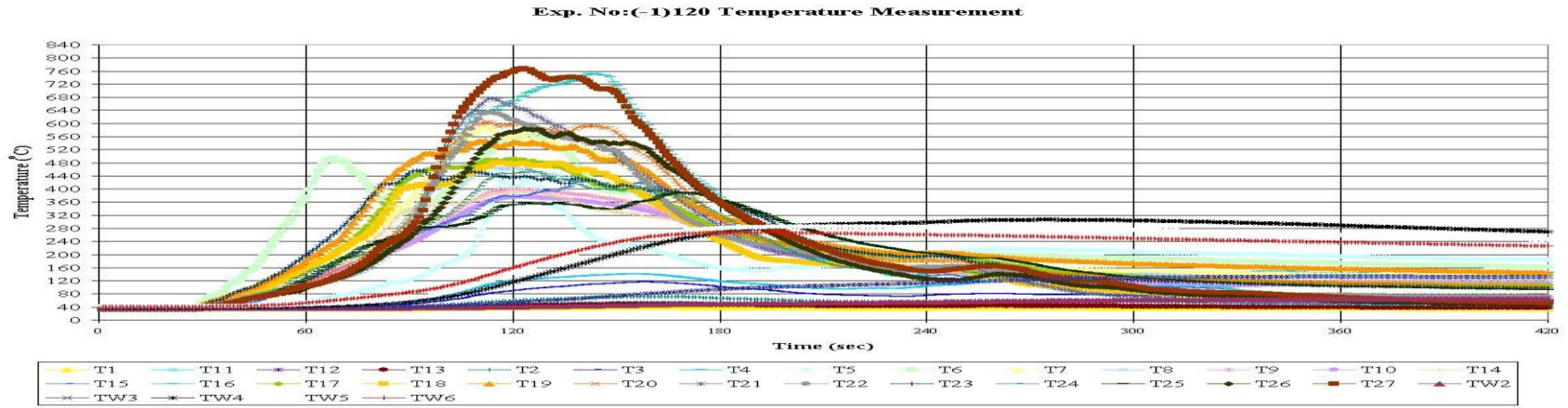


Figure D.50 Experiment No: (-1)120

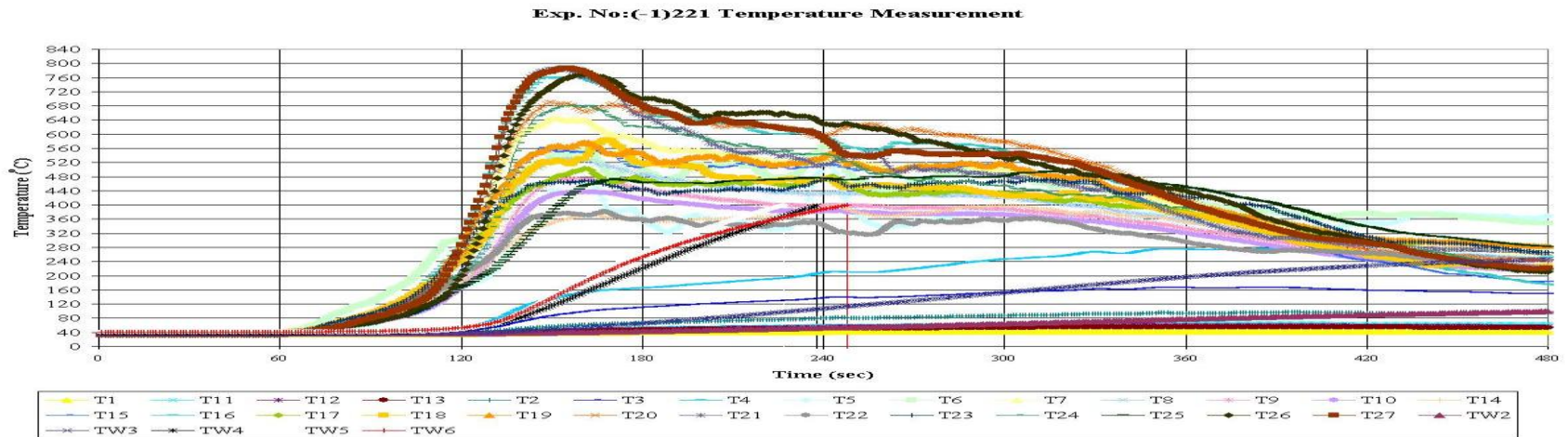


Figure D.51 Experiment No: (-1)120

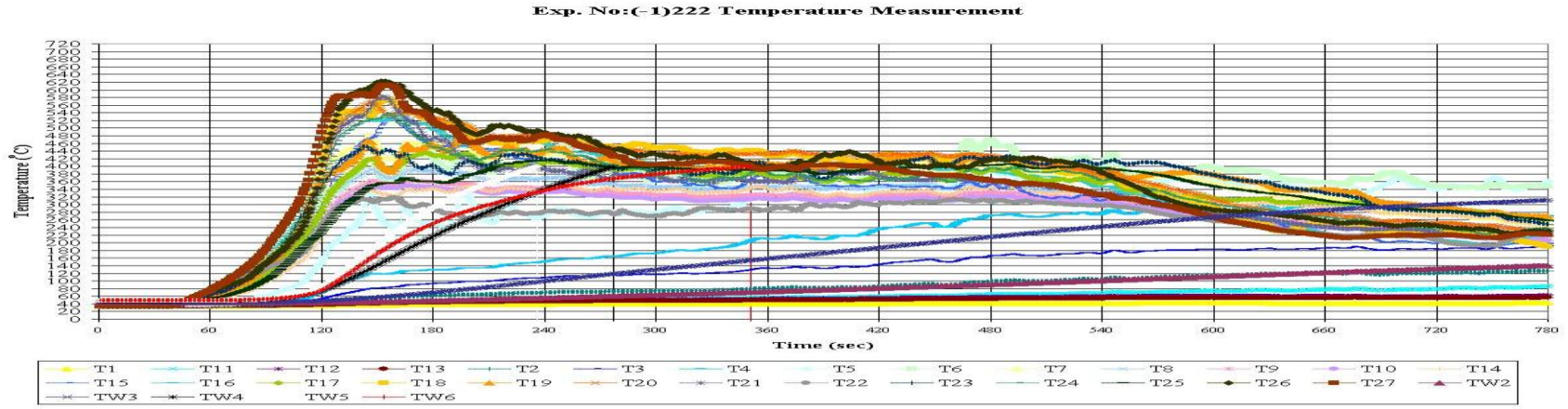


Figure D.52 Experiment No: (-1)222

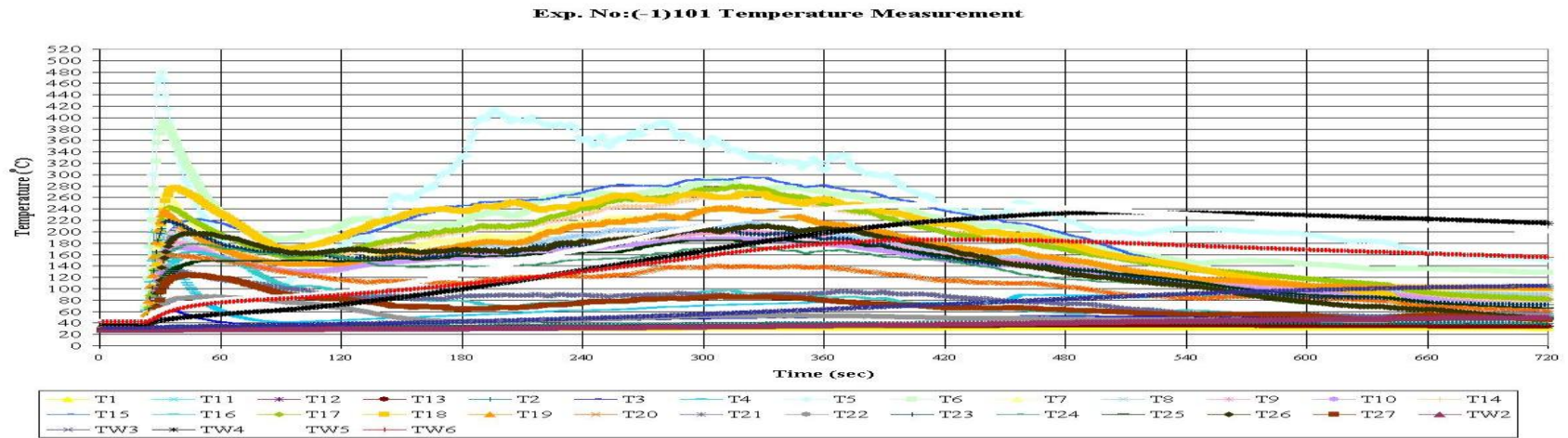


Figure D.53 Experiment No: (-1)101

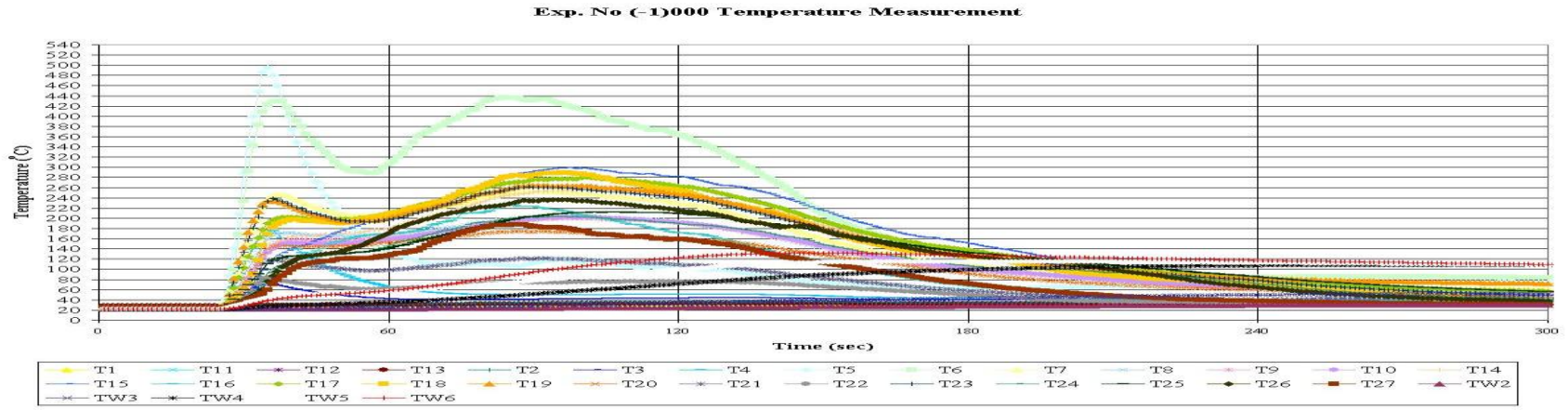


Figure D.54 Experiment No: (-1)000

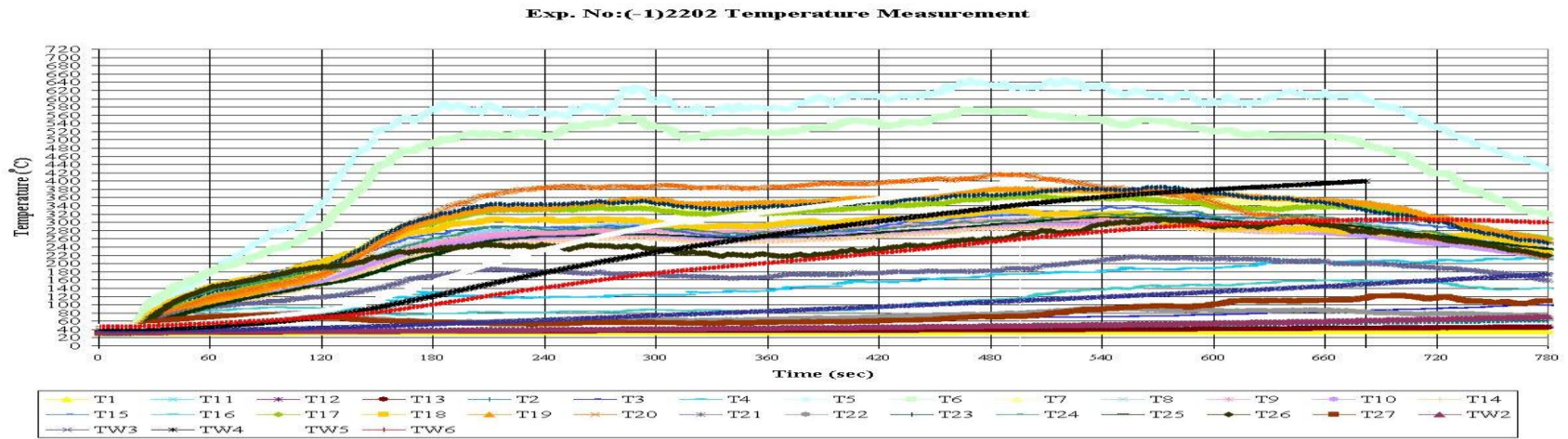


Figure D.55 Experiment No: (-1)2202

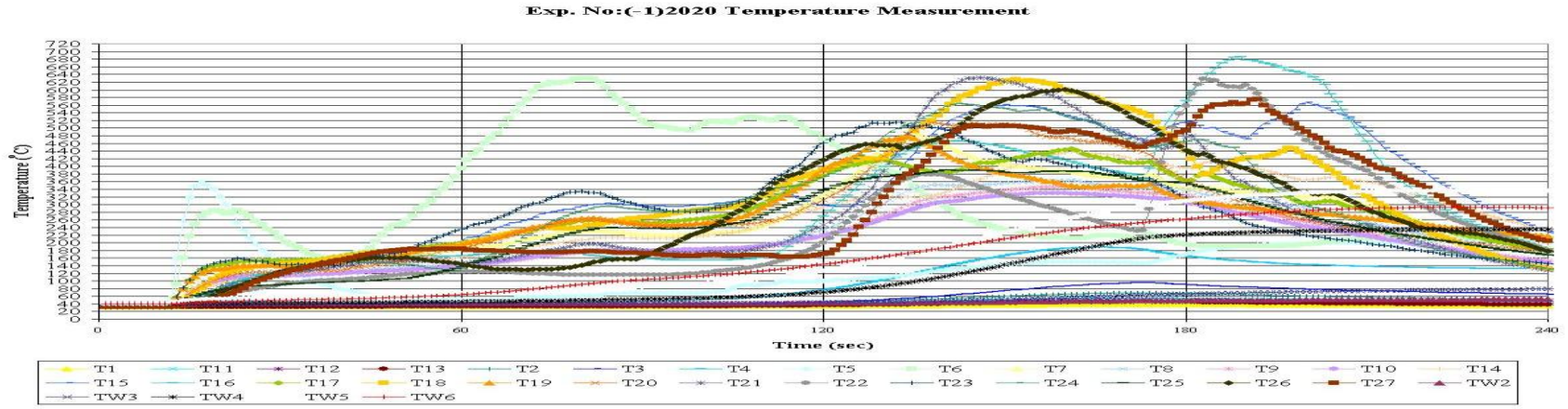


Figure D.56 Experiment No: (-1)2020

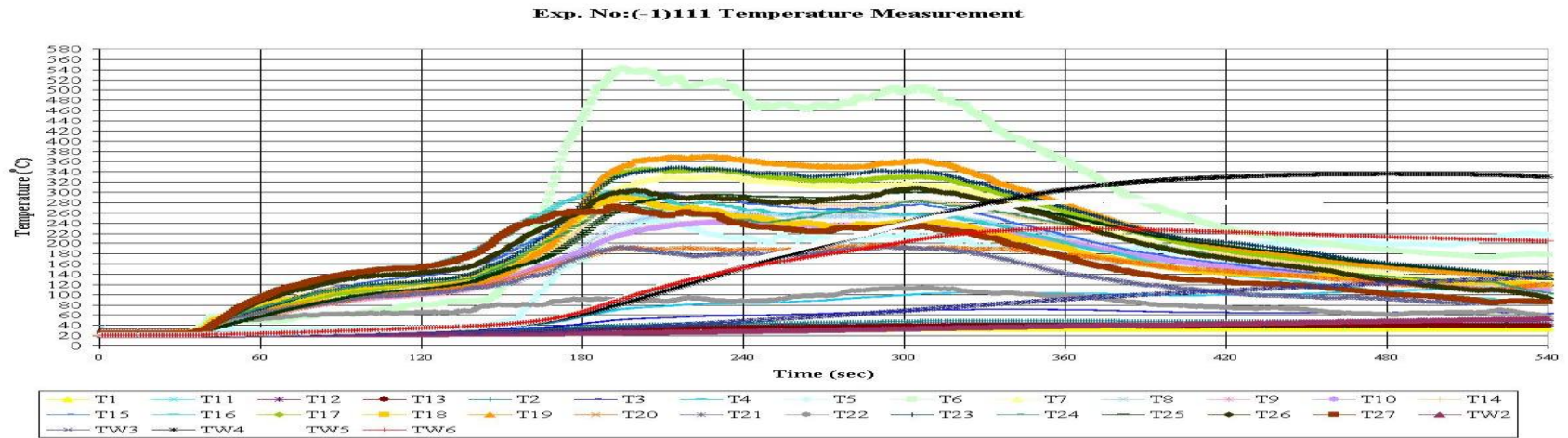


Figure D.57 Experiment No: (-1)111

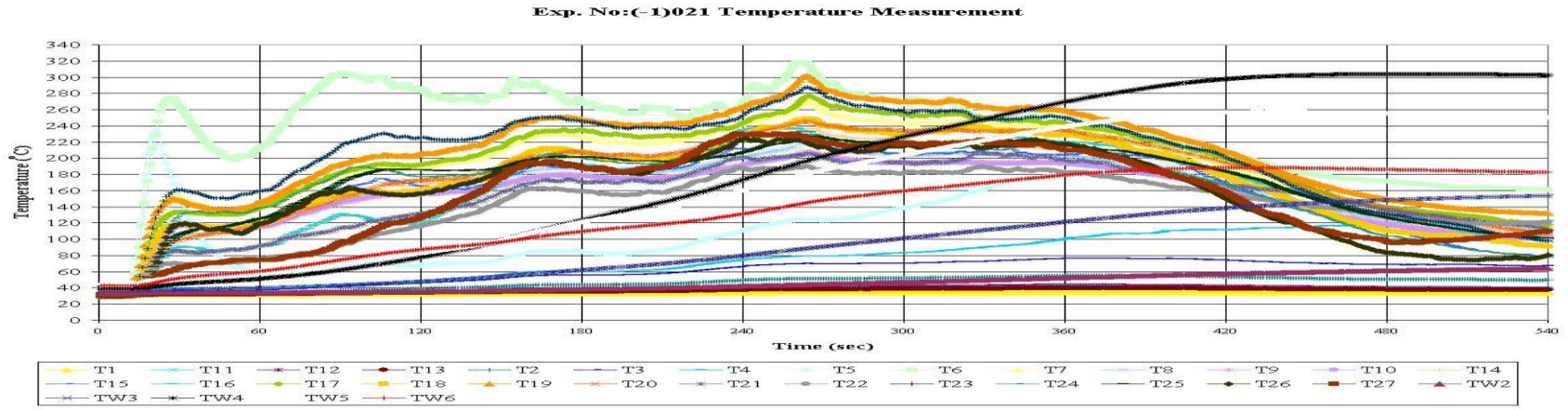


Figure D.58 Experiment No: (-1)021

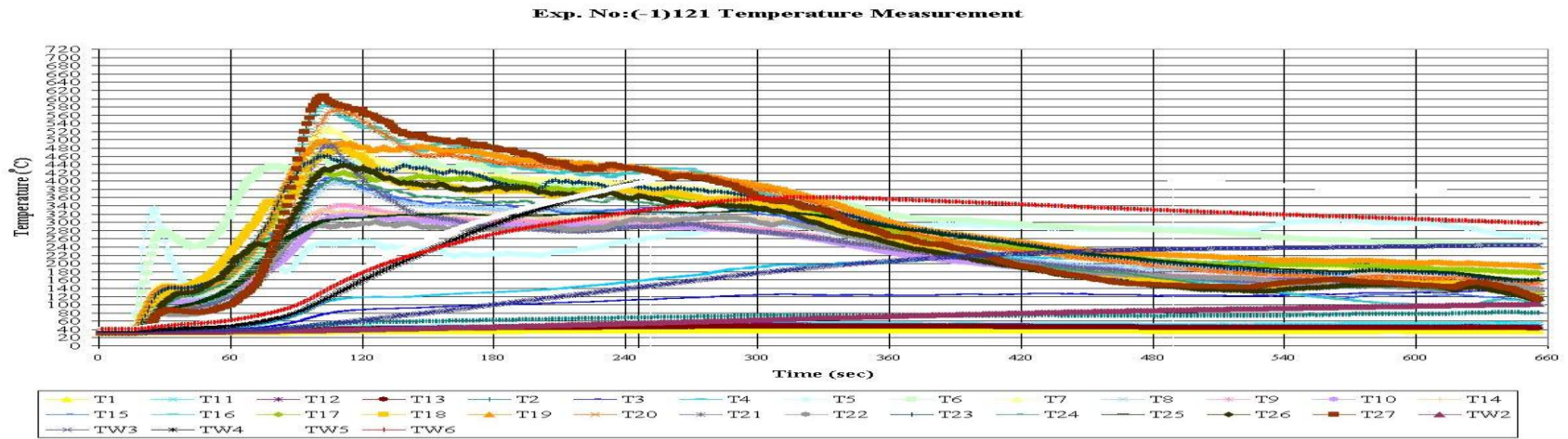


Figure D.59 Experiment No: (-1)121

Table D. 1 Amount of Energy Released in Certain Experiments

Design Code	V (m/s)	H (cm)	L (cm)	W (cm)	T (cm)	Mass (g)	Energy ReleasedQ (kJ)	
							I. TRIAL	II. TRIAL
(-1)000	0,5	12	10	10	1	158,2	1859,8	1843,7
0000	1	12	10	10	1	160,3	3503,49	3369,5
1000	2	12	10	10	1	159,5	4569,16	4741,6
20000	3	12	10	10	1	157,8	4896,04	4422,3

CURRICULUM VITAE

PERSONAL INFORMATION

Surname, Name : KAYILI, SERKAN
Date & Place of Birth : 31 July 1979 - ILGAZ
Nationality : Turkish (TC)
Phone : +90 312 210 25 96
E- mail : serkankayili@gmail.com

EDUCATION

Degree	Institution	Year of Graduation
M.S.	MIDDLE EAST TECHNICAL UNIVERSITY Department of Mechanical Engineering	2005
B.S.	MIDDLE EAST TECHNICAL UNIVERSITY Department of Mechanical Engineering	2002
High School	Ankara Atatürk Anatolian High School	1997

WORK EXPERIENCE

Year	Place	Enrollment
2002 – Present	MIDDLE EAST TECHNICAL UNIVERSITY Department of Mechanical Engineering	Teaching Assistant
2005 – Present	Taru Engineering Inc.	Researcher
2002 – 2005	Ostim Investment Co.	Mechanical Engineer
2001 August	Mitaş Bolt Factory	Intern Engineering Student
2000 August	Turkish Aerospace Industries, Inc.	Intern Engineering Student

FOREIGN LANGUAGE

Advanced English

PUBLICATIONS & PROCEEDINGS

- Kayılı, S., Köktürk, T., Eralp, O.C., “Design Criteria and Technical Issues on Emergency and Comfort Ventilation Of Underground Rail Transit (Urt) Systems, Focus On Turkey”, VIII. International HVAC+R Technology Symposium and Exhibition, 12-14 May 2008 (in Turkish)
- Kayılı, S., Eralp, O.C., “Simulation of Fire And Ventilation in the Stations of Underground Transportation Systems with CFD” Journal of HVAC & Sanitary Engineering, Issue 102 , pages 19-27 , November –December 2007 (in Turkish)
- Kayılı, S., Eralp, O.C., “Simulation of Fire And Ventilation in the Stations of Underground Transportation Systems with CFD”, VIII. National HVAC & Sanitary Engineering Congress, 25-28 October 2007 (in Turkish)
- Eralp, O. C., Kayılı, S., Kayhan, C. , Koç, G., “Application of Jet Fans for Emergency Ventilation in Tunnels of Underground Transportation Systems”, VII. International HVAC+R Technology Symposium and Exhibition, 8-10 May 2006 (in Turkish)
- Eralp, O. C., Basesme E., Kayılı, S., Musluoglu E., “A CFD Analysis of Station Fire Incidents and Determination of Passenger Evacuation Scenarios”, Safety Innovation Criteria inside Tunnels, Gijon-Spain, 2005
- Eralp O.C., Musluoğlu, E, Kayılı, S., “CFD Analysis of Fire Incidents around Crossover Located on the Tunnels Connecting ODTÜ and Bilkent Stations in Ankara Metro System”, Safety Innovation Criteria inside Tunnels, Gijon-Spain, 2005

PROJECTS PARTICIPATED

- Tests for Performance Evaluation of Diaphragm Pumps, METU, October 25th, 2009
- Tests for Evaluation of Piston Effects in Hastane Station Ankara Metro System METU, October 25th, 2008
- Simulation of Tunnel Fires and Emergency Ventilation and Piston Effect; Design of the Emergency Ventilation System in İstanbul Railway Mass Transit of Sanayi- Haciosman Section, September 2008
- CFD Analysis of Station Fire in Sanayi Station, Atatürk Oto Sanayi Station, İTÜ Ayazağa Station in İstanbul Railway Mass Transit of Sanayi- Haciosman Section, June -September 2008
- Marmaray Project TBM Tunnel Key Segment Fire Test, GAMA & NUROL JV, January 15, 2008
- CFD Analysis of Station Fire in Başak Konutları-4, Çiçin Stations of İstanbul Başak Konutları-4 Kirazlı-1 Rail Transportation System, April 2007
- CFD Analysis of Temperature Distribution inside Concrete for RWS & Hydrocarbon Fire Curves, Marmaray Consortium, 2006

- Simulation of Tunnel Fires and Emergency Ventilation and Piston Effect; Design of the Emergency Ventilation System in İstanbul Esenler Bağcılar Light Rail Transportation System, 2006
- Simulation of Tunnel Fires, Emergency Ventilation and Station Comfort, Design of the Emergency Ventilation System in Ulus – Keçiören Metro System., Yüksel Proje AŞ., 2005-2006
- Simulation of Tunnel Fires and Emergency Ventilation and Piston Effect; Design of the Emergency Ventilation System in Ankara Metro 3rd Phase, Giriş İnş. AŞ., 2002-2003.
- Simulation of Tunnel Fires, Emergency Ventilation and Station Comfort, Design of the Emergency Ventilation System in Ankara Söğütözü-Çayyolu Metro System. Yüksel Proje AŞ., 2003-2004
- Simulation of Tunnel Fires, Emergency Ventilation and Station Comfort, Design of the Emergency Ventilation System in Ankara Söğütözü-Karakusunlar Light-Rail Ankaray System, Yüksel Proje AŞ., 2004
- Simulation of Tunnel Fires, Emergency Ventilation and Station Comfort, Design of the Emergency Ventilation System in Ankara Kızılay-Söğütözü Metro System–Preliminary Study, Giriş İnş. AŞ., 2003
- Simulation of Tunnel Fires, Emergency Ventilation and Station Comfort, Design of the Emergency Ventilation System in Ankara Ulus-Keçiören Metro System –Preliminary Study. Yüksel Proje AŞ., 2003
- Simulation of Tunnel Fires, Emergency Ventilation and Station Comfort, Design of the Emergency Ventilation System in Ankara Ulus-Keçiören Metro System, Yüksel Proje AŞ., 2004
- Simulation of Tunnel Fires, Emergency Ventilation and Station Comfort, CFD Analysis of Station Fires, Design of the Emergency Ventilation System in Krakow Metro System – Poland, 2004
- Performance Tests for ASELSAN Meteorological Sensors (IRDAM 2156 & METSMAN MK II), 2004
- A Preliminary Simulation and Analysis of Tunnel Fires in the Marmaray-İstanbul Bosphorous Pass System, 2003

MEMBERSHIPS

Chamber of Turkish Mechanical Engineers

HOBBIES

Football, Movies, Motor Sports, Books, Computer Technologies, Music